Cranfield University

John Davenport

UV Spectroscopic Instrumentation for Formaldehyde Detection in the Indoor Environment

January 2014

School of Engineering

Supervised by Dr. Jane Hodgkinson and Prof. Ralph P. Tatam

Academic Year 2013 / 2014

PhD Thesis

Acknowledgements

There are a number of people without whom this project would not have been possible and who deserve my thanks.

I would like to thank my supervisor Jane Hodgkinson whose help and advice was invaluable and who, I feel, went over and above the required duties to ensure the success of this project.

My thanks also go to Ralph Tatam for his academic advice, Stephen Staines for his support in the laboratory, AlphaSense for co-sponsoring and supporting the project and John Saffell for his industrial advice.

Finally, I would like to thank my wife Rebecca for her invaluable emotional support, proof reading and for putting up with me whilst writing up.

Abstract

The aim of this project was to assess the feasibility of using UV spectroscopy for a simple detection system for formaldehyde gas in the indoor environment. Formaldehyde gas is hazardous to human health causing irritation of the eyes, nose and throat, headaches, limited pulmonary function and is a potential carcinogen. Formaldehyde derivatives are used in plywood and fibre board, carpeting, fabrics and some paints. The gas can be emitted from these materials and can build up in the indoor environment. Current methods for detecting formaldehyde gas that are simple, reliable and inexpensive are limited.

A literature study of chemicals common to the indoor environment was carried out, and their UV absorption spectra compared to that of formaldehyde. 85 substances and substance groups were considered, 11 of which had absorption spectra that overlapped with the formaldehyde UV absorption band. A region was found between 320 and 360nm with very little spectral interference. Given the number of gases considered, this was a surprising result.

Formaldehyde has several strong absorption peaks between regions of very low absorption, allowing for low resolution detection using a single LED source. Two prototype detection systems were developed. The first used a UV LED light source and used a beam splitter to provide one detection channel and one reference channel. The channels used narrow band (laser-line) optical filters.

It was thoroughly optimised for noise performance, giving a best case limit of detection of 4.2ppm, limited by source fluctuation and shot noise, and LED thermal drift. Future developments could include a temperature controller inside the casing of the LED, or a multi-pass gas cell to increase sensitivity. With only two channels, the two filter system was susceptible to spectral interference from nitrogen dioxide and nitric acid.

The second prototype system was developed using a novel method of passing un-collimated light through a laser-line filter to produce multiple wavelength channels with an angular spread. The principle was validated using two-channel detection with a limit of detection of 6ppm.

Contents

List of symbols

A	Normalised absorbance signal
A_{trans}	Einstein A co-efficient
A_D	Detector area
a_1	First Steinhart–Hart parameter
a_2	Second Steinhart–Hart parameter
a_3	Third Steinhart–Hart parameter
C	Capacitance
c	Free space speed of light ($3\times10^{8}ms^{-1}$)
d	Distance
E	Photon energy
E_G	Electron band gap
ΔE	Uncertainty in photon energy
f_0	Initial frequency
f_d	Doppler shifted frequency
Δf_{ca}	Frequency change due to adiabatic collision broadening
Δf_{cd}	Frequency change due to diabatic collision broadening
Δf_e	Noise equivalent bandwidth
G	On-chip amplifier gain
G_1	Off-chip amplifier gain
h	Planck constant ($6.63\times10^{-34}Js$)
$\hbar$	Reduced Planck constant ($h/2\pi$).
I_0	Initial intensity
I	Final intensity

I_{0D}	Initial intensity at detection band
I_D	Final intensity at detection band
I_{0R}	Initial intensity at reference band
I_R	Final intensity of reference band
ΔI	Intensity variation
J_D	Dark current density
k_B	Boltzmann constant ($1.38\times10^{-23}JK^{-1}$)
l	Path length
m	Molecular mass
N	Molecular number density
N_{bit}	Converter bit rate
N_{well}	Electron well capacity
N_x	Number density of perturbing molecules
n_0	Refractive index of air (1)
n_f	Effective refractive index
n_{dark}	Number of dark current electrons
n_{pe}	Number of photoelectrons
n_{reset}	Reset noise electron number
$n_{on\text{-}chip}$	On-chip amplifier noise electron number
$n_{off\text{-}chip}$	Off-chip amplifier noise electron number
n_{ADC}	Analogue to digital conversion noise electron number
n_{prnu}	Photo-response non-uniformity electron number
P	Pressure
q_e	Electron charge ($1.6\times10^{-19}C$)
R	Reflectivity of the mirrors

R_{nm}	Transition moment the *n*-*m* electronic transition
S	Signal current
T	Temperature
t_{int}	Integration time
Δt	Time uncertainty of electronic transfer
U	Fixed pattern ratio
V	Volume
V_{on}	Noise voltage after the on-chip amplifier
V_{off}	Noise voltage after the off-chip amplifier
v	molecular velocity
α_G	Dark current factor (between 1 and 2)
ε_0	Electric permittivity of free space
θ	Filter angle of incidence
λ	Photon wavelength
λ_0	Initial filter central wavelength
λ_f	Filter central wavelength when tilted
μ	Magnetic permeability
σ	Absorption cross-section
σ_a	Adiabatic collision optical cross-section
τ_d	Diabatic collision lifetime
$\tau_{ring\text{-}down}$	Ring-down time

List of units

A	Amperes
AU	Absorbance units
bit	Binary digits
C	Coulombs
°C	Degrees Celsius
e^-	Electron charges (1.60×10^{-19}C)
Hz	Hertz
hr	Hours
J	Joules
K	Degrees Kelvin
Kg	Kilograms
l	Litre
m	Metres
mol	Moles
Pa	Pascal
ppb	Parts per billion (10^9) of a gas by molecule in air
ppm	Parts per million (10^6) of a gas by molecule in air
ppt	Parts per trillion (10^{12}) of a gas by molecule in air
s	Seconds
V	Volts
W	Watts
%	Per cent
°	Degrees (angles)

Publications

Noise analysis of a CCD based ultra-violet spectrometry system
JJ Davenport, J Hodgkinson, JR Saffell and RP Tatam
Photonics Europe, Brussels, April 2012, Proc SPIE **8349**, 8349-61 (10pp), 2012.

Evaluation of the feasibility of a non-dispersive UV detection technique for measurement of gaseous formaldehyde
JJ Davenport, J Hodgkinson, JR Saffell and RP Tatam
Photon 12, Durham, September 2012

Gas Analyser
JJ Davenport, J Hodgkinson, JR Saffell and RP Tatam
Patent application GB1213640.4

Journal Publications in progress

Noise comparison of CCD based ultra-violet spectrometers for use in spectroscopy
JJ Davenport, J Hodgkinson, JR Saffell and RP Tatam

Identification of a Region of the Formaldehyde Absorption Spectrum with Very Limited Interference from Indoor Pollutants
JJ Davenport, J Hodgkinson and RP Tatam

A novel method for indoor formaldehyde gas detection using low resolution, non-dispersive spectroscopy (working title)
JJ Davenport, J Hodgkinson, JR Saffell and RP Tatam

A novel method for using a single optical filter to provide multiple measurement channels for low resolution, non-dispersive spectroscopic formaldehyde gas detection (working title)
JJ Davenport, J Hodgkinson, JR Saffell and RP Tatam

Chapter 1: Introduction

Formaldehyde (CH_2O), also known as methanal, methyl aldehyde and methylene oxide, is a valuable industrial chemical. Its resin is used in the production of fibre boards, carpeting, fabrics and many other products [1] [2]. Formaldehyde gas is hazardous to human health, being, among other things, toxic, allergenic and potentially carcinogenic [1] [2] [3]. It has been shown to cause health problems in enclosed urban areas [4], especially when ventilation is low [5] and is a possible contributor to "sick building syndrome".

The potential for formaldehyde build-up is a serious problem in industrial buildings and offices. Many of the materials used in modern offices contain formaldehyde and can emit background levels for multiple years [6]. It is common to refurbish entire rooms or even entire buildings, adding a large number of formaldehyde sources all at one time. Factories, warehouses or hospitals that work with formaldehyde based substances are also at risk of high formaldehyde build-up [7] [8] [9] [10].

Indoor formaldehyde detection would be desirable for a number of reasons [11]. Firstly, for verification and enforcement of international standards, such as the European Standard (EN) [12] (EN 717), the American Society for Testing and Materials (ASTM) [13] (ASTM E1333 – 10) and the International Organisation of Standardisation (ISO) [14] (ISO 14184). Secondly, for use with new buildings being 'burned-in' (heating run hot for several days with the windows open) to expel formaldehyde [11]. Thirdly, for use in offices or working environments, for detecting background formaldehyde levels and ensuring safe working conditions.

At the time of writing, while several formaldehyde detection methods exist, they tend to be expensive, complex to operate or have issues with selectivity [15] [16] [17] [18]. Methods of simply and reliably detecting hazardous levels of formaldehyde are extremely limited, with a single electrochemical system being the only exception [19]. More details on other methods of gas detection are given in Chapter 2.

This project aimed to investigate the feasibility of a formaldehyde detector based on ultra-violet (UV) spectroscopy. Spectroscopy tends to have good selectivity and sensitivity [20] but can be a complicated process, requiring trained operators. This project aimed to use knowledge of the formaldehyde absorption spectrum to build a less complex system, targeted specifically at formaldehyde.

Formaldehyde exhibits absorption in both the UV and IR regions of the spectrum. The UV region was used because the main infra-red (IR) formaldehyde absorption regions overlap with those of several other gases. For example the absorption region between 5.5 and 6.0μm overlaps with an absorption region of water vapour [21] [22], and the absorption region between 3.3μm and 3.8μm partially overlaps with an absorption region of methane [21]. Also the formaldehyde absorption spectrum in the UV had some interesting properties and gave an opportunity to investigate a relatively unexplored region.

1.1. Aims

The main aim of this project was to design, build and assess the feasibility of a system to detect the presence and concentration of formaldehyde gas in the indoor environment. The primary intended application was for factories, offices and other industrial buildings. The project was co-sponsored by Alphasense Ltd, a UK supplier of gas sensor modules. Below is the list of aims for the system that was set at the beginning of the project. They were decided upon in discussion with Alphasense based on the desired application of the system, and on what was considered practically feasible.

- Limit of detection of 0.1ppm (parts per million by volume). This is the recommended indoor limit set by a number of countries including Canada, Singapore and South

Korea [5]. It is necessary that the limit of detection is at least as low as the action limit for the user. Some countries and organisations have more stringent limits, but 0.1ppm made for a realistically achievable target. The system should be able to reliably measure at this limit, with minimal false negatives.

- Good selectivity. Selectivity is defined as the ability of the device to avoid cross-sensitivity from other gases or airborne particles, particularly those present in the target environment. "Good" can only be defined relative to the environment in question. It is not possible to guarantee that all gases have been considered, making selectivity a difficult property to quantify. In general it is given as a list of substances known to have cross-sensitivity and a list of substances verified to be cross-sensitivity free. Ideally typical concentrations of gases in the indoor environment should not give cross sensitivity above the limit of detection of the device.

- Response time t_{90} of no longer than 60s. This is the time between individual measurements. t_{90} refers to time taken to reach a reading corresponding to 90% of the equilibrium value following a step change. Formaldehyde concentrations have been shown to vary with temperature and with humidity [23] [18], and would be expected to vary on about the minutes time scale. It is important that formaldehyde does not reach dangerous levels between measurements. Additionally if the system were to be used as a hand held device then it would be inconvenient to the operator if measurements took much longer than sixty seconds.

- Simple to manufacture. The system should be simple enough that it can be easily produced and not prohibitively expensive. It should be constructed of readily available components and should avoid complex components where possible. The sponsors desired a total cost of components in a final instrument to be less than £100.

- Robust. The system should be able to operate reliably in a range of conditions. It should therefore avoid the use of moving parts and delicate components where possible. Indoor temperature varies less than outdoor temperatures, but the system needed to withstand any changes it may encounter in transit etcetera. Ideally the system should be able to operate reliably between 10 - 30°C for indoor air, and

remain un-damaged from 0°C to 50°C for outdoor air. Operating up to 40°C may be desirable for use during back-out.

- Easy to operate. Ultimately, a scientific education or significant training should not be required to operate the system. It should be simple to set up and give results that are easily interpreted. This should either be a readout of formaldehyde concentration or simply an indication of its presence above or below safe levels.

1.2. Novelty

This section provides a summary of work in this project that was considered to be novel.

- At the time of writing, methods of measuring formaldehyde that were both simple and inexpensive were extremely limited. One manufacturer did produce an electrochemical detector [19] but no others were found.

- The application of UV spectroscopy to formaldehyde detection in indoor air was a novel one. Much work in indoor spectroscopic gas detection takes place in the IR region with the UV remaining relatively unexplored. Recent developments in UV LEDs has opened up potential for new areas of research.

- A full and detailed analysis of the noise limitations affecting a number of CCD based spectrometers was made, and the results are given in Chapter 3. Tests were performed to identify and quantify a range of common noise phenomena, making a comparison between the spectrometers. As an investigation of the limits of the technology, this was a contribution to the field of instrumentation.

- A detailed study was undertaken into the spectra of gases commonly found in the indoor environment, given in Chapter 4. The intention was to find the potential extent of interference in the formaldehyde UV absorption region. This was an important consideration for many of the systems developed in this project.

A band of the formaldehyde spectrum was found between 320 and 360nm with very limited interference, which was a surprising result given the number of gases considered. The band is also used for differential optical absorption spectroscopy (DOAS) [24] [25] [26] [27] for formaldehyde detection. However this was generally used for outdoor measurements, which differs substantially from the indoor environment. These points form the basis of a patent application (see Publications List, page XI).

- Over the course of the project, several detection systems have been designed and implemented. Some of them showed independent novelty as detection systems. For example, exploitation of the angular dependence of interference filters to provide multiple wavelength channels is believed to be novel. This also forms the basis of a patent application (see Publications List, page XI). At the time of writing, application GB1213640.4 was intended to be divided into these two parts, but this had not yet taken place.

- The detection systems developed in this project also provided some unique advantages as gas detection methods. Using optical methods allowed for a greater degree of selectivity and long term stability than some other methods (such as electrochemical). The decreased components and the specific use of formaldehyde spectral features allowed for a lower cost than typical of optical detection methods.

1.3. Thesis summary

The first chapter of this document introduces the project, summarises the aims and objectives, and outlines the targets. The aim of this project was to investigate the feasibility of UV spectroscopy for detecting gaseous formaldehyde and to design and build a series of prototype devices. This chapter also summarises the rest of the document.

Chapter 2 gives the background to the project including a number of relevant literature reviews. The properties of formaldehyde are explained, along with its observed concentrations in indoor environments and a detailed description of its effects on health. Details are given on common gas detection methods used at the time of writing, including

their principle advantages and disadvantages and identifying which of them can be used to detect formaldehyde.

Chapter 3 covers spectroscopy, starting with a theoretical description including the behaviour of light passing through an absorbing medium and the origin of the absorption bands. Sources of spectral broadening are described along with the effect they have on formaldehyde under different conditions. Finally a theoretical description is given of the principles of operation of the systems used in this project.

Chapter 4 is a detailed study of the spectra of gases expected to be present in the indoor environment. This included a review of published spectra considering 85 chemicals and chemical groups common to the indoor environment. It was found that the region between 320 – 360nm is relatively free from interference from indoor gases, with nitrogen dioxide and nitrous acid being the only major interferents. From this region some sets of low resolution wavelength bands were selected to be used for prototype systems. Each set included bands for detection and for reference.

Chapter 5 describes the UV spectrometer that was used in this project. The criteria by which it was selected are given. The performance of the spectrometer was thoroughly investigated including comparisons to two similar spectrometers and a detailed investigation into noise phenomena. This information was used to find a set of operation procedures which optimised the performance of the spectrometer and which were used throughout the project.

Chapter 6 concerns the preliminary system. This was a conventional dispersive spectroscopy system using a broad-band light source and a UV spectrometer. It was used throughout the project as a research tool for testing fundamental principles and as a benchmark for later designs. The main components of the system are described in this chapter, as are some of the tests carried out on the system for characterisation and optimisation. The methods of formaldehyde generation used in this project are also described in this chapter.

Chapter 7 describes the two-filter detection system. This system used a UV LED as a light source and two laser line filters to give a detection and a reference channel. The system was optimised and tested with formaldehyde. This chapter gives the results and discusses the advantages and disadvantages of the system.

Chapter 8 describes the single-filter, multi-channel system. This builds on the two-filter detection system, and exploits the angular dependence of a single laser-line filter to provide multiple measurement channels to a photodiode array. This system was also optimised and tested, and the results are discussed in this chapter.

The ninth and final chapter summarises the project and gives the conclusions that were drawn. The project dealt with the question of whether it was feasible to use UV spectroscopy to detect formaldehyde gas, and the considered answer is given here. The limitations of the current system are given along with suggestions for future work in this area.

1.4. Chapter summary

Formaldehyde is a chemical used in a wide range of products such as fibre boards, carpeting and many others. These materials can then emit formaldehyde gas which can build up in the local environment. Formaldehyde is hazardous to human health, as it is toxic, allergenic and potentially carcinogenic.

The aim of this project was to design, build and test a formaldehyde gas detector based on UV spectroscopy. The primary intended application was for use in the indoor environment, specifically industrial buildings such as offices or factories. This device had the following targets:

- Limit of detection of 0.1ppm or lower, the recommended indoor limit of several countries.
- Low cross-response to gases commonly found in the indoor environment.
- Response time of 60s or less to prevent formaldehyde concentrations reaching dangerous levels between measurements.
- Simple to manufacture, containing a minimum of complex components.
- Robust and able to operate over a 10 - 30°C range, approximately corresponding to the indoor air temperature range.
- Simple to operate, requiring no extensive training.

For the novelty of the project, at the time of writing there were very few options for measuring formaldehyde gas that were both simple and reliable. The application of UV spectroscopy to indoor formaldehyde detection was also novel. Chapter 3 includes an analysis into the noise performance of the UV spectrometer used in this project, which was considered a contribution to the field of instrumentation.

Chapter 4 covers a detailed study into the absorption spectra of common indoor gases and their potential to interfere with formaldehyde measurements, which yielded novel information. Finally the prototype systems designed during this project held novelty, specifically the use of the angular dependence of interference filters.

The next chapter gives some more detail on the background to the project. This includes the properties of formaldehyde, a review of studies into its concentrations in the indoor environment, and details of its effect on human and animal health. Also included is a review of current gas detection methods, listing which are applicable to formaldehyde detection.

1.5. References

[1] Y. Lu, J. Liu, B. Lu, A. Jiang and C. Wan, "Study on the removal of indoor VOCs using microtechnology," *Jounal of Hazardous Materials,* vol. 182, pp. 204-209, 2010.

[2] S. Kim, "Control of formaldehyde and TVOC emission from wood-based flooring composites at various manufacturing processes by surface finishing," *Journal of Hazardous Materials,* vol. 176, pp. 14-19, 2010.

[3] G. D. Nielsen and P. Wolkoff, "Cancer effects of formaldehyde: a proposal for an indoor air guideline value," *Archives of Toxicology,* vol. 84, pp. 423-446, 2010.

[4] A. Elia, V. Spagnolo, C. Di Franco, P. M. Lugarà and G. Scamarcio, "Trace gas sensing using quantum cascade lasers and a fiber-coupled optoacoustic sensor: application to formaldehyde," *Journal of Physics: Conference Series,* vol. 214, no. 1, p. 012037, 2010.

[5] T. Salthammer, S. Mentese and R. Marutzky, "Formaldehyde in the indoor enviroment," *Chemical Reviews,* vol. 110, pp. 2536-2572, 2010.

[6] T. W. Zinn, D. Cline and W. F. Lehmann, "Long-term study of formaldehyde emission decay from particleboard," *Forest Products Journal,* vol. 40, pp. 15-18, 1990.

[7] T. Malaka and A. M. Kodama, "Respiratory health of plywood workers occupationally exposed to formaldehyde," *Archive of Environmental Health,* vol. 45, pp. 288-294, 1990.

[8] H. G. Bourne and S. Seferian, "Formaldehyde in wrinkle-proof apparel produces-Tears for milady," *Industrial Medicine and Surgery,* vol. 28, pp. 232-238, 1959.

[9] E. P. Horvath, H. Anderson, W. E. Pierce, L. P. Hanrahan and J. O. Wendlick, "Effects of formaldehyde on the mucous membranes and lungs: a study of an industrial population," *Journal of the American Medical Association,* vol. 259, pp. 701-707, 1988.

[10] R. De Zottle, L. Petronio, C. Negro, "Occupational exposure to formaldehyde in hospitals environmental and health survey of exposed staff in operating rooms and other departments," *Medicina del Lavoro,* vol. 76, no. 3, pp. 246-252, 1985.

[11] Personal communication with J. Saffell, Technical Director of Alphasense Ltd., Great Notley, UK, 2013.

[12] H. Schwab, R. Marutzky and B. Meyer, European Regulations for Formaldehyde, Braunschweig, Germany: Fraunhofer Institute for Wood Research Wilhelm-Klauditz-Institut, 2007.

[13] Designation: E1333 − 10, Standard Test Method for Determining Formaldehyde Concentrations in Air and Emission Rates from Wood Products Using a Large Chamber, West Conshohocken, USA: ASTM International, 2010.

[14] ISO 14184-1:2011, Textiles -- Determination of formaldehyde -- Part 1: Free and hydrolysed formaldehyde (water extraction method), Geneva, Switzerland: ISO, 2005.

[15] J. A. Dirksen, K. Duval and T. A. Ring, "NiO thin-film formaldehyse gas sensor," *Sensors and Actuators,* vol. 80, pp. 106-115, 2001.

[16] H. Bagheri, M. Ghambarian, A. Salemi and A. Es-Haghi, "Trace determination of free formaldehyde in DTP and DT vaccines and diphtheria–tetanus antigen by single drop microextraction and gas chromatography–mass spectrometry," *Journal of Pharmaceutical and Biomedical Analysis,* vol. 50, pp. 287-292, 2009.

[17] C. Wang and P. Sahay, "Breath analysis using laser spectroscopic techniques: breath biomarkers, spectral fingerprints, and detection limits," *Sensors,* vol. 9, pp. 8230-8262, 2009.

[18] H. Kudo, Y. Suzuki, T. Gessei, D. Takahashi, T. Arakawa and K. Mitsubayashi, "Biochemical gas sensor (bio-sniffer) for ultrahigh-sensitive gaseous formaldehyde

monitoring," *Biosensors and Bioelectonics,* vol. 26, pp. 854-858, 2010.

[19] Monitor, PPM FormaldemeterTM htV 3 Parameter IAQ, *operation manual,* PPM Technology Ltd., Caernarfon, UK, 2008.

[20] G. Man, B. Stoeber and K. Walus, "An assessment of sensing technologies for the detection of clandestine methamphetamine drug laboratories," *Forensic Science International,* vol. 189, pp. 1-13, 2009.

[21] Eds. P. J. Linstrom, W. G. Mallard, "Evaluated Infrared Reference Spectra," in *NIST Chemistry WebBook, NIST Standard Reference Database Number 69,* Gaithersburg, USA, National Institute of Standards and Technology, 2013.

[22] S.E. Stein, Eds. P. J. Linstrom, W. G. Mallard, "Infrared Spectra," in *NIST Chemistry WebBook, NIST Standard Reference Database Number 69,* Gaithersburg, USA, National Institute of Standards and Technology, 2013.

[23] G. E. Myers, "The effects of temperature and humidity on formaldehyde emission from UF-bonded boards: a literature critique," *Forest Products Journal,* vol. 35, no. 9, pp. 20-31, 1985.

[24] A. M. Winer, "Long pathlength differential optical absorption spectroscopy (DOAS) measurements of gaseous HONO, NO2 and HCHO in the California South coast air basin," *Research on Chemical Intermediates,* vol. 20 (3/4/5), pp. 423-445, 1994.

[25] W. Thomas, E. Hegels and S. Slijkhuis, "Detection of biomass burning combustion products in Southeast Asia from backscatter data taken by the GOME spectrometer," *Geophysical Research Letters,* vol. 25 (9), pp. 1317-1320, 1998.

[26] I. D. Smedt, J. F. Muller, T. Stavrakou, R. van der A, H. Eskes and M. V. Roozendael, "Twelve years of global observations of formaldehyde in the troposphere using GOME and SCIAMACHY sensors," *Atmospheric Chemistry and Physics,* vol. 8, p. 4947–4963, 2008.

[27] F. Wittrock, A. Richter, H. Oetjen, J. P. Burrows, M. Kanakidou, S. Myriokefalitakis, R. Volkamer, S. Beirle, U. Platt and T. Wagner, "Simultaneous global observations of glyoxal and formaldehyde from space," *Geophysical Research Letters,* vol. 33, 2006.

Chapter 2: Background: formaldehyde and methods of detection

This chapter covers some of the background material and literature that was important to the project. Details are given of the properties of formaldehyde, as it was the focus of study. A representative selection of studies into formaldehyde concentrations in the indoor environment is given. The effects of the gas on human and animal health are discussed in detail.

Finally the results of a review into common gas detection methods in use at the time of writing are given. This gives descriptions of the operations of many of the main types of detection methods, including ionisation detection, semiconductor detection, electrochemical detection, gravimetric detection, gas chromatography, optical absorption spectroscopy and fluorescence detection. Advantages and disadvantages are given along with a listing of those which are applicable to formaldehyde detection.

2.1. Formaldehyde

Formaldehyde, also known as methanal, methyl aldehyde and methylene oxide, is the first member of the aldehyde chemical family. It has the chemical formula CH_2O and the molecular structure shown in Figure 2.1 [1] . Under standard conditions it is a colourless gas. It is toxic, allergenic and a potential human carcinogen [2] [3] [4]. It has been shown to cause

inflammation in lung epithelial cells [5] and to be harmful at a level of 2ppm (parts per million in air by volume) [6] [7].

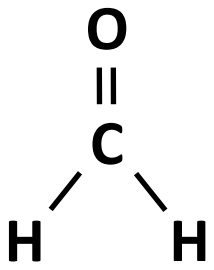

Figure 2.1: Molecular structure of formaldehyde. It consists of one central carbon atom covalently bonded to two hydrogen atoms and covalently double-bonded with one oxygen atom.

The World Health Organisation (WHO) has set a guideline maximum level for prolonged or acute formaldehyde exposure at 80ppb (parts per billion, one ppb being 10^{-3} ppm), and many countries have set theirs in line with this [1] [8]. Some countries have guideline levels as high as 100ppb, such as Canada, Singapore and South Korea [1].

Formaldehyde is also a valuable industrial chemical with limited alternatives [1] [2] [3]. Formaldehyde resin is used as an adhesive in plywood and medium density fibre board [9] [10] and in carpeting [11], and is also used in the production of paints [12] and wallpapers [13], Formaldehyde is also a by-product of incomplete combustion [1] and is present in various cleaning products [1]. Small amounts have been found in human breath [14], although it is unclear whether this was absorbed from the environment or produced by the body.

Many of these materials emit low concentrations of formaldehyde over time. Emission levels are highest when materials are new, generally decreasing exponentially, but can take multiple years to reach safe levels [8] [1] [15]. Formaldehyde gas can build up in enclosed areas, particularly when new furnishings or carpeting have been installed and where premises are not adequately ventilated.

A list of properties of formaldehyde is given in Table 2.1. It readily dissolves into water at room temperature, producing *formalin*, a common preservative [16]. For industrial uses, formaldehyde is generally produced by the oxidation of methanol. In the laboratory the most

common method of production is the dissociation of *paraformaldehyde*, a white powder formed of polymerised formaldehyde molecules precipitated from formalin. This process is described in more detail in Chapter 6. Formaldehyde gas is flammable, but at concentrations much higher than were used in this project.

Table 2.1: Properties of formaldehyde

Property	**Formaldehyde**
Formula	CH_2O [1]
CAS number	50-00-0 [1]
Molar mas	30.026gmol^{-1} [16]
Melting point	181K (-92°C) [16]
Boiling point	252K (-21°C) [16]

The UV absorption spectrum of formaldehyde is shown in Figure 2.2. It consists of a number of strong absorption peaks containing many spectral features that are narrower than the resolution of this graph. Between the main peaks there are wavelength regions of lower absorption cross-section. At higher wavelengths the absorption of these regions is close to zero. More detail and a better resolved graph of the formaldehyde absorption spectrum is given in Chapter 3.

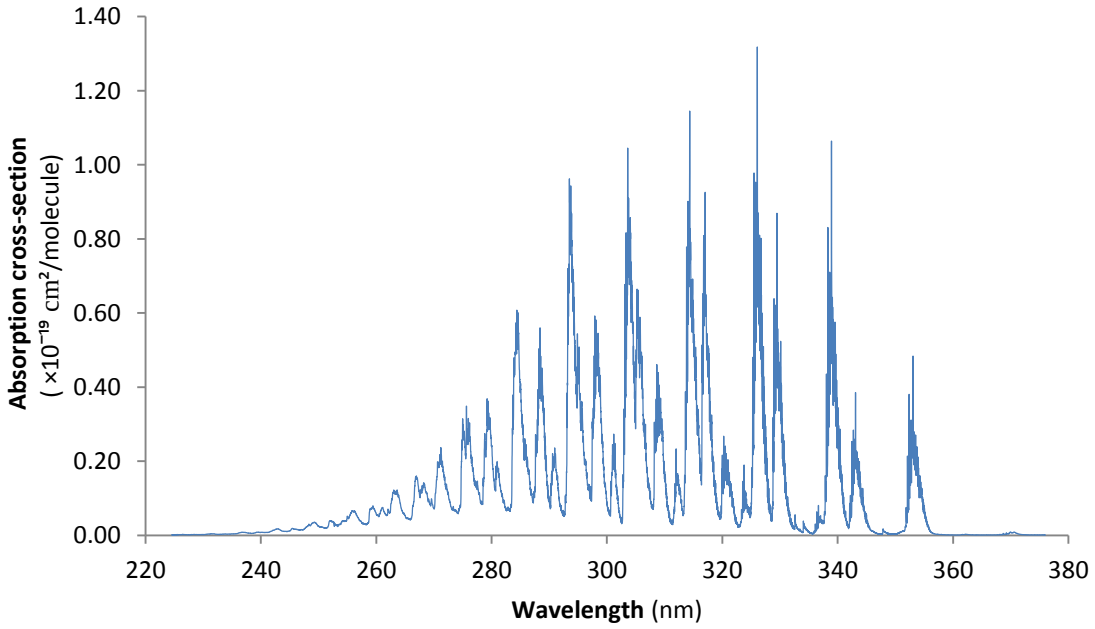

Figure 2.2: Graph of the formaldehyde UV absorption spectrum, re-plotted from data from Meller *et al* [17]. The spectrum is not fully resolved in this graph.

2.1.1. Indoor concentrations

Indoor formaldehyde concentration varies significantly by building, by country and by time. Formaldehyde is generally measured in studies of specific buildings either randomly selected or where there is specific concern. This makes it difficult to draw broad conclusions. A significant majority of studies have been carried out in homes or areas where children are likely to be present with offices and industrial buildings making up a relatively small fraction of the published work. A selection of relevant studies is summarised in Table 2.2. 50-P refers to the 50th percentile of data collected. 95-P refers to the 95th percentile.

Table 2.2: Selection of world-wide studies into indoor formaldehyde concentration.

Location	**Type of building**	**Year**	**Concentration** (ppb)	**Source**	**Notes**
Germany	Residences	1995	9.6 – 520	[18]	
Germany	Offices	2003	4.8	[19]	50-P
Finland	Offices	2009	8.8	[20]	Geometric mean
Sweden	Schools	2001	2.4	[21]	Geometric mean
Poland	Offices	2005	1.84 – 25.9	[22]	
USA	Mobile homes	1989	70	[23] [24]	Arithmetic mean
USA	Residences	2007	16.1 26.0	[25] [26]	50-P 95-P
Quebec	Residences	2008	7.7 – 72.1	[27]	
South Korea	Schools	2009	150 (summer) 100 (winter)	[28]	Geometric mean
Japan	Residences	2004	30.1	[29]	Geometric mean
Hong Kong	Offices	2006	25.6 in 2006	[30]	Air conditioned, geometric mean
China	Hotel ball rooms	2004	23.8	[31]	Geometric mean
Egypt	Residences	2000	77.4	[32]	Arithmetic mean
Australia	Residences	2002	0.8 – 133	[33]	Dependent on room
Brazil	Laboratories		<1 – 65.7	[34]	
N/A	Submarines	2006	<10	[35]	Submerged operations

The levels measured in South Korean schools and the highest levels measured in German and Australian residences were above the 100ppb target measurement concentration of this project. Several exceed the WHO guideline limit of 80ppb but none of them reach the short term sensory irritation threshold of around 2ppm (see Section 2.1.2). In general these results show that there is a significant variation in formaldehyde concentrations in the indoor

environment, even between similar buildings. This makes concentration difficult to predict, emphasising the requirement for readily available formaldehyde detection.

2.1.2. Effects of formaldehyde gas on health

Formaldehyde gas is toxic, allergenic and potentially carcinogenic to humans [2] [3] [4]. This section gives a detailed description of observed effects of formaldehyde on human and animal health. The effects of the gas can vary significantly between subjects for both humans and other animals [36]. It is not uncommon for symptoms to manifest in some individuals at much lower concentrations than in others [37] [38], making it difficult to give definitive safe levels.

It can also be difficult to distinguish the effects of formaldehyde from other gases or conditions that may be present during testing [36] [39]. Links between formaldehyde and asthma or cancer are still under debate [40] [41] [42]. In general, sensory irritation has been found to be dependent on the peak exposure concentration rather than integrated concentration over exposure time [36] [43]. Some studies have suggested that slightly lower concentrations may still be harmful when the subject is exposed over a full working day but these findings are still under debate [36] [44]. However, it was important to take measurements sufficiently frequently to prevent concentration rising above safe levels.

Sensory irritation, specifically of the eyes and throat, is one of the most common health effects of atmospheric formaldehyde. At concentrations of 2ppm or below, these effects tend to be merely unpleasant and do not cause severe health issues [45] [46]. Studies into sensory irritation as well as odours generally rely on test subjects reporting their experiences. This can pose problems such as a lack of quantitative measurements and the placebo effect [47]. Problems also arise for studies into long term work place exposure where other gases may also be present [36].

Kulle *et al.* [47] exposed nineteen subjects to concentrations of formaldehyde between 0ppm and 2.0ppm. Some were also exposed to concentrations as low as 500ppb or up to 3.0ppm. The study demonstrated that there were no significant differences from 0 to 500ppb, and that

more than 50% of subjects experienced odour and eye irritation at 2.0ppm. 37% experienced throat irritation at 2.0ppm.

Many other studies show similar findings with little significant irritation below 500ppb, eye irritation in more than 50% of subjects at 2.0ppm and throat or nasal irritation in 25-50% at 2.0ppm [6] [7] [46]. Reports of odours varied between studies; Schachter *et al.* [46] found that 47% of subjects reported odours when no formaldehyde was present. This makes it difficult to accurately quantify the effects of formaldehyde at low concentrations. The target limit of detection was set at 0.1ppm (100ppb) to ensure detection safely below these levels.

As concentrations increase, symptoms become more severe. Discomfort starts almost immediately after exposure between 4 and 5ppm [48] [36]. Intense lachrymation (watering eyes), severe irritation of the eyes, nose and throat and difficulty breathing can occur between 10 and 20ppm [49]. Many formaldehyde symptoms have been shown to be reversible [44] [50] after about 4 weeks of non-exposure [51].

Several studies have been carried out to determine if there is a link between asthma and formaldehyde sensitivity or if asthmatic symptoms are exacerbated by formaldehyde. Green *et al.* [52] gave 3ppm of formaldehyde to sixteen asthmatic subjects during moderate, intermittent exercise and to twenty one healthy subjects during heavy, intermittent exercise. Both groups experienced sensory irritation to a similar level. No acute asthmatic episodes were observed.

Witek *et al.* [53] exposed fifteen asthmatic subjects to 0ppm and 2ppm of formaldehyde. Again levels of sensory irritation were similar to expected levels for healthy subjects. Several other studies have shown similar results and it has been concluded that if there is any relationship [54] [52] [55] between formaldehyde and asthmatic reactions, it is weak.

The question of whether formaldehyde has carcinogenic properties has received significant debate. Hauptmann *et al.* [40] identified a link with nasopharyngeal cancer. This finding has been criticized by Marsh and Youk [56] and by Marsh et al. [57], questioning the re-analysis, the cancer risk model and the isolation of other factors such as exposure to sulfuric acid mists, mineral acid, metal dusts. At the time of writing a consensus has not yet been reached

In animals, acute exposure to formaldehyde gas has been shown to cause severe breathing difficulties, cramps, vomiting and death [58] [59] [60]. Ivanoff found an LC50 (lethal concentration for 50% of subjects) of 81ppm for rats with no exposure duration reported [61]. The National Institute of Occupation Safety and Health found an LC50 of 664ppm for cats exposed for 8hrs [62].

Such concentrations are much higher than have been observed in homes, offices or factories. In addition, other symptoms such as sensory irritation will begin at much lower concentrations which will give a warning of the presence of the gas. It is thought unlikely that humans would be exposed to concentrations high enough to risk death. For the purposes of this project, systems were intended to detect formaldehyde below the level of observable symptoms.

2.2. Methods of gas detection

Gas detection is used in a wide range of areas such as mining, industrial chemical processing, environmental atmospheric studies, oil rigs, fire fighting and many more [63] [64] [65] [66]. It is frequently used to identify specific chemicals that may pose a health risk, such as toxic or explosive gases. Gas detection can also be used to alert operators to the absence of oxygen, for example in confined space entry [67]. There are many gases besides formaldehyde for which detection is desirable. This Section reviews some of the gas detection methods that are currently in use.

Some of the most common methods of gas detection are described here. They are ionisation, semiconductor, electrochemical, gravimetric, gas chromatography and finally optical [68] [66]. Table 2.3 below is a summary of gas detection methods. This is not an exhaustive list. Formaldehyde can be detected by single use detection strips [69] which were not included as this project focused on systems and methods that can be re-used. There are also other, less common types such as Inscentinel detectors which use trained bees to identify target gases, although bees need regular re-training which adds significant cost [70].

Table 2.3: Summary of common gas detection methods

Method	Subtypes	Advantages	Disadvantages	Formaldehyde Detection?
Ionisation [1] [71] [10]	Mobility spectrometers, photoionisation detectors	Good sensitivity	Poor selectivity	No
Semiconductor [8] [72] [73]	Biochemical detectors	Low cost	Poor selectivity, requires high temperature	Yes
Electrochemical [74]	Voltage mode, current mode, solid state	Low cost, good sensitivity	Does not work for all gases, limited lifetime	Yes
Gravimetric [75]	Acoustic wave detectors, microcantilever detectors	Good sensitivity	Poor selectivity	No
Gas chromato-graphy [76]	Micro gas chromatography	Very accurate and reliable	Long response time, very expensive and complex	Yes
Optical absorption spectroscopy [75] [77] [78] [79] [80]	UV spectroscopy, TDLS, cavity ringdown spectroscopy, photo-acoustic spectroscopy, etc.	Good sensitivity and selectivity	Can be expensive and complex (less than gas chromatography)	Yes
Tuneable diode laser spectroscopy [80] [77] [81]	TDLS with quantum cascade lasers	Good sensitivity and selectivity	Complex to build and operate	Yes
Photoacoustic spectroscopy [75]	-	Good sensitivity and selectivity	Susceptible to background noise	Yes
Cavity ringdown spectroscopy [17]	-	Good sensitivity, independent of source fluctuation	Complex to build and align	Yes
Differential optical absorption spectroscopy [82] [83]	UV DOAS	Good sensitivity and selectivity	Complex construction and post processing	Yes
Fluorescence [8]	Time resolved UV fluorescence	Very good selectivity if time resolved	Complex, needs pulses shorter than a few nanoseconds	Yes
Non-dispersive infra-red [84] [85] [86] [87]	IR LED, IR filament bulb	Low cost, simple to operate	Only works in the IR	No

2.2.1. Ionisation detectors

There are two main types of ionisation detectors, ion mobility spectrometers (IMS) [1] [71] and photoionisation detectors (PID) [10]. In IMS the gas sample is ionised and is then moved down a drift tube by an applied electric field. A carrier buffer gas opposes this motion and gases in the sample can be identified by their transit times in the manner of a chromatograph.

In PID the sample is exposed to light (usually UV [68]) with energy higher than the ionisation potential of the target gas but lower than that of the main components of air (such as N_2 and O_2). Both types of ionisation detector can be reasonably sensitive (25 ppb reported by Cross *et al.* (1997) [1]) but both also suffer from a lack of selectivity. No examples of this method being used for formaldehyde were found in the literature.

2.2.2. Semiconductor detectors

The internal resistance of a semiconductor detector is altered by the presence of the target gas. Concentrations can be measured by the change in current or voltage [73] [72]. The disadvantage of this method is that it is poor at distinguishing between different potential target gases and so requires a carefully chosen chemically-selective material. Some types suffer from low sensitivity [8] and others from slow response (~35 minutes) [68]. Semiconductor devices can require high temperatures for optimal performance [73] [72]. The main advantage of semiconductor detectors is that they can be made small and very cheaply due to their simple construction.

Formaldehyde detection with a semiconductor sensor was demonstrated by Dirkson *et al*. (2001) [73] and by Lee *et al*. (2007) [72]. Both groups used thin films of NiO, the conductivity of which was changed by the presence of formaldehyde gas. Neither group reported sensitivity better than 1ppm and both showed cross-sensitivity with acetone and methanol. Furthermore the devices displayed optimal performance only at 600ºC, adding additional complexity and power consumption to the design.

2.2.3. Electrochemical detectors

In electrochemical detection the target gas passes through a porous membrane and then undergoes reaction with an electrode in the manner of a battery [74]. The current or voltage generated by this reaction can then be used to detect the gas. These detectors can be made small and cheaply and have shown sensitivity as low as a few parts per billion [74]. However some target gases have non-electroactive functional groups and so cannot in principle be detected by this method.

One electrochemical formaldehyde detector has been produced (PPM Technologies Formaldemeter) [88] although no scientific publications were found on the subject. At low concentrations (roughly around 1ppm or less) it has a response time of one minute. A limit of detection is not quoted by the manufacturers. Information on selectivity was also not given.

2.2.4. Gravimetric detectors

There are two main types of gravimetric detectors: acoustic wave detectors [75] and microcantilever detectors [68]. Both types can be made small, cheaply and with reasonable sensitivity. However, the selectivity of both types is highly dependent on the sensing layer used, making the choice of sensing layer very important. Microcantilever detectors have the additional advantage of being able to function in vacuum or in liquid as well as in gas, although they have a lower range of detectable target gases. No examples of either method being used for formaldehyde were found in the literature.

2.2.5. Gas chromatography

A common method of detecting formaldehyde is gas chromatography [89] [90] [76] [91]. A gas sample is mixed with a carrier gas such as helium or nitrogen. This is then passed through a long cylindrical column filled with a solid or high-boiling-point liquid. Gases migrate through the column in approximate order of volatility and are detected at the far end (frequently using a flame ionisation detector). Components can be identified by their

retention time (time taken to pass through the column) but it is sometimes necessary to use a mass spectrometer for confirmation.

Gas chromatographs can be very accurate and reliable, particularly when combined with a mass spectrometer [76]. The limit of detection for formaldehyde has been reported as low as 136ppb [92]. However it can take time (a few minutes to several hours) for samples to pass through the column [76] [91]. Furthermore, the method can only operate when a sample of the target gas is injected into the device and the device itself is kept sealed. This is a problem for taking continuous, real-time gas measurements and could allow time for gases in a sample to decay or react before being detected.

2.2.6. Optical detectors

There is currently a wide variety of optical gas detection methods, including spectrometry, chemiluminescence, colorimetric and fluorescence [93] [94] [95] [96]. Optical detectors often demonstrate excellent selectivity and may be able to measure the concentration of multiple target gases with a single reading. They are often able to sense gases remotely, detecting them along an optical path rather than requiring direct detection of gases within a sample. Extra attention is given to optical methods here as they are particularly relevant to this project.

Spectroscopy has proved to be an effective method for detecting formaldehyde [78]. Many of these types have been used for formaldehyde detection including tuneable diode laser spectroscopy (TDLS), photoacoustic spectroscopy (PAS), cavity ringdown spectroscopy (CRDS) differential optical absorption spectroscopy (DOAS) and non-dispersive infrared (NDIR) Many chemical species have their own region of spectral absorption. Formaldehyde has an absorption region in the UV between 250nm and 360nm [79]. The fundamental principles of spectroscopy are described in more detail in Chapter 3.

2.2.7. Tuneable diode laser spectroscopy

In TDLS, a tuneable diode laser is used as a light source and its wavelength is tuned to scan across the absorption spectrum of the target gas. TDLS is extremely sensitive; Rehle *et al.* (2001) [80] reported formaldehyde detection at 0.32ppb using a 353nm laser, where formaldehyde has a significant peak [78] [79]. Richter *et al.* [97] achieved an even greater sensitivity of 74ppt at 3.5μm but at a decreased response time (once per minute rather than once every few seconds). TDLS systems demonstrate good sensitivity and signal–to-noise ratio, but are expensive and complex to manufacture.

Formaldehyde detectors using quantum cascade lasers have been demonstrated by Horstjann *et al.* using 3.53μm [77] and by Elia *et al.* using 5.621μm [81] in TDLS detection. Both groups report good sensitivity (30ppb and 600ppb respectively) and good selectivity, although it seems that the devices used would still be complex to build.

2.2.8. Photoacoustic spectroscopy

PAS relies on the photo-acoustic effect whereby sound is produced by the transfer of mechanical energy to a sample by a modulated light beam. When a sample of gas is used, the amount of energy transferred is proportional to the absorption coefficient of the sample. It is therefore possible to determine the light energy absorbed at a given wavelength by measuring the amplitude of sound produced, allowing the absorption spectrum of the sample to be found if the source can be tuned across it.

PAS has been shown to give reasonable sensitivity and response time (detection of formaldehyde at 3ppb at one measurement per three minutes being shown by Angelmahr *et al.* [75]) but is quite susceptible to background acoustic noise. This makes it less suitable for uncontrolled environments such as an unknown building.

2.2.9. Cavity ringdown spectroscopy

In CRDS the light source is used to illuminate an optical cavity containing a sample of the gas. The rate at which intensity decays after the source has been switched off allows the rate of absorption of the gas to be found. For small concentrations, the decay time $\tau_{ring\text{-}down}$, also known as the ring-down time [78], is given by:

$$\tau_{ring-down}(\lambda) = \frac{d}{c(1-R+\sigma(\lambda)Nd)} \quad (2.1)$$

where d is the equivalent path length, c is the speed of light, R is the reflectivity of the mirrors, $\sigma(\lambda)$ is the absorption cross-section at wavelength λ and N is the molecular number density.

Provided that the properties of the optical cavity are known, the absorbance of the sample can be calculated. An advantage of CRDS is that it is not affected by fluctuations in light source intensity as it is the decay rate that is measured. Meller *et al.* [17] reports a sensitivity of 150ppb for formaldehyde.

2.2.10. Differential optical absorption spectroscopy

DOAS uses high resolution spectrometers and differential post-measurement analysis to identify narrow band features in absorption spectra. It is frequently used for atmospheric pollution measurements and for trace gas identification [98] [99]. Stutz and Platt [100] have published algorithms required to separate measurements of concentrations of ozone, nitrogen dioxide, sulfur dioxide and formaldehyde in the atmosphere. High resolution spectral measurements are required.

Hausmann [82] has estimated the level of error when using UV DOAS techniques to measure concentrations of OH, SO_2, $C_{10}H_8$, and formaldehyde in the atmosphere, in the presence of instrumental noise. Both papers reveal the high degree of complexity in spectral post-processing required to separate these species at trace atmospheric levels using their UV absorption spectra.

Dooly *et al.* [83] have shown the corrections required to measure NO concentrations in the presence of other vehicle exhaust gases, in particular including UV-absorbing species NO_2 and SO_2. A high resolution (0.7nm) spectrometer was used for this work. Absorbances at a wavelength of 227nm had to be corrected by measurements made at 287nm and 413nm to account for the presence of two additional absorbing species. Use of narrow spectral bins simplified the analysis required by limiting the range of potential interferents at each wavelength. Nevertheless, some cross-response to the interfering species remained.

2.2.11. Fluorescence detectors

Fluorescence detection is a form of optical detection where light absorbed by a specific chemical is re-emitted and can be detected. Kudo *et al.* (2010) [8] demonstrated a formaldehyde detector using the fluorescence of nicotinamide adenine dinucleotide. This is a product of the formaldehyde dehydrogenase reaction which takes place when formaldehyde is present in the device. This method has good sensitivity, detecting formaldehyde at 2.5ppb [8]. It shows very good selectivity from acetaldehyde (fluorescent intensity only 1.3% of formaldehyde signal), and no cross-sensitivity with acetone, benzene, methanol and ethanol. However the paper does not quote a response time.

2.2.12. NDIR

Non-dispersive infra-red (NDIR) gas detection is a method based on low-resolution absorption spectroscopy. It is used in a wide range of applications such as ventilation control, industrial safety and process control and even in monitoring of fruit ripening. It is one of the few methods capable of detecting carbon dioxide at the ppm level.

NDIR generally uses the 'fingerprint region', a region of the IR spectrum below about 1,500cm^{-1} wavenumbers (~6.7µm) [101] in which many species of gas have unique absorption patterns. While formaldehyde does absorb in the fingerprint region but overlaps with a several very common gases such as water and carbon dioxide. It is therefore difficult to detect formaldehyde using NDIR.

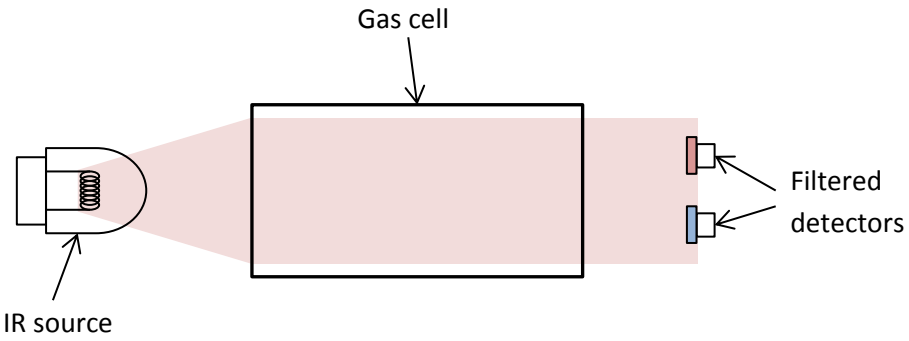

Figure 2.3: Diagram of a typical NDIR system. Light from the IR source passes through the gas cell, to be partly absorbed. Filtered detectors provide detection and reference channels.

Figure 2.3 is a diagram of a typical NDIR setup. It fundamentally consists of an IR light source, a gas cell or volume containing the sample, and several filtered detectors. Light from the IR source passes through the sample where part of it is absorbed. The absorption of light passing through a sample is determined by the Beer-Lambert law, shown in Equation (2.2) [102]. This is described in more detail in Chapter 3, as are the other principles of absorption spectroscopy.

$$\frac{I(\lambda)}{I_0(\lambda)} = e^{-\sigma(\lambda) l N} \tag{2.2}$$

where I is the final intensity of light transmitted through a sample at wavelength λ, I_0 is the initial intensity at that wavelength, σ is the absorption cross-section per molecule of absorbing gas at that wavelength, l is the light path length through the sample and N is the number density of absorbing gas molecules. The absorption cross-section is determined by the gas in question and is characteristic of each species.

The filters on the detectors limit the light that reaches them so they only respond to light within a specific wavelength. One filter is used as a reference channel, and one more is used for each gas being detected. Some systems use an LED as a relatively narrow-band source instead of a broad band source and a filter [103] [84]. These may use pre-determined intensities as references [84], although this precludes real-time control of variations.

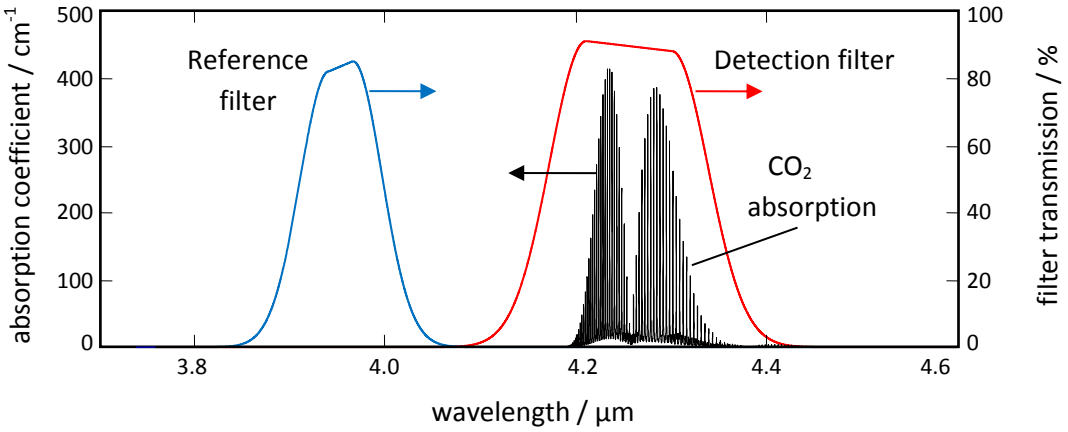

Figure 2.4: Graph of NDIR spectra taken from Hodgkinson *et al.* [85]. The carbon dioxide absorption spectrum (100% vol, 1 atm) was re-calculated from the HITRAN database [104]. The spectra of a detection filter and a reference filter were also included, approximated from data from [105]). The arrows indicate the relevant axis for each data set.

Figure 2.4 is a graph of NDIR spectra taken from Hodgkinson *et al.* [85]. It shows the IR absorption spectrum of carbon dioxide, re-plotted from data taken by the HITRAN database [104]. It also shows the transmission spectra of a detection filter and a reference filter [105]. The detection filter covers the region where formaldehyde absorbs and so intensity will be decreasing when it is present according to Equation (2.2). The reference channel covers a region with little or no absorption from carbon dioxide and is used to control for fluctuations in source intensity or other variations.

In order to build an NDIR system, it is necessary to find spectral regions for the detection channel and the reference channel that are both within the range of the IR source. It is also desirable that no other gases should absorb in either region, or interference will occur. Spectroscopic interference is described in more detail in Chapter 3 and Chapter 4.

Aleksandrov *et al.* [84] tested a prototype NDIR carbon dioxide detector. It used an IR LED (LED42Sc) with a central emission wavelength at 20ºC of 4.11µm and a photodiode (PD42Sc) with a maximum emission wavelength of 4.08µm. A limit of detection of 10ppm was found, with the main source of error being temperature dependence of the LED and photodiode. It was not clear if this system used a separate reference channel or a pre-measured reference value.

Hodgkinson *et al.* [85] designed an NDIR carbon dioxide detector to fit in a small volume (20mm diameter × 16.5mm height). It used a broad-band IR filament bulb as a source, modulated with a 2.25Hz square wave. It used two detectors, one for detection with a 4.2µm filter, and one for reference with a 3.95µm filter. A noise equivalent absorption (NEA) of 3×10^{-5}AU, effected by detector noise and by thermal effects. This gave a carbon dioxide limit of detection of 1ppm.

Fonollosa *et al.* [86] built and characterised an NDIR ethylene detector for monitoring fruit ripening in store-houses. The system used a four channel detector used for reference, for ethylene detection and for rejection of potential interference such as ammonia and ethanol. It used a thermal IR emitter and a multi-pass white cell (1.6m path length). Optical filters were used with the four detector channels with central wavelengths of 3.4µm (ethanol), 9.7µm for ammonia, 3.9µm for the reference band and 10.6µm for ethylene. It had a limit of detection of 30ppm for ethylene and 160ppm for ammonia.

Lou *et al.* [87] demonstrated an NDIR like system using UV absorption to detect sulphur dioxide. It used a 300nm UV LED (UVTOP300) as a light source. Light, modulated by a chopper fan, passes through a gas sample. A beam splitter devides light into an unfiltered detection channel and a reference channel with a second gas cell. The second gas cell contains about 10^4ppm of sulphur dioxide, making it largely opaque at the main absorption peaks and essentially acting as a filter.

A sulphur dioxide sensitivity of 0.4ppm was reported, which is very low for an NDIR type system. It would be more difficult to achieve a similar level for formaldehyde which has peak UV absorption cross-section of around 10^{-19}cm^2/molecule [17], while sulphur dioxide has around 10^{-18}cm^2/molecule [106]. Lou *et al.* states that the 300nm region is largely free from interference from other gases. Formaldehyde [17], acetaldehyde [107], nitrogen dioxide [108], hexanal [109] and ozone [110] do all have absorption in the region.

The method is non-dispersive as it uses filters to limit the band of each filter, rather than dispersive optical gratings as in a conventional spectrometer. A key advantage of NDIR is that it uses few, simple components in comparison to conventional spectrometers. They can also be built relatively small (20mm diameter × 16.5mm height, Hodgkinson *et al.* [85]). They give only single measurements for each of their channels so channel positions have to be

specifically tailored to a given gas. NDIR achieves many of the aims of this project and a similar approach in the UV was considered promising.

2.2.13. Suitability for this project

This project aimed to design a simple, sensitive and selective formaldehyde detector for indoor air. **Table 2.4** shows a summary of the gas detection methods discussed in this chapter, with reference to their suitability to this project. UV spectroscopy was selected as it had good selectivity and sensitivity like most optical detection methods, but had the potential for a more simple design, specific to formaldehyde.

Table 2.4: Summary of gas detection methods and their suitability to this project

Method	Benefits	Problems	Suitable?
Ionisation	N/A	Does not detect formaldehyde	No
Semiconductor	Low purchase cost	Requires 600°C, high power consumption and running cost	No
Electrochemical	Low cost, good sensitivity	Difficulty detecting formaldehyde, limited selectivity, limited lifetime.	No
Gravimetric	N/A	Does not detect formaldehyde	No
Gas chromatography	Very accurate and reliable	Long response time, very expensive and complex	No
Tuneable diode laser spectroscopy	Good sensitivity and selectivity	Complex to build and operate	No
Photoacoustic spectroscopy	Good sensitivity and selectivity	3 minute response time, susceptible to background noise	No
Cavity ringdown spectroscopy	Good sensitivity, independent of source fluctuation	Complex to build and align	No
Differential optical absorption spectroscopy	Good sensitivity and selectivity	Complex construction and post processing	No
Fluorescence	Very good selectivity if time resolved	Complex, needs pulses shorter than a few nanoseconds	No
Non-dispersive infra-red	Low cost, simple to operate	Only works in the IR	No
UV spectroscopy	Potential for good sensitivity, selectivity and simple design	None	Yes

2.3. Chapter summary

This chapter covered a representative selection of the background literature used in this project and was important to understanding the context of the work. This included several literature reviews into areas of particular relevance. The main areas covered were details of formaldehyde gas and details of current gas detection methods.

Formaldehyde, CH_2O, is the first member of the aldehyde chemical family. It is a colourless gas at room temperature, boiling at -21°C and melting at -92°C. Formaldehyde has a spectroscopic absorption region in the UV between 240 – 360nm which includes a number of high absorption peaks in between regions of very low absorption.

Formaldehyde is hazardous to health in humans and animals. Unpleasant odours and irritation of the nose, eyes and throat have been observed in humans at around 2ppm. At higher concentrations of 10 – 20ppm symptoms such as intense eye watering, severe irritation and decreased pulmonary function have been seen. Acute exposure in animals found an LC50 of 81ppm for rats and 664ppm for cats. Several studies have investigated a potential link between formaldehyde and asthma, finding no strong correlation. The potential carcinogenic properties of formaldehyde are still under debate.

A literature review was carried out into the formaldehyde concentrations measured in various buildings from around the world. Buildings studied included offices, residences, schools, mobile homes, hotels, laboratories and even submarines. It was found that while dangerous levels of formaldehyde were uncommon, concentration could vary significantly, even between similar buildings. This emphasises the requirement for readily available formaldehyde detection.

Semiconductor formaldehyde detectors using NiO films have been demonstrated. Sensitivity was found to be around 1ppm and cross-sensitivity with acetone and methanol was an issue. Semiconductor gas detectors also require high temperatures, 600ºC in this case. One electrochemical formaldehyde detection system has been produced, although a limit of detection was not quoted. At low concentrations it has a response time of around two minutes.

Gas chromatography is a common method for detecting formaldehyde, and can be very accurate and reliable. However measurements can take several hours and trained operators are required. Equipment is often both bulky and expensive.

Optical methods cover a wide range of detection methods including TDLS, PAS, CRDS, DOAS and fluorescence detection. Optical detection methods can be extremely accurate, one PAS study reporting a formaldehyde limit of detection of 3ppb. However they frequently require many complex components, often needing high resolution spectrometers.

The principle aim of this project was to design and test a formaldehyde gas detector for use in indoor air. The project limit of detection of detection target was 0.1ppm. This was lower than the majority of concentrations reported to affect humans, and significantly lower than concentrations reported to cause severe health issues.

While formaldehyde concentrations can be measured accurately and reliably, there are not many methods that will do so simply or quickly. Formaldehyde detection methods tend to require expensive equipment and/or trained operators to interpret results. This project aimed to use non-dispersive UV detection to develop a simple and reliable detection system based on few components. The theory of spectroscopy and the underlying principles the method are described in the next chapter.

2.4. References

[1] J. H. Cross, T. F. Limero, J. L. Lane and F. Wang, "Determination of ammonia in ethylene using ion mobility spectrometry," *Talanta,* vol. 45, pp. 19-23, 1997.

[2] Y. Lu, J. Liu, B. Lu, A. Jiang and C. Wan, "Study on the removal of indoor VOCs using microtechnology," *Jounal of Hazardous Materials,* vol. 182, pp. 204-209, 2010.

[3] S. Kim, "Control of formaldehyde and TVOC emission from wood-based flooring composites at various manufacturing processes by surface finishing," *Journal of Hazardous Materials,* vol. 176, pp. 14-19, 2010.

[4] G. D. Nielsen and P. Wolkoff, "Cancer effects of formaldehyde: a proposal for an indoor air guideline value," *Archives of Toxicology,* vol. 84, pp. 423-446, 2010.

[5] C. Persoz, S. Achard, C. Leleu, I. Momas and N. Seta, "An in vitro model to evaluate the inflammatory response after gaseous formaldehyde exposure of lung epithelial cells," *Toxicology Letters,* vol. 195, pp. 99-105, 2010.

[6] E. A. Schuck, E. R. Stephens and J. T. Middleton, "Eye irritation response at low concentrations," *Archives of Environmental Health,* vol. 13, pp. 570-575, 1966.

[7] J. R. Bender, L. S. Mullin, G. J. Graepel and W. E. Wilson, "Eye irritation response of humans to formaldehyde," *American Industrial Hygiene Association Journal,* vol. 44, p. 463–465, 1983.

[8] H. Kudo, Y. Suzuki, T. Gessei, D. Takahashi, T. Arakawa and K. Mitsubayashi, "Biochemical gas sensor (bio-sniffer) for ultrahigh-sensitive gaseous formaldehyde monitoring," *Biosensors and Bioelectonics,* vol. 26, pp. 854-858, 2010.

[9] T. Jiang, D. J. Gardner and M. G. D. Baumann, "Volatile organic compound emissions arising from the hot-pressing of mixed-hardwood particleboard," *Forest Products Journal,* vol. 52, pp. 66-67, 2002.

[10] P. G. Sim, C. M. Elson and M. A. Quilliam, "Use of the photoionisation detector in packed-column supercritical fluid chromatography," *Journal of Chromatography,* vol. 445, pp. 239-243, 1988.

[11] C. J. Weschler, M. Brauer and P. Koutrakis, "Indoor ozone and nitrogen dioxide: a potential pathway to the generation of nitrate radicals, dinitrogen pentaoxide, and nitric acid indoors," *Environmental Science and Technology,* vol. 26, pp. 179-184, 1992.

[12] J. C. S. Chang, R. Fortmann, N. Roache and H. C. Lao, "Evaluation of low-VOC latex paints," *Indoor Air-International Journal of Indoor Air Quality and Climate,* vol. 9, pp. 253-258, 1999.

[13] M. Nicolas, O. Ramalho and F. Maupetit, "Reactions between ozone and building products: Impact on primary and secondary emissions," *Atmospheric Environment,* vol. 41, pp. 3129-3138, 2007.

[14] B. Moser, F. Bodrogi, G. Eibl, M. Lechner, J. Rieder and P. Lirk, "Mass spectrometric profile of exhaled breath—field study by PTR-MS," *Respiratory Physiology & Neurobiology,* vol. 145, pp. 295-300, 2005.

[15] T. W. Zinn, D. Cline and W. F. Lehmann, "Long-term study of formaldehyde emission decay from particleboard," *Forest Products Journal,* vol. 40, pp. 15-18, 1990.

[16] D. R. Lide, Handbook of Chemistry and Physics, 82nd Edition, Boca Raton: CRC Press, 2001-2002.

[17] R. Meller and G. K. Moortgat, "Temperature dependence of the absorption cross sections of formaldehyde between 223 and 323 K in the wavelength range 225-375 nm," *Journal of Geophysical Research-Atmospheres,* vol. 105, pp. 7089-7101, 2000.

[18] T. Salthammer, F. Fuhrmann, S. Kaufhold, B. Meyer and A. Schwarz, "Effects of climatic parameters on formaldehyde concentrations in indoor air," *Indoor Air - International Journal of Indoor Air Quality and Climate,* vol. 5, no. 2, pp. 120-128, 1995.

[19] W. Bischof, M. Bullinger-Naber, B. Kruppa, B. H. Müller and R. Schwab, Expositionen und gesundheitliche beeinträchtigungen in bürogebäuden - Ergebnisse des ProKlimA - projektes, Stuttgart: Fraunhofer IRB Verlag, 2003.

[20] H. Salonen, A.-L. Pasanen, S. Lappalainen, H. Riuttala, T. Tuomi, P. Pasanen, B. Back and K. Reijula, "Volatile organic compounds and formaldehyde as explaining factors for sensory irritation in office environments," *Journal of Occupational And Environmental Hygiene,* vol. 6, no. 4, pp. 239-47, 2009.

[21] G. Smedje and D. Norback, "Irritants and allergens at school in relation to furnishings and cleaning," *Indoor Air - International Journal of Indoor Air Quality and Climate,* vol. 11, no. 2, pp. 127-133, 2001.

[22] M. Posniak, I. Makhniashvili and E. Koziel, "Volatile organic compounds in the indoor air of warsaw office buildings," *Indoor and Built Enviroment,* vol. 14, no. 3-4, pp. 269-275, 2005.

[23] K. Sexton, M. X. Petreas and K. S. Liu, "Formaldehyde exposures inside mobile homes," *Environmental Science & Technology,* vol. 23, no. 8, pp. 985-988, 1989.

[24] K. S. Liu, F. Y. Huang, S. B. Hayward, J. Wesolowski and K. Sexton, "Irritant effects of formaldehyde exposure in mobile homes," *Environmental Health Perspectives,* vol. 94, pp. 91-94, 1991.

[25] W. Liu, J. Zhang, L. Zhang, B. J. Turpin, C. P. Welsel, M. T. Morandi, T. H. Stock, S. Colome and L. R. Korn, "Estimating contributions of indoor and outdoor sources to indoor carbonyl concentrations in three urban areas of the United States," *Atmospheric Environment,* vol. 40, no. 12, pp. 2202-2214, 2006.

[26] W. Liu, J. J. Zhang, L. R. Korn, L. Zhang, C. P. Weisel, B. Turpin, M. Morandi, T. Stock and S. Colome, "Predicting personal exposure to airborne carbonyls using residential measurements and time/activity data," *Atmospheric Environment,* vol. 41, no. 25, pp. 5280-5288, 2007.

[27] N. L. Gilbert, M. Guay, D. Gauvin, R. N. Dietz, C. C. Chan and B. Levesque, "Air change rate and concentration of formaldehyde in residential indoor air," *Atmospheric*

Environment, vol. 42, no. 10, pp. 2424-2428, 2008.

[28] W. Yang, J. Sohn, J. Kim, B. Son and J. Park, "Indoor air quality investigation according to age of the school buildings in Korea," *Journal of Environmental Management,* vol. 90, no. 1, pp. 348-354, 2009.

[29] K. Sakai, D. Norback, Y. Mi, E. Shibata, M. Kamijima, T. Yamada and Y. Takeuchi, "A comparison of indoor air pollutants in Japan and Sweden: formaldehyde, nitrogen dioxide, and chlorinated volatile organic compounds," *Environmental Research,* vol. 94, no. 1, pp. 75-85, 2004.

[30] L. T. Wong, K. W. Mui and P. S. Hui, "A statistical model for characterizing common air pollutants in air-conditioned offices," *Atmospheric Environment,* vol. 40, no. 23, pp. 4246-4257, 2006.

[31] Y. Feng, S. Wen, X. Wang, G. Sheng, Q. He, J. Tang and J. Fu, "Indoor and outdoor carbonyl compounds in the hotel ballrooms in Guangzhou, China," *Atmospheric Environment,* vol. 38, no. 1, pp. 103-112, 2004.

[32] M. I. Khoder, A. A. Shakour, S. A. Farag and A. A. Abdel Hameed, "Indoor and outdoor formaldehyde concentrations in homes in residential areas in Greater Cairo," *Journal of Environmental Monitoring,* vol. 2, no. 2, pp. 123-126, 2000.

[33] P. Dingle and P. Franklin, "Formaldehyde levels and the factors affecting these levels in homes in Perth, Western Australia," *Indoor and Built Environment,* vol. 11, no. 2, pp. 111-116, 2002.

[34] R. M. Cavalcante, C. S. Campelo, M. J. Barbosa, E. R. Silveira, T. V. Carvalho and R. F. Nascimento, "Determination of carbonyl compounds in air and cancer risk assessment in an academic institute in Fortaleza, Brazil," *Atmospheric Environment,* vol. 40, no. 29, pp. 5701-5711, 2006.

[35] O. Persson, C. Oestberg, J. Pagels and A. Sebastian, "Air contaminants in a submarine equipped with air independent propulsion," *Journal of Environmental Monitoring,* vol. 8, no. 11, pp. 1111-1121, 2006.

[36] D. Paustenbach, Y. Alarie, T. Kulle, N. Schachter, R. Smith, J. Swenberg, H. Witschi and S. B. Horowitz, "A recommended occupational exposure limit for formaldehyde based on irritation," *Journal of Toxicology and Environmental Health,* vol. 50, no. 3, pp. 217-263, 1997.

[37] I. Andersen and L. Molhave, Controlled human studies with formaldehyde. In Formaldehyde toxicity, Washington, DC: Hemisphere, 1983.

[38] I. N. Ritchie and R. G. Lehnen, "Formaldehyde-related health complaints of residents

living in mobile and conventional homes," *American Journal of Public Health,* vol. 77, p. 323–328, 1987.

[39] T. Malaka and A. M. Kodama, "Respitory health of plywood workers occupationally exposed to formaladehyde," *Archives of Environmental Health,* vol. 45, pp. 288-294, 1990.

[40] M. Hauptmann, J. H. Lubin, P. A. Stewart, R. B. Hayes and A. Blair, "Mortality from Solid Cancers among Workers in Formaldehyde Industries," *American Journal of Epidemiology,* vol. 159, no. 12, p. 1117–1130, 2004.

[41] A. Blair, R. Saracci, P. A. Stewart, R. B. Hayes and C. Shy, "Epidemiologic evidence on the relationship between formaldehyde exposure and cancer.," *Scandinavian Journal of Work, Environment & Health,* vol. 16, no. 6, pp. 381-393, 2013.

[42] J. K. McLaughlin, "Formaldehyde and cancer: a critical review," *International Archives of Occupational and Environmental Health,* vol. 66, pp. 295-301, 1994.

[43] E. P. Horvath, H. Anderson, W. E. Pierce, L. P. Hanrahan and J. O. Wendlick, "Effects of formaldehyde on the mucous membranes and lungs: a study of an industrial population," *Journal of the American Medical Association,* vol. 259, pp. 701-707, 1988.

[44] R. Alexandersson, B. Kolmodin-Hedman and G. and Hedenstierna, "Exposure to formaldehyde: Effects on pulmonary function.," *Archives of Environmental Health,* vol. 37, p. 279–284, 1982.

[45] J. J. Day, R. E. M. Less, R. H. Clark and P. L. Patter, "Respiratory response to formaldehyde and off-gas of urea formaldehyde foam insulation," *Canadian Medical Association Journal,* vol. 131, p. 1061–1065, 1984.

[46] E. N. Schachter, T. J. Witek, D. J. Brody, T. Tosun, G. J. Beck and B. P. Leaderer, "A study of respiratory effects from exposure to 2 ppm formaldehyde in healthy subjects," *Archives of Environmental Health,* vol. 41, p. 229–234, 1986.

[47] T. J. Kulle, L. R. Sauder, J. R. Hebel, D. J. Green and M. D. Chatham, "Formaldehyde dose-response in healthy nonsmokers," *The International Journal of Air Pollution Control and Hazardous Waste Management,* vol. 37, no. 8, p. 919–924, 1987.

[48] P. C. Conlon and A. M. Mason, Emergency action guide for formaldehyde solution, Washington DC, USA: Association of Americal Railroads, 1984.

[49] N. Zurlo, "Formaldehyde and derivatives," in *Encyclopedia of occupational health and safety,* Geneva, Switzerland, International Labor Office, 1983, pp. 914-916.

[50] J. F. Gamble, A. J. McMichael, T. Williams and M. Battigelli, "Respiratory function and formaldehdye type resine," *American Industrial Hygiene Association Journal,* vol. 37, pp. 499-513, 1976.

[51] R. Alexandersson and G. Hedenstierna, "Pulmonary function in wood workers exposed to formaldehyde: A proposed study," *Archive of Environmental Health,* vol. 44, pp. 5-11, 1989.

[52] D. J. Green, L. R. Sauder, T. J. Kulle and R. Bascom, "Acute response to 3.0 ppm formaldehyde in exercising healthy nonsmokers and asthmatics," *The American Review of Respiratory Disease,* vol. 135, p. 1261–1266, 1987.

[53] T. J. Witek, E. N. Schachter, T. Tosun, G. J. Beck and B. P. Leaderer, "An evaluation of respiratory effects following exposure to 2.0 ppm formaldehyde in asthmatics: Lung function, symptoms, and airway reactivity," *Archives of Environmental Health,* vol. 42, p. 230–237, 1987.

[54] L. R. Sauder, D. J. Green, M. D. Chatham and J. T. Kulle, "Acute pulmonary response of asthmatics to 3.0 ppm formaldehyde.," *Toxicology and Industrial Health,* vol. 3, p. 569–578, 1987.

[55] D. Sheppard, W. L. Eschenbacher and J. Epstein, "Lack of bronchomotor response to up to 3 ppm formaldehyde in subjects with asthma," *Environmental Research,* vol. 35, p. 133–139, 1984.

[56] G. M. Marsh and A. O. Youk, "Reevaluation of mortality risks from nasopharyngeal cancer in the formaldehyde cohort study of the National Cancer Institute," *Regulatory Toxicology and Pharmacology,* vol. 42, no. 3, pp. 275-283, 2005.

[57] G. M. Marsh, A. O. Youk and P. Morfeld, "Mis-specified and non-robust mortality risk models for nasopharyngeal cancer in the National Cancer Institute formaldehyde worker cohort study," *Regulatory Toxicology and Pharmacology,* vol. 47, no. 1, pp. 59-67, 2007.

[58] K. C. Gupta, A. G. Ulsamer and P. W. Preuss, "Formaldehyde in indoor air: sources and toxicity," *Environmental International,* vol. 8, pp. 349-358, 1982.

[59] E. Skog, "A toxicological investigation of lower aliphatic aldehydes," *Acta Pharmacol,* vol. 6, p. 299, 1950.

[60] A. W. Horton, R. Type and K. L. Stemmer, "Experimental carcinogenesis of the lung, inhalation of gaseous formaldehyde or an aerosol of coal tar by C3H mice," *Journal of the National Cancer Institute,* vol. 30, pp. 31-43, 1963.

[61] N. Ivanoff, "On some aldehydes of practical importance (German)," *American*

Industrial Hygiene Association Journal, vol. 73, p. 307–319, 1911.

[62] National Institute of Occupational Safety and Health, Criteria for a recommended standard. Occupational exposure to formaldehyde, Washington DC, USA: Department of Health, Education, and Welfare, 1976.

[63] W. Armerding, M. Spiekermann, J. Walter and F. J. Comes, "Multipass optical absorption spectroscopy: a fast-scanning laser spectrometer for the in situ determination of atmospheric trace-gas components, in particular OH," *Applied Optics,* vol. 35, pp. 4206-4219, 1996.

[64] E. Hawe, C. Fitzpatrick, P. Chambers, G. Dooly and E. Lewis, "Hazardous gas detection using an integrating sphere as a multipass gas absorption cell," *Sensors and Actuators A,* vol. 141, pp. 414-421, 2008.

[65] M. Triki, P. Cermak, G. Mejean and D. Romanini, "Cavity-enhanced absorption spectroscopy with a red LED source for NOx trace analysis," *Applied Physics B,* vol. 91, pp. 195-201, 2008.

[66] J. Hodgkinson and R. P. Tatam, "Optical gas sensing: a review," *Measurement Science & Technology,* vol. 24, no. 1, p. 012004, 2013.

[67] U. Svedberg, J. Samuelsson and S. Melin, "Hazardous Off-Gassing of Carbon Monoxide and Oxygen Depletion during Ocean Transportation of Wood Pellets," *Annals of Occupational Hygiene,* vol. 52, pp. 259-266, 2008.

[68] G. Man, B. Stoeber and K. Walus, "An assessment of sensing technologies for the detection of clandestine methamphetamine drug laboratories," *Forensic Science International,* vol. 189, pp. 1-13, 2009.

[69] X. Q. Wang, Y. Si, X. Mao, Y. Li, J. Y. Yu, H. P. Wang and B. Ding, "Colorimetric sensor strips for formaldehyde assay utilizing fluoral-p decorated polyacrylonitrile nanofibrous membranes," *Analyst,* vol. 138, no. 17, pp. 5129-5136, 2013.

[70] Inscentinel, Rothamsted Research: Harpenden, AL5 2JQ, UK, www.inscentinel.com, 2011 .

[71] M. Utriainen, E. Karpanoja and H. Paakkanen, "Combining miniaturized ion mobility spectrometer and metal oxide gas sensor for the fast detection of toxic chemical vapors," *Sensors and Actuators,* vol. 93, pp. 17-24, 2003.

[72] C. Lee, C. Chiang, Y. Wang and R. Ma, "A self-heating gas sensor with integrated NiO thin-film for formaldehyde detection," *Sensors and Actuators B,* vol. 122, pp. 503-510, 2007.

[73] J. A. Dirksen, K. Duval and T. A. Ring, "NiO thin-film formaldehyse gas sensor," *Sensors and Actuators,* vol. 80, pp. 106-115, 2001.

[74] N. Nakano and S. Ogawa, "Preparation of thin gold-film electrode for an electrochemical gas sensor for phosphine and arsine," *Sensors and Actuators B,* vol. 21, pp. 51-55, 1994.

[75] M. Angelmahr, A. Miklos and P. Hess, "Photoacoustic spctroscopy of formaldehyde with tunable laser radiation at the parts per billion level," *Applied Physics B,* vol. 85, pp. 285-288, 2006.

[76] R. A. Trenholm, F. L. Rosario-Ortiz and S. A. Snyder, "Analysis of formaldehyde formation in wastewater using on-fiber derivatization– solid-phase microextraction–gas chromatography–mass spectrometry," *Journal of Chromatography,* vol. 1210, pp. 25-29, 2008.

[77] M. Horstjann, Y. A. Bakhirkin, A. A. Kosterev, R. F. Curl, F. K. Tittel, C. M. Wong, C. J. Hill and R. Q. Yang, "Formaldehyde sensor using interband cascade laser based quartz-enhanced photoacoustic spectroscopy," *Applied Physics B,* vol. 79, pp. 799-803, 2004.

[78] C. Wang and P. Sahay, "Breath analysis using laser spectroscopic techniques: breath biomarkers, spectral fingerprints, and detection limits," *Sensors,* vol. 9, pp. 8230-8262, 2009.

[79] L. Borland, M. Brickhouse, T. Thomas and A. W. Fountain, "Review of chemical signature databases," vol. 397, pp. 1019-1028, 2010.

[80] D. Rehle, D. Leleux, M. Erdelyi, F. Tittel, F. M. and S. Friedfeld, "Ambient formaldehyde detection with a laser spectrometer based on difference-frequency generation in PPLN," *Applied Physics B,* vol. 72, pp. 947-952, 2001.

[81] A. Elia, V. Spagnolo, C. Di Franco, P. M. Lugarà and G. Scamarcio, "Trace gas sensing using quantum cascade lasers and a fiber-coupled optoacoustic sensor: application to formaldehyde," *Journal of Physics: Conference Series,* vol. 214, no. 1, p. 012037, 2010.

[82] M. Hausmann, U. Brandenburger and T. Brauers, "Simple Monte Carlo methods to estimate the spectra evaluation error in differential-optical-," *Applied Optics,* vol. 38, no. 3, pp. 462-475, 1999.

[83] G. Dooly, C. Fitzpatrick and E. Lewis, "Deep UV based DOAS system for the monitoring of nitric oxide using ratiometric separation techniques," *Sensors and actuators B-chemical,* vol. 134, no. 1, pp. 317-323, 2008.

[84] S. E. Aleksandrov, G. A. Gavrilov, A. A. Kapralov, B. A. Matveev, G. Y. Sotnikova and M. A. Remennyi, "Simulation of Characteristics of Optical Gas Sensors Based on Diode Optopairs Operating in the Mid-IR Spectral Range," *Quantum Electronics,* vol. 79, no. 6, pp. 112-118, 2008.

[85] J. Hodgkinson, R. Smith, W. O. Hob, J. R. Saffell and R. P. Tatam, "Non-dispersive infra-red (NDIR) measurement of carbon dioxide at 4.2 mu m in a compact and optically efficient sensor," *Sensors and Actuators B: Chemical,* vol. 186, pp. 580-588, 2013.

[86] J. Fonollosa, B. Halford, L. Fonseca, J. Santander, S. Udina, M. Moreno, J. Hildenbrand, J. Wöllenstein and S. Marco, "Ethylene optical spectrometer for apple ripening monitoring in controlled atmosphere store-houses," *Sensors and Actuators B,* vol. 136, pp. 546-554, 2009.

[87] X. T. Lou, G. Somesfalean, Z. G. Zhang and S. Svanberg, "Sulfur dioxide measurements using an ultraviolet light-emitting diode in combination with gas correlation techniques," *Applied Physics B,* vol. 94, pp. 699-704, 2009.

[88] Monitor, PPM FormaldemeterTM htV 3 Parameter IAQ, *Operation Manual,* PPM Technology Ltd., Caernarfon, UK, 2008.

[89] H. Bagheri, M. Ghambarian, A. Salemi and A. Es-Haghi, "Trace determination of free formaldehyde in DTP and DT vaccines and diphtheria–tetanus antigen by single drop microextraction and gas chromatography–mass spectrometry," *Journal of Pharmaceutical and Biomedical Analysis,* vol. 50, p. 287–292, 2009.

[90] A. Takeuchi, T. Takigawa, M. Abe, T. Kawai, Y. Endo, T. Yasugi, G. Endo and K. Ogino, "Determination of formaldehyde in urine by headspace gas chromatography," *Bulletin of Environmental Contamination and Toxicology,* vol. 79, pp. 1-4, 2007.

[91] A. L. Rice, "Isotopic analysis of atmospheric formaldehyde by gas chromatography isotope ratio mass spectrometry," *Analytical Chemistry,* vol. 78, pp. 6320-6326, 2006.

[92] Š. V. Bolta, L. Zupančič-Kralj and J. Marsel, "Gas chromatographic determination of formaldehyde in air using solid-phase microextraction sampling," *Chromatographia,* vol. 48, no. 1-2, pp. 95-100, 1998.

[93] F. Evangelisti, A. Baroncelli, P. Bonasoni, G. Giovanelli and F. Ravegnani, "Differential optical absorption spectrometer for measurement of tropospheric pollutants," *Applied Optics,* vol. 34, no. 15, pp. 2732-2744, 1995.

[94] M. Belz, F. A. Klein and H. Habhegger, "UV LED fiber optic detection system for DNA and protein," *Proceedings of SPIE,* vol. 6433, pp. H4330-H4330, 2007.

[95] E. P. Kantzas and A. J. S. McGonigle, "Ground based ultraviolet remote sensing of volcanic gas plumes," *Sensors,* vol. 8, pp. 1559-1574, 2008.

[96] B. A. Patterson, J. P. Lenney, W. Sibbett, B. Hirst, N. K. Hedges and M. J. Padgett, "Detection of benzene and other gases with an open-path, static Fourier-transform UV spectrometer," *Applied Optics,* vol. 37, no. 15, pp. 3172-3175, 1998.

[97] D. Richter, A. Fried, B. P. Wert, J. G. Walega and F. K. Tittel, "Development of a tunable mid-IR difference frequency laser source for highly sensitive airborne trace gas detection," *Applied Physics B-Lasers and Optics,* vol. 75, pp. 281-288, 2002.

[98] U. S. J. Platt, Differential optical absorption spectroscopy : principles and applications, Berlin: Springer, Physics of Earth and Space Environments, 2008.

[99] M. W. Sigrist, Air Monitoring by Spectroscopic Techniques. Chemical Analysis, Hoboken: John Wiley & Sons, 1994.

[100] J. Stutz and U. Platt, "Numerical analysis and estimation of the statistical error of differential optical absorption spectroscopy measurements with least-squares methods," *Applied Optics,* vol. 35, no. 30, pp. 6041-6053, 1996.

[101] J. P. Maity, S. Kar, C. M. Lin, Y. C. Chen, Y. F. Cheng, J. S. Jean and T. R. Kulp, "Identification and discrimination of bacteria using Fourier transform infrared spectroscopy," *Spectrochimica Acta Part A: Molecular and Biomolecular Spectroscopy,* vol. 116, p. 478–484, 2013.

[102] L. Chomaz, L. Corman, T. Yefsah, D. Desbuquois and J. Dalibard, "Absorption imaging of a quasi-two-dimensional gas: a multiple scattering analysis," *New Journal of Physics,* vol. 14, p. 055001, 2012.

[103] J. G. Crowder, H. R. Hardaway and C. T. Elliott, "Mid-infrared gas detection using optically immersed, room-temperature, semiconductor devices," *Measurement Science and Technology,* vol. 13, pp. 882-884, 2002.

[104] L. S. Rothman et al., "The HITRAN 2008 molecular spectroscopic database," *Journal of Quantitative Spectroscopy & Radiative Transfer ,* vol. 110, no. 9-10, pp. 533-572, 2009.

[105] Infratec GmbH, Pyroelectric and Multispectral Detectors, *Product Brochure,* Infratec GmbH, Dresden, Germany, 2005.

[106] A. C. Vandaele, C. Hermans and S. Fally, "Fourier transform measurements of SO2 absorption cross sections: II. Temperature dependence in the 29000–44000/cm (227–345nm) region," *Journal of Quantitative Spectroscopy & Radiative Transfer,* vol. 110, 2009.

[107] W. Schneider and G. Moortgat, Personal communication to E. P. Röth, R. Ruhnke, G. Moortgat, R. Meller, and W. Schneider, Berichte des Forschungszentums Jülich, 3341, 1997.

[108] K. Bogumil, J. Orphal, T. Homann, S. Voigt, P. Spietz, O. C. Fleischmann, A. Vogel, M. Hartmann, H. Kromminga, H. Bovensmann, J. Frerick and J. P. Burrows, "Measurements of molecular absorption spectra with the SCIAMACHY pre-flight model: instrument characterization and reference data for atmospheric remote-sensing in the 230–2380 nm region," *Journal of Photochemistry and Photobiology A: Chemistry*, vol. 157, pp. 167-184, 2003.

[109] H. Plagens, R. Bröske, M. Spittler, L. Ruppert, I. Barnes and H. K. Becker, "Atmospheric loss processes of hexanal. Photolysis and reaction with OH and Cl radicals", Proceedings of the Second Workshop of the EUROTRAC-2 Subproject Chemical Mechanism Development: Karlsruhe, Germany, GPP10-1-GPP10-4, 1998.

[110] D. Daumont, J. Brion, J. Charbonnier and J. Malicet, "Ozone UV spectroscopy I: Absorption cross-section at room-temperature," *Journal of Atmospheric Chemistry*, vol. 15, pp. 145-155, 1992.

Chapter 3: Theory of spectroscopy

This chapter explains the theoretical background of the project. The fundamental principles of spectroscopic gas detection are explained, including many of the important equations. A detailed explanation is given of how the principles of spectroscopy were specifically applied to this project with hypothetical examples. An explanation of spectral line broadening effects is given, along with some information on how they apply to formaldehyde.

3.1. Theory of UV spectroscopy

The formaldehyde detection systems developed in this project were based on UV spectroscopy. This is one of many forms of spectroscopy, in which light passes through a sample and the absorption is used to identify or quantify it. The UV was a relatively un-explored region for spectroscopic applications and included some interesting formaldehyde features. Spectroscopy relies on the fact that atoms and molecules only absorb a photon when its energy matches a transition to a more exited state. The energy of a photon is dependent on its wavelength as expressed by [1]:

$$E = \frac{hc}{\lambda} \tag{3.1}$$

where E is the energy of the photon, h is the Planck constant, c is the free space speed of light and λ is the wavelength of the photon.

Photons with an energy that does not match a transition are not absorbed and, provided they are not scattered or otherwise impeded, pass through the sample. This results in a specific set of wavelengths which will be absorbed by a given atom or molecule, and so every species has a characteristic absorption spectrum.

The degree of absorption through a given sample is governed by the Beer-Lambert law shown in Equation (3.2) [2]. The Beer-Lambert law describes an exponential decrease in intensity as light of a specific wavelength passes through a sample. This law is essential to the understanding of absorption spectroscopy and gives one of the most important equations for this project:

$$\frac{I(\lambda)}{I_0(\lambda)} = e^{-\sigma(\lambda) l N} \tag{3.2}$$

where I is the final intensity of light transmitted through a sample at wavelength λ, I_0 is the initial intensity at that wavelength, σ is the absorption cross-section per molecule of absorbing gas at that wavelength, l is the light path length through the sample and N is the number density of absorbing gas molecules.

The proportional decrease of intensity is related to the absorption cross-section of a molecule and the number of molecules encountered. For wavelengths that correspond to a major energy transition of the sample, the absorption cross-section is large and the intensity drops off very quickly. For wavelengths that do not, the absorption cross-section is small or zero and the intensity remains relatively unchanged. Wavelength-dependent absorption cross-sections are well documented for many species allowing samples to be identified.

A useful way of describing this effect is to define the *absorbance* of a sample. This is the ratio of absorbed intensity to initial intensity and is given by:

$$\frac{\Delta I(\lambda)}{I_0(\lambda)} = \frac{I(\lambda) - I_0(\lambda)}{I_0(\lambda)} \tag{3.3}$$

Systems used in this project were designed for detecting small concentrations, the target being 0.1ppm and the maximum testes being 40ppm. This allowed the Beer-Lambert to be approximated to Equation (3.4), the derivation of which can be seen in Appendix 1:

$$\frac{\Delta I(\lambda)}{I_0(\lambda)} = \sigma(\lambda) l N \tag{3.4}$$

The sensitivity of a spectroscopy device can be quantified as its *noise equivalent absorbance* (NEA), with dimensionless units AU (absorbance units). This is the minimum absorbance which will give a measurement equal to the noise in a given system. It is not specific to a given gas or path length the through sample.

A diagram of Beer-Lambert absorption through a body of gas is shown in Figure 3.1. Darker colour represents more intense light, demonstrating the exponential decrease in intensity as light passes through the sample. If the absorbance, the path length and the absorption cross-section are known then the number density of the absorbing species can be calculated and hence the concentration.

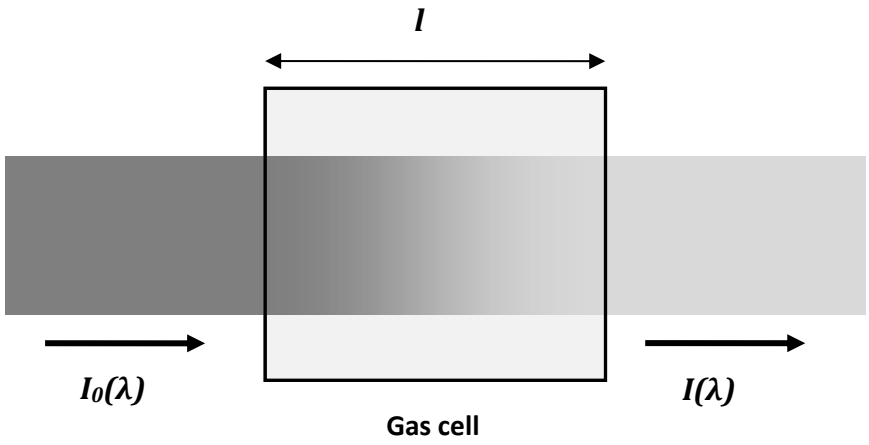

Figure 3.1: Diagram of Beer-Lambert absorption. Light of wavelength λ passes through a body of absorbing gas and decreases in intensity. In this diagram, darker colour represents more intense light.

There are two main ways in which an atom or molecule may transition to a more exited state and therefore absorb a photon. The first is electronic promotion, whereby an atomic electron absorbs a photon in the process of transitioning from one discrete energy level to another [1].

The energy levels around an atom are quantised and electrons cannot exist between two energy levels. Therefore, the photons that can be absorbed in this way are limited to those matching the band gap of a specific energy transition. Electronic promotion is the dominant absorption process for monatomic gases [3].

The second is vibrational or rotational transition. Molecules, being made up of a number of atoms bonded together, also have a range of vibration and rotation states [3]. These include vibration of inter-atomic bonds, flexing between bonds and the various rotation axes of the molecule itself. The energy of these states is dependent on the shape of the molecule and the arrangement of the bonds. Formaldehyde is subject to, among other things, symmetric C-H and C-O stretching, anti-symmetric C-H stretching, symmetric C-H bending and rotation about all of the x, y and z axes [4].

In general, both types of transition have many possible combinations, leading to many absorption peaks. Absorption peaks often overlap each other, superposing and becoming difficult to resolve independently. For a given species under a given set of conditions this will lead to a series of absorption peaks and troughs which add together to give a characteristic absorption spectrum.

A graph of the absorption spectrum of formaldehyde gas is given in Figure 3.2, re-plotted from data measured by Meller *et al.* [5]. Some of the major absorption peaks are labelled, following the scheme of Clouthier and Ramsey [6]. Labels follow the form M^a_b, representing a vibronic transition of the vibration state *M*, *a* representing the quantum number in the upper energy state and *b* the quantum number in the lower state [6].

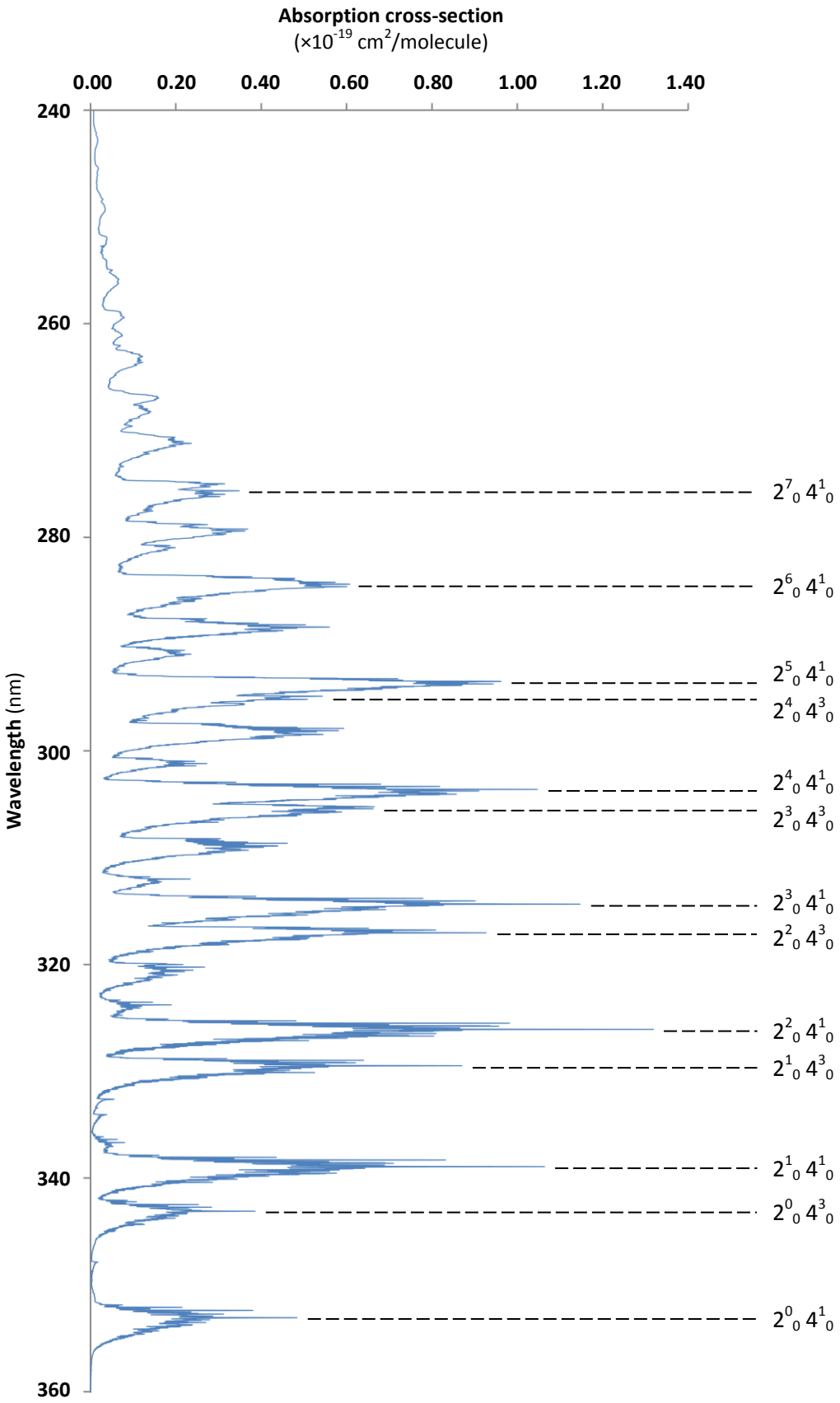

Figure 3.2: Graph of the formaldehyde absorption spectrum in the UV range, re-plotted from data from Meller *et al.* [5] with some of the major vibration state peaks marked [6].

Figure 3.2 shows the UV absorption range of formaldehyde between 240nm and 360nm. The spectrum consists of several strong absorption peaks, predominantly caused by molecular vibration [6]. Figure 3.3 is a higher resolution graph of the $2^1_0\ 4^1_0$ absorption peak in which a number of much finer spectral features can be seen. These are typical of the peaks in the formaldehyde UV. Between the main peaks are regions of low absorption which, particularly in the longer wavelength part of the spectrum, can drop to almost zero.

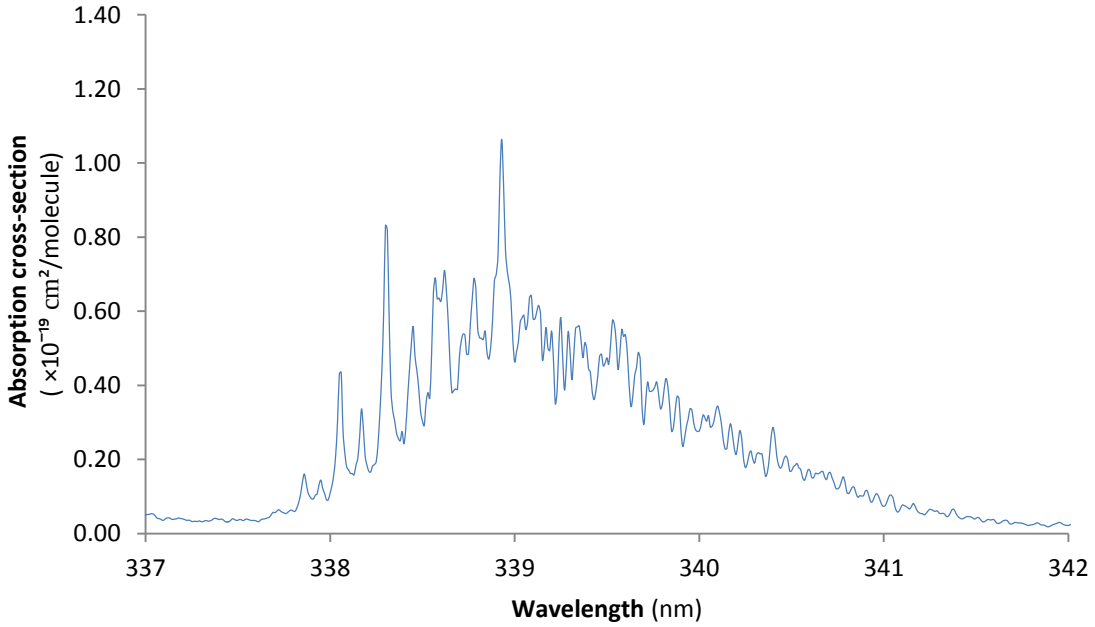

Figure 3.3: Graph of the $2^1_0\ 4^1_0$ formaldehyde absorption peak showing the fine spectral features that are typical across the UV spectrum, re-plotted from data from Meller *et al.* [5]. Fine spectral features were attributed to electronic transitions.

In practice, spectroscopy is not as straightforward as simply identifying the absorption spectrum of a recognised species. In most samples taken in the field there will be more than one gaseous species present. This makes spectroscopic identification much more difficult, as absorption peaks can overlap. As the number of gases increase, so does the probability of overlapping peaks. Equation (3.5) describes the wavelength dependant intensity decrease that takes place when two species that absorb in the same region are present:

$$\frac{I(\lambda)}{I_0(\lambda)} = e^{-l(\sigma_1(\lambda)N_1+\sigma_2(\lambda)N_2)} \tag{3.5}$$

where $\sigma_1(\lambda)$ and $\sigma_2(\lambda)$ are the absorption cross-sections of the two gases and N_1 and N_2 are their number densities.

It is not always possible to isolate individual absorption spectra from the spectrum of a complicated sample. It becomes necessary to know the spectra of specific chemical species and then search for recognisable spectral patterns. For example, Figure 3.4 shows the absorption spectra of all the indoor gases identified to overlap with formaldehyde in the UV region (see Chapter 4). It would be difficult to identify formaldehyde from a spectrum including all of these gases.

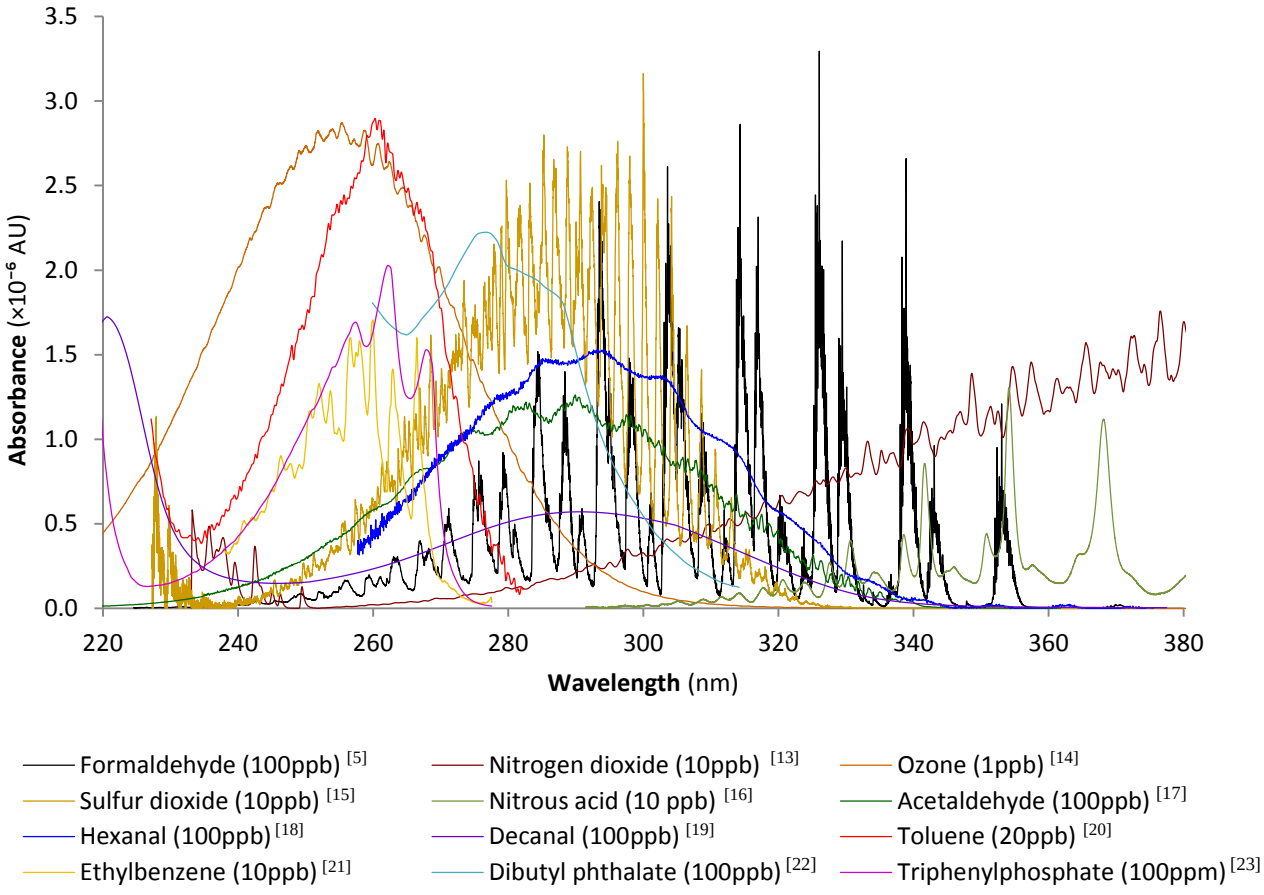

Figure 3.4: Absorbance spectra of formaldehyde, together with all identified gases with spectra that overlap with it, re-plotted from other studies. Concentrations were chosen arbitrarily so as to allow easy comparison to 100ppb of formaldehyde and a 10cm path length is assumed throughout.

3.2. Spectroscopy in this project

This section gives an overview of the application of spectroscopy to formaldehyde concentration measurement as used in this project. This includes many of the most significant equations in the project and a discussion of the purpose and application of measurement channels. Finally, an example is given using a hypothetical system with several low-resolution channels, two for measurement and two for reference. In general the number of channels required is one for detection, one for reference and one more for additional piece of information required.

3.2.1. Principles of operation

In this project initial light intensities were generally found using a separate, reference channel. This allowed for an accurate initial intensity measurement as well as controlling for variations in signal intensity not related to formaldehyde absorption, such as presence of other gases or fluctuation of source intensity. A reference measurement that varied in the same manner could control for such issues. The normalised absorbance signal, *A*, can be defined as in Equation (3.6) [7]:

$$A = 1 - \frac{I_D}{I_R}\frac{I_{0R}}{I_{0D}} \tag{3.6}$$

where I_{0D} is the initial intensity of the detection band, I_{0R} is the initial intensity of the reference band, I_D is the final intensity of the detection band and I_R is the final intensity of the reference band.

Variation in source intensity can cause problems, as it may lead to incorrect assumptions as to the relationship between initial and final intensity. This causes errors in the absorbance calculations and in turn leads to errors in the concentration calculations. Variations in source intensity can be caused by variations in drive current, temperature changes or source fluctuation noise. Variations in optical coupling efficiency from mechanical instability, temperature changes or impurities on the gas cell windows can also affect the amount of light reaching the detectors.

Variations like this can be controlled by having a separate reference channel along with the detection channel(s). Reference channels are required not to be affected by the presence of formaldehyde. Assuming any effects are broad band and affect both channels equally, they can be used to provide reliable measurements of the source's initial intensity. This can be done in a number of different ways.

Firstly, a separate optical path can be used, bypassing the gas cell such that no absorption from formaldehyde occurs. This has the advantage of taking reference measurements simultaneously with detection measurements and so controlling for variations over time. However it does not control for any variations that take place after the paths have divided, such as variations in coupling efficiency. There will also tend to be a decrease in light along the main optical path, caused by components such as the beam splitter.

Secondly, reference measurements can be taken at a different time, before or after the sample is introduced. This will only control for long-term variations such as temperature effects. Sometimes the introduction of the sample itself may cause variation such as cell repositioning error. It is also not appropriate for systems where a source of clean air for the reference channel is not available.

Finally, reference measurements can be taken across a different wavelength band. This method is specifically appropriate to formaldehyde as it has several wavelength regions in which there is little or no absorption (see Figure 3.2). This method has the advantage of providing simultaneous reference measurements in the same optical path as the detection measurements. However, it does not control for wavelength-variable fluctuations and is susceptible to potential interference from other gases.

In this project, reference measurements were generally taken across different wavelength bands. Occasionally this was not possible and reference measurements were taken at a different time. A detection and a reference measurement allow the absorbance of light passing through a sample to be found, and therefore the concentration of the absorbing gas to be calculated.

Figure 3.5 shows a hypothetical example of four channels used for a spectroscopic measurement of formaldehyde. Channels A and C are measurement channels, channels B and D are reference channels. Each is defined by a mathematically determined Gaussian function with a FWHM of 3nm, typical of laser-line narrow band-pass filters (see Chapter 7). In this example regions of minimal absorption are used for reference channels. This part of the formaldehyde absorption spectrum also has some selectivity advantages as described in Chapter 4.

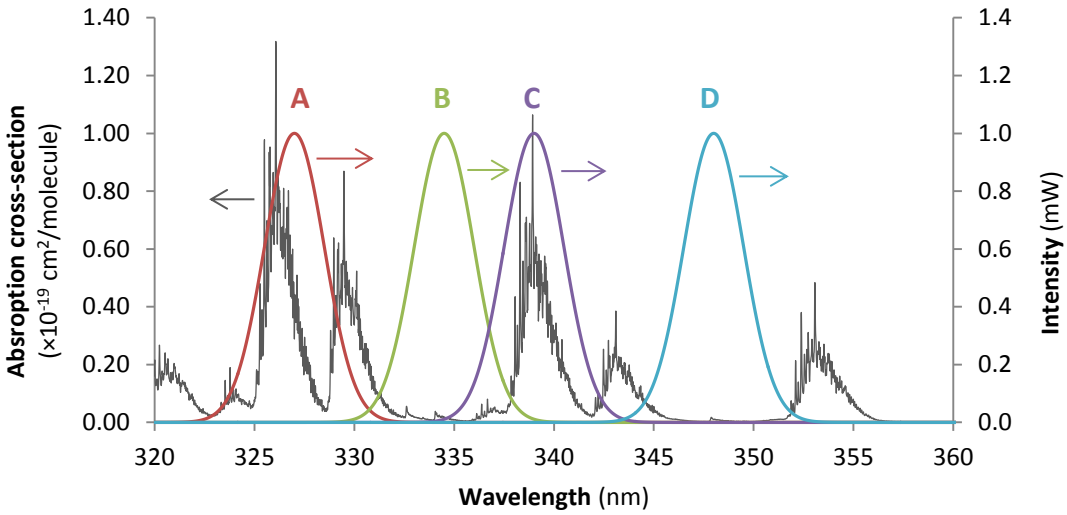

Figure 3.5: Example channels as mathematically determined Gaussian distributions with 3nm FWHM and arbitrarily selected intensity, along with the absorption spectrum of formaldehyde. A: measurement channel, B: reference channel, C: measurement channel, D: reference channel.

The spectra of each of the four channels are used in Equation (3.4) along with the formaldehyde spectrum. The changes in intensity spectra for these channels were calculated for an example concentration of 10ppm of formaldehyde in a 10cm gas cell. The results are shown in Figure 3.6. This shows that the two measurement channels give a significant intensity variation from formaldehyde while the two reference channels give a much smaller intensity variation.

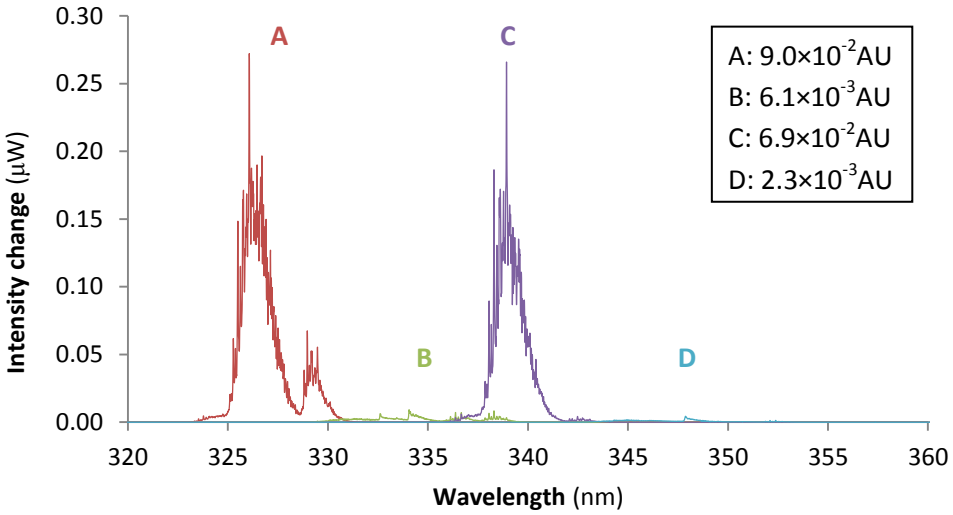

Figure 3.6: Absorbance spectra of the four channels calculated for 10ppm of formaldehyde in a 10cm gas cell. In this example, absorbances are 9.0×10^{-2}AU, 6.1×10^{-3}AU, 6.9×10^{-2}AU and 2.3×10^{-3}AU for channels A, B, C and D respectively.

The total area under each line, being the integral, gives the absorbance for each channel. In this example absorbance values were found to be 8.96×10^{-2}AU, 6.11×10^{-3}AU, 6.86×10^{-2}AU and 2.25×10^{-3}AU for channels A, B, C and D respectively. Absorbances for detection channels A and C are significantly greater than for reference channels B and D. If formaldehyde is the only gas present, the ratio between them will remain consistent and its concentration can be found by Equation (3.4). In principle only two of these channels are required, one measurement and one reference, but the additional channels would make the system more robust to errors and interference.

3.3. Spectral broadening and environmental effects

Even spectral lines from electronic promotion are not truly monochromatic but are broadened out in a distribution of wavelengths around the central line. These distributions frequently merge into one another, creating wide regions of the spectrum in which absorption occurs. Spectral broadening and effects are caused by a range of phenomena, some of which are constant while others vary with environmental factors such as temperature and pressure. It is therefore important to understand spectral line broadening in order to predict and control for variations in the absorption spectra of the gases.

3.3.1. Natural broadening

This determines the natural width of a spectral line as determined by the Heisenberg uncertainty principle [8]. The uncertainty principle as relates to spectral lines is described by Equation (3.7):

$$\Delta E \Delta t \geq \hbar/_2 \tag{3.7}$$

where ΔE is the uncertainty in energy, Δt is the uncertainty in time and ħ is the reduced Planck constant *(h/2π)*.

If Δt is taken to be the lifetime of the excited state, then the frequency spread due to natural broadening is given by Equation (3.8):

$$\Delta f \geq \frac{A_{trans}}{2\pi} \tag{3.8}$$

where A_{trans} is the Einstein A coefficient for a given electronic transition given by Equation (3.9) [9]:

$$A_{trans} = \frac{64\pi^4}{(4\pi\varepsilon_0)3h\lambda^3} |\boldsymbol{R_{trans}}|^2 \tag{3.9}$$

where ε_0 is the electric permittivity of free space and $\boldsymbol{R_{trans}}$ is the transition moment.

The distribution of excited state lifetime is given by a Lorentzian relationship and thus the natural-broadening line profile is as well [10]. Natural broadening equations contain no environmental terms such as temperature and pressure and so the line width will not decrease below this level. It is also wavelength dependent, being more significant at shorter wavelengths.

3.3.2. Doppler broadening

The molecules of a body of gas move around in random directions. The frequency of a photon to be absorbed by a moving molecule will be shifted by the Doppler effect, depending on velocity. Molecules travelling towards the source will absorb photons with lower frequencies. Molecules travelling away from the source will absorb photons with higher frequencies. For non-relativistic molecular velocities the shifted frequency is given by Equation (3.10) [9]:

$$f_d = f_0/(1 - {}^{v}/_{c}) \tag{3.10}$$

where f_d is the Doppler shifted frequency, f_0 is the initial frequency of the spectral line, v is the velocity of the molecule and c is the free space speed of light.

Molecule velocities are determined by the Maxwell–Boltzmann distribution leading to a Gaussian distribution of frequency with a FWHM given by Equation (3.11) [9]:

$$\Delta f_d = \frac{f_0}{c}\left(\frac{2\,k_B\,T\,ln2}{m}\right)^{1/2} \tag{3.11}$$

where T is the temperature of the gas, k_B is the Boltzmann constant and m is the mass of a single molecule.

As increasing temperature increases the mean particle velocity within a gas, Doppler broadening increases with increasing temperature. Wavelength is of course related to frequency by:

$$c = f\lambda \tag{3.12}$$

where f is the frequency and other symbols have their previous meanings. Hence a spread in frequency leads directly to a spread in wavelength, causing further broadening of the spectral lines.

3.3.3. Collision broadening

Collision broadening arises from collisions between molecules in the sample, which changes their energy states. These are known as diabatic collisions and can increase or decrease transition energies [10]. Collision broadening increases with the concentration of colliding molecules and so is sometimes known as pressure broadening. When diabatic collisions exist between like molecules the phenomena is known as resonance broadening or Holzmark broadening [10]. When diabatic collisions exist between different molecules it is known as foreign gas broadening or Lorentz broadening [10].

Both types have a FWHM given by Equation (3.13) [10].

$$\Delta f_{cd} = {}^{1}/_{\pi\tau_d} \tag{3.13}$$

where τ_d is the diabatic collision lifetime and Δf_{cd} refers to the change frequency due to diabatic collision broadening.

Adiabatic collisions also contribute to collision broadening, where they cause changes in the phase of the atomic oscillators. Broadening from adiabatic collisions also has a Lorentzian line profile with a FWHM given by Equation (3.14) [10]:

$$\Delta f_{ca} = \left(\frac{8k_B T}{\pi^3 \mu}\right)^{1/2} \sigma_a N_x \tag{3.14}$$

where μ is the magnetic permeability, σ_a is the adiabatic collision optical cross-section, N_x is the density of perturbing molecules lifetime and Δf_{ca} refers to the change in frequency due to adiabatic collision broadening.

Under standard temperature and pressure, adiabatic collision broadening tends to dominate over both natural broadening and diabatic collision broadening. Adiabatic collision broadening can also cause minor shifts in central line wavelength, generally towards longer wavelengths, as well as slight asymmetry of line profile [10]. It is therefore important to account for this when making spectroscopic measurements.

3.3.4. Other spectral effects

While the main spectral effects have been covered above, there are a number of others that can also take place. Many of these will only apply under specific circumstances. Examples include Stark and Zeeman broadening, which result from electric or magnetic fields respectively, and macroscopic Doppler shift, in which the gas has a net flow. Power broadening and saturation broadening can occur in the presence of high levels of radiation such as high power lasers [10]. For the purposes of this project these phenomena will be ignored as the conditions they require are unlikely to be present when measurements are taken.

The total line broadening in a sample is the result of a convolution of all line broadening phenomena taking place. Natural broadening and collision broadening both have Lorentzian profiles while Doppler broadening has a Gaussian profile. The resulting convolution is known as Voigt profile [10]. The dominant conditions that affect spectral broadening are temperature and pressure, both of which tend to increase line width. It is therefore important to be aware of the temperature and pressure of a sample when taking spectral measurements.

3.4. Spectral effects on formaldehyde

A general description of spectral broadening was given in Section 3.3. Here it was stated that a number of factors influence the width of a spectral line with the main factors depending on temperature and pressure. In this section the effects of pressure and temperature on the formaldehyde absorption spectrum are investigated.

3.4.1 Temperature dependant effects

The effect of temperature on the formaldehyde absorption spectrum was investigated by Meller and Moortgat (2000) [11]. They demonstrated variations to the spectrum at three different temperatures, 223K (-50°C), 289K (16°C), and 323K (50°C). Measurements were taken at a pressure of 100kPa (approximately 1 atmosphere). Figure 3.7 shows data between 337 and 342nm and is representative of the rest of the formaldehyde absorption spectrum.

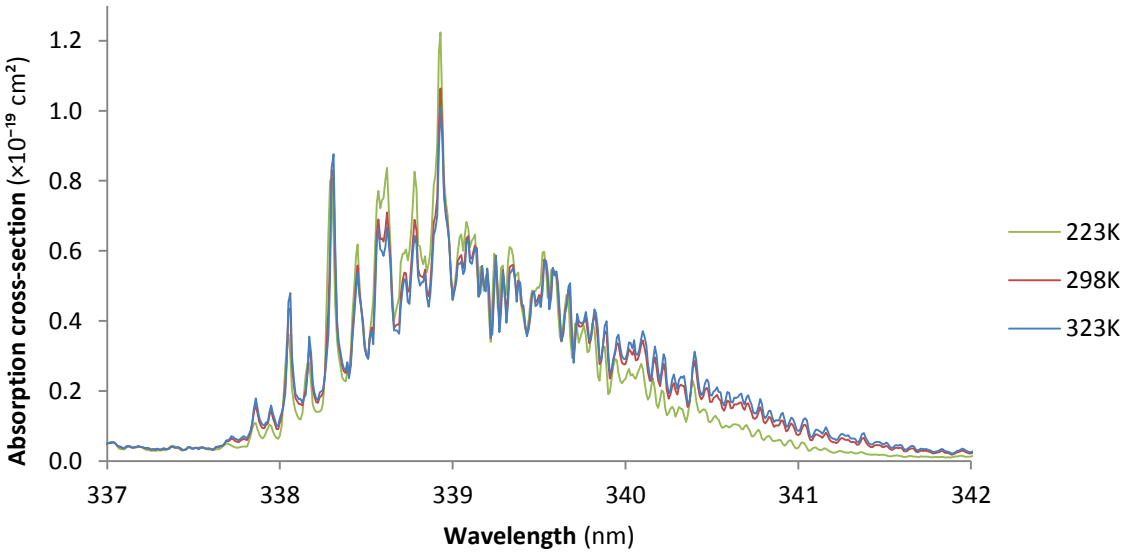

Figure 3.7: Graph showing the effects of temperature variation on part of the formaldehyde absorption spectrum as measured by Meller and Moortgat (2000) [11]. Temperature dependence in this region is representative of the rest of the spectrum.

Temperature can be seen to have some effect on the spectrum with the relative height of some of the sub-nanometre peaks varying with temperature. There may also be some spectral broadening of the main peak with increasing temperature. In spectroscopic measurements, the absorbance is integrated across the full range of the wavelength channel. Mathematically integrating across this data yields a change in absorbance of between 2.7 and -3.8% over a 100K temperature change. It was considered that this would be unlikely to be significant for the 10 – 30°C target range for this project.

3.4.2. Pressure dependant broadening

The effect of pressure on the formaldehyde absorption spectrum was measured by Co *et al.* [12] and the results are shown in Figure 3.8. This study covers only 350.877-355.871nm which makes up a small part of the region of interest. Pressure levels range from 10-53kPa, which is substantially below atmospheric pressure at 101kPa. Data for pressure variation around atmospheric was not found from a single study. The temperature during these measurements was at the more appropriate level of 289K.

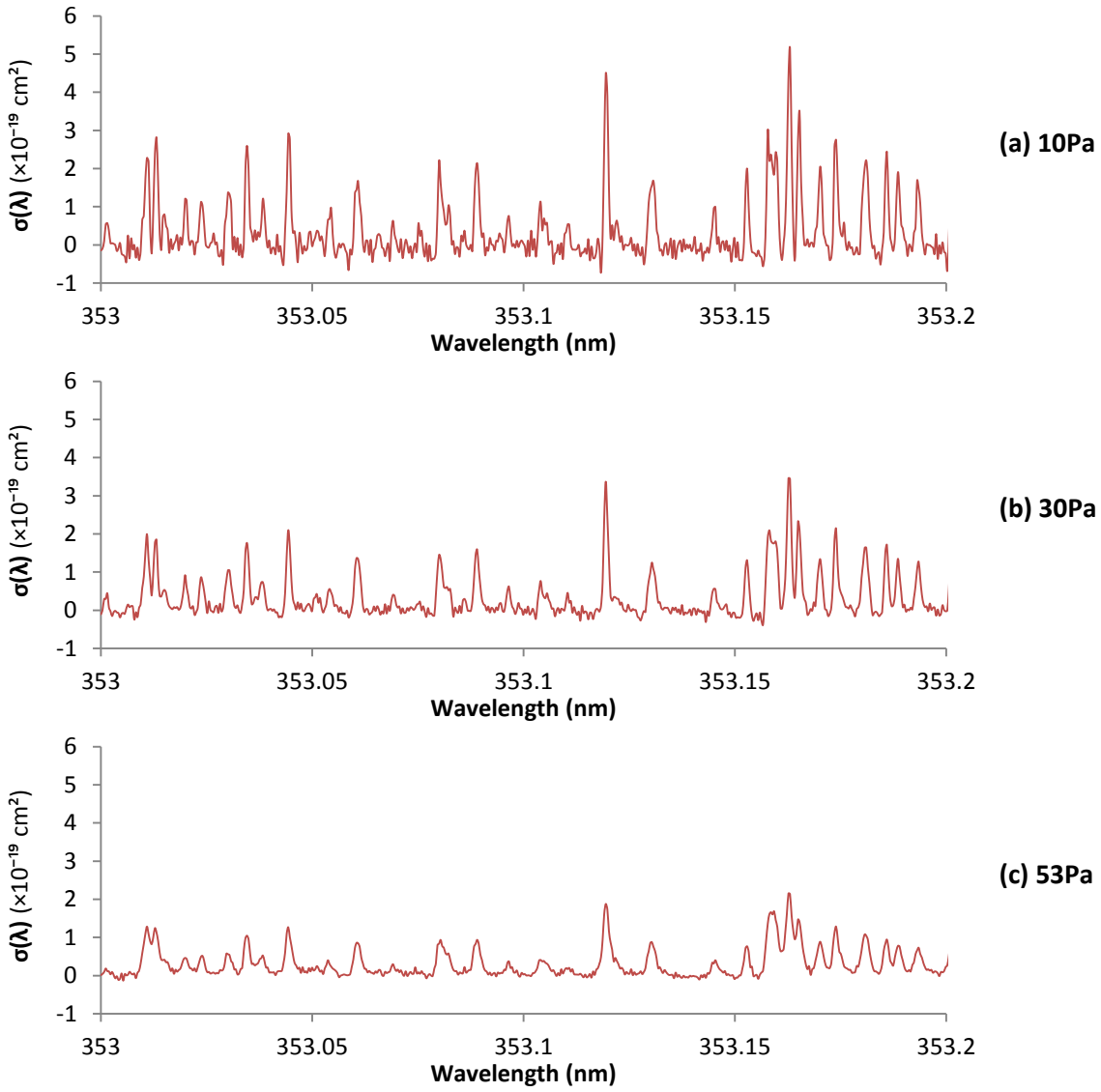

Figure 3.8: Graphs of a small part of the formaldehyde absorption spectrum at (a) 10Pa, (b) 30Pa and (c) 53Pa re-plotted from data from Co *et al.* [12]. It can be seen that peaks broaden with increasing pressure as expected.

The graphs in Figure 3.8 show an increase in peak width with increasing pressure as expected from pressure broadening. Peak height decreases with increasing pressure, which is also consistent since when a peak experiences pressure broadening its absorption is spread over a greater range of wavelengths. It should be noted that molecular number density was not controlled and is likely to have increased with increasing pressure.

Again these effects are small in comparison to the measurement resolution of 3nm typically used in this project. Spectral broadening is likely to increase approaching atmospheric pressure. By integrating over the wavelength band and by keeping within the linear region of the Beer-Lambert law it was thought likely that temperature and pressure would not significantly affect results.

This section demonstrates that while the formaldehyde does undergo broadening effects from temperature and pressure, they are small in comparison to the spectral resolutions used. The total absorbance from a peak did not change due to broadening effects. It was concluded that broadening effects could be neglected in the course of this project.

3.5. Chapter summary

The principles of spectroscopy and spectroscopic gas detection are the theoretical basis for this project. When light passes through a sample of gas, it will only be absorbed if it matches an energy transition of the molecules present. Energy transitions may be from electronic promotion between orbits or vibrational or rotational states within molecules and will result in a characteristic absorption spectrum, unique to each species. The absorption through a sample of gas is described by the Beer-Lambert law:

$$\frac{I(\lambda)}{I_0(\lambda)} = e^{-\sigma(\lambda)lN} \tag{3.2}$$

The absorption cross-section of a gas can be changed by a number of factors, usually resulting in spectral broadening. Examples include natural broadening, Doppler broadening, and collision broadening. Broadening phenomena often depend on local conditions such as temperature and pressure. It is important to take these effects into account when taking spectroscopic measurements. Formaldehyde demonstrated broadening under both temperature and pressure increases. However, the effects were small in comparison to spectral resolutions used in the project and it was concluded that broadening effects could be ignored.

Within the context of this project absorption was measured as intensity variation integrated across wavelength bands. Formaldehyde concentrations tended to be close to the limit of detection of measurements systems. This meant that absorption was small in comparison to initial intensities and so limiting case approximations could be used. Across a given measurement channel, the intensity shift was found to be proportional to the molecular number density:

$$\frac{\Delta I(\lambda)}{I_0(\lambda)} = \sigma(\lambda) l N \tag{3.4}$$

This was used for calculating concentrations during the project. Spectroscopic measurement channels may be either detection channels, using a region of the spectrum with strong absorption, or reference channels using regions of little or no absorption. Formaldehyde is unusual in that it has several such regions very close together in its absorption spectrum. In the next chapter the absorption spectra of a wide range of gases common to the indoor environment are reviewed in order to find out how they interfere with the formaldehyde spectrum. This was used to select the wavelength bands for the detection and reference channels to be used in later prototype systems.

3.6. References

[1] D. W. Brow, A. J. Floyd and M. Sainsbury, Organic Spectrocopy, Chichester: John Wiley & Sons, 1998.

[2] L. Chomaz, L. Corman, T. Yefsah, D. Desbuquois and J. Dalibard, "Absorption imaging of a quasi-two-dimensional gas: a multiple scattering analysis," *New Journal of Physics,* vol. 14, p. 055001, 2012.

[3] D. L. Pavia, G. M. Lampman and G. S. Kriz, Introduction to Spectroscopy, third edition, Stamford: Thomson Learning, 2001.

[4] J. Lahilahti, Rotation-vibration spectroscopic studies of formaldehyde and formic acid molecules, Department of Physical Sciences, University of Oulu, Finland, 2006.

[5] R. Meller and G. K. Moortgat, "Temperature dependence of the absorption cross sections of formaldehyde between 223 and 323 K in the wavelength range 225-375 nm,"

Journal of Geophysical Research-Atmospheres, vol. 105, pp. 7089-7101, 2000.

[6] D. J. Clouthier and D. A. Ramsay, "The spectroscopy of formaldehyde and thioformaldehyde," *Annual Review of Physical Chemistry,* vol. 34, pp. 31-58, 1983.

[7] J. Hodgkinson, R. Smith, W. O. Hob, J. R. Saffell and R. P. Tatam, "Non-dispersive infra-red (NDIR) measurement of carbon dioxide at 4.2 mu m in a compact and optically efficient sensor," *Sensors and Actuators B: Chemical,* vol. 186, pp. 580-588, 2013.

[8] J. Y. Ping and D. G. Rancourt, "Thickness effects with intrinsically broad absorption-lines," *Hyperfine Interactions,* vol. 71, no. 1-4, pp. 1433-1436, 1992.

[9] J. Michael Hollas, Modern Spectroscopy, New Jersey: John Wiley & Sons, 2007.

[10] J. D. Ingle and S. R. Crouch, Spectrochemical Analysis, London: Prentice Hall, 1988.

[11] R. Meller and G. K. Moortgat, "Temperature dependence of the absorption cross sections of formaldehyde between 223 and 323 K in the wavelength range 225-375 nm," *Journal of Geophysical Research,* vol. 105, pp. 7089-7101, 2000.

[12] D. Co, T. Hanisco, J. Anderson and F. Keutsch, "Rotationally resolved absorption cross sections of formaldehyde in the 28100-28500 cm-1 (351-356 nm) spectral region: Implications for in situ LIF measurements," *Journal of Physical Chemistry A,* vol. 109, pp. 10675-10682, 2005.

[13] K. Bogumil, J. Orphal, T. Homann, S. Voigt, P. Spietz, O. C. Fleischmann, A. Vogel, M. Hartmann, H. Kromminga, H. Bovensmann, J. Frerick and J. P. Burrows, "Measurements of molecular absorption spectra with the SCIAMACHY pre-flight model: instrument characterization and reference data for atmospheric remote-sensing in the 230–2380 nm region," *Journal of Photochemistry and Photobiology A: Chemistry,* vol. 157, pp. 167-184, 2003.

[14] D. Daumont, J. Brion, J. Charbonnier and J. Malicet, "Ozone UV spectroscopy I: Absorption cross-section at room-temperature," *Journal of Atmospheric Chemistry,* vol. 15, pp. 145-155, 1992.

[15] A. C. Vandaele, C. Hermans and S. Fally, "Fourier transform measurements of SO2 absorptioncrosssections: II. Temperature dependence in the 29000–44000/cm (227–345nm) region," *Journal of Quantitative Spectroscopy & Radiative Transfer,* vol. 110, 2009.

[16] J. Stuts, E. S. Kim, U. Platt, P. Bruno, C. Perrino and A. Febo, "UV-visible absorption cross section of nitrous acid," *Journal of Geophysical Research,* vol. 105 (D11), pp. 14,585-14,592, 2000.

[17] W. Schneider and G. Moortgat, Personal communication to E. P. Röth, R. Ruhnke, G. Moortgat, R. Meller, and W. Schneider, Berichte des Forschungszentums Jülich, jül-3341, 1997.

[18] H. Plagens, R. Bröske, M. Spittler, L. Ruppert, I. Barnes and H. K. Becker, Atmospheric loss processes of hexanal. Photolysis and reaction with OH and Cl radicals, Proceedingsof the Second Workshop of the EUROTRAC-2 Subproject Chemical Mechanism Development: Karlsruhe, Germany, GPP10-1-GPP10-4, 1998.

[19] H. R. Cooper and H. W. Melville, "The Kinetics of the Autoxidation of n-Decanal. Part I. The Mechanism of Reaction," *Journal of the Chemical Society,* pp. 1984-1993, 1951.

[20] W. Koban, J. D. Koch, R. K. Hanson and C. Schulz, "Absorption and fluorescence of toluene vapor at elevated temperatures," *Physical Chemistry Chemical Physics,* vol. 6, pp. 2940-2945, 2004.

[21] T. Etzkorn, B. Klotz, S. Sorensen, I. V. Patroescu, I. Barnes, K. H. Becker and U. Platt, "Gas-phase absorption cross sections of 24 monocyclic aromatic hydrocarbons in the UV and IR spectral ranges," *Atmospheric Environment,* vol. 33, pp. 525-540, 1999.

[22] V. S. Fihtengolts, et al., Atlas of UV Absorption Spectra of Substances Used in Synhetic Rubber Manufacture, 171: 1969.

[23] L. Lang (Editor), Absorption Spectra in the Ultraviolet and Visible Region.

Chapter 4: Interfering gases and wavelength selection

All spectrometry systems are susceptible to interference from other gases but this is particularly the case for the low-resolution methods developed in this project. This chapter presents a thorough literature based review into the gases expected to be present in the target environment and highlight which ones have the potential to interfere with formaldehyde.

85 substances and substance groups were identified as likely to be present in the indoor environment based largely on a study of pollutants in indoor air by C. J. Weschler [1] . 32 of these had significant absorption in the UV-Visible region. Data on the absorption spectra were obtained from other studies and analysed, finding that 11 of them overlapped with the formaldehyde absorption spectrum. Following this analysis, a region of the formaldehyde absorption spectrum was identified with potential for low cross-interference.

4.1. Gases considered

Weschler's study focused mainly on homes in the United States and collected and compared published data from many other studies [1]. Some of the underlying data in these sources was obtained using gas detection methods such as chromatographs or mass spectrometers [2] [3]. Other data was inferred from the presence of emitting materials such as medium density fibreboard (MDF).

Many gas detection methods take multiple hours to run [4] [5] and so short lived species may have gone undetected and been left out of the study. Nitrous acid is produced from the heterogeneous hydrolysis of nitrogen dioxide with wet surfaces [6] and can exist for as little as 10 minutes in forest atmospheres [7].

Several other studies found nitrous acid to be present in the indoor environment [6] [8] and so nitrous acid was added to the list of compounds considered here. Otherwise, Weschler's report appears to be a reasonably thorough study and is well regarded by several others [9] [10]. It has therefore been used as the benchmark for formaldehyde selectivity in this report.

The substances identified for this review can be divided into three basic categories: inorganic gases, volatile organic compounds (including semi-volatiles) and airborne particles. Each of these categories has some broadly similar properties and gases in a category will frequently have similar sources. In this review, gases in each of these categories are considered separately.

The source of many polluting inorganic gases in modern buildings is cooking and heating appliances [11] as well as indoor smoking and various industrial processes. In the UK, indoor concentrations of carbon monoxide, nitrogen dioxide and nitric oxide have been on the decrease in recent years due to a decrease in smoking and other factors [1] [12] [13]. The trend of indoor ozone is less clear [14].

The category 'volatile organic compounds' covers a wide variety of large molecules that can still readily be gaseous at room temperature. Formaldehyde is a volatile organic compound, as are some other members of the aldehyde group. This category also includes alkanes, aromatics such as benzene and toluene and many more.

Indoor sources of these gases include emissions from resins, rubber and carpets, smoking and indoor chemistry [1] [15]. Indoor concentrations of some compounds such as aromatics and some of the more volatile compounds, are currently decreasing or remaining constant due to decreases in source abundance [16] [17] [18]. Some longer-chain aldehydes and many semi-volatile organic compounds are currently increasing, potentially due to increased indoor chemistry and certain cosmetic products [1] [19] [20].

Recent increases in awareness of environmental issues and high energy prices have resulted in increased building insulation. This may have led to reduced ventilation and potentially caused increases in the indoor concentrations of many gases [1]. More volatile compounds are more likely to evaporate and be found in gaseous form. They will, however, then disperse: provided that the source does not continue to emit, they will tend to remain in the indoor environment for a shorter time than other pollutants.

The final category includes metal particles, mineral fibres, dust components, mould spores and many others [1]. Their sources are widespread, including lead-based paints, indoor smoking, industrial processes and even human skin. The concentrations of many airborne particles are decreasing due to legal restrictions on certain sources, but it is difficult to draw general trends [1] [21] [22].

Small particles are known to exhibit a spectroscopic scattering effect that is analogous to the absorption cross-section. It is variable with wavelength and so airborne particles can exhibit broad spectral features similar to light absorption features [23]. Some airborne particles also exhibit fluorescence effects in the UV [23] [24]. Airborne particles were not considered in this project but may have to be considered or eliminated when using a detection system 'in-situ', potentially by filtering.

4.2. Spectral interference with formaldehyde

A full list of all substances and substance groups considered in this review is given in Appendix 2. In total, 85 substances and substance groups were identified by Weschler [1]. 32 of these had absorption spectra in the UV-Visible region. Of these gases, 11 were found to overlap with the formaldehyde UV absorption region.

Figure 4.1 shows the absorption spectra of the 11 gases identified to overlap with formaldehyde. The spectrum of formaldehyde is included for comparison. Data was acquired from a number of sources, generally reported as absorption cross-section but occasionally the *absorption coefficient* (using the base 10, molar equivalent of the Beer-Lambert law. See Appendix 3). Interference may come from a mix of organic and inorganic gases. The aldehyde group is represented here, as are some aromatics.

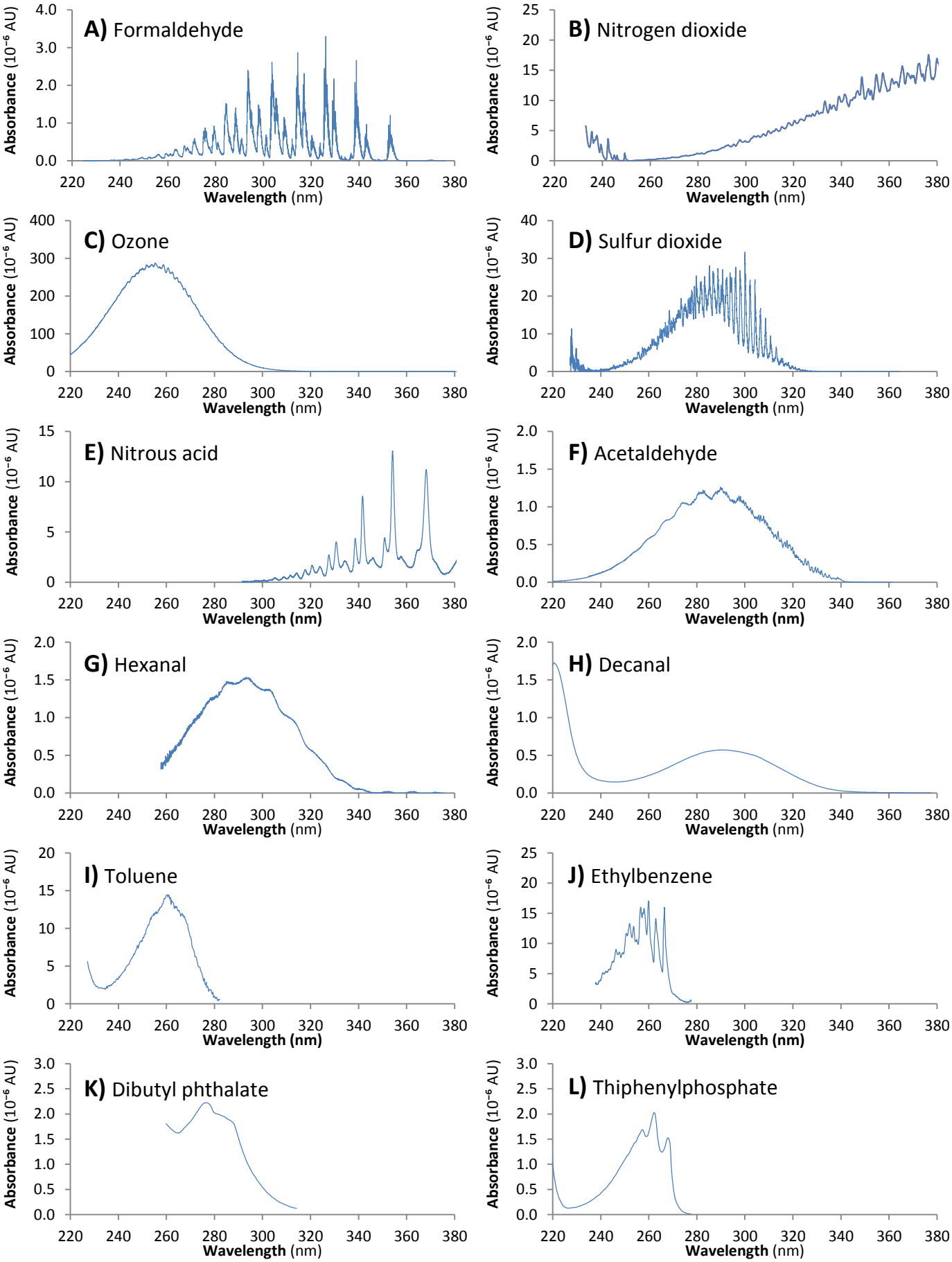

Figure 4.1: Re-plotted absorbance spectra of formaldehyde along with all identified gases with spectra that overlap with it. **A)** Formaldehyde [25] **B)** Nitrogen dioxide [26] **C)** Ozone [27] **D)** Sulfur dioxide [28] **E)** Nitrous acid [29] **F)** Acetaldehyde [30] **G)** Hexanal [31] **H)** Decanal [32] **I)** Toluene [33] **J)** Ethylbenzene [34] **K)** Dibutyl phthalate [35] **L)** Triphenylphosphate [36]. All absorbances assume concentrations of 100ppb and path lengths of 100mm.

On examining this data, the spectral region between 320nm and 360nm was identified as having very limited spectral interference from the other gases listed here. An extended graph of this region is shown in Figure 4.2. It shows an expansion of the identified region with the gas that absorb here, corrected for expected concentrations.

Concentration data comes from a number of studies. Saraga *et al.* [38] studied air quality in a museum, a primary industry and an office from which mean concentration data for nitrogen dioxide, ozone, sulphur dioxide and acetaldehyde is used. Peng *et al.* [39] measured pollutants in multiple locations of a single office building from which mean concentration data for decanal is used. Marchan *et al.* [40] measured aldehyde concentrations in 16 homes from which hexanal concentration is used.

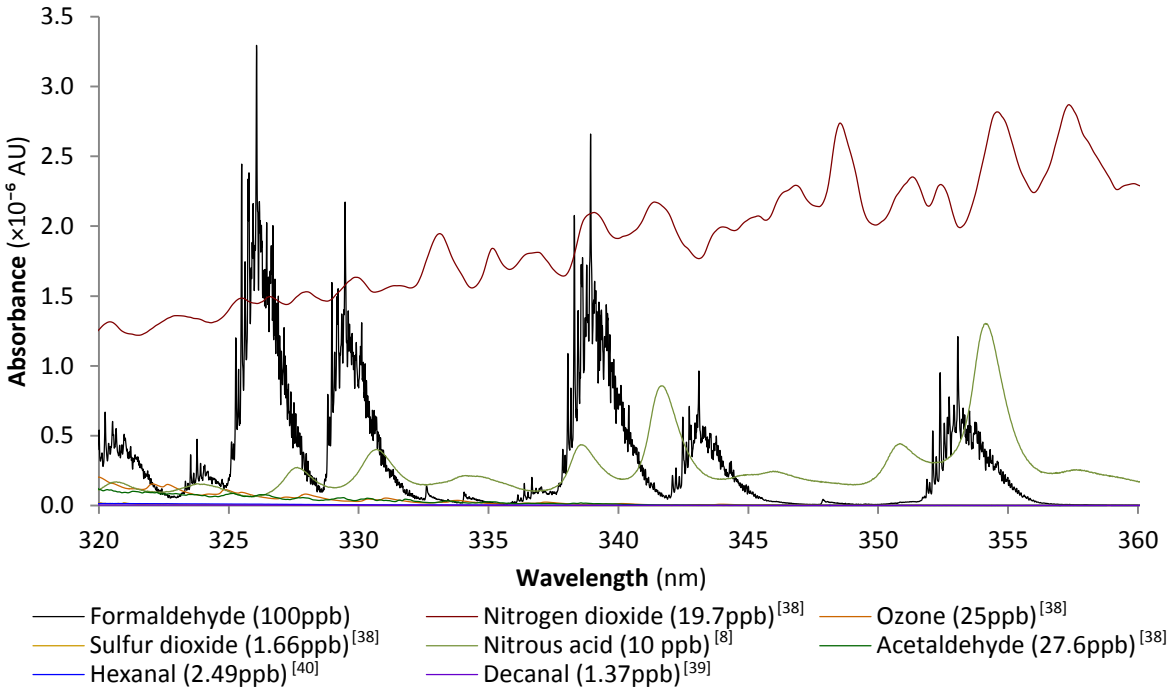

Figure 4.2: Graph of absorbance of gases in the identified region. Concentrations are based on values found by a number of studies [38] [39] [40] [41] [42] but are expected to vary substantially between locations. A 10cm path length is assumed throughout.

Every indoor environment is different, being subject to a wide range of gas sources and having a significant variation in levels of ventilation. Measured concentrations tend to vary between and within individual studies [38] [39]. The concentrations used in Figure 4.2 are therefore examples of concentrations that may arise and should be used as a general guide.

Nitrogen dioxide appears to be the most significant interfering gas in this region, with some interference from nitrous acid. Nitrogen dioxide is produced by indoor smoking and combustion appliances, and has been on the decrease in recent years [1]. Nitrous acid is produced by reactions of nitrogen dioxide with wet surfaces [6] and would require both to be present to be produced.

Finding significant interference from only nitrogen dioxide and nitrous acid was a surprising result given the number of species present. The general region around 320 – 360nm is used in DOAS for detection of outdoor formaldehyde [43] [44] [45] [46]. This analysis shows that it is equally useful for indoor measurements.

4.3. Wavelength selection

In the identified region, the formaldehyde spectrum shows a number of absorption peaks as marked on Figure 4.2. It also shows a number of regions with very minimal absorption, 332-338nm, 345-352nm and 356 and above. These regions of minimal absorption are peculiar to formaldehyde, with most gases having a more gradual transition between high absorption and low absorption. These unusual features allow for reference channels and measurement channels to be placed very close together on the formaldehyde spectrum. These can then be used to measure the formaldehyde concentration as described in Chapter 3.

Two sets of wavelength bands were selected from this region to be used as detection and reference channels. These bands are low resolution, around 3nm FWHM, compatible with the transmission spectra of laser-line filters. Individual channels were selected to have wavelengths close together (preferably within the 10-15nm range typical of the FWHM of an UV LED) as it was desirable to use a single light source for each set of measurements to control for variations. In this section the two sets of wavelength channels are discussed.

4.3.1. The 339nm wavelength band set

The 339nm wavelength band set has a pair of detection bands centred at 339nm over the $2^1_0\,4^1_0$ peak and at 329nm over the $2^1_0\,4^3_0$ and the $2^2_0\,4^1_0$ peaks. It also had a single reference band centred at 335nm over a region of low absorption. Figure 4.3 shows the UV absorption spectrum of formaldehyde along with mathematically generated channels in the position of the 339nm wavelength band set. They are given a FWHM of 3nm, in keeping with the typical performance of a laser-line filter.

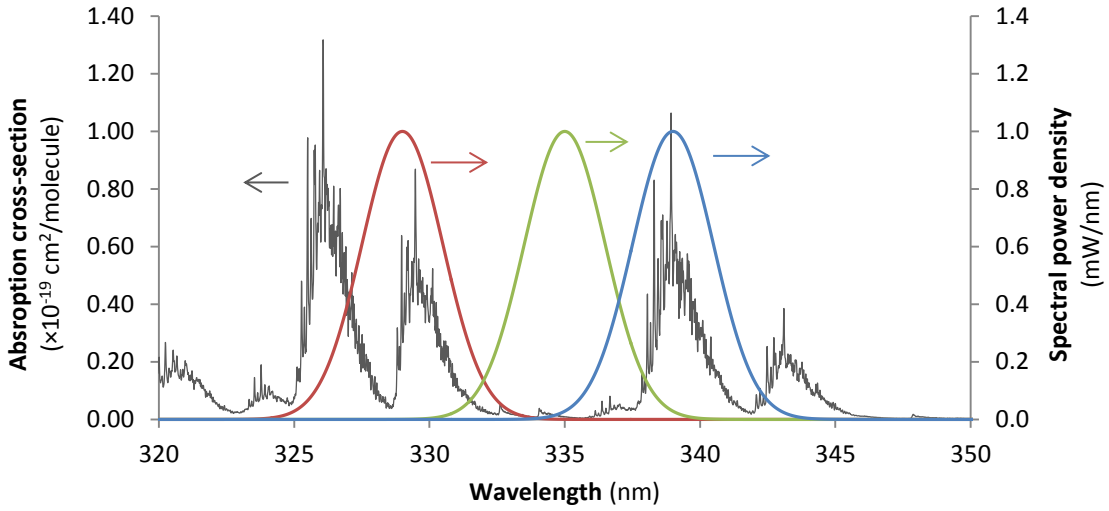

Figure 4.3: UV absorption spectrum of formaldehyde along with mathematically generated channels in the position of the 339nm wavelength band set. The blue line represents the 339nm detection channel, the green line the 335nm reference channel and the red line the 329nm.

Figure 4.4 shows the theoretical change in spectral power density of the three channels when light passes though 10cm of 10ppm of formaldehyde gas. This gives the change in intensity due to absorption by the gas as described in Chapter 3. The total intensity change due to formaldehyde in each channel is given by the area under the spectrum, i.e. the integral of spectral power density by wavelength. This example gives absorbance values of 7.03×10^{-2}AU for the 339nm detection channel, 7.01×10^{-3}AU for the 335nm reference channel and 6.86×10^{-2}AU for the 329nm detection channel.

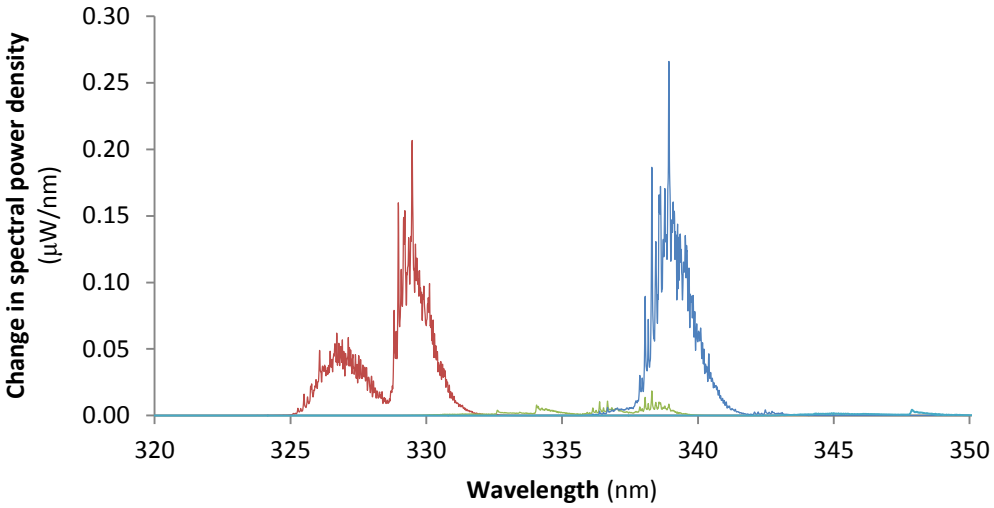

Figure 4.4: Theoretical change in spectral power density of the three channels when light passes though 10cm of 10ppm of formaldehyde gas. In this example the absorbances are 7.03×10^{-2}AU for the 339nm detection channel (Blue), 7.01×10^{-3}AU for the 335nm reference channel (Green) and 6.86×10^{-2}AU for the 329nm detection channel (Red) respectively.

The main advantage of the 339nm wavelength band set is that it uses one of the strongest formaldehyde absorption peaks in the identified region. The $2^2_0\ 4^1_0$ peak is slightly stronger, but not as close to potential reference regions. The main disadvantage is that while the three peaks were within 10nm of each other, at the time of writing there did not exist a single commercially available LED that covered this range. This issue is discussed in more detail in Chapter 7 and Chapter 8.

4.3.2. The 353nm wavelength band set

The 353nm wavelength band set had a pair of detection bands centred at 353nm over the $2^0_0\ 4^1_0$ peak and at 343nm over the $2^0_0\ 4^3_0$ peak. It also had a single reference band centred at 348nm over a region of low absorption. Figure 4.5 shows a diagram of the intensity spectra of measurement channels across these three wavelength bands, together with the formaldehyde spectrum in the identified region.

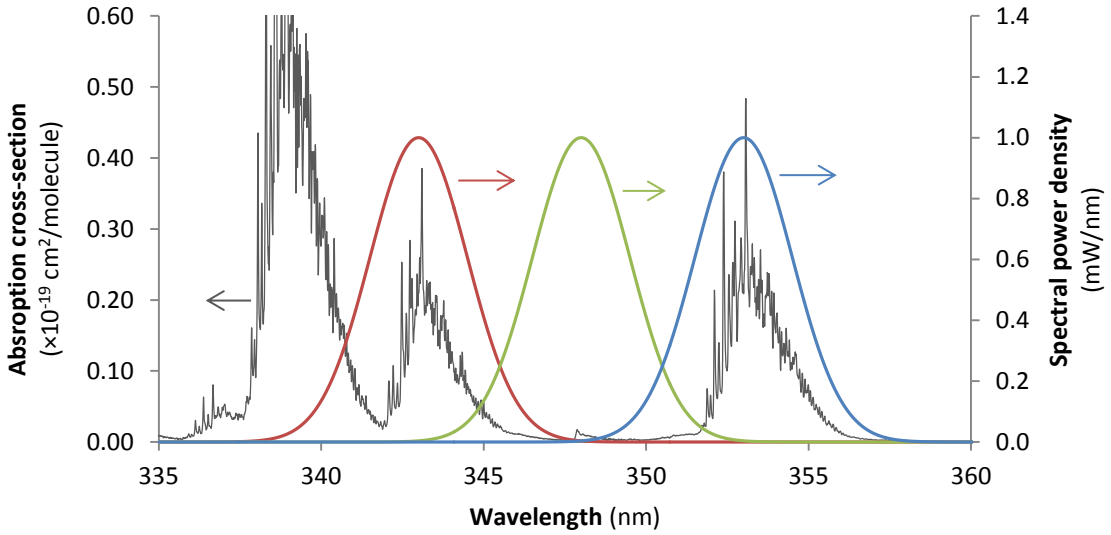

Figure 4.5: UV absorption spectrum of formaldehyde along with mathematically generated channels in the position of the 339nm wavelength band set. The blue line represents the 353nm detection channel, the green line the 348nm reference channel and the red line the 343nm.

The theoretical change in spectral power density of the three channels is shown Figure 4.6, for light passes though 10cm of 10ppm of formaldehyde gas. The total intensity change due to formaldehyde in each channel is given by the area under the multiplied spectrum, i.e. the integral of the spectral power density by wavelength. This example gives absorbance values of 3.01×10^{-2}AU for the 353nm detection channel, 2.25×10^{-3}AU for the 348nm reference channel and 3.06×10^{-2}AU for the 343nm detection channel.

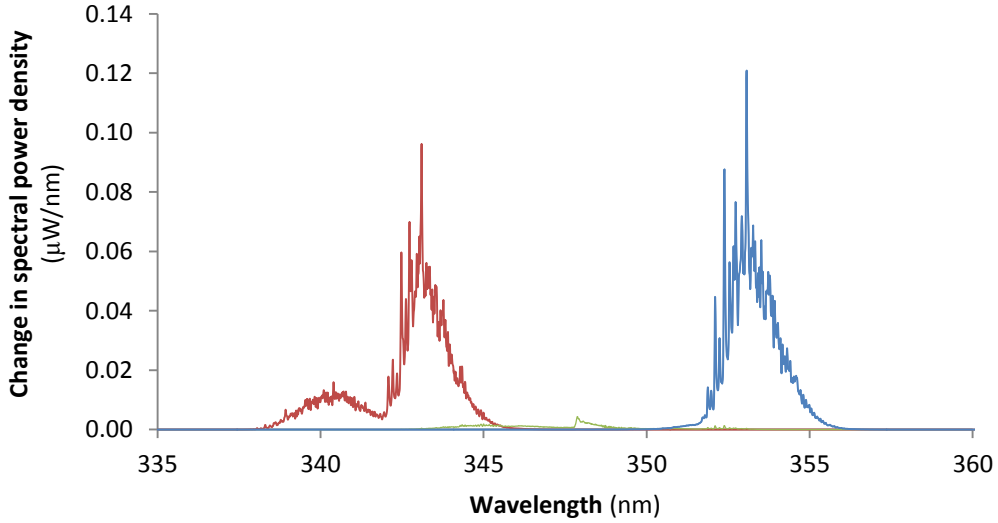

Figure 4.6: Theoretical change in spectral power density of the three channels when light passes though 10cm of 10ppm of formaldehyde gas. In this example the absorbances are 3.01×10^{-2}AU for the 353nm detection channel (Blue), 2.25×10^{-3}AU for the 348nm reference channel (Green) and 3.06×10^{-2}AU for the 343nm detection channel (Red) respectively.

The main advantage of the 353nm wavelength band set is that all three bands fall within the FWHM of a single, commercially available LED (the 350nm source described in Chapter 8). The main disadvantage is that the two peaks used as detection channels are relatively weak, potentially leading to a less sensitive system. However it is aligned to the commercially available 355nm laser-line filter (see Chapter 8), and photodiode based detectors tend to be more responsive at longer UV wavelengths. This set covers aims of selectivity and low complexity outlined in Chapter 1.

4.4. Chapter summary

The region 320-360nm is used for the spectroscopic measurement of formaldehyde in forest and outdoor environments using DOAS. However its potential for detection in indoor air was not well established. This is due to the increased potential range of spectral interferents and differing (potentially significantly higher) concentrations present.

By considering 85 substances and substance groups, the region of the formaldehyde spectrum between 320nm and 360nm was identified as having a minimum of potential interferents in the indoor environment. The main interfering species found were nitrogen dioxide and nitrous acid, with minimal interference from sulphur dioxide, acetaldehyde, ozone, hexanal and decanal. Given the number of species believed to be present in the indoor environment, it was surprising that a region could be found with so little interference.

The identified region included some wavelength regions with high formaldehyde absorption and some in which absorption was minimal. Spectroscopic measurements taken in the former regions will have significant response from formaldehyde. Measurements taken in the latter regions will have very little. These can be used as detection and reference channels respectively for a low resolution detection method specifically targeted at formaldehyde.

Two sets of wavelength bands were selected, which included detection and reference bands appropriate for use in prototype systems. Each had two detection bands and one reference band. The 339nm band set covered one of the strongest formaldehyde absorption peaks but all three channels could not be covered by a single LED source.

This was not the case for the 353nm band set, but did not include such strong absorption peaks. Each set was selected to require only one LED and filter type. The 353nm band set was preferable as it both the selectivity and low complexity aims outlined in Chapter 1. Chapter 8 and Chapter 9 describe the systems that made use of these findings.

4.5. References

[1] C. J. Weschler, "Changes in indoor pollutants since the 1950s," *Atmospheric Enviroment,* vol. 43, pp. 153-169, 2009.

[2] A. Wisthaler, G. Tamas, D. P. Wyon, P. Strom-Tejsen, D. B. J. Space, A. Hansel, T. D. Mark and W. C. J., "Products of ozone-initiated chemistry in a simulated aircraft environment," *Environmental Science and Technology,* vol. 39, pp. 4824-4832, 2005.

[3] J. Nøjgaard, A. Nørgaard and P. Wolkoff, "On-line analysis of secondary ozonides from cyclohexene and D-limonene ozonolysis using atmospheric sampling townsend discharge ionization mass spectrometry," *Atmospheric Environment,* vol. 41, pp. 8345-8354, 2007.

[4] R. Pal and K. Kim, "Gas chromatographic approach for the determination of carbonyl compounds in ambient air," *Microchemical Journal,* vol. 90, p. 147–158, 2008.

[5] H. Bagheri, M. Ghambarian, A. Salemi and A. Es-Haghi, "Trace determination of free formaldehyde in DTP and DT vaccines and diphtheria–tetanus antigen by single drop microextraction and gas chromatography–mass spectrometry," vol. 50, p. 287–292, 2009.

[6] K. A. Ramazan, D. Syomin and B. J. Finlayson-Pitts, "The photochemical production of HONO during the heterogeneous hydrolysis of NO," *Physical Chemistry Chemical Physics,* vol. 6, pp. 3836-3843, 2004.

[7] M. Sorgel, I. Trebs, A. Serafimovich, A. Moravek, A. Held and C. Zetzsch, "Simultaneous HONO measurements in and above a forest canopy: influence of turbulent exchange on mixing ratio differences," *Atmospheric Chemistry and Physics,* vol. 11, p. 841–855, 2011.

[8] S. S. Park, J. H. Hong, J. H. Lee, Y. J. Kim, S. Y. Cho and S. J. Kim, "Investigation of nitrous acid concentration in an indoor environment using an in-situ monitoring system," *Atmospheric Environment,* vol. 42, p. 6586–6596, 2008.

[9] T. Salthammer, S. Mentese and R. Marutzky, "Formaldehyde in the indoor enviroment," *Chemical Reviews,* vol. 110, p. 2536–2572, 2010.

[10] R. A. Rudel and L. J. Perovich, "Endocrine disrupting chemicals in indoor and outdoor air," *Atmospheric Environment,* vol. 43, pp. 170-181, 2009.

[11] G. J. Raw, S. K. D. Coward, V. M. Brown and D. R. Crump, "Exposure to air pollutants in English homes," *Journal of Exposure Analysis and Environmental Epidemiology,* vol. 14, p. S85–S94, 2004.

[12] F. H. Shair and K. L. Heitner, "Theoretical model for relating indoor pollutant," *Environmental Science and Technology,* vol. 8, p. 444–451, 1974.

[13] J. A. Mott, M. I. Wolfe, C. J. Alverson, C. S. Macdonald, C. R. Bailey, L. B. Ball, J. E. Moorman, J. H. Somers, D. M. Mannino and S. C. Redd, "National vehicle emissions policies and practices and declining U.S. carbon monoxide-related mortality," *JAMA-Journal of the American Medical Association,* vol. 288, p. 987–989, 1974.

[14] J. London and J. Kelly, "Global trends in total atmospheric ozone," *Science,* vol. 184, p. 987–989, 1974.

[15] P. Wolkoff, "Volatile organic compounds – sources, measurements, emissions, and the impact on indoor air quality. Indoor Air," *Indoor Air,* vol. 5, no. S3, pp. 5-73, 1995.

[16] S. K. Brown, M. R. Sim, M. J. Abramson and C. N. Gray, "Concentration of volatile organic compounds in indoor air - a review," *Indoor Air,* vol. 4, pp. 123-134, 1994.

[17] A. T. Hodgson and H. Levin, "Volatile organic compounds in indoor air: a review of concentrations measured in North America since 1990," *Lawrence Berkeley National Lab Report,* LBNL-51715, 2003.

[18] N. T. Program, Report on Carcinogens, U.S. Department of Health and Human Services, Public Health Service, Washington, DC.: 2005, 11th ed.

[19] Y. Xu and J. C. Little, "Predicting emissions of SVOCs from polymeric materials and their interaction with airborne particles," *Environmental Science and Technology,* vol. 40, p. 456–461, 2006.

[20] C. J. Weschler and W. W. Nazaroff, "Semivolatile organic compounds in indoor environments," *Atmospheric Environment,* vol. 42, p. 9018–9040, 2008.

[21] Executive Summary: ThirdExecutive Summary: Third National Report on Human Exposure to Environmental Chemicals, Atlanta, GA: CDC (Centers for Disease Control and Prevention), 2005.

[22] E. Abt, H. H. Suh, P. Catalano and P. Koutrakis, "Relative contribution of outdoor and indoor particle sources to indoor concentrations," *Environmental Science and Technology,* vol. 34, p. 3579–3587, 2000.

[23] K. Davitt, Y. K. Song, A. V. Nurmikko, S. R. Jeon, M. Gherasimova, J. Han, Y. L. Pan and R. K. Chang, "UV LED arrays for spectroscopic fingerprinting of airborne biological particles," *Current Topics in Solid State Physics,* vol. 2, no. 7, p. 2878–2881, 2005.

[24] K. Davitt, Y.-K. Song, W. R. P. III and A. V. Nurmikko, "290 and 340 nm UV LED arrays for fluorescence detection from single airborne particles," *Optics Express,* vol. 13, no. 23, pp. 9548-9555, 2005.

[25] R. Meller and G. K. Moortgat, "Temperature dependence of the absorption cross sections of formaldehyde between 223 and 323 K in the wavelength range 225-375 nm," *Journal of Geophysical Research-Atmospheres,* vol. 105, pp. 7089-7101, 2000.

[26] K. Bogumil, J. Orphal, T. Homann, S. Voigt, P. Spietz, O. C. Fleischmann, A. Vogel, M. Hartmann, H. Kromminga, H. Bovensmann, J. Frerick and J. P. Burrows, "Measurements of molecular absorption spectra with the SCIAMACHY pre-flight model: instrument characterization and reference data for atmospheric remote-sensing in the 230–2380 nm region," *Journal of Photochemistry and Photobiology A: Chemistry,* vol. 157, pp. 167-184, 2003.

[27] D. Daumont, J. Brion, J. Charbonnier and J. Malicet, "Ozone UV spectroscopy I: Absorption cross-section at room-temperature," *Journal of Atmospheric Chemistry,* vol. 15, pp. 145-155, 1992.

[28] A. C. Vandaele, C. Hermans and S. Fally, "Fourier transform measurements of SO2 absorptioncrosssections: II. Temperature dependence in the 29000–44000/cm (227–345nm) region," *Journal of Quantitative Spectroscopy & Radiative Transfer,* vol. 110, 2009.

[29] J. Stuts, E. S. Kim, U. Platt, P. Bruno, C. Perrino and A. Febo, "UV-visible absorption cross section of nitrous acid," *Journal of Geophysical Research,* vol. 105 (D11), pp. 14,585-14,592, 2000.

[30] W. Schneider and G. Moortgat, Personal communication to E. P. Röth, R. Ruhnke, G. Moortgat, R. Meller, and W. Schneider, Berichte des Forschungszentums Jülich, jül-3341, 1997.

[31] H. Plagens, R. Bröske, M. Spittler, L. Ruppert, I. Barnes and H. K. Becker, Atmospheric loss processes of hexanal. Photolysis and reaction with OH and Cl radicals, Proceedingsof the Second Workshop of the EUROTRAC-2 Subproject Chemical

Mechanism Development: Karlsruhe, Germany, GPP10-1-GPP10-4, 1998.

[32] H. R. Cooper and H. W. Melville, "The Kinetics of the Autoxidation of n-Decanal. Part I. The Mechanism of Reaction," *Journal of the Chemical Society,* pp. 1984-1993, 1951.

[33] W. Koban, J. D. Koch, R. K. Hanson and C. Schulz, "Absorption and fluorescence of toluene vapor at elevated temperatures," *Physical Chemistry Chemical Physics,* vol. 6, pp. 2940-2945, 2004.

[34] T. Etzkorn, B. Klotz, S. Sorensen, I. V. Patroescu, I. Barnes, K. H. Becker and U. Platt, "Gas-phase absorption cross sections of 24 monocyclic aromatic hydrocarbons in the UV and IR spectral ranges," *Atmospheric Environment,* vol. 33, pp. 525-540, 1999.

[35] V. S. Fihtengolts, et al., Atlas of UV Absorption Spectra of Substances Used in Synhetic Rubber Manufacture, 171: 1969.

[36] L. Lang (Editor), Absorption Spectra in the Ultraviolet and Visible Region.

[37] D. J. Clouthier and D. A. Ramsay, "The spectroscopy of formaldehyde and thioformaldehyde," *Annual Review of Physical Chemistry,* vol. 34, pp. 31-58, 1983.

[38] D. Saraga, S. Pateraki, A. Papadopoulos, C. Vasilakos and T. Maggos, "Studying the indoor air quality in three non-residential environments of different use: A museum, a printery industry and an office," *Building and Environment,* vol. 46, pp. 2333-2341, (2011).

[39] C. Y. Peng, C. H. Lan and T. J. Wu, Investigation of indoor chemical pollutants and perceived odor in an area with complaints of unpleasant odors, Building and Environment: Vol 44, 2106–2113.

[40] C. Marchand, B. Bulliot, S. Le Calve and P. Mirabel, Aldehyde measurements in indoor environments in Strasbourg (France), Atmospheric Environment: Vol 40, 1336–1345.

[41] R. J. Shaughnessy, T. J. McDaniels and C. J. Weschler, Indoor Chemistry: Ozone and Volatile Organic Compounds Found in Tobacco Smoke, Environmental Science & Technology: Vol 35, 2758-2764.

[42] P. S. S., J. H. Hong, J. H. Lee, Y. J. Kim, S. Y. Cho and S. J. Kim, "Investigation of nitrous acid concentration in an indoor environment using an in-situ monitoring system," *Atmospheric environment ,* vol. 42, p. 6586–6596, (2008).

[43] A. M. Winer, "Long pathlength differential optical absorption spectroscopy (DOAS) measurements of gaseous HONO, NO2 and HCHO in the California South coast air basin," *Research on Chemical Intermediates,* vol. 20 (3/4/5), pp. 423-445, 1994.

[44] W. Thomas, E. Hegels and S. Slijkhuis, "Detection of biomass burning combustion products in Southeast Asia from backscatter data taken by the GOME spectrometer," *Geophysical Research Letters,* vol. 25 (9), pp. 1317-1320, 1998.

[45] I. D. Smedt, J. F. Muller, T. Stavrakou, R. van der A, H. Eskes and M. V. Roozendael, "Twelve years of global observations of formaldehyde in the troposphere using GOME and SCIAMACHY sensors," *Atmospheric Chemistry and Physics,* vol. 8, p. 4947–4963, 2008.

[46] F. Wittrock, A. Richter, H. Oetjen, J. P. Burrows, M. Kanakidou, S. Myriokefalitakis, R. Volkamer, S. Beirle, U. Platt and T. Wagner, "Simultaneous global observations of glyoxal and formaldehyde from space," *Geophysical Research Letters,* vol. 33, 2006.

[47] R. Meller and G. K. Moortgat, "Temperature dependence of the absorption cross sections of formaldehyde between 223 and 323 K in the wavelength range 225-375 nm," *Journal of Geophysical Research-Atmospheres,* vol. 105, pp. 7089-7101, 2000.

Chapter 5: Spectrometers

A tool that was used extensively throughout this project was a CCD based UV spectrometer (Avantes AvaSpec-3648-USB2-SPU2). It was an important component of the evaluation system (Chapter 6), characterisation of UV light sources and filters and finally for aligning and setting up later detection systems. A detailed analysis of spectrometer performance was undertaken, characterising it as a research tool and assessing its potential as a detection device.

Two other spectrometers were used for comparison (Ocean Optics OEM S2000 and Hamamatsu TG-UV: C9404MC Mini Spectrometer z). Identified noise phenomena included source fluctuation noise, photo-response non-uniformity (PRNU), dark current noise, fixed pattern noise (FPN) and read noise. These were identified and characterised by varying light source, spectrometer settings or temperature. A number of noise limiting techniques are proposed.

5.1. CCD operation

Charge coupled devices (CCDs) are a common type of photo-detector based around generating a measureable voltage proportional to the number of incident photons over an array. They are used in a wide range of applications such as cameras and scientific and industrial light sensors as well as spectrometers. Some spectrometers use complementary metal–oxide–semiconductor (CMOS) arrays, which serve a broadly similar purpose. Spectrometers using CCD arrays tend to have a slightly faster readout and a slightly lower noise than CMOS arrays.

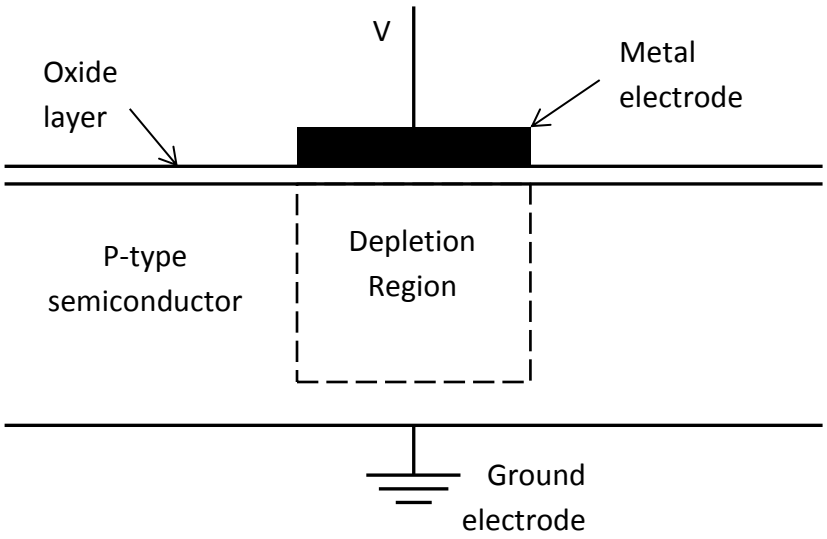

Figure 5.1: Diagram of a basic metal oxide gate of a CCD. Photoelectrons are collected in the depletion region and can then be transferred between electron wells by varying the control voltage (V).

A diagram of a basic CCD is shown in Figure 5.1, although devices may differ in detail. Incident photons strike the depletion region which is a p-type semiconductor. If a photon's energy is greater than the semiconductor band gap and it is absorbed, it creates an electron-hole pair. In this example the electron remains in the depletion region while the hole is removed by the ground electrode. The total number of photoelectrons that can be held in the depletion region is dependent on it dimensions and material and is known as the electron well capacity.

The second stage of CCD operation is transfer of charge across electron wells. The purpose is to collect charges from multiple pixels to be measured. Charge is transferred from well to well by manipulating their control voltages and it is this coupling of charge that gives the CCD its name [1]. The coupling architecture depends on the layout of the array.

The final stage of CCD operation is conversion of charge into a measurable voltage. This is carried out by a floating diode acting as a capacitor. It produces a voltage proportional to the CCD charge as described by Equation (5.1):

$$V = \frac{N_e G_{on}}{C} \tag{5.1}$$

where V is the voltage, N_e is the number of electrons, G_{on} is the on-chip amplifier gain, and C is the floating diode capacitance. CCDs are typically connected to further electronics that amplify the voltage and digitally encode it.

The total number of photoelectrons collected by a CCD pixel by a given incident intensity over a given time is described by Equation (5.2) [1]:

$$n_{pe} = A_D t_{int} R_e(\lambda) I(\lambda) \tag{5.2}$$

where A_D is the area of the pixel, t_{int} is the integration time and R_e is the spectral responsivity of the CCD pixel.

5.2. Spectrometer selection

A comparison of available spectrometers was carried out in order to decide which was the most appropriate for use in this project. A spectral range of at least 200 – 400nm was desired as it covered the formaldehyde spectrum as well as most of the indoor gases that interfered with it (see Chapter 4).

The UV formaldehyde absorption spectrum showed some fine peaks on the scale of about 0.04nm and it was desirable to be able to have a spectral resolution that could distinguish them. Also a CCD detector array was preferred as, while CMOS arrays appeared to have generally faster readouts, CCDs tended to have lower noise.

Table 5.1: Summary of UV spectrometers considered for preliminary system.

Spectrometer	Spectral range (nm)	Resolution (nm)	Sensor	Pixels	Bit Res	Stray light	Interface	Cost
Hamamatsu								
C10082CA	200-800	6	CCD	2048	16 bit	0.05%	USB	?
C10082CAH	200-800	1	CCD	2048	16 bit	0.05%	USB	?
C10082MD	200-800	6	CMOS	1024	16 bit	0.03%	USB	?
C9404CA	200-400	3	CCD	1024	16 bit	0.03%	USB	?
C9404CAH	200-400	1	CCD	1024	16 bit	0.03%	USB	£3,580
C9404MC	200-400	3	CMOS	512	16 bit	0.03%	USB	?
Ocean Optics								
Maya2000 Pro	175-1100	0.035	CCD	2048	116 bit	?	USB	$5,800
USB4000	200-1100	0.3-10	CCD	3648	16 bit	<0.1%	USB or RS232	$2,540
USB4000-FL	200-1100	10	CCD	3648	16 bit	<0.05%	USB or RS233	$2,887
USB2000-UV-VIS	200-850	1.5	CCD		24 bit	<0.1%	USB	$3,160
Spectronic devis								
Unispec CCD	200-1100	'high'	CCD	2048	12 bit	<0.1%	USB, PP or RS232	$1,500
Unispec PDA	190-1100	'high'	PD	1024	12 or 16 bit	<0.1%	USB, PP or RS233	$1,500
CRO-MMS UV VIS I	190-720	7	?	'low'	12 or 16 bit	<0.1%	USB, PP or RS234	£1,900
CRO-MMS (UV)	190-400	3	?	'low'	12 or 16 bit	<0.1%	USB, PP RS235	£1,900
Avantes								
Avaspec-2048-USBSPU2	200-450	0.1	CCD	2048	14 bit	<0.1%	USB	£2,889
Avaspec-3648-USB2-SPU2	**200-450**	**0.01**	**CCD**	**3648**	**16 bit**	**<0.04%**	**USB**	**£3,079**
Horiba Scientific								
VS140	190-800	2.3	CCD	3864	?	0.025%	USB	£3,182

Table 5.1 is the table used for selecting the spectrometer. The final decision made was to use the Avaspec-3648-USB2-SPU2 UV spectrometer made by Avantes BV and bought from Knight Photonics Ltd. This spectrometer has a better spectral range than required and one of the best spectral resolutions. It uses a CCD detector with better-

than-average pixel resolution and bit rate. It also came with the option of 'ultra-low stray light', which allowed the stray light to be decreased from 0.1% to 0.04%.

5.3. Spectrometers used

The AvaSpec spectrometer (Avantes AvaSpec-3648-USB2-SPU2) [2] was the main spectrometer used in this project. The UV absorption spectrum of formaldehyde lies between 220nm – 380nm [3]. It was therefore necessary for the spectrometer to cover this range. Spectral resolution was also important for resolving formaldehyde sub-nanometre spectral features. Finally, good noise performance was necessary for improving the limit of detection.

The Ocean Optics spectrometer (Ocean Optics OEM S2000) [4] was used for comparison as it was one of the most commonly used laboratory spectrometers at the time of writing. However it had a spectral range in the visible and near IR and so was not appropriate for making UV spectral measurements. The Hamamatsu spectrometer (Hammamatsu TG-UV: C9404MC Mini Spectrometer z) was a potential contender with the AvaSpec spectrometer for use in this project, and came on a short term loan from the manufacturer. Table 5.2 shows details of the three spectrometers as quoted by the manufacturers.

Table 5.2: Details of the spectrometers given by manufacturers.

	AvaSpec-3648-USB2-SPU2	**Ocean Optics OEM S2000**	**Hamamatsu TG-UV: C9404MC**
Spectral range	200 – 400nm	514 – 1,177nm	200 – 400nm
Spectral resolution	0.083nm	0.27 – 0.38nm	3nm
Detector	CCD	CCD	CCD
Pixels	3,648 pixels	2,048 pixels	512 pixels
Bit resolution	16 bits	16 bits	16 bits
Signal to noise	350:1	250:1	No details given
Dark noise	40 counts	No details given	No details given
Stray light	0.04%	No details given	0.03%

All three spectrometers were designed for use with optical fibres and had SMA optical fibre inputs. For this project they were all used with the same UV resistant optical fibre (Avantes FC-UV600-0.5-SR solarisation resistant optical fibre for deep UV). The fibre was 0.5m long and had a core radius of 600µm. It had an SMA connector at both ends and a minimum recommended bend radius of 0.36m.

A photograph of the AvaSpec spectrometer is shown in Figure 5.2 showing the input optical fibre. The spectrometer was controlled from a laptop computer, where measurement parameters were set by the Avasoft software package (Avantes Avasoft 7.5.3 USB1/USB2 Version 4.0). A diagram of the internal optics of the AvaSpec spectrometer is shown in Figure 5.3. It used the classical Czerny-Turner optical design [5] [6].

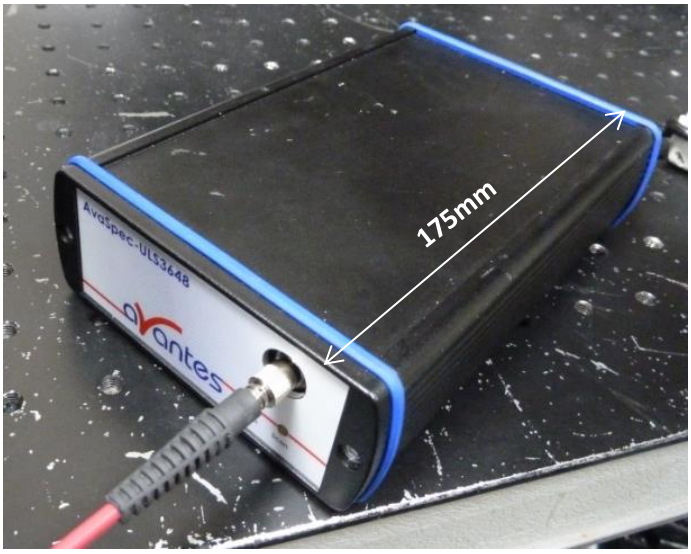

Figure 5.2: Photographs of the AvaSpec UV spectrometer (Avantes AvaSpec-3648-USB2-SPU2) with its input optical fibre.

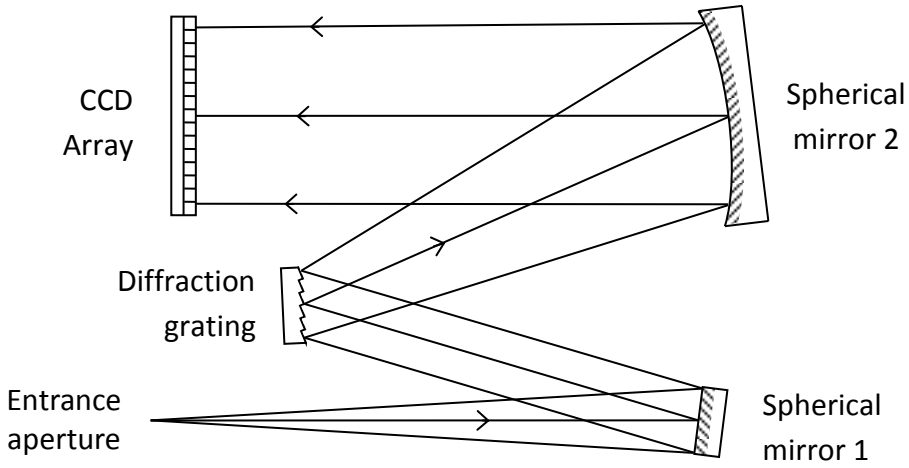

Figure 5.3: Diagram of the internal optics of the AvaSpec spectrometer (classical Czerny-Turner design). Light entered the spectrometer at the entrance aperture and was collimated by mirror 1. It was diffracted by the grating and directed by mirror 2 onto the CCD array.

In this design, light from the sample enters the spectrometer through the optical fibre. Spherical mirror 1 collimates it onto the diffraction grating. Diffracted light then falls incident onto Spherical mirror 2 which directs it onto the CCD array. Each pixel received photons from only a narrow band of wavelengths. The profile of the spectrum can be found by the intensity of signal generated by the CCD pixels.

The Ocean Optics spectrometer had a spectral range of 514 – 1,177nm (visible and near IR). A photograph is shown in Figure 5.4 and a diagram of the internal optics in Figure 5.5. It used the crossed-beam Czerny-Turner optical design [6]. The crossed Czerny-Turner design permits a longer optical path within a given size of instrument whilst the standard Czerny-Turner design reduces the angle of incidence between elements.

Figure 5.4: Photographs of an Ocean Optics spectrometer (Ocean Optics OEM S2000).

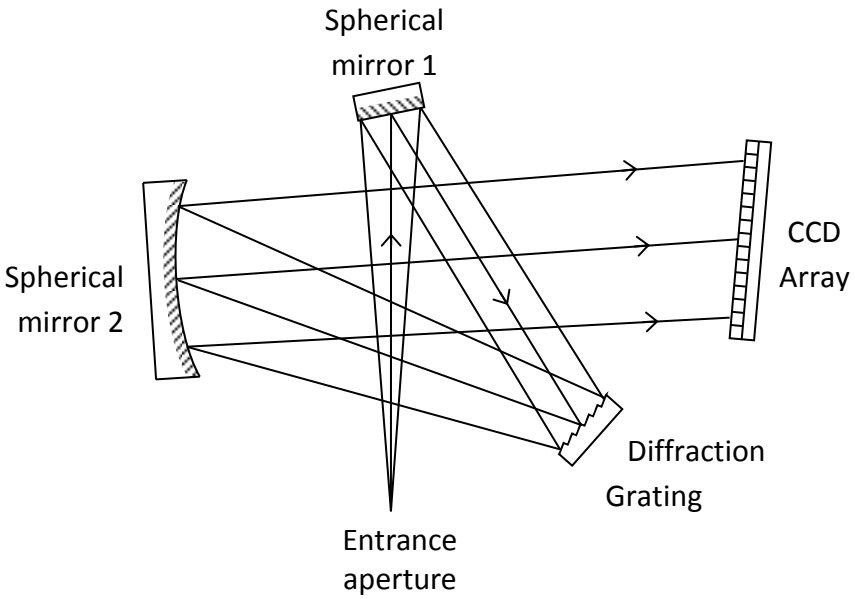

Figure 5.5: Diagram of the internal optics of the Ocean Optics spectrometer (Czerny-Turner optical design). Light entered the spectrometer at the entrance aperture and was collimated by mirror 1. It was then diffracted by the grating and directed by mirror 2 onto the CCD array.
Finally a photograph of the Hamamatsu spectrometer is shown in Figure 5.6, taken

from the supplier's website, and a diagram of its internal optics is shown in Figure 5.7. Unlike the other two spectrometers, this device uses transmissive rather than reflective optics. Transmissive optics allows deviations in the angle of the optical axis to be limited but can be subject to chromatic aberration effects. Light from the optical

fibre is collimated into the transmission grating by the first lens. Dispersed light is then directed onto the CCD array by the second lens.

Figure 5.6: Photograph of the Hamamatsu spectrometer (Hamamatsu TG-UV: C9404MC Mini Spectrometer z), taken from the supplier's website. The SMA connection where input fibre is attached can be seen at the front.

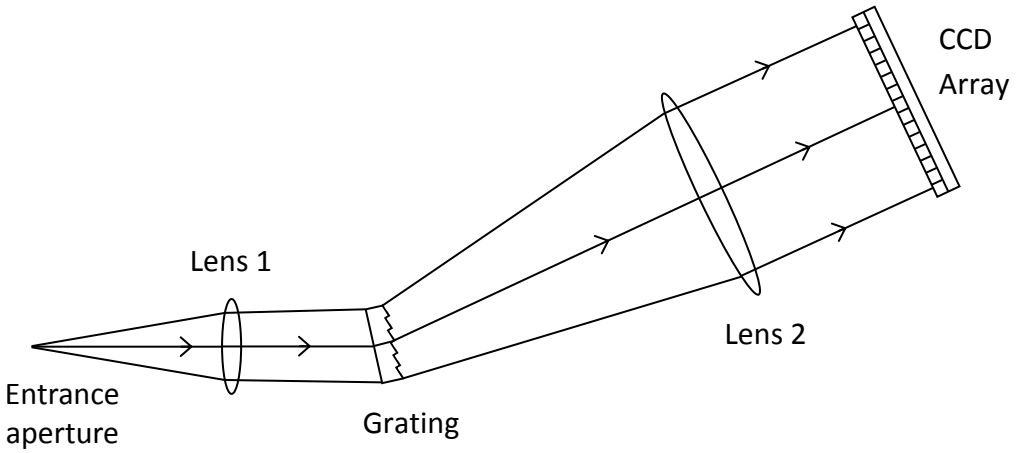

Figure 5.7: Diagram of the internal optics of the Hamamatsu spectrometer. Light entered the spectrometer at the entrance aperture and was collimated by the first lens. It was then dispersed by the transmission grating and directed by the second lens onto the CCD array.

5.4. Light sources

Two different light sources were used for characterising the spectrometers. The first was a broad spectrum deuterium UV lamp. The second was a narrow spectrum UV LED.

5.4.1. UV Lamp

The UV lamp (Hamamatsu L10671 UV-Vis light source, incorporating an S2D2 deuterium lamp) [7] has a spectral range of 200nm to 1,600nm. The lamp was quoted as having a drift of ±0.25nm and a fluctuation of 0.004% (4×10^{-5}A.U.). Figure 5.8 shows photographs of A) the UV Lamp and B) a metal box designed to contain it and protect it from damage.

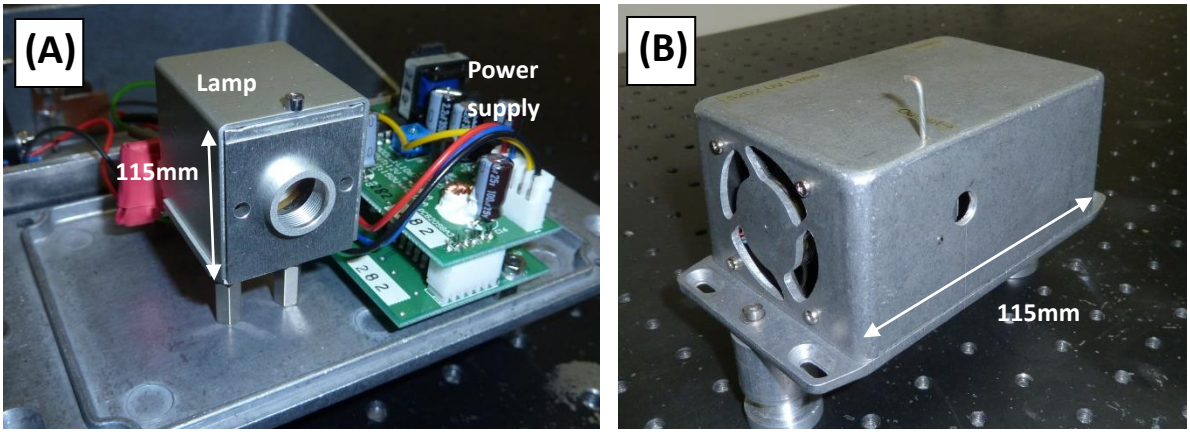

Figure 5.8: Photograph of the UV Lamp A) open and B) closed showing the protective box.

The lamp required ventilation for heat dissipation, so holes were cut in the box and a fan was included. A shutter was also included as the lamp took around 20s to warm up. The total output power that left the aperture of the box was measured as 0.1mW with the use of a photodiode (the photodiode's responsivity was not constant with wavelength so a middle wavelength was used for calculations).

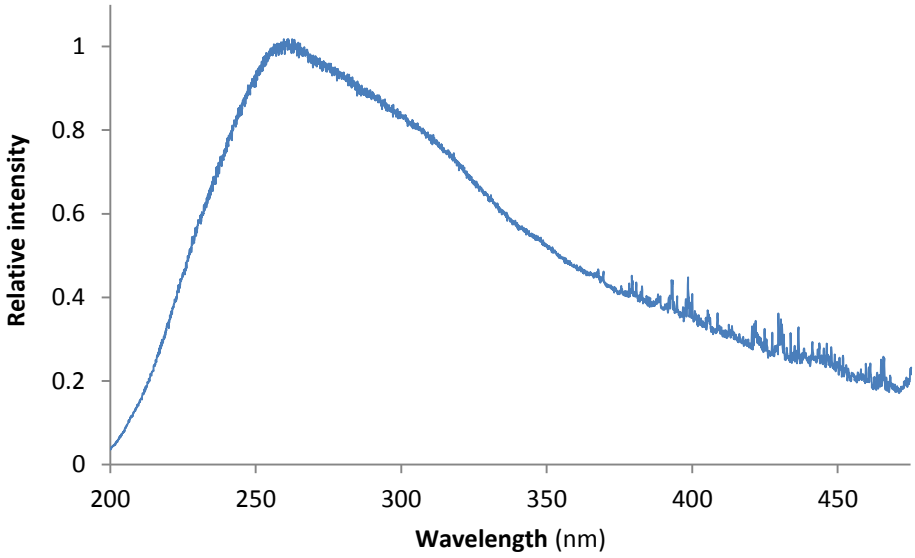

Figure 5.9: Graph of the relative intensity output of the UV lamp, measured by the AvaSpec spectrometer.

The spectral distribution of intensity of the UV lamp, as measured by the AvaSpec spectrometer, is given in Figure 5.9. It is not immediately clear whether the spectrum shown in Figure 5.9 is a true representation of the lamp output or is affected by the CCD responsivity. From a single source and a single measurement device it is difficult to distinguish features originating from the source from features originating from the measurement.

Figure 5.10 shows an image of typical spectral distribution as given by the manufacturer [7] as raw data was not available. There is reasonably good correspondence between Figure 5.9 and Figure 5.10 between around 260 and 400nm. However, below 260nm the manufacturer's data continues to increase whereas data measured in this project decreases. This was suspected to be due to decreased spectrometer responsivity. It was also suspected that the fine structure seen on top of the main curve is due to the spectrometer photo-response non-uniformity (see Chapter 5).

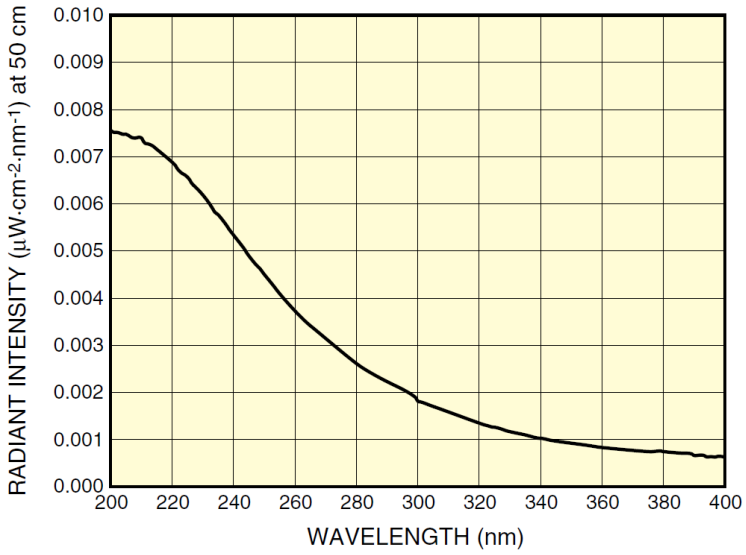

Figure 5.10: Image of the typical intensity spectrum of the UV lamp as given by the manufacturer. Raw data was not available.

5.4.2. 340nm UV LEDs

The 340nm UV LED (SETi UVTOP335TO39BL) [8] had a quoted central wavelength of 340nm and an FWHM of 15nm. It came with an internal parabolic mirror and a front ball lens with a 3.18mm radius. It had a focal spot at a quoted distance between 15 and 20mm and a spatial divergence of approximately 6°. The ball lens option was selected as it had a tight spatial divergence which allowed for minimum loss of light through the system.

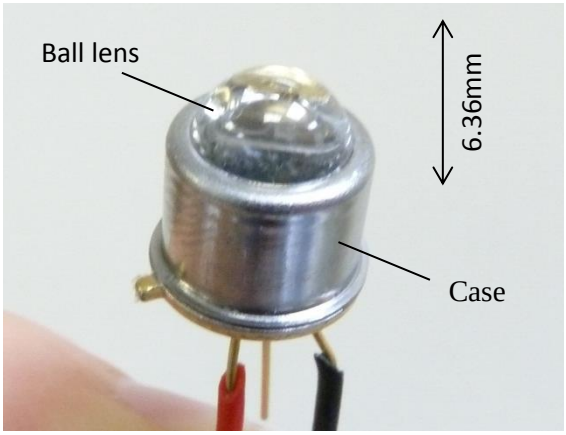

Figure 5.11: Photograph of the 340nm LED showing the casing and the ball lens.

Figure 5.11 is a photograph of the 340nm LED showing the casing and the ball lens. During preliminary testing a connection wire of one of the 340nm LED was burned out. Therefore the case and the ball lens were removed to examine the element and internal layout. Figure 5.12 shows some microscope images of the LED element.

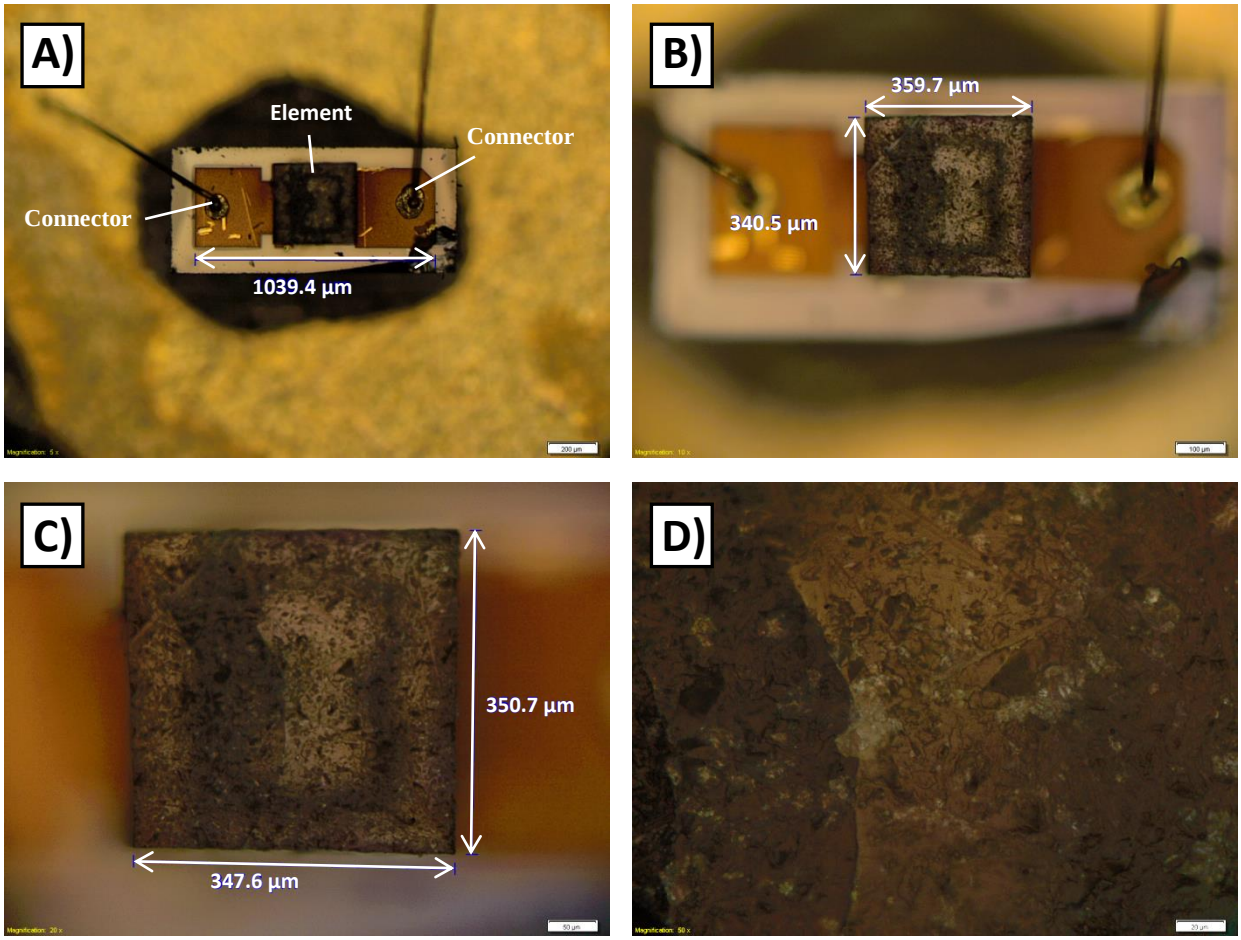

Figure 5.12: Microscope images of the LED element and mounting magnified at **A)** 5 times, **B)** 10 times, **C)** 20 times and **D)** 50 times. The element of this LED is not perfectly square, as shown in the scales of images B) and C).

Using measurements taken from the opened LED and details from the manufacture, a computer model of the LED was created using the Zemax optical design program (Figure 5.13). It shows the position of the LED element, parabolic mirror and front ball lens; and some example rays of the LED output were also generated. This model was used for optimising the setup of the rest of the system.

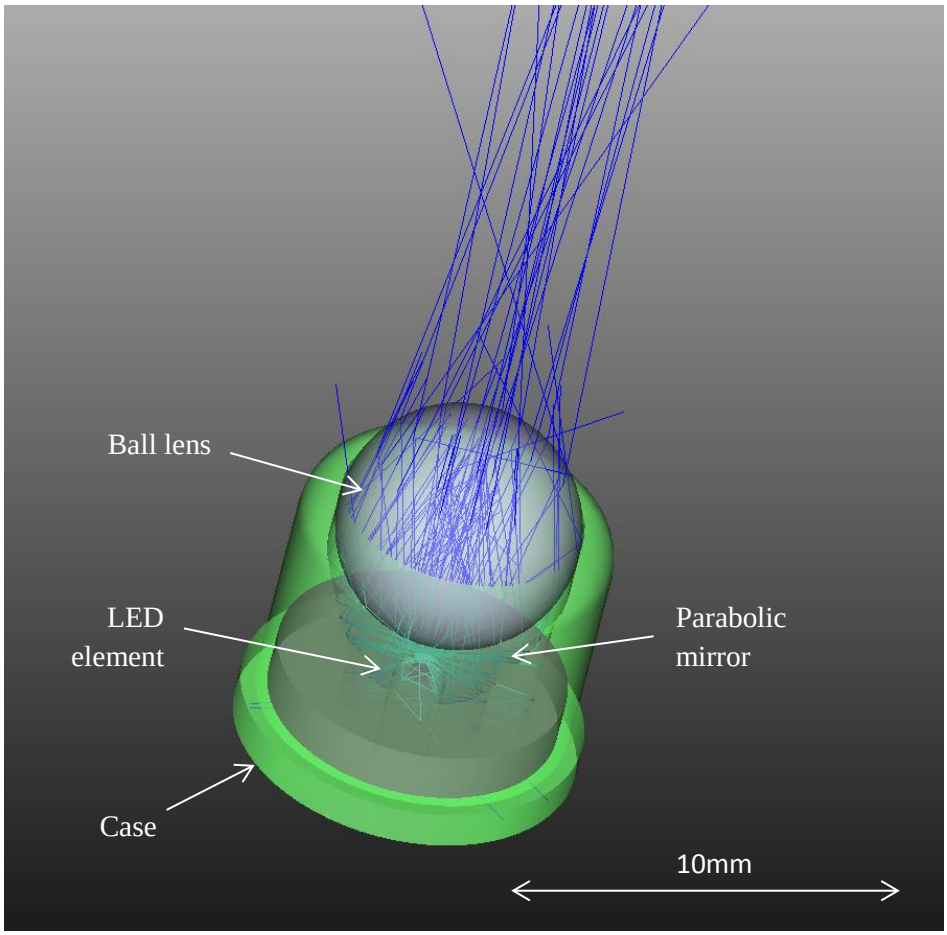

Figure 5.13: Zemax model of the UV LED and its optical output (non-sequential ray tracing). Inside the case is the LED element and an approximately parabolic mirror finishing with the ball lens. Some example output rays are also shown.

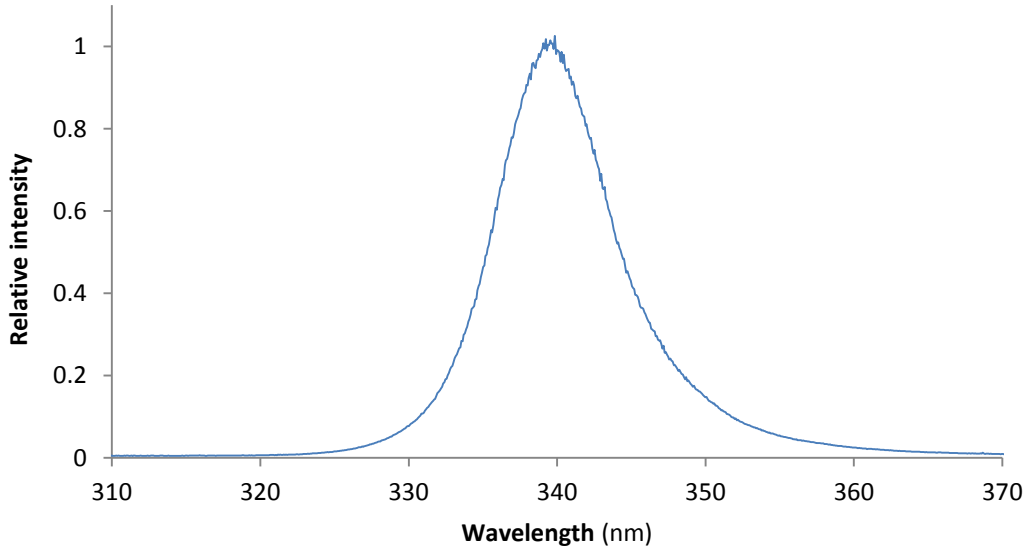

Figure 5.14: Graph of the relative intensity spectrum of the 340nm LED as measured by the AvaSpec UV spectrometer.

The intensity spectrum of the 340nm LED was measured with the AvaSpec spectrometer and the results are shown in Figure 5.14. The peak was found to be at 339.7nm, very close to the quoted value. The FWHM was found to be 9.2nm, significantly lower than the quoted value of 15nm.

5.4.3. Nd:YAG laser

A Nd:YAG laser (Spectra Physics GCR Series Nd:YAG laser) [9] was used as a narrow spectrum source to test spectral resolution of the spectrometers. This is described in Section 5.4.2. A photograph is shown in Figure 5.15 . The laser had a Q-switched laser pulse with a frequency of 10Hz. Pulses had an 8ns duration, a pulse energy of 2.5J and a peak output wavelength of 266nm. The exact line width was not known but was found to be no greater than 0.14nm by the AvaSpec spectrometer (see section 5.4.2).

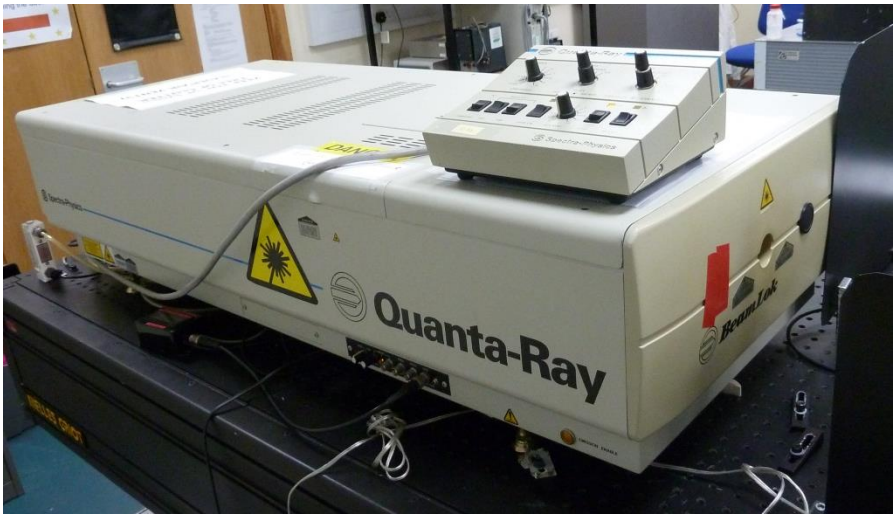

Figure 5.15: Photograph of the Nd:YAG laser. The box on the top controls the laser output.

5.5. Performance

The performance of a spectrometer is generally given in terms of its spectral range, spectral resolution and noise stability. Spectral range is defined as the limits of wavelengths which can be reliably detected by the spectrometer, and spectral

resolution as the range of each spectral bin. Spectrometer noise and stability have rather more involved definitions.

In this chapter details are given of a thorough, quantitative analysis of the performance of the AvaSpec UV spectrometer. Comparisons with the other two spectrometers are given where possible. Source shot noise and fluctuation noise were also analysed as they were thought likely to be significant in any spectrometry system.

5.5.1. Spectral range

The spectral range of a spectrometer describes the range of wavelengths it will respond to and detect. It describes the range of wavelengths angled onto the photodiode array by the optical grating. Other wavelengths will either fail to fall incident onto the array or fail to be diffracted or transmitted by the grating. In the ideal case, wavelengths outside this range will not affect the spectrometer's output.

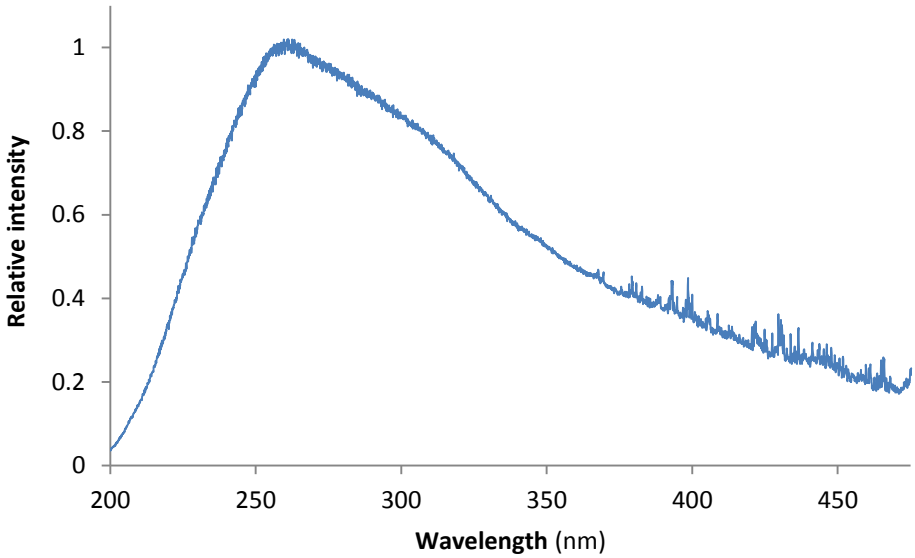

Figure 5.16: Spectral distribution of the UV lamp as measured by the AvaSpec spectrometer.

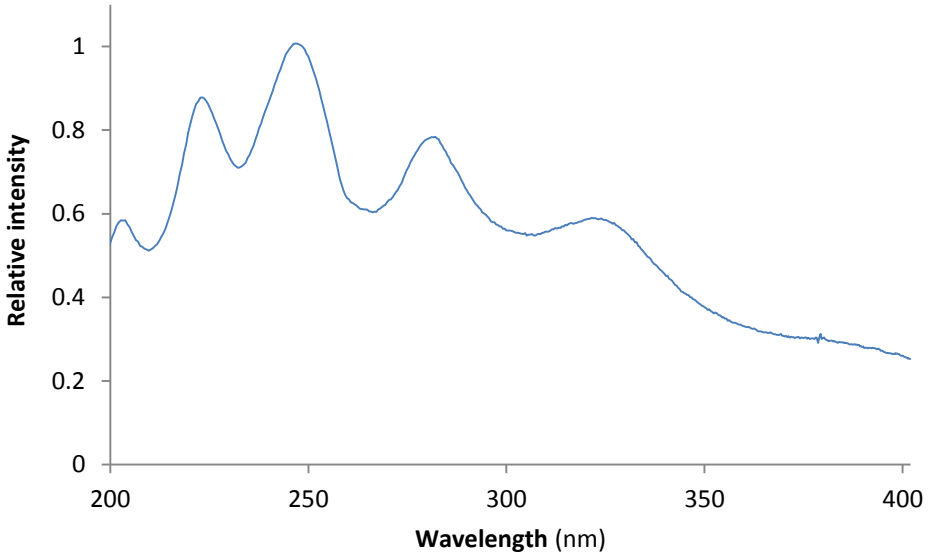

Figure 5.17: Spectral distribution of the UV lamp as measured by the Hamamatsu spectrometer.

Figure 5.16 and Figure 5.17 show the output of the AvaSpec and Hamamatsu spectrometers in response to the UV lamp. This gives a spectral range for the AvaSpec spectrometer of 200 – 475nm, slightly wider than the quoted range. The spectral range of the Hamamatsu spectrometer was 200 – 400nm, in keeping with the quoted values. It should be noted that these ranges assume that the single output was representative of the true incident wavelength.

It is noticeable that the two spectrometers gave a different output spectrum for the UV lamp, and both are different from the spectral distribution reported by the manufacturer (discussed in Chapter 6). This is because detector's responsivity, as a function of wavelength, is not identical from spectrometer to spectrometer as described in more detail in Section 5.4.6.

5.5.2. Spectral resolution

The spectral resolution of a spectrometer is the minimum separation of spectral features that can be resolved. This is dependent on the range of wavelengths reaching each detector array element. Depending on the geometry of the internal optics,

spectral resolution will not always be constant across the detectable spectrum. There is often a trade-off between spectral range and spectral resolution, as both are limited by the number of detector array elements.

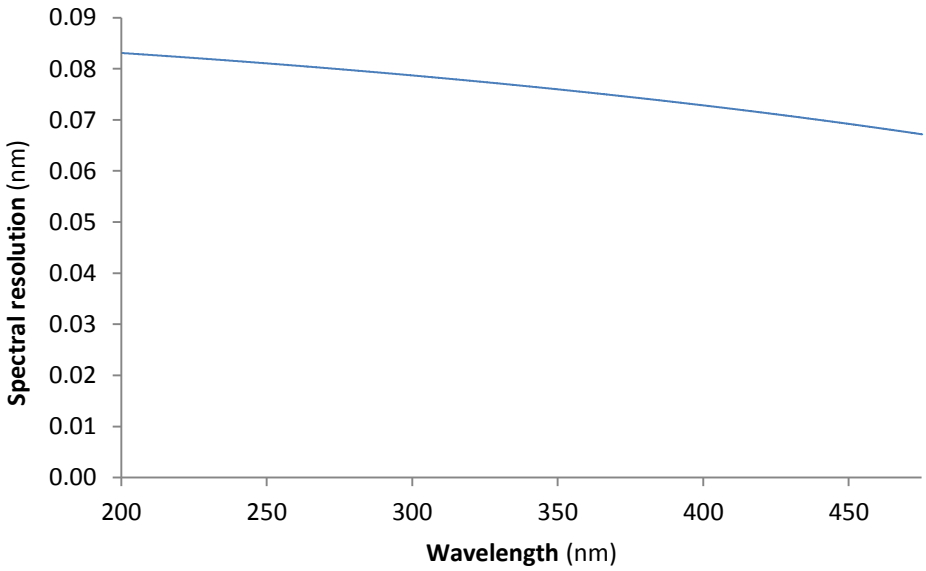

Figure 5.18: Array precision of the AvaSpec spectrometer across wavelength. It varies between 0.083nm and 0.067nm. The quoted value was 0.083nm

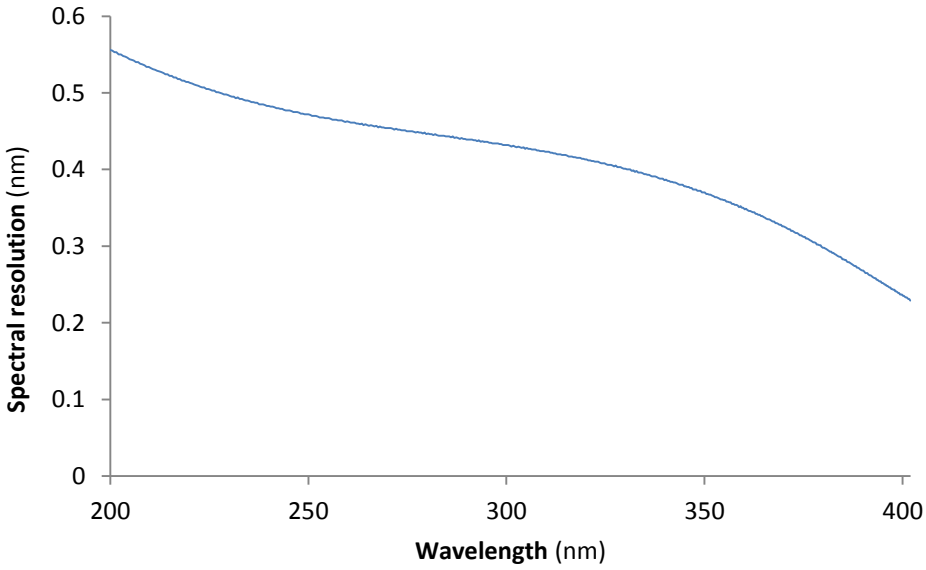

Figure 5.19: Array precision of the Hamamatsu spectrometer across wavelength. It varies between 0.55nm and 0.24nm

The array precisions of the AvaSpec and Hamamatsu spectrometers are given in Figure 5.18 and Figure 5.19. This is the difference in reported wavelength between one pixel and the next across the array and is related to spectral resolution. The variations come from the spectrometers' internal optics giving a change in angular and spectral distribution across the detector array.

The array precision of the AvaSpec spectrometer varies between 0.083nm and 0.067nm, the first of which corresponds to the quoted spectral resolution of 0.083nm. The array precision of the Hamamatsu spectrometer varies between 0.233nm and 0.558nm, much smaller than the quoted spectral resolution of 3nm.

Spectral resolution may not be as low as the array precision for a number of reasons. Resolution may be limited by optics resulting in light spreading across several pixels. Stray light effects can lead to photons hitting the "wrong" detector element. Mis-positioning of the array may lead to a shift in reported wavelength, moving the spectral range up or down. These effects can be tested with a light source of known wavelength.

The spectral resolution was tested using the Nd:YAG laser. The laser had a known central wavelength and approximately known spectral distribution, allowing it to determine whether the spectrometers were giving realistic values. A proportion of the laser light was launched into the optical fibre of the AvaSpec and Hamamatsu spectrometers, taking care to keep the intensity below saturation levels.

The results are shown in Figure 5.20. Both spectrometers show a peak in signal at 266nm, as expected for the Nd:YAG laser. The AvaSpec spectrometer shows a minimum spectral resolution of 0.14nm, a little above the quoted value. The Hamamatsu spectrometer shows a much wider spectral distribution of 1.85nm FWHM. This demonstrates a higher spectral resolution for this spectrometer, although still lower than the quoted 3nm. No spectral width information was available from the laser manufacturer.

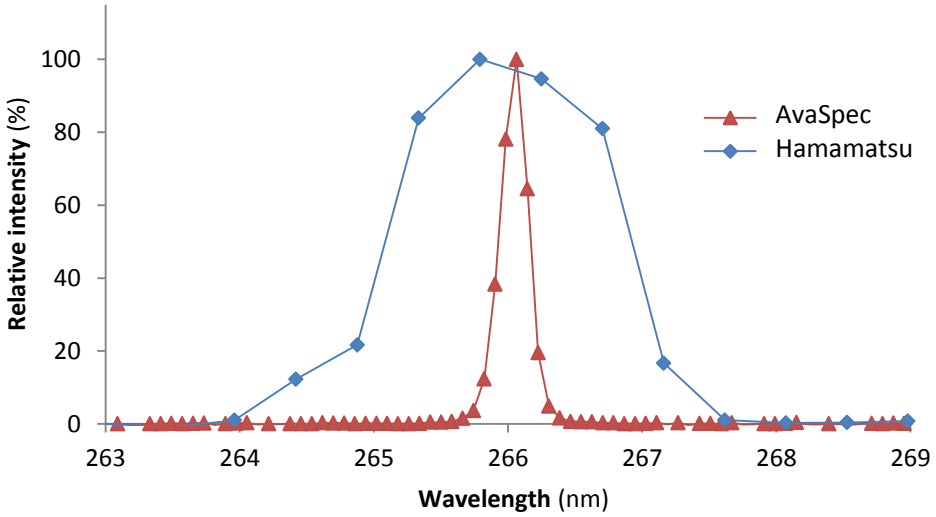

Figure 5.20: Graphs of the Nd:YAG laser spectrum taken by the AvaSpec spectrometer (Red) and the Hamamatsu spectrometry (Blue). The AvaSpec spectrometer measured a FWHM of 0.14nm, larger than its quoted spectral resolution of 0.083nm. The Hamamatsu spectrometer measured a FWHM of 1.85nm, smaller than its quoted resolution of 3nm.

5.5.3. Shot noise and source fluctuation noise

Shot noise is caused by statistical variability in the rate of arrival of photons at the detector due to the quantised nature of light. Since photons arrive from their source independently of one another, shot noise is white noise and follows a Poisson distribution. It is described by the Schottky formula, Equation (5.3) [10] [11]:

$$\langle i_{sh} \rangle = \sqrt{2 q_e i_{pe} \Delta f_e} \tag{5.3}$$

where i_{sh} is the shot noise current, q_e is the charge on the electron, i_{pe} is the current caused by photoelectrons and Δf_e is the noise equivalent bandwidth. In terms of number of collected photoelectrons this can be given as:

$$\langle n_{pe} \rangle = \sqrt{2 q_e n_{pe} \Delta f_e} \tag{5.4}$$

Source fluctuation noise behaves in a similar statistical manner to shot noise, being white noise with a Poisson distribution in the rate of arrival of photons [10]. Together source fluctuation and shot noise follow the generalised Equation (5.5). Unless the

transmitted intensity is very low, source fluctuation noise tends to dominate shot noise.

$$\langle n_{f\text{-}s} \rangle \propto \sqrt{n_{pe}} \tag{5.5}$$

where $n_{f\text{-}s}$ is the combined number of electrons from source fluctuation and shot noise. The signal to noise ratio increases as the square root of signal intensity. It is not dependent on temperature and is a fundamental limit of any photon detection system. Increasing the integration time has the same effect on shot noise as increasing intensity, since the CCD chip has more time to gather photons.

The total number of electrons collected was varied to test shot noise and source fluctuation noise phenomena. Measurement time period was varied, thereby varying the number of photons arriving at the detector. Preliminary testing found that source fluctuation noise depended on the total measurement period with no observed difference between a long integration time and summation over many measurements.

The fraction of source fluctuation noise was found for the AvaSpec and Ocean Optics spectrometers using Equation (5.6):

$$\frac{\langle n_{f\text{-}s} \rangle}{\sqrt{n_{pe}}} = \frac{\mathrm{stdev}(n_{pe})}{\sqrt{\mathrm{mean}(n_{pe})}} \tag{5.6}$$

where stdev(n_{pe}) is the standard deviation of photoelectron number and mean(n_{pe}) is the mean average of photoelectron number.

Measurements were taken with an integration time of 30ms (see Section 5.4.4.) and the number of measurements averaged was changed to vary the total measurement time. Averages were taken of the values measured by all active pixels and are shown in Figure 5.21. Theoretical predictions from Equation (5.5) are included with empirically fitted proportionality factors of 1.1 for the AvaSpec spectrometer and 1.47 for the Ocean Optics spectrometer. Errors were estimated as a percentage of signal for each individual pixel before averaging across them.

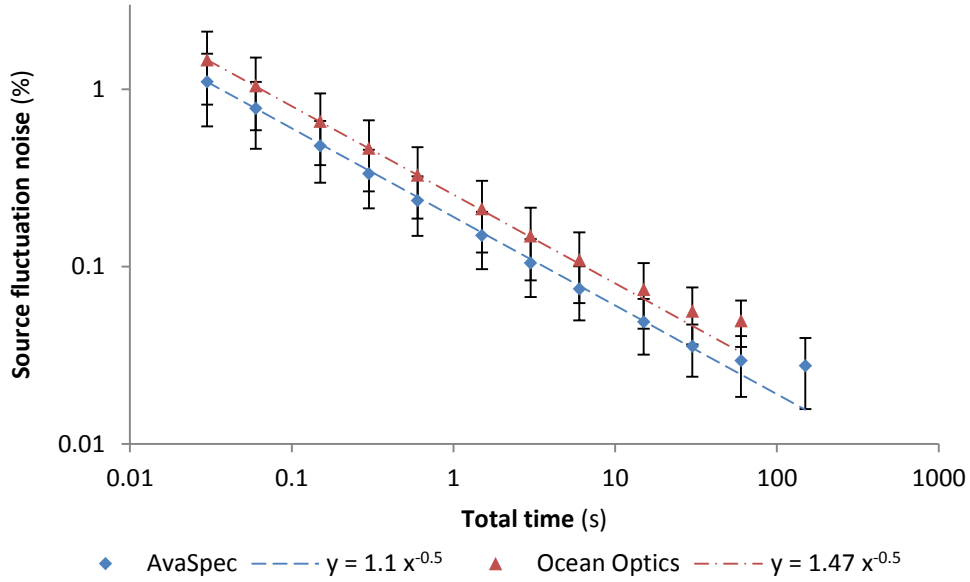

Figure 5.21: Effect of summing over multiple readings of source fluctuation noise from the two spectrometers. Theoretical prediction from Equation (5.5) are included, with scaling factors empirically to data between 0.03 and 30s.

The two spectrometers showed similar behaviour and good correspondence with theory for measurement times below 30s. For measurement times above 30s the source fluctuation noise increases above expected values. We attribute this to long-timescale drift effects (order of minutes) caused by slight temperature variations or mechanical instability. These would have been magnified by the increased measurement period, eventually dominating over Equation (5.5).

While the measurements from the two spectrometers were within one another's error bars, they maintained a systematic difference and gave different proportionality factors. In general a single source should produce the same results for different spectrometers. However the difference may have been caused by the different wavelength operational ranges of the two spectrometers.

For the purposes of this project, a total measurement time period of 30s was used as the standard for the AvaSpec spectrometer. This was because it gave the optimum source fluctuation noise performance for minimum response time. Total measurement

time period was controlled by setting the integration time and the number of averages for each measurement. The settings used are discussed in Section 5.4.4.

5.5.4. Dark current and fixed pattern noise

This section describes a number of effects which occur independently of the intensity of input light. In CCD chips, most dark current arises from thermal excitation of electrons in the semiconductor active material. It can also arise from background thermal radiation within the spectrometer, but this is probably not significant in the UV.

The number of dark current electrons affecting a given CCD element is given by [1]:

$$n_{dark} = \frac{J_D A_D t_{int}}{q} \tag{5.7}$$

where A_D is the area of the detector, t_{int} is the integration time of the spectrometer and J_D is the dark current density given by [1]:

$$J_D \approx k_B \, exp\left(-\frac{E_G}{\alpha_G k_B T}\right) \tag{5.8}$$

where E_G is the semiconductor band gap, α_G is the dark current factor for the semiconductor material ($1 \leq \alpha_G \leq 2$), k_B is the Boltzmann constant and T is temperature in Kelvin.

The intensity of background radiation is given by [12]:

$$I_{bg}(\lambda, T) = \frac{2\pi hc^2}{\lambda^5} \cdot \frac{1}{e^{hc/k_B T\lambda} - 1} \tag{5.9}$$

where h is the Planck constant and c is the free space speed of light. This is the blackbody radiation curve and tends to be strongest in the IR region. It was thought

unlikely to be a significant factor in the UV range for operation at ambient temperature. The mean dark current is constant for fixed conditions but the noise on individual readings follows a Poisson distribution. Hence, dark current noise has the same relationship with signal magnitude as shot noise, described by as Equation (5.5).

Fixed pattern noise (FPN) arises from differences in the mean dark current between pixels, generally caused by variations in the detector area or the dark current density. It does not generally vary with time, and is present irrespective of signal [1]. These variations tend to be caused by imperfections in CCD manufacture and so FPN remains constant between measurements. FPN is unique to each spectrometer, and must therefore be identified, but when this has been done it can simply be subtracted from measurements [13].

In order to characterise signal-independent noise phenomena, measurements were taken under dark conditions. Dark current was measured at a range of integration times for both spectrometers and the results are shown in Figure 5.22. For each data point counts were averaged across all pixels to control for FPN. Error bars were estimated from the standard deviations of ten measurements.

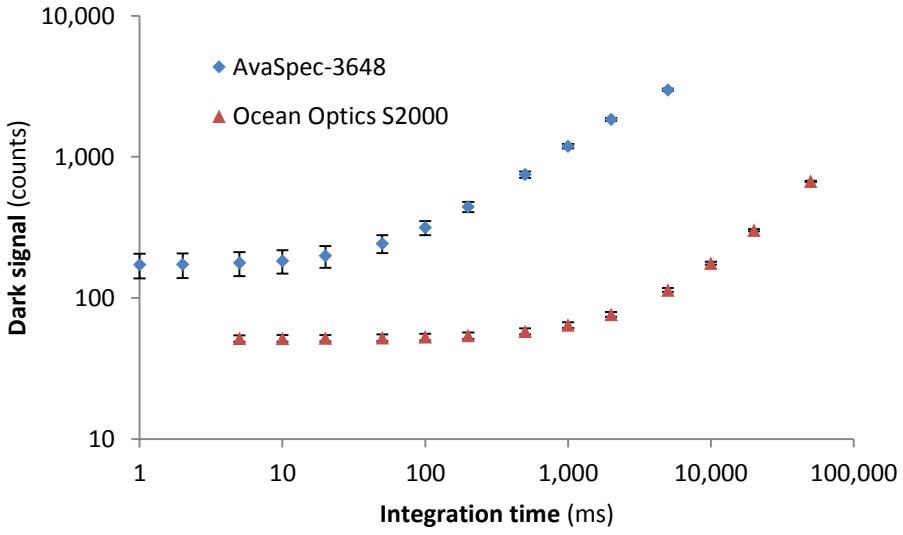

Figure 5.22: Change in average dark signal with integration time for the two spectrometers. Both spectrometers show a region where dark signal increases with integration time as expected, and a region where it remains constant, attributed to read noise

Both sets of data show a region where dark current increases with integration time as expected, because the CCD chips had more time to gather dark signal. However, for low integration times there is a region where dark current is constant. This was attributed to read noise, which is independent of integration time (see Section 5.4.5). The minimum dark current level was 170±30 counts for the AvaSpec-3648 and 52±3 counts for the Ocean Optics S2000.

For the purposes of this project the standard integration time period for the AvaSpec spectrometer was set at 30ms. Longer periods would cause increases in dark signal while read noise would dominate at shorter periods. With the 30s total measurement period stated earlier, this required averages to be taken over 1,000 measurements.

Dark current noise was tested in the same way as for shot noise and source fluctuation noise, by varying the total measurement time and thereby the photons collected. The results for the AvaSpec and Ocean Optics spectrometers are shown in Figure 5.23. Theoretical predictions from Equation (5.5) are included with empirically fitted proportionality factors of 35 for the AvaSpec spectrometer and 2.87 for the Ocean Optics spectrometer. Errors were found as the standard deviation between pixels.

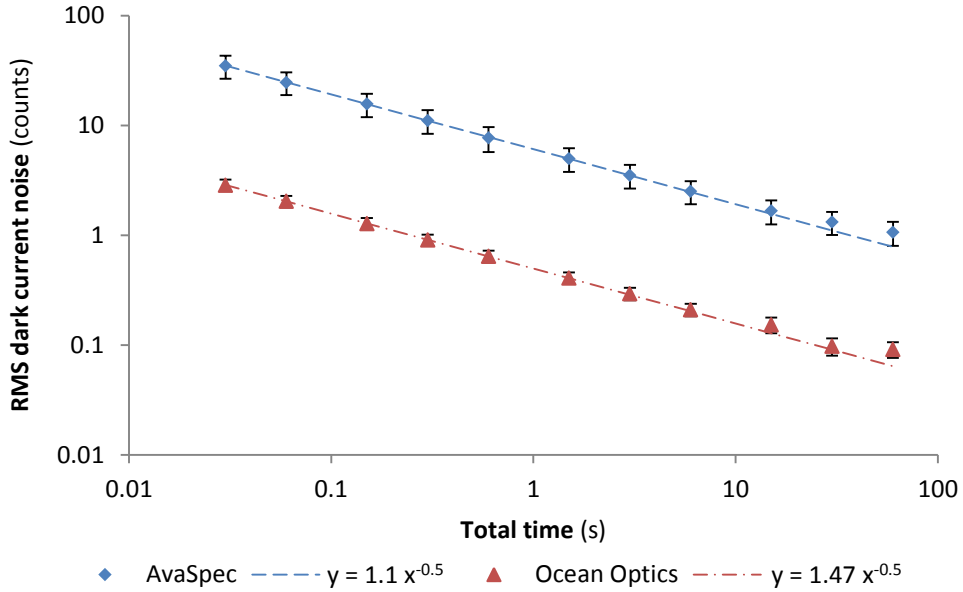

Figure 5.23: Effect of averaging over multiple measurements on dark current noise from the two spectrometers. Theoretical predictions from Equation (5.5) are included, with scaling factors empirically to data between 0.03 and 30s ($y = 35\ x^{-0.5}$ for the AvaSpec-3648 and $y = 2.87\ x^{-0.5}$ for the Ocean Optics S2000).

The behaviour of the two spectrometers was very similar to that seen for shot noise and source fluctuation noise. Both spectrometers showed good correspondence with theory for measurement times below 30s. As before, noise values for measurement times above 30s increase above theoretical values, attributed to drift effects. This supports the decision to use 30ms as the standard measurement time for this project.

The FPN for the two spectrometers is presented in Figure 5.24 and Figure 5.25, taken under dark conditions. The patterns were very repeatable, the AvaSpec-3648 and the Ocean Optics S2000 having RMS variation between measurements of 0.5% and 0.15% respectively. The AvaSpec-3648 spectrometer data shows three statistically significant peaks at 278nm, 369nm and 409nm. They remained when signal was introduced although were quickly dominated by other noise phenomena at higher intensities. They may have been due to stray light or possibly some electronic source.

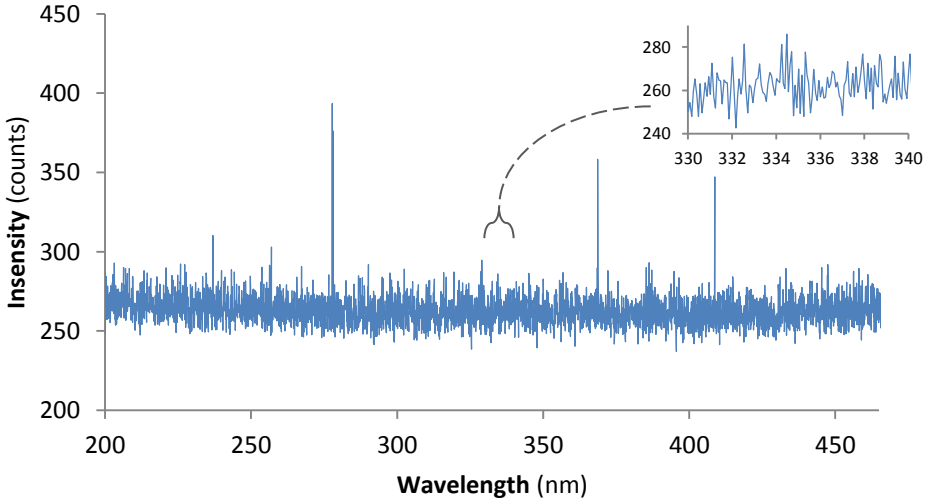

Figure 5.24: AvaSpec-3648 FPN measured with an integration time of 30ms and averaged over 10,000 readings. Between 200 and 450nm the FPN had an average value of 263 counts and an RMS variation of 9.4 counts. Outliers can be seen at 278nm, 369nm and 409nm. Average RMS variation between measurements was 0.5%. The insert shows a typical section of the data at full resolution.

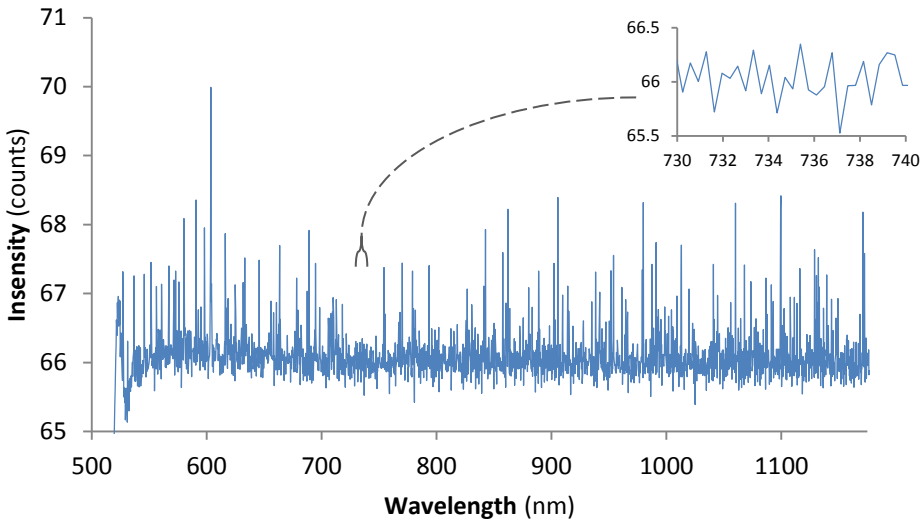

Figure 5.25: Ocean Optics S2000 FPN measured with an integration time of 30ms and averaged over 10,000 readings. Between 514 and 1,177nm the FPN had an average value of 66 counts and an RMS variation of 0.38 counts. Average RMS variation between measurements is 0.15%. The insert shows a typical section of the data at full resolution.

The effect of temperature on FPN was found by placing the spectrometer in an environmental oven at a series of elevated temperatures. The entrance aperture was covered to provide dark conditions. At least 1 hour was allowed between temperature changes to allow the system to reach thermal equilibrium. The test was run several times with different integration times, varying the number of averages in order to keep the time period of each measurement the same. The FPN variation was then determined as the RMS deviation from the mean across the spectral range of each spectrometer.

A sample of the results from the AvaSpec spectrometer is shown in Figure 5.26. They did not behave as expected. According to Equation (5.7) and Equation (5.8), the dark current of each pixel should increase with temperature, resulting in an increase in both magnitude and position of FPN variations on the intensity axis. As can be seen in Figure 5.26, the position of the FPN decreased with increasing temperature.

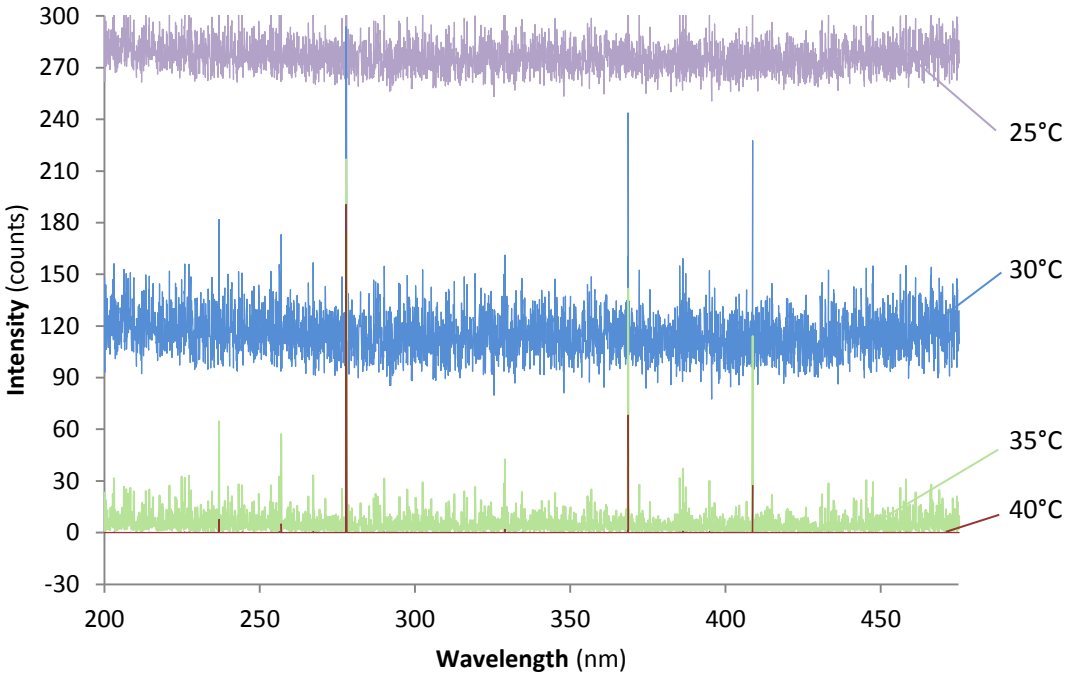

Figure 5.26: Sample FPN of the AvaSpec spectrometer measured at different temperatures. The position decreases with increasing temperature instead of increasing as expected, attributed to a voltage offset on the detector. Not all of the 25°C data is shown in this graph.

In the extreme case, this decreases the signal to zero counts, at which point it could not be measured. Some of the data taken at 35°C can be seen to fall to zero counts in Figure 5.26. At 40°C, only the highest values can be measured above zero counts. In a private conversation with the manufacturer, this behaviour was identified as a voltage offset on the detector [14] from which the signal baseline decreased with increasing temperature.

Data showing a significant number of points at zero counts was removed from the subsequent analysis. Figure 5.27 and Figure 5.28 show that the FPN variation of the two spectrometers increased with temperature as expected. Results from a range of integration times are included, demonstrating a variation in FPN as expected. In both spectrometers the voltage offset dominated dark current for high temperature and low integration time measurements, and meaningful FPN variation figures could not be found.

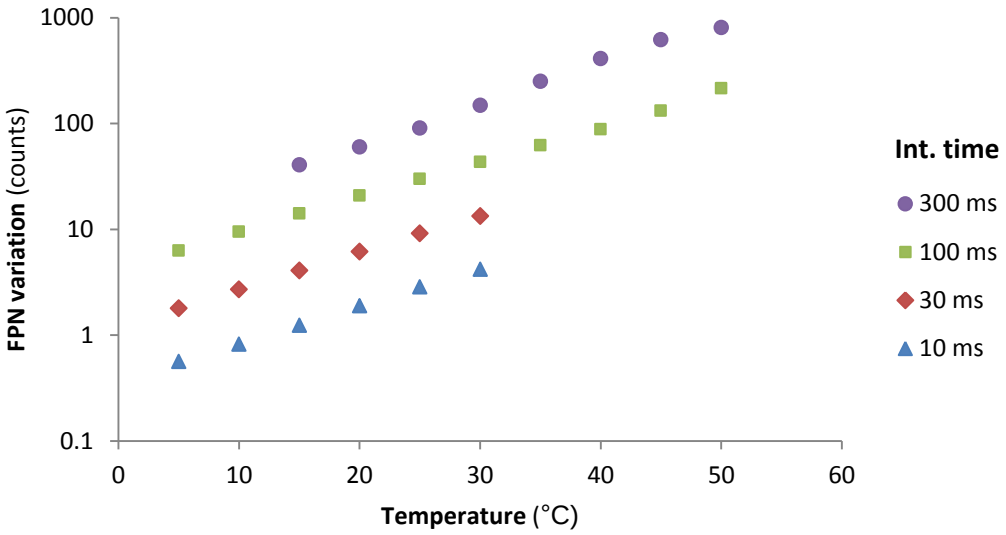

Figure 5.27: AvaSpec spectrometer temperature dependence of FPN, found as RMS variation of dark current and over a range of integration times. FPN variation increases with increasing temperature as expected.

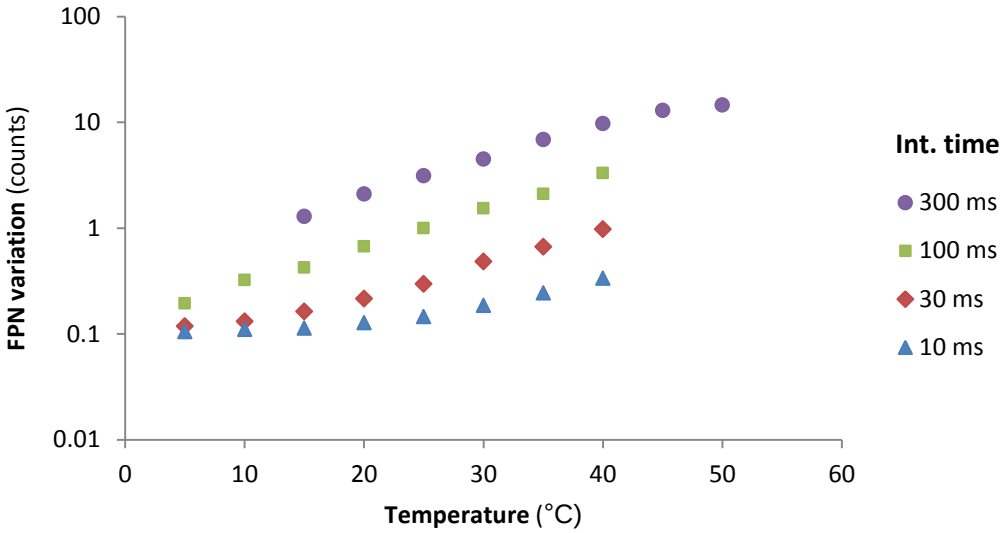

Figure 5.28: Ocean Optics spectrometer temperature dependence of FPN, found as RMS variation of dark current and taken over multiple integration times. It behaved similarly AvaSpec spectrometer but FPN variation did not decrease below about 0.1counts due to count digitisation following averaging.

It was important, when using either spectrometer, that the signal did not become unreadable as a result of high temperature operation. Therefor longer integration times

should be used for low-signal or high-temperature measurements. This was not an issue during this project as high-signal measurements were generally used for spectroscopy. The measured variation between pixels of the Ocean optics spectrometer did not drop below 0.1 counts, as seen in Figure 5.28. This was because averages were taken across ten measurements, and only integer numbers of counts were possible for each.

5.5.5. Read noise

This category includes noise phenomena which occur when charge carriers in the CCD are converted into electrical signals, as described in Section 5.1. CCDs are typically connected to further electronics that amplify the voltage referred to as off-chip amplifiers [1], which also cause read noise. The final phenomenon included in this category comes from voltage analogue to digital conversion.

(i) Reset noise comes from thermodynamic variations in the resetting voltage at the sense node capacitor between readings [15]. It is described by Equation (5.10), where C is the sense node capacitance [1]:

$$\langle n_{reset} \rangle = \frac{\sqrt{k_B T C}}{q_e} \tag{5.10}$$

(ii) The on-chip amplifier converts charge packets to current [16] and has noise described by Equation (5.11), where V_{on} is the noise voltage after the on-chip amplifier [1]:

$$\langle n_{on\text{-}chip} \rangle = \frac{C}{q_e G} V_{on} \sqrt{\Delta f_e} \tag{5.11}$$

(iii) Off-chip amplifier noise has a very similar form, being described by Equation (5.12), where G_1 is the off-chip amplifier gain and V_{off} is the noise voltage after the off-chip amplifier [1].

$$\langle n_{off\text{-}chip} \rangle = \frac{C}{q_e G G_1} V_{off} \sqrt{\Delta f_e} \tag{5.12}$$

(iv) Finally quantisation noise is produced by analogue to digital conversion and follows Equation (5.13), where N_{well} is the electron well capacity and N_{bit} is the bit resolution of the converter [1]:

$$\langle n_{ADC} \rangle = \frac{N_{well}}{2^{N_{bit}} \sqrt{12}} \tag{5.13}$$

Read noise is not dependent on integration time as it only occurs when the signal is taken from the CCD. The total read noise can be found by combining the different components as in Equation (5.14). The read noise is generally expected to be fixed for any given pixel.

$$\langle n_{read} \rangle^2 = \langle n_{reset} \rangle^2 + \langle n_{on-chip} \rangle^2 + \langle n_{off-chip} \rangle^2 + \langle n_{ADC} \rangle^2 \tag{5.14}$$

As read noise occurs once per measurement, it is difficult to reliably identify and isolate it. Other noise phenomena in signal transfer systems or in computer or data logging devices may well behave in the same way. Distinguishing between different types of read noise can also be difficult. In practice, however, a single value can be given for a spectrometer which describes all noise phenomena behaving in this manner.

Figure 5.22 in Section 5.4.4 shows the dark current of the AvaSpec and Ocean Optics spectrometers, measured at a range of integration times. Both spectrometers show behaviour consistent with read noise. Dark current levels off with decreasing integrations times instead of continuing to decrease as expected for random dark noise. This gave a minimum dark current attributed to read noise of 171±34 counts for the AvaSpec-3648 and 51.5±3 counts for the Ocean Optics S2000.

5.5.6. Photo-response non-uniformity

Photo-response non-uniformity (PRNU) is a variation in responsivity between CCD elements caused by variations in detector area or spectral responsivity (see Equation (5.2)). Like FPN, it is caused by imperfections in CCD manufacture and is unique to each spectrometer [13]. PRNU is most significant for high intensity measurements and bright conditions while FPN is most significant in low intensity measurements and dark conditions. PRNU responds proportionally to signal intensity, and so is difficult to distinguish from variations in source intensity across the measured spectrum.

PRNU is described by Equation (5.15), where *U(λ)* is the fixed pattern ratio (a scaling factor that applies to each pixel independently [1]).

$$\langle n_{prnu} \rangle = U(\lambda) n_{pe} \tag{5.15}$$

An estimation of PRNU was found for the two independent light sources by subtracting the assumed 'true' spectra. This was found by using a seven term polynomial equation, computer fitted to the measured data. It allowed a smooth shape to be fitted to the measured spectra whilst ignoring sub-nm wavelength structure. It did not account for any spectrally narrow features of the source, or spectrally broad PRNU features. Values were then normalised for power due to the linear relationship of PRNU with signal (from Equation (5.2)).

The AvaSpec spectrometer was used with a deuterium UV lamp and again with a 340nm LED to estimate PRNU. The Ocean Optics spectrometer also used the deuterium UV lamp and a visible LED, as the 340nm LED was out of its spectral range. The visible LED (RS Components HLMPC515) had a central wavelength of 570nm and a 15nm FWHM. Samples of the results from the two spectrometers are shown in Figure 5.29 and Figure 5.30.

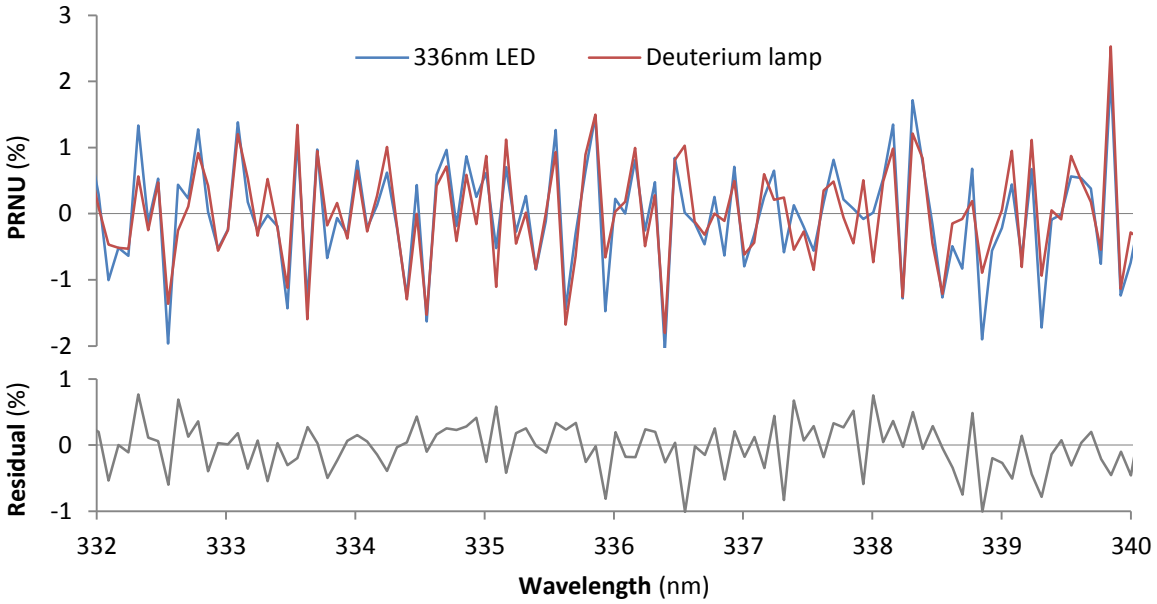

Figure 5.29: Comparison of PRNU of the AvaSpec spectrometer with the 336nm LED and the deuterium UV lamp. Percentages are given in terms of total signal.

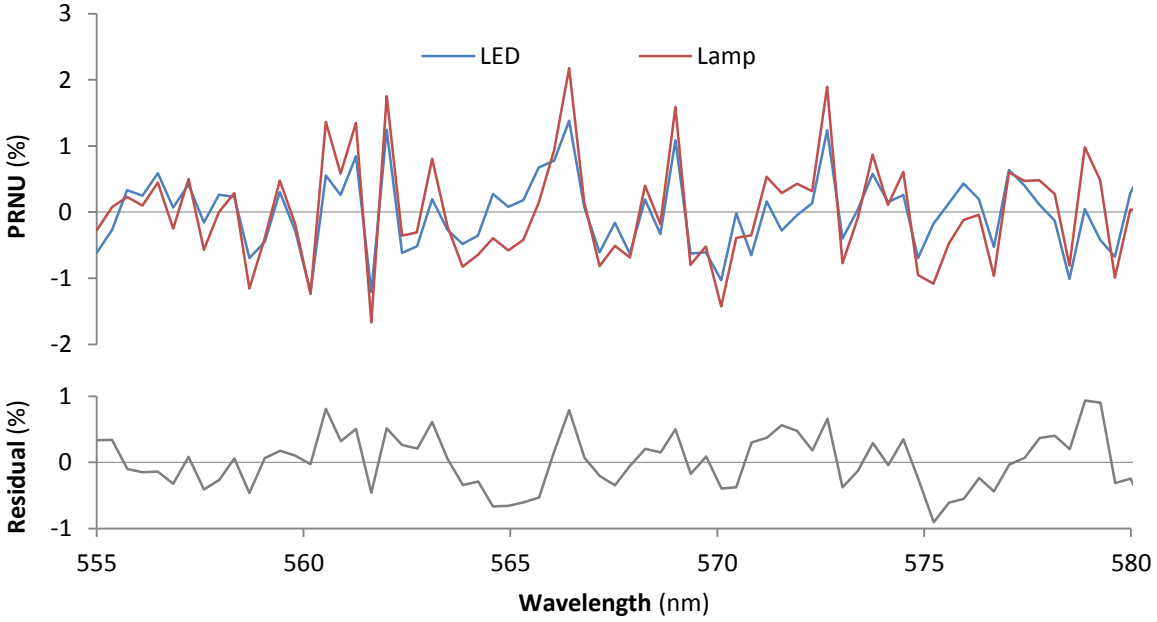

Figure 5.30: Comparison of PRNU of the Ocean Optics spectrometer with the 570nm LED and the deuterium UV lamp. Percentages are given in terms of total signal.

The average RMS PRNU in these regions was found to be 0.6±0.2% for the AvaSpec-3648 and 0.54±0.17% for the Ocean Optics S2000. The majority of the errors on these values come from the residual differences between sources, as it is not easy to

distinguish between PRNU and systematic variations in source intensity. The residual is the worst case PRNU assuming it is responsible for all differences between the two data sets.

5.6. Performance optimisation

The following settings and procedures were used to optimise the performance of the AvaSpec spectrometer by limiting the noise phenomena identified above. Once found, these settings and procedures were used as standard during this project. A summary initial and controlled levels of noise phenomena is given at the end of the section.

5.6.1. Increased sampling

Noise phenomena which vary randomly with time such as shot noise, source fluctuations and dark current noise can be decreased by increased sampling using one of two methods:

(i) Longer integration times within the CCD itself. Higher integration time can increase dark current and can cause saturation for high-intensity signals.

(ii) Averaging over multiple CCD readouts. A lag time of up to 7ms between readouts must be considered, and therefore this method will only provide an advantage for integration times longer than 10ms. Use of multiple readouts may also cause an increase in read noise.

In this project a total measurement time of 30s was achieved by using a 30ms integration time and averaging over 1,000 measurements. Improvements from increased sampling were limited by long-term drift effects which came to dominate for longer term measurements.

5.6.2. Temperature control

Many of the noise phenomena described in this chapter were temperature-dependent. Variations in temperature could affect the dark current noise and cause shifts in the baseline of measurements. Temperature stability was therefore highly desirable during spectrometer measurements.

The room temperature of the main laboratory used for this project varied between 22 and 24ºC. For most tests this was found to be sufficiently stable, although an alcohol thermometer was placed with the system to allow temperature to be recorded during testing. For some particularly sensitive measurements it was necessary to control the temperature with an environmental oven.

Care was taken to avoid decreasing the temperature to the point of damaging the apparatus, for example by causing condensation or even ice crystals to form. Spectrometers were kept from dropping below 0°C. Also, when the signal was very low, the voltage offset described in Section 5.4.4 could dominate the signal. This would render measurements impossible. Consequently, the temperature was kept at 39°C or below except in high signal cases.

5.6.3. Dark current correction

Two methods were identified to correct for dark current and FPN.

(i) Dynamic dark correction is an automatic function that can be implemented on a spectrometer to correct for dark current in real time. It subtracts the same dark current from readings across the full wavelength range and so makes no correction for variations due to pattern noise. It was therefore best suited to measurements of rapidly changing conditions with short integrations times. This method was generally avoided as the spectrometer did not record data on the amount of dark noise subtracted and because conditions were generally kept stable.

(ii) The second method was to record the dark current of the spectrometer across all pixels and manually subtract it from readings. This was the preferred method. It corrects for both dark current and FPN. As described above, dark current is not constant with temperature and so it needed to be recorded in conditions as close to measurement conditions as possible. Generally this involved recording dark noise immediately before or immediately after experiments. Where temperature was controlled, pre-recorded dark current values could be used.

5.6.4. Photo-response non-uniformity scaling

Figure 5.29 gives the measured PRNU of a selected part of the spectrum of the AvaSpec spectrometer. Its response to increasing signal intensity was linear according to Equation (5.15). Once the PRNU is characterised, it becomes possible to scale measured signal to account for it. As stated above, PRNU is unique to each spectrometer and so must be determined before any scaling is done, requiring at least two independent light sources to isolate it from source spectral variation.

A single source with a known and smoothly varying spectrum such as a blackbody source could be used for characterising PRNU. However a black body would be problematic for the UV. For example the Heitronic SW 11 B blackbody radiation source [17] can run at up to 1,000ºC but with Planck curve of only 500 – 600nm..

For spectroscopic measurements, such as those carried out in this project, a comparison is made between the measured spectrum of a light source with a sample of gas present and without it. It is therefore not necessary to isolate spectral variation of the spectrometer and the source, as both should remain constant between readings and the two could be scaled together. For spectroscopic measurements taken in this project, spectral variations in source intensity and PRNU were treated as constants between measurements and could be considered together.

5.6.5. Optimisation results

Noise phenomena identified in this project fell into two main categories: those that were dependent on the external signal and those that were not, and would apply to dark conditions. Table 5.3 gives a summary of noise phenomena in these two categories including initial levels measured and levels after methods of limitation have been employed. Controlled figures assume the 30ms integration times and 1,000 averages mentioned earlier.

Table 5.3: Noise values before and after controls for the AvaSpec spectrometer

Phenomenon	**Initial level**	**Controls**	**Controlled level**
Signal-dependent			
PRNU	0.60±0.2%	Scaling	0.19±0.1%
Light source fluctuation noise	0.78±0.3% (60ms readings)	Increased sampling (Drift limit at 30s)	0.036±0.01%
Total	0.98±0.4%	-	0.20±0.1%
Signal-independent (dark conditions)			
Dark noise & fixed pattern noise (~20°C)	263±9 counts	Dark correction	1.3±0.3 counts
Dark current noise	24.7±6 counts (60ms readings)	Increased sampling (Drift limit at 30s)	1.3±0.3 counts
Total	264±11 counts	-	1.3±0.3 counts

In general signal-independent phenomena, such as dark current noise, FPN and read noise, will dominate for low intensity measurements. Signal-dependent phenomena, such as source fluctuation noise and PRNU, will dominate for high intensity measurements. Stray light is more difficult to define quantitatively and so does not fall into either category. Noise figures are given as a percentage of signal for signal-dependent phenomena and as an absolute count rate for signal-independent phenomena. Total noise of each type is found by taking the square root of the sum of squared values.

For this project the signal comes from a light source and is decreased only by gas absorption. For expected concentrations, absorption is unlikely to reduce intensity substantially and so signal-dependent phenomena are expected to dominate. This gives a noise level of 0.2% which corresponds to a minimum measurable absorbance of 2×10^{-3}AU for a single pixel. This is much higher than the absorbances of formaldehyde peaks at 100ppb (between 1 and 3). Some additional accuracy may be obtained from averaging over many pixels within an absorption band but the high variation of formaldehyde absorbance within bands limits this option.

By removing PRNU, NEA drops to 2.5×10^{-4}AU, predominantly limited by source fluctuation from the UV lamp. The $2^1_0\,4^1_0$ formaldehyde peak at 340nm has an absorption cross-section of 6.0×10^{-20}cm^2/molecule [18]. A path length of 17m would be required to detect a formaldehyde concentration of 100ppb. It is likely that this would be impractically long for a portable detection system. Some improvement could be gained by averaging over the entire spectrum, but that would lead to increased cross-sensitivity as shown in Chapter 4.

5.7. Chapter summary

The AvaSpec UV spectrometer was an important piece of equipment for this project. It was used in the evaluation system described in Chapter 6 and for the characterisation of later components and systems. It was selected based on the requirements for spectral range and resolution, array type and element number, and sensitivity and noise performance. A list of currently available UV spectrometers was compiled, from which the desired spectrometer was selected.

A detailed characterisation and comparison was made between the AvaSpec spectrometer and two others with broadly similar properties. The Hamamatsu spectrometer was a close contender for use in this project and operated over a similar range. The Ocean Optics spectrometer is one of the most commonly used mini spectrometers for scientific applications and had a similar internal layout.

The properties that were characterised included spectral range, spectral resolution, shot noise and source fluctuation noise. Also included were dark and fixed pattern noise, read noise and photo-response non-uniformity. For the spectroscopic measurments taken in this project, the most significant noise phenomenon was source fluctuation noise. A temperature-dependent offset of fixed pattern noise was observed in both the AvaSpec and the Ocean Optics spectrometer. This was caused by a voltage offset on the detector.

A set of procedures was chosen to optimise the performance of the AvaSpec spectrometer for this project. A 30ms integration time was used and averages were taken over 1,000 measurements. This gave a total measurement period of 30s, allowing randomly varying noise phenomena such as source fluctuation noise and dark current noise to be reduced. The maximum measurement period was limited by long term drift effects mainly attributed to temperature changes. Source fluctuation noise was the main short term noise phenomenon.

Temperature was controlled by an environmental oven for some tests, but in general the temperature in the laboratory was sufficiently stable. Dark current was removed by measuring it before or after taking measurements and subtracting it from the final values. PRNU could be corrected from measurements by first quantifying it and then scaling it out. This was not necessary for spectroscopic measurements as it behaved the same way as variations in source spectrum and so varied proportionally with absorption measurements.

The spectrometers described in this chapter are complex instruments that require detailed knowledge to use, and so would not be appropriate for a simple detection system. However they are also very versatile, the AvaSpec spectrometer giving high resolution spectral information over the full UV range. Chapter 6 describes an evaluation system using the AvaSpec spectrometer.

5.8 Bibliography

[1] G. C. Holst, CCD Arrays, Cameras, and Displays, Washington: SPIE Press, 1996.

[2] Avantes AvaSpec-3648-USB2-SPU2, *Technical Data Sheet,* Avantes, Apeldoorn, The Netherlands, 2010.

[3] L. Borland, M. Brickhouse, T. Thomas and A. W. Fountain, "Review of chemical signature databases," *Analytical and Bioanalytical Chemistry,* vol. 397, pp. 1019-1028, 2010.

[4] Ocean Optics OEM S2000, *Technical Data Sheet,* Ocean Optics, Dunedin, Florida, USA, 2011.

[5] K. Lee, K. P. Thompson and J. P. Rolland, "Broadband astigmatism-corrected Czerny–Turner spectrometer," *Optics Express,* vol. 18, no. 22, pp. 23378-23378, 2010.

[6] J. M. Simon, M. A. Gil and A. N. Fantino, "Czerny-Turner monochromator: astigmatism in the classical and in the crossed beam dispositions," *Applied Optics,* vol. 25, no. 20, pp. 3715-3720, 1986.

[7] L. Hamamatsu S2D2 UV-Vis Light Source, *technical data sheet,* Hamamatsu, Hamamatsu, Japan, 2010 .

[8] SETi UVTOP335, *Technical Data Sheet,* Sensor Electronic Technology Inc., Columbia, USA.

[9] Spectra-Physics, Quanta-Ray, Pulsed Nd: YAG Lasers, *User Manual,* Spectra-Physics, Santa Clara, USA, 2011.

[10] J. D. Winefordner, R. Avni, T. L. Chester, J. J. Fitzgerald, L. P. Hart, D. J. Johnson and F. W. Plankey, "A comparison of signal-to-noise ratios for single channel methods (sequential and multiplex) vs multichannel methods in optical spectroscopy," *Spectrochimica Acta Part B-Atomic Spectroscopy,* vol. 31(1), pp. 1-19, 1976.

[11] S. Engelberg, "The Wiener-Khinchin theorem and applications," in *Random signals and noise; a mathematical introduction*, Boca Raton, CRC Press, 2006, pp. 110-114.

[12] E. Hecht, Optics, Second Edition, Reading, Massachusetts: Addison-Wesley Publishing Company, 1987.

[13] G. Zonios, "Noise and stray light characterization of a compact CCD spectrophotometer used in biomedical applications," *Applied Optics,* vol. 49, no. 2, pp. 163-169, 2010.

[14] Private conversation with Neville Davies, Senior Applications Scientist, Account Manager, Ocean Optics, 2013.

[15] J. Hynecek, "Spectral Analysis of Reset Noise Observed in CCD Charge-Detection Circuits," *IEEE Transactions on Election Devices,* vol. 37, no. 3, pp. 640-647, 1990.

[16] P. Centen, "CCD On-Chip Amplifiers: Noise Performance versus MOS Transistor Dimensions," *IEEE Transactions on Eletron Devices,* vol. 38, no. 5, pp. 1206-1216, 1991.

[17] Heitronics SW 11 B Blackbody Radiation Source , *Technical Data Sheet,* Heitronics, Wiesbaden, Germany, 2013.

[18] R. Meller and G. K. Moortgat, "Temperature dependence of the absorption cross sections of formaldehyde between 223 and 323 K in the wavelength range 225-375 nm," *Journal of Geophysical Research-Atmospheres,* vol. 105, pp. 7089-7101, 2000.

Chapter 6: Evaluation system

In the early stages of the project an evaluation system was built, based on the principles of UV spectroscopy. It used high performance components, including the AvaSpec spectrometer described in Chapter 5, and was used as a research tool during the project. The evaluation system was designed to be versatile and easily modified. After testing, lessons learned with the evaluation system were used for the design of prototypes, which were simpler and more specialised systems.

6.1. Setup

A photograph of the evaluation system is shown in Figure 6.1 and Figure 6.2 is a schematic diagram. The system is shown with a 101mm long gas cell. Some minor variations in the exact setup were made during the project, but the basic operation remained consistent.

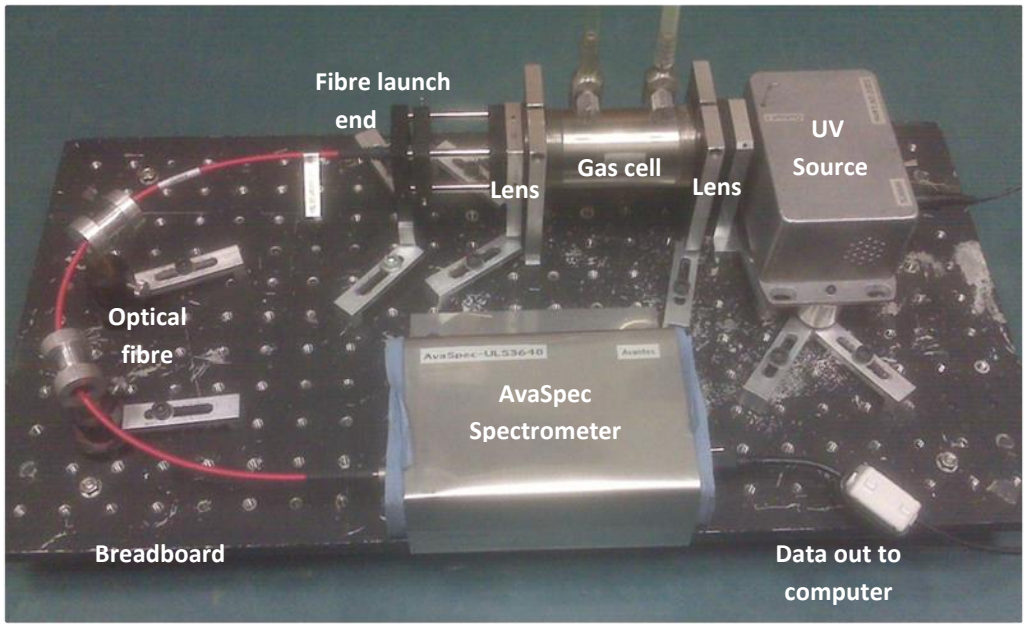

Figure 6.1: Photograph of the evaluation spectrometry system. The light path starts at the UV lamp at the top right, travels left to the fibre launch end, the optical fibre then delivering it to the AvaSpec spectrometer at the bottom.

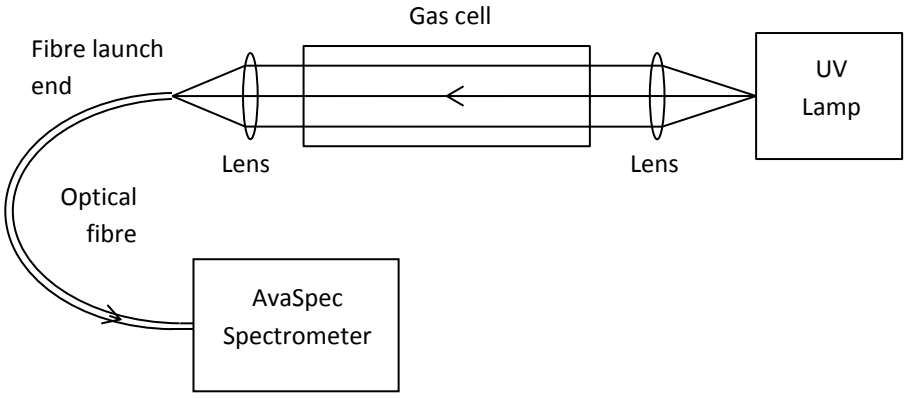

Figure 6.2: Diagram of the evaluation spectrometry system. Light from the UV source is collimated into the cell by the first lens, where the sample absorbs parts of the spectrum. Light is then focused on to the fibre launch end by the second lens and is delivered to the spectrometer by the optical fibre.

The system works on the principle of UV spectroscopy as described in Chapter 3. Light is transmitted by the UV lamp and collimated into the gas cell by the first lens. The gas cell contains the sample which absorbs some of the light as it passes through. The remaining light is then coupled into the optical fibre by the second lens. The light then travels along the optical fibre, and its spectrum is analysed by the spectrometer.

6.2. Apparatus

The evaluation system used a UV lamp, a gas cell, some fused silica lenses, an optical fibre and the AvaSpec spectrometer. The UV spectrometer was described in detail in Chapter 5 and used an integration time of 30ms and averaged over 1,000 measurements to maximise noise performance. The gas cells and the fused silica lenses were used in later prototype systems as well, as described in Chapter 7 and Chapter 8.

6.2.2. Gas cells

In order to allow for greater control of test samples, a gas cell was generally used in this project rather than taking open path measurements. This was a small, cylindrical container with a window at each end into which was placed the gas sample to be tested. Two different gas cells were used during this project, one with an internal length of 101mm and removable windows and one with an internal length of 195mm and fixed windows. Dimensions were determined by availability of equipment.

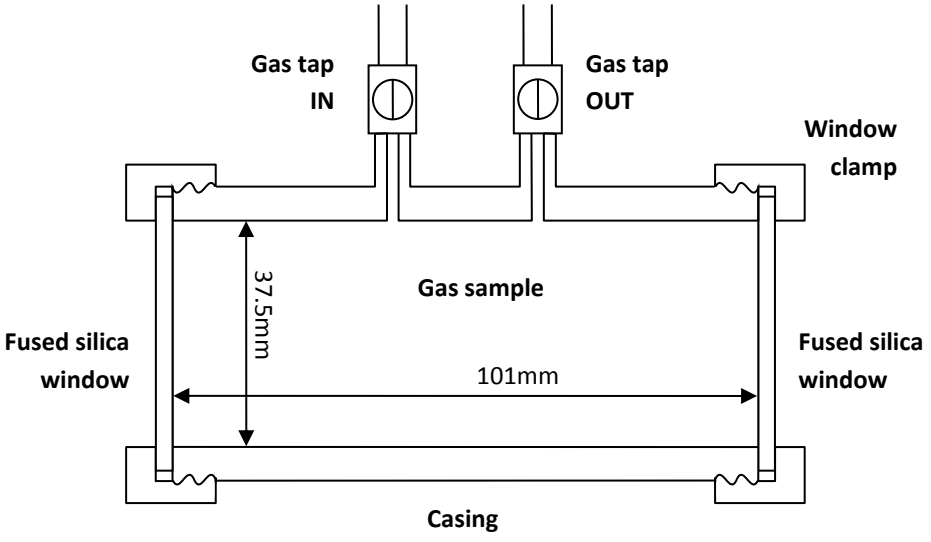

Figure 6.3: Diagram of the 101mm gas cell. Gas samples are exchanged through the gas taps. Light from the UV lamp then passes in through one fused silica window, through the gas sample, and out through the other fused silica window. Window clamps can be unscrewed to remove windows.

The 101mm gas cell was the first gas cell to be used in this project. A schematic diagram of the 101mm gas cell is shown in Figure 6.3. 101mm was the internal length and it had an internal diameter of 37.5mm. It therefore had an internal volume of 112cm^3, not including the volume of the gas taps. The cell was held in place by fitted holders attached to the window clamps.

The 101mm gas cell had a pair of gas taps on one side, one for gas in and one for gas out. The windows were held in place by a screw-in clamp. When taking a measurement some of the sample was pumped into the gas cell. Initially both taps were left open to permit gas to leave the cell, purging it of any contamination. Then the input was closed, followed shortly by the output to prevent surrounding gases diffusing back, and prevent pressure increase inside the cell.

The cell was tested for leaks by filling it with a low (non-explosive) concentration of methane gas and then testing joints using a flammable gas detector around the outside. The detector responded to the presence of methane, thus locating any leaks or confirming that the cell was gas tight. The cell was found to have slight leaks around the window clamp screw fittings. Sealant tape was applied to the joins, which did stop the leaks, but proved to be easily damaged and unreliable.

The 195mm gas cell was constructed to be an improvement on the 101mm gas cell. It was constructed from a length of aluminium tubing into which holes were drilled for the two gas taps. Instead of being held by window clamps the windows were glued directly onto the ends of the gas cell using a two part epoxy adhesive. This provided a much better seal at the cost of some versatility. A photograph of this cell is shown in Figure 6.4 and a schematic diagram in Figure 6.5.

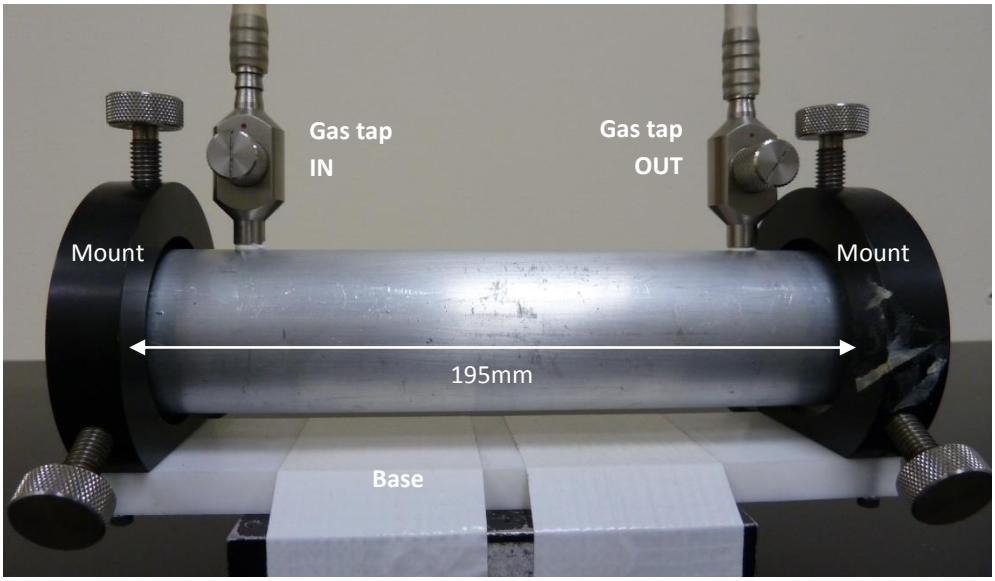

Figure 6.4: Photograph of the 195mm gas cell. Three point mounts can be seen on either side with the plastic base below.

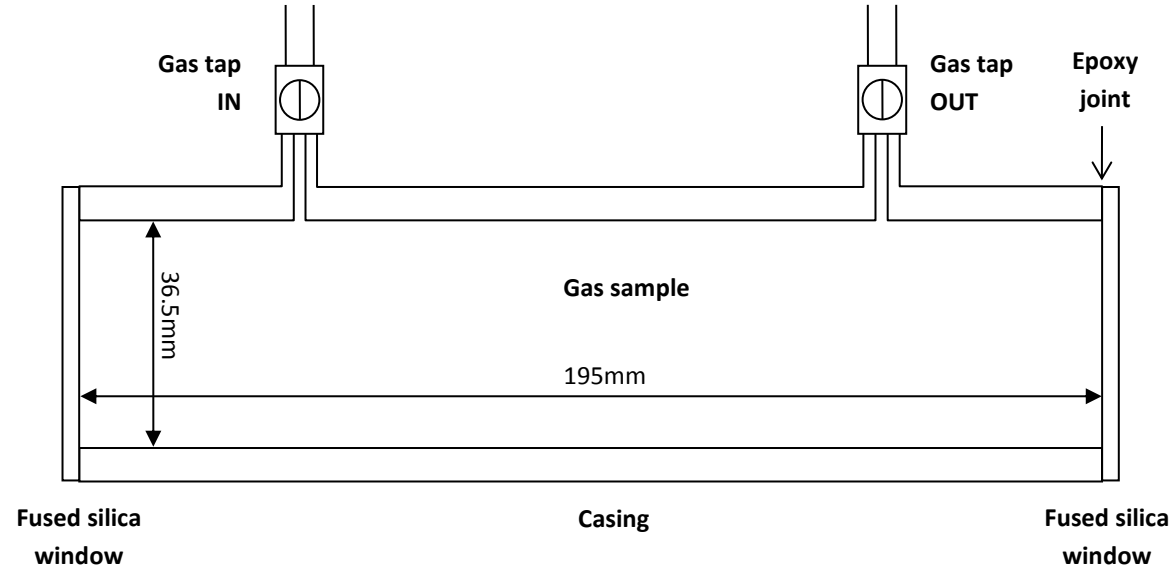

Figure 6.5: Diagram of the 195mm gas cell. Gas exchange operated as for the 101mm gas cell. Windows were glued to the ends of the casing to prevent gas leakage.

The 195mm gas cell was longer and narrower than the 101mm gas cell. 195mm was the internal length and the internal diameter was 36.5mm. The cell's internal volume was therefore 204cm^3, not including the volume of the gas taps. This volume was slightly higher than for the 101mm gas cell, so a larger sample was required to fill it. It did not have a fitted

holder and so was mounted in a pair of three point mounts, which were themselves mounted to a specially constructed plastic base. The mounting system can be seen in Figure 6.4.

The windows at each end of both cells were made out of UV grade fused silica, which is transparent in the region of interest (verified with the UV spectrometer). The 101mm cell used 3mm thick windows with a 50mm diameter, the 195mm cell used 2mm thick windows with a 45mm diameter. In general the 195mm gas cell was superior as, while it required a slightly large sample volume, it had a longer optical path length and a better gas seal.

6.2.3. Lenses

Two lenses were used for this system, not counting those integrated into other components such as the UV spectrometer. The first (UQG FSL-2560) [1] was a plano-convex lens with a focal length of 60mm. The second (UQG FSL-2540) [1] was also a plano-convex lens with a focal length of 40mm. Both were made of UV grade fused silica.

To the author's knowledge fused silica was the most commonly available UV lens material. This means that spectral dispersion cannot easily be optically corrected. The design wavelength of the lenses was 587nm whilst the UV absorption spectrum of formaldehyde lies between 250nm and 360nm. Figure 6.6 shows a diagram of the effect of spectral dispersion on focal length at three different wavelengths.

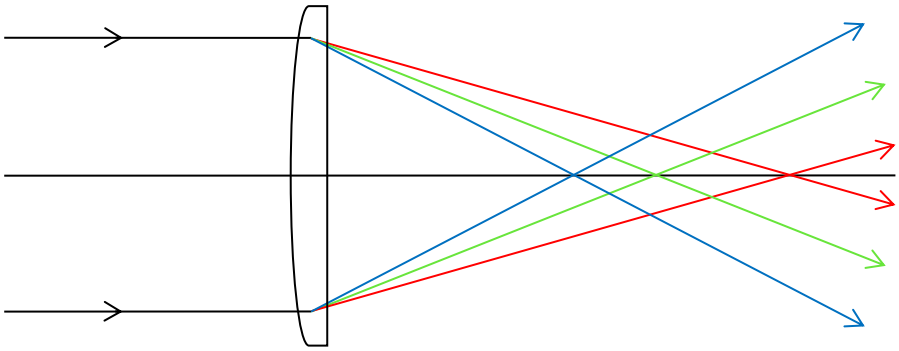

Figure 6.6: Diagram of the effect of spectral dispersion on focal length. Green lines are at the design wavelength, red lines are at a longer wavelength and blue lines are at a shorter wavelength. The extent of spectral dispersion varies by material as well as by wavelength.

The general effect of spectral dispersion is to vary the position of the focal point for different wavelengths. For narrow band measurements, such as those taken with the narrow band laser line filters used later, this is less of a problem. For broader band measurements it is often possible to place measuring elements (photodiodes or the launch end of optical fibres) outside the focal region to ensure that at least some light from all wavelengths was measured.

6.3. Limit of detection

In Chapter 3 the noise equivalent absorbance (NEA) was defined as the minimum intensity variation from absorbance that will give a signal equal to the RMS noise of the system. When the variation is much smaller than the signal, as is the case for spectroscopic measurements close to the limit of detection, the absorbance of a sample can be approximated to:

$$\frac{\Delta I(\lambda)}{I_0(\lambda)} = \sigma(\lambda) l N \qquad (6.\ 1)$$

Chapter 5 described the optimum settings for the AvaSpec spectrometer, which were used with this system. The system used a single light source operating in the high intensity regime of the spectrometer. This meant that signal-independent noise phenomena could be ignored and PRNU did not need to be independently identified from the intensity spectrum of the source.

This gave an NEA of 2.5×10^{-4}AU. The value of σ(340nm) for formaldehyde is given by Meller *et al.* (2000) [2] as 6.0×10^{-20}cm^2/molecule. This corresponds to the $2^1_0\,4^1_0$ formaldehyde peak, one of the strongest peak in the low interference section identified in Chapter 4. The length of the gas cell in the evaluation system was 19.5cm. This gives a limit of detection of 2.1×10^{14} molecules cm^{-3}. Under standard atmospheric conditions this equates to a limit of detection of 8.5ppm.

6.4. Formaldehyde generation and testing

During this project several methods of producing and delivering formaldehyde gas from paraformaldehyde were used. Factors like safety requirements, desired concentration and precision of calibration and delivery rate were taken into account. The tests described in this section were intended to test both the evaluation system and also the generation methods. The UV absorption spectrum of formaldehyde is shown in Figure 6.7 for reference.

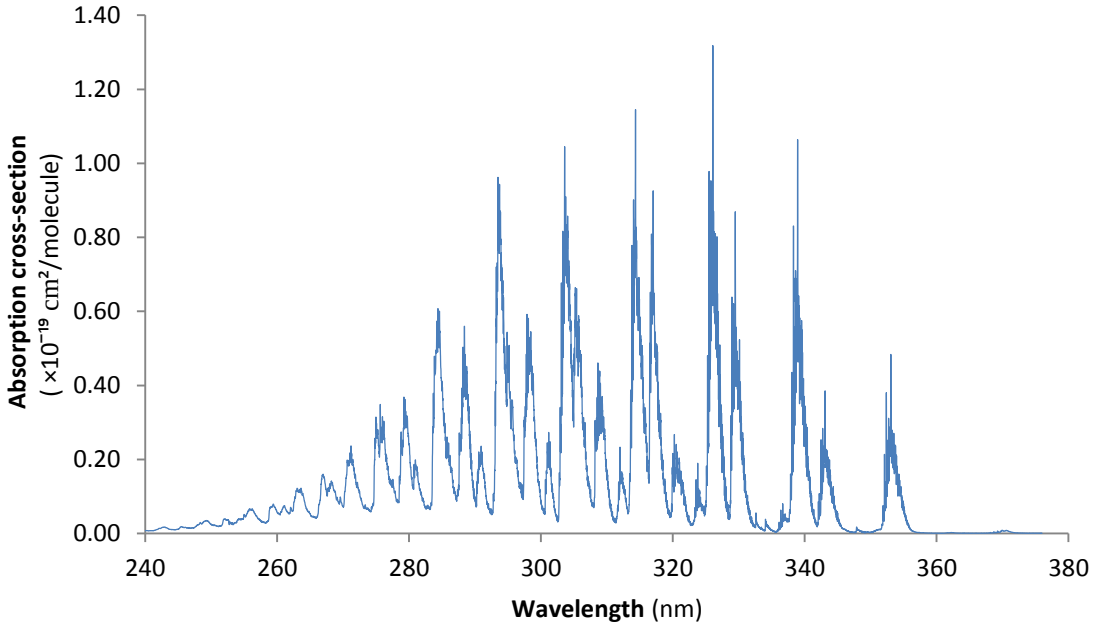

Figure 6.7: Graph of the formaldehyde UV absorption spectrum, re-plotted from data from Meller *et al.* [2].

In this project formaldehyde was generated by heating paraformaldehyde. Paraformaldehyde is a white powder that forms as a precipitate in aqueous formaldehyde solution. This powder, when heated, dissociates into formaldehyde gas. It is a polymer composed of a number of formaldehyde molecules. The molecular structure is shown in Figure 6.8.

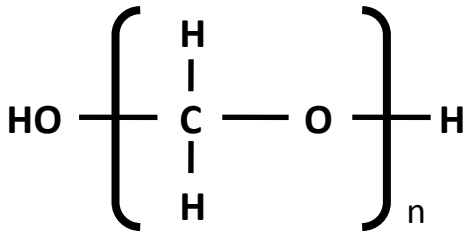

Figure 6.8: Molecular structure of paraformaldehyde. It is a polymer made of many (n) formaldehyde molecules. When heated it dissociates into gaseous formaldehyde.

6.4.1. Direct paraformaldehyde heating

Direct heating of paraformaldehyde had the potential to produce high concentrations of formaldehyde gas but it was hard to be sure how much would be produced. Such concentrations and the risk of contact with paraformaldehyde made safety of paramount importance. The safety procedures used for direct paraformaldehyde heating in this project are described in detail in Appendix 4. A 25g container of paraformaldehyde powder was obtained for formaldehyde generation. Several techniques of heating and gas delivery were considered.

The first technique was to use the formaldehyde that had accumulated in the head space of the container. This was also a worthwhile test for safety reasons as headspace gas could have posed a threat, particularly as the history of the pot was not known. The lid was opened and a quantity of the headspace gas was extracted by syringe and transferred into the gas cell to be measured. It was found that insufficient formaldehyde was present for any of the detection systems used in this project. However it showed that the container could be safely opened.

The second technique was heating paraformaldehyde inside a syringe. A small quantity of paraformaldehyde powder (less than 1g) was placed inside the syringe and the end sealed to contain all gas produced. Generating it directly in the syringe reduced the extent of loss and leaks during transfers. The syringe was placed in contact with a heated gel pack for several minutes, heating it to approximately 50ºC. The content was then transferred to the gas cell, taking care to safely dispose of any remaining powder.

On testing this technique, it was also found to produce insufficient formaldehyde to be detected. Further, there was no obvious decrease in the amount of paraformaldehyde powder in the syringe. It was concluded that if any paraformaldehyde had been made to dissociate, it had not been enough to produce sufficient formaldehyde gas. It was decided to heat a larger quantity of paraformaldehyde.

The third technique for direct paraformaldehyde heating was to gently heat the entire pot. The pot was placed in contact with the heated gel pack for a few minutes, after which a quantity of the headspace gas was removed by syringe. As before this was transferred into the gas cell for detection. A detectable quantity was produced and the results are shown in Figure 6.9.

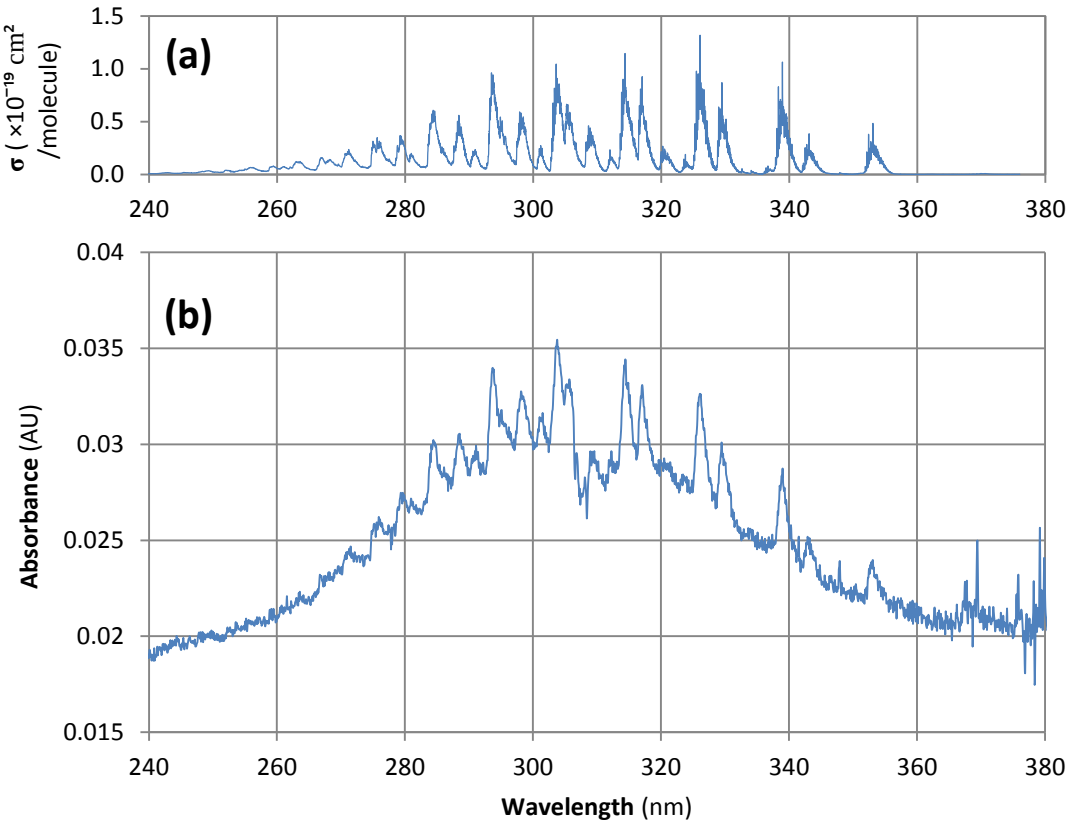

Figure 6.9: A) Absorption spectrum measured by Meller *et al.* [2] for comparison. **B)** Absorbance of formaldehyde generated by heating the paraformaldehyde pot and measured with the evaluation system.

The results in Figure 6.9 show clear correspondence to the absorption spectrum of formaldehyde Figure 6.7. The positions of peaks are well matched between the two data sets.

The absorbance above the base line of the 2^1_0 4^1_0 peak at 339nm was found to be $4.0\times10^{-3}\pm6\times10^{-4}$AU. This peak had an absorption cross section of 6.0×10^{-20}cm^2/molecule, therefore giving a formaldehyde concentration of 140±20ppm.

Figure 6.9 (b) shows a significant degree of cell repositioning error, evident by the position of the baseline. This occurs when the gas cell was removed and replaced between reference and detection measurements to allow generation to take place in the glove box. Errors were caused by differences in the position of the gas cell. Direct paraformaldehyde heating showed that the system responded to formaldehyde but was not appropriate for more detailed testing.

6.4.2. Permeation tube

This generation method used a calibrated paraformaldehyde permeation tube (Trace Source HRT-010.00-3024/100) heated in a calibration vapour generator (Owlstone OVG-4) [3]. The vapour generator delivered an air flow from 50-500cm^3 per minute and had an oven temperature range of 35-100°C. It had a quoted warm-up period from room temperature to 100°C of 15 minutes and had temperature stability to ±0.1°C.

The permeation tube contained paraformaldehyde powder. When the tube was heated, formaldehyde gas permeated though the wall of the tube. The generator system then mixed it with compressed air to produce the desired concentration. It delivered a repeatable concentration of formaldehyde set by controlling the temperature and the air flow rate, as described by Equation (6.2) [3]:

$$C = p_1(T_1)/F_{air} \tag{6.2}$$

where C is the concentration of generated formaldehyde gas, F_{air} is the air flow rate from the vapour generator and $p_1(T_1)$ is the permeation rate at temperature T_1 given by Equation (6.3)

$$\log p_1(T_1) = \log p_0(T_0) + \alpha(T_1 - T_0) \tag{6.3}$$

where $p_0(T_0)$ is the permeation rate at temperature T_0 and α is the temperature coefficient.

The main advantage of this method was that it produced reliable and repeatable concentrations. By keeping the temperature constant at 100°C it was necessary only to find the permeation rate at that temperature. This allowed the concentration to be varied by varying the air flow rate. Concentrations could be reliably kept within the safe levels for the fume cupboard. Therefore the gas cell did not need to be separated from the rest of the system to be passed into the glove box and so repositioning error could be avoided.

A limitation of the method was that higher concentrations could only be achieved with low air flow rates. The lowest flow rate that could be reliably produced by the vapour generator was 50cm^3 per minute and the 195mm gas cell had an internal volume of 204cm^3. Setting the air flow rate to get lower concentrations than this could cause it to take multiple minutes to fill the gas cell, potentially introducing errors from long term drift effects.

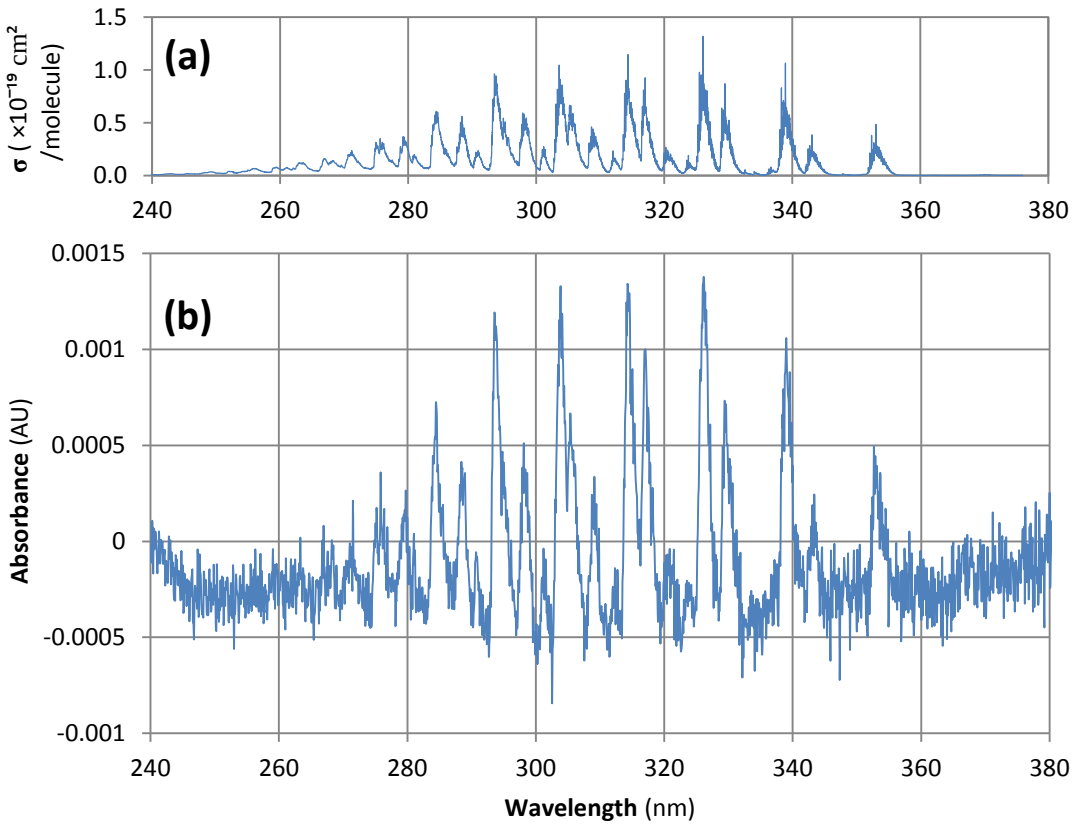

Figure 6.10: A) Absorption spectrum measured by Meller *et al.* [2] for comparison. B) Absorbance of formaldehyde generated from the permeation tube and measured by the evaluation system.

The evaluation system was tested with formaldehyde generated using the permeation tube. A change in flow rate was used to take reference measurements to avoid interfering with the system by changing connections. The flow was varied between 50 and 500cm^3 per minute providing a difference of 450cm^3 per minute. The resulting absorbance spectrum is shown in Figure 6.10, along the formaldehyde absorption cross-section as measured by Meller *et al.* [2].

As for direct paraformaldehyde heating, the position of absorbance peaks shows a good correspondence with the literature data. The absorbance above the base line of the 2^1_0 4^1_0 peak at 339nm was found to be (1.2±0. 2×10^{-3})AU. This peak had an absorption cross section of 6.0×10^{-20}cm^2/molecule, therefore giving a formaldehyde concentration of 40±7ppm. This corresponds to a permeation rate of (1.8±0.3×10^{-4})cm^3 per minute.

Figure 6.10 also shows a significant improvement in the baseline, resulting from removal of cell repositioning error. The formaldehyde concentration used for this data was taken not far above the system limit of detection of 8.5ppm. As described in Chapter 5, noise at this level predominantly comes from shot and source fluctuation noise and from long term drift effects. The former is visible in Figure 6.10 as the random variations of the base-line, and the latter as the position of the baseline below 0AU.

Although direct paraformaldehyde heating gave a higher concentration of formaldehyde, permeation tube generation was calibrated and more precise. In addition, permeation tube generation removed the need to move the gas cell, eliminating cell repositioning error. It was decided that permeation tube generation was the preferred method for use in this project.

6.5. Testing with other gases

As well as formaldehyde, the system was tested with a number of other gases in order to verify that it operated as expected. Also the concentration of formaldehyde available for testing was severely limited by safety considerations. Using other gases with absorption spectra in the UV region allowed the performance of the system to be tested at higher concentrations.

All of the gases tested in this section were supplied by gas bottle, imposing some limits on the maximum available concentration. Test gases were combined either with synthetic air (nitrogen and oxygen with no other gases) or with atmospheric air including many other species and trace gases. The gas cell was thoroughly flushed with synthetic air between measurements to ensure that there was no contamination from previous samples.

The absorption region of nitrogen lies below 100nm and so is not within the spectral range of the spectrometer. A comparison was made between pure nitrogen and synthetic air (80% nitrogen), showing no detectable variation. The absorption of carbon dioxide lies below 190nm, which is also outside the range of the spectrometer.

A comparison was made between lab air (minimum of approximately 390ppm carbon dioxide) and synthetic air (no carbon dioxide), again with no detectable variation. Oxygen had some absorption in the spectrometer's range but always below 2×10^{-23}cm^2/molecule. A comparison was made between pure oxygen and synthetic air (20% oxygen), showing no detectable variation.

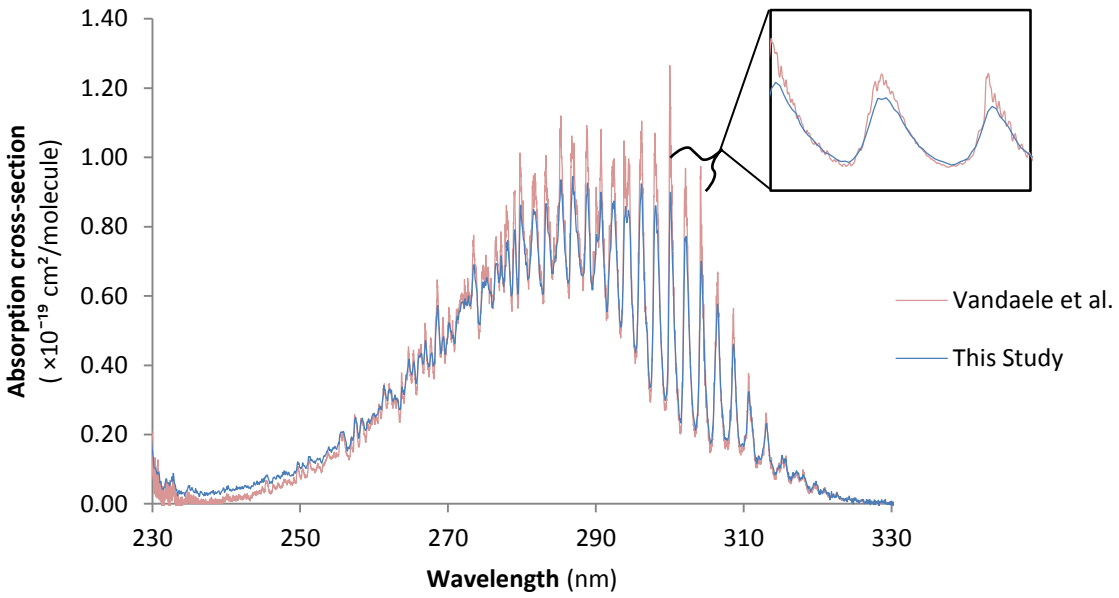

Figure 6.11: Graph of Absorption spectrum of sulfur dioxide measured by the evaluation system at 1% (blue) and by Vandaele *et al*. at 100% [4] (red). An inset is included of an expansion of 300 to 305nm. It can be seen that the two data sets have reasonable absorption cross-section correspondence and very good wavelength correspondence.

Sulfur dioxide showed very clear absorption spectra when used to test the evaluation system. The data from the sulfur dioxide measurement is presented in Figure 6.11, along with re-plotted data taken from Vandaele *et al*. (2009) [4]. The Vandaele study had a better spectral resolution and so could resolve the sub-nanometre features within the main absorption peaks. However it can clearly be seen that the main spectral peaks correspond well between the two data sets.

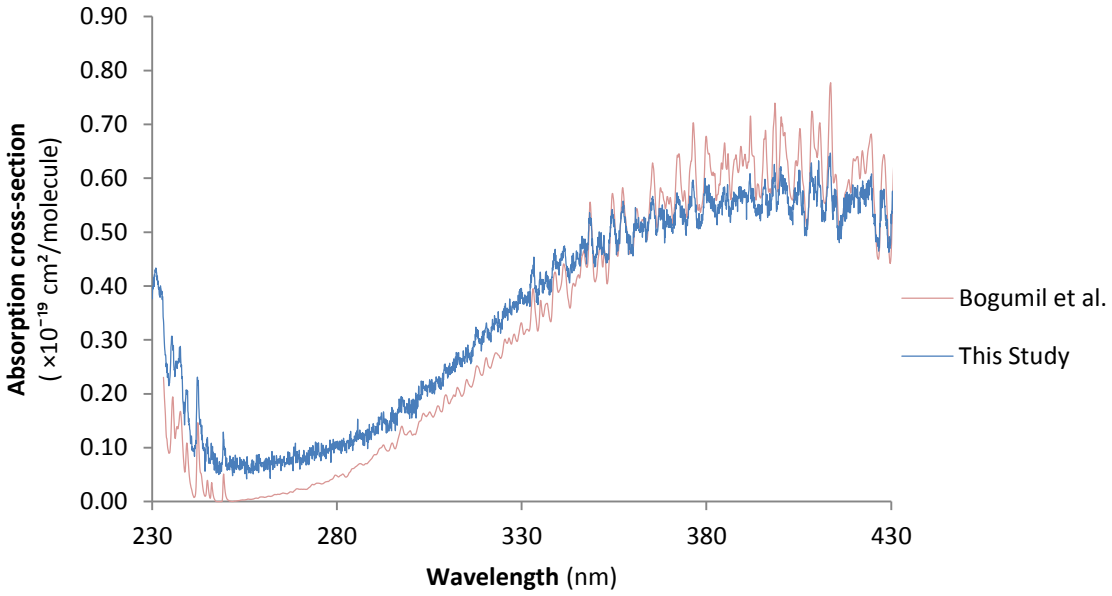

Figure 6.12: Graph of Absorption spectrum of nitrogen dioxide measured by the evaluation system at 1% (blue) and by Bogumil *et al*. at 1% [4] (red). It can be seen that the two data sets have a good wavelength correspondence and a reasonable absorption cross-section correspondence.

Nitrogen dioxide showed a similar wavelength correspondence to literature data [5] as shown in Figure 6.12. The absorption cross-section correspondence, while reasonable, was less simarlar than for sulfur dioxide. Hydrogen sulfide and nitric oxide were on the limit of the spectrometer's range, and so gave a weaker signal, but were still clearly detectable and corresponded to literature [6] [7]. These results demonstrate that the evaluation system worked as expected for gases besides formaldehyde.

6.6. Chapter summary

The evaluation system was a spectroscopic detection system for formaldehyde based on commercially available components. It was designed to test the principles of formaldehyde spectroscopy and to be used as a research tool during the project. The system used a deuterium lamp as a light source and a CCD UV spectrometer. Gas samples were contained within a gas cell through which light was collimated by UV grade silica lenses.

The system and constituent components were characterised in detail. Some components, such as the UV lenses and the gas cells, were also used in later systems. The theoretical limit of detection was found using the optimum performance of the spectrometer described in Chapter 5. This gave an NEA of 2.5×10^{-4}AU which, for the 195mm gas cell and the absorption cross-section of formaldehyde at 340nm, gave a limit of detection of 8.5ppm for a single measurement point.

The system was tested using formaldehyde gas generated from paraformaldehyde powder. Firstly paraformaldehyde was heated directly to produce the gas. While a wide range of concentrations could be produced by varying the time and temperature of the heating period, the concentration was uncalibrated and difficult to predict. Also gas delivery had to take place in a glove box into which the gas cell had to be passed into, bringing in significant cell repositioning errors.

The second method of generating formaldehyde was to use a permeation tube and a vapour generator. The permeation tube was pre-calibrated and produced a much more reliable supply of the gas. Further, it could be piped directly to the gas cell to avoid cell repositioning errors. Measurements of the formaldehyde spectrum using this method corresponded well to literature results, to within the limits of the UV spectrometer.

The system was also tested with other gases, many of which could safely be supplied at much higher concentrations than formaldehyde. Sulfur dioxide and nitrogen dioxide both had strong absorption regions within the range of the spectrometer and gave results with good correspondence to literature results. Nitrogen, oxygen and carbon dioxide were shown to have little or no absorption within the range of the spectrometer. This was as expected and an important result as these gases are always present in air and could interfere with results.

Results show that the evaluation system could detect formaldehyde as well as other gases within its spectral range and within the limits of the UV spectrometer. It was used to test formaldehyde detection and to verify the generation methods used in the project. Prototype systems that simplify and optimise the basic principles of the evaluation system are described in Chapter 7 and Chapter 8. These systems were designed to reduce the required complexity by specifically targeting formaldehyde absorption regions.

6.7 References

[1] UQG Optics UV Fused Silica - Spectrosil, *technical data sheet,* UQG Optics, Cambridge, UK, (2010).

[2] R. Meller and G. K. Moortgat, "Temperature dependence of the absorption cross sections of formaldehyde between 223 and 323 K in the wavelength range 225-375 nm," *Journal of Geophysical Research-Atmospheres,* vol. 105, pp. 7089-7101, 2000.

[3] Owlstone GEN-SYS User Manual, Owlstone, Norwalk, USA, 2008.

[4] A. C. Vandaele, C. Hermans and S. Fally, "Fourier transform measurements of SO2 absorption cross-sections: II. Temperature dependence in the 29000–44000/cm (227–345nm) region," *Journal of Quantitative Spectroscopy & Radiative Transfer,* vol. 110, pp. 2115-2126, 2009.

[5] K. Bogumil, J. Orphal, T. Homann, S. Voigt, P. Spietz, O. C. Fleischmann, A. Vogel, M. Hartmann, H. Kromminga, H. Bovensmann, J. Frerick and J. P. Burrows, "Measurements of molecular absorption spectra with the SCIAMACHY pre-flight model: instrument characterization and reference data for atmospheric remote-sensing in the 230–2380 nm region," *Journal of Photochemistry and Photobiology A: Chemistry,* vol. 157, pp. 167-184, 2003.

[6] T. Etzkorn, B. Klotz, S. Sorensen, I. V. Patroescu, I. Barnes, K. H. Becker and U. Platt, "Gas-phase absorption cross sections of 24 monocyclic aromatic hydrocarbons in the UV and IR spectral ranges," *Atmospheric Environment,* vol. 33, pp. 525-540, 1999.

[7] Y. Iida, F. Carnovale, S. Daviel and C. Brion, "Absolute oscillator strengths for photoabsorption and the molecular and dissociative photoionization of nitric oxide," *Chemical Physics,* vol. 105, no. 1-2, p. 211–225, 1986.

Chapter 7: Two filter system

The two filter system was constructed as a first proof of concept device using lessons learned with the evaluation system. This system was designed to meet the aims of sensitivity and response time given in Chapter 1. However it used only a single detection channel and a single reference channel, specifically targeted at formaldehyde, limiting its selectivity.

The two filter system was designed to test whether formaldehyde could be detected using low resolution spectral measurements and to test a method of tilting laser-line filters to fine tune their transmission wavelength to specific spectral features. However this system only used two channels, detection and reference, limiting its selectivity.

7.1. Setup

A photograph of the optical setup of the two filter system is shown in Figure 7.1. A close-up of the transmission and reflection arms of the beam splitter is shown in Figure 7.2 where they can be seen more clearly. The system used two channels on the two arms of the beam splitter, one for detection and one for reference.

Laser-line filters were used to limit the input light to the desired wavelength range, as set by the 339nm wavelength band set described in Chapter 4. The channels were selected to be sufficiently close together to use the same LED as a light source, taking advantage of the proximity of high and low-absorption regions in the formaldehyde spectrum.

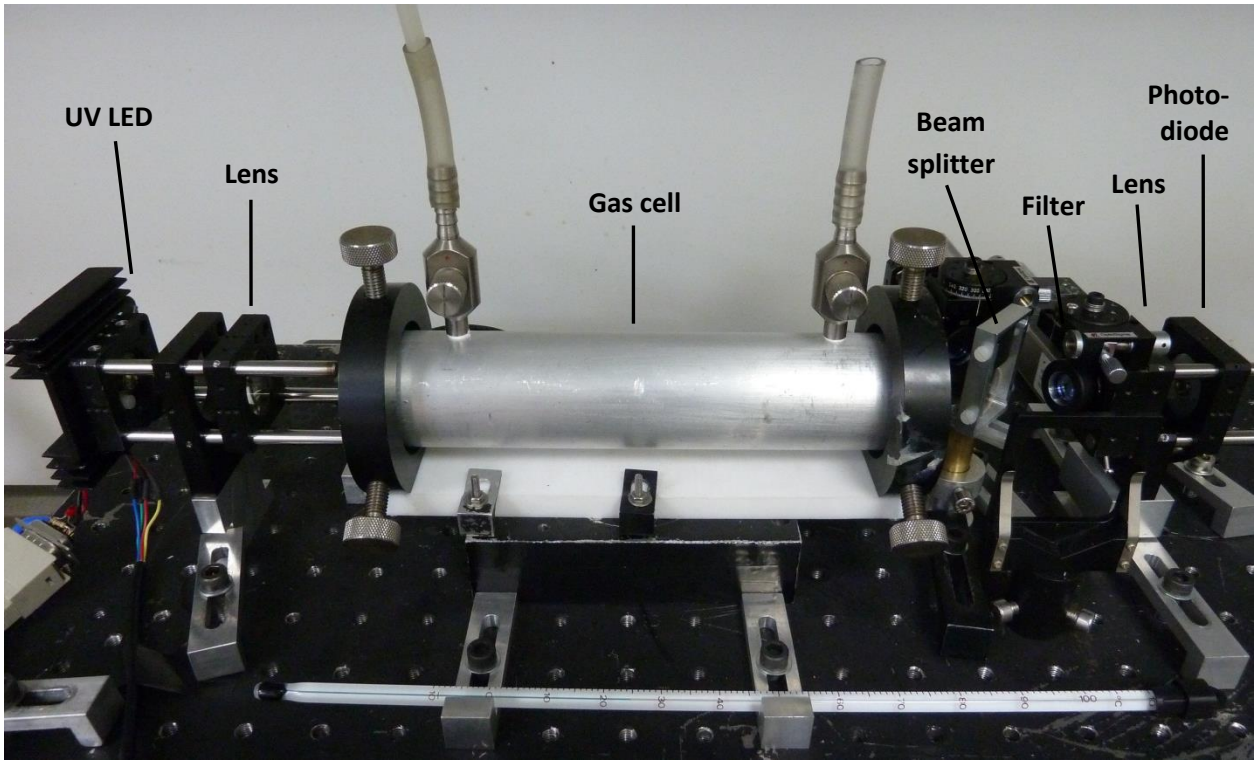

Figure 7.1: Photograph of the optical setup of the two filter system. A close-up of the two arms of the beam splitter is shown in more detail in Figure 7.3.

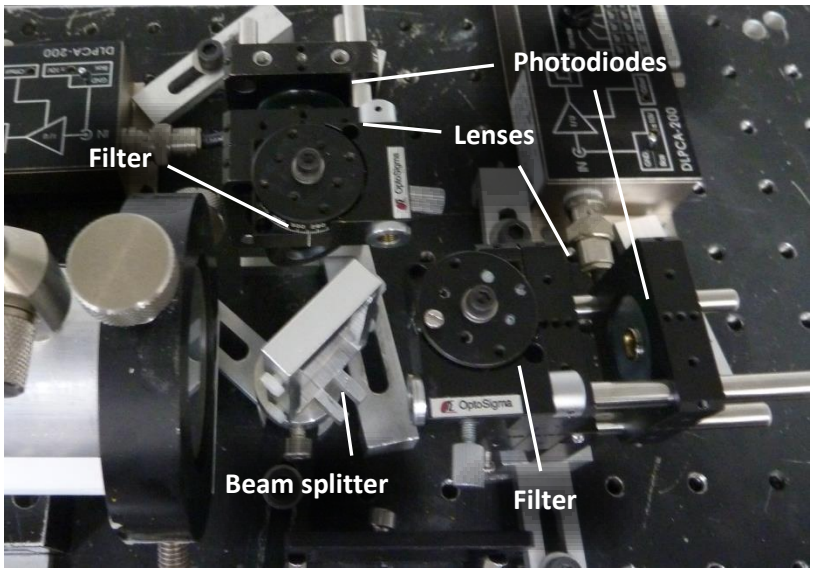

Figure 7.2: Close-up of the transmission and reflection arms of the two filter system for easier viewing.

A diagram of the optical setup is shown in Figure 7.3. Light from a 340nm UV LED was collimated into the gas cell by the 60mm focal length lens. The beam splitter divided the light

into two channels. Light from each channel then passed through a laser-line filter, angled to tune the transmission wavelength to the desired range. Finally, the light of each channel was focused by the 16mm focal length lenses onto a photodiode for detection.

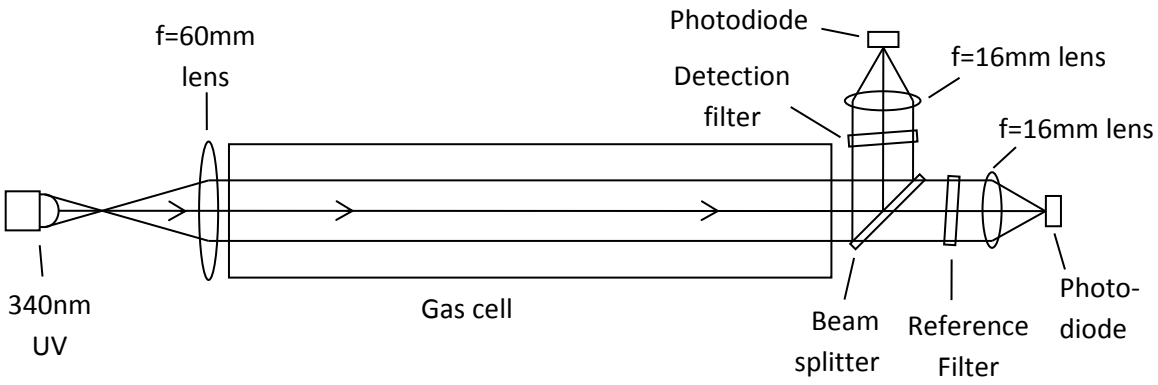

Figure 7.3: Diagram of the optical system. Light from a 340nm LED was collimated through the gas cell by the 60mm lens. The beam splitter divided the light into a detection channel (reflection) and a reference channel (transmission). The desired spectral range was then selected by the filters before the 16mm lenses focused light onto the photodiodes for detection.

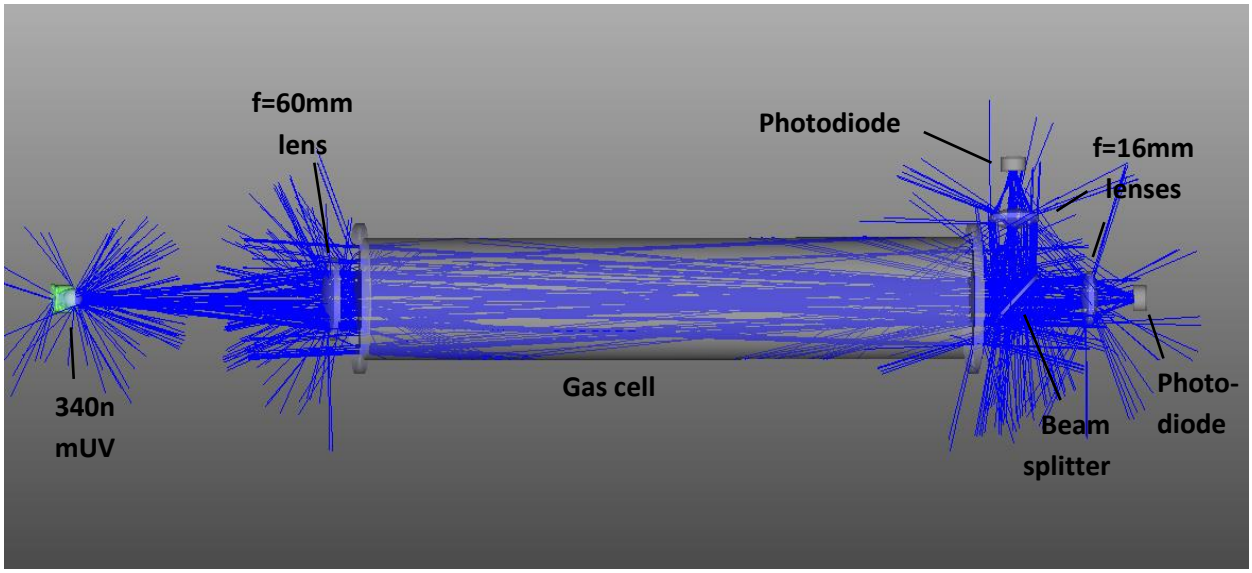

Figure 7.4: Computer model of the optical layout of the two filter system as optimised by the Zemax optical design program. A number of example light rays are shown in blue.

The optical setup of the two filter system was optimised using the Zemax optical design program running in non-sequential mode [1]. The program changes a set of defined variables,

such as optical element position and curvature, to optimise the system according to the desired criteria defined by the user. In this case, the positions of optical elements were varied from a starting arrangement to maximise the amount of light reaching the photodiode whilst allowing space for the 195mm gas cell and the filters. Several arrangements were tested, with the best optimisation selected. Figure 7.4 shows the layout of the system as modelled. These specifications were used to set up the two filter system.

7.2. Apparatus

The two filter system made use of photodiodes, a Peltier temperature control module, custom made 339nm laser-line optical filters and a range of electronic devices for driving the LED, modulation, for amplification and for noise reduction. Also used was the 340nm UV LED described in Chapter 5 and the fused silica lenses and the 195mm gas cell described in Chapter 6. The characterisation of the new apparatus is described in detail in this section.

7.2.1. Photodiodes

Two photodiodes were used for the two channels (RS Components OSD5.8-7QSD5.8-7Q) [2]. The chip material was silicon with a photosensitive area of 5.8mm^2. The photodiodes were UV enhanced (using UV-grade silica front windows), giving improved performance in the regions used by the two filter system. The photodiodes had a quoted typical dark current of 3pA. There photodiodes were selected as they absorbed in the UV region and had a photosensitive area a little larger than the focal spot of the system (Figure 7.4).

An image of typical responsivity of this type of photodiode is shown in Figure 7.5, as given by the manufacturer as raw data was not available. The responsivity of a photodiode using a quartz window was included in the graph but was not used in this project. The data gives a photodiode responsivity between 0.16 - 0.17AW^{-1} over the wavelength range used with the two filter system.

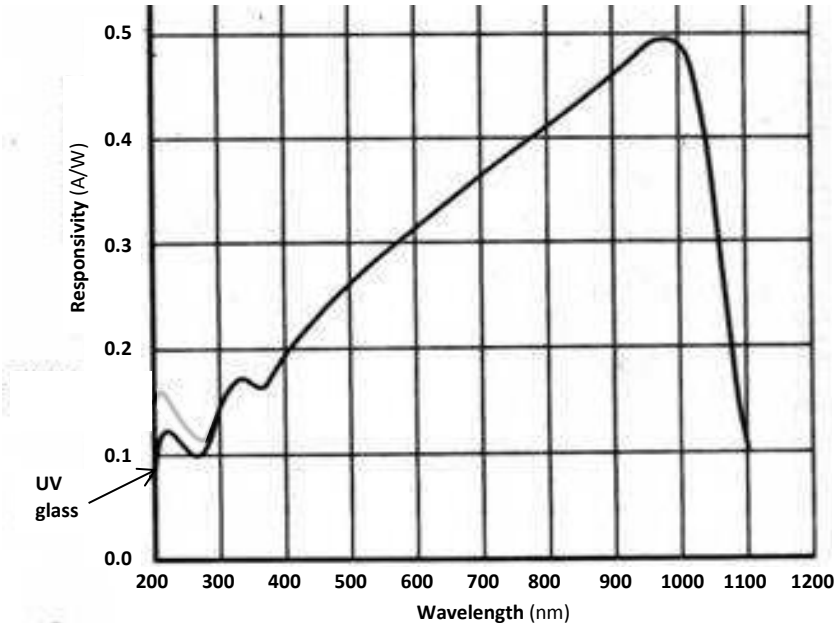

Figure 7.5: Image of the typical responsivity of the RS Components photodiode as given by the manufacturer [2]. The photodiode used a UV glass window. Raw data was not available.

Although the photodiodes were UV enhanced, they still had a significant responsivity in the visible part of the spectrum. They were therefore susceptible to interference from visible light from outside the optical axis or that had not been blocked by the filters. It was therefore important to use beam blockers or covers, or to switch room lights off. The lock-in amplifiers (described in Section 7.2.5) also helped by removing any signal not matching the reference frequency used to modulate the LED.

7.2.2. Peltier module

A Peltier module (Global Component Sourcing Thermoelectric module ET-007-06-11) [3] was included in the system to control and stabilise the temperature of the LED. The temperature behaviour of the LED is described in Section 7.2.3, showing a slight shift of the transmission spectrum towards longer wavelengths with increasing temperature. By connecting a thermistor (EPCOS NTC thermistor B57550G103J) [4] [5] [6] and a temperature controller (Thorlabs Temperature Controller Ted 200) [7], the temperature of the LED could be set and controlled.

Figure 7.6 shows a photograph and a diagram of Peltier module and the thermistor on the back of the 340nm LED. The Peltier module and the thermistor were placed in thermal contact with the back of the 340nm LED with thermal grease to improve conduction. This was as close to the LED element as they could be placed without cutting the case and risking damage to parts of the LED.

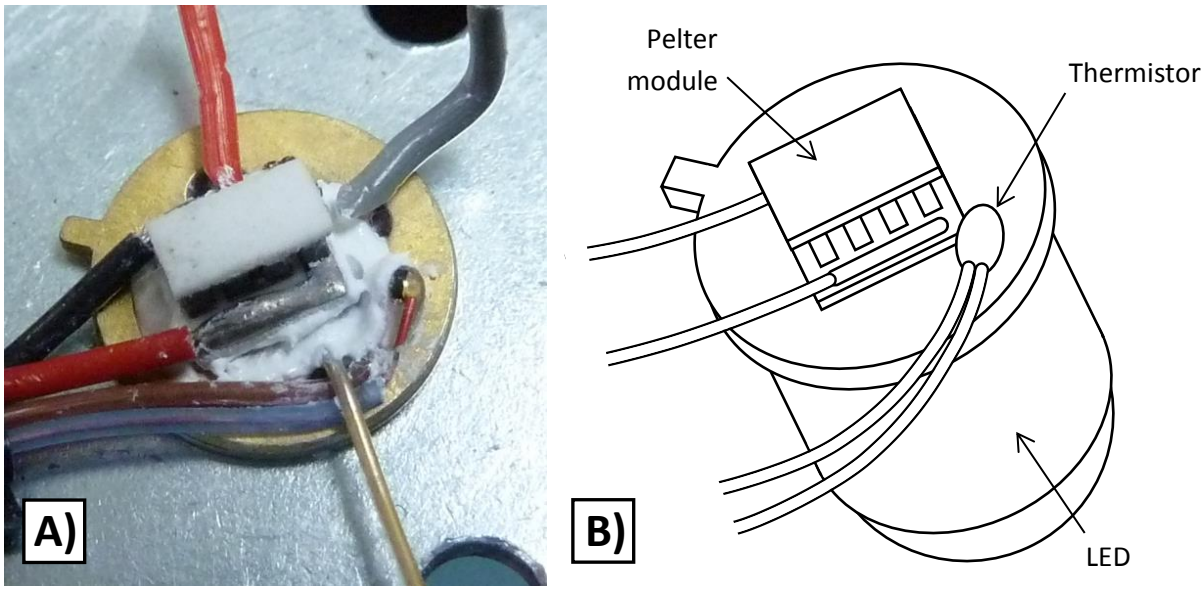

Figure 7.6: A) Photograph of the Pelter module and thermistor attached to the back of the 340nn LED. **B)** Diagram of the same thing. In the photograph thermal grease can be seen around the module and the thermistor and the LED is held in a mount. In the diagram the LED wires have been omitted for simplicity.

The opposite side of the Peltier module was placed in contact with a heat sink. A layer of packing foam was placed around the Peltier module to insulate the LED from the heat sink and avoid a feedback loop. The Peltier module was controlled by the temperature controller, through which it could be heated or cooled depending on the temperature measured by the thermistor. A diagram of this setup is given in Figure 7.7.

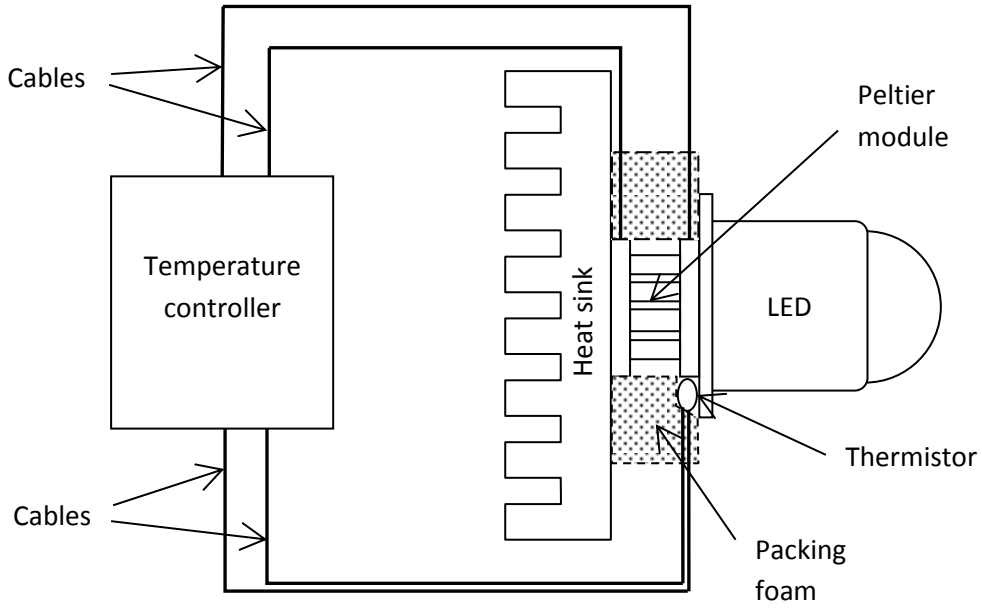

Figure 7.7: Diagram of the Peltier module attached to the LED along with supporting components. Temperature was measured by the thermistor and the Peltier module was controlled by the temperature controller. The packing foam was to decrease thermal contact between the two sides of the module.

7.2.3. Laser-line filters

While it was not necessary to distinguish the sub-nanometre spectral features of the formaldehyde spectrum, the main bands still had widths of around 3nm. Commercially available 'narrow' band-pass filters had typical transmission bandwidths of 10nm, which was too wide for this system. 'Laser-line' filters presented a better prospect, typically having transmission bandwidths of between 2 and 3nm. These are filters designed to permit transmission from a specific laser but block all other light and so have very precisely defined transmission spectra.

The transmission spectrum of an interference filter is based on the thicknesses of its coating layers. The pass wavelength of each layer is based on the distance the light passes through it before reflecting. If the filter is not perpendicular to the optical axis, this distance increases. This results in a shift in central wavelength of the filter with angle as described by Equation (7.1) [8]:

$$\lambda_f = \lambda_0 \left(1 - \left(n_0/n_f\right)^2 \sin^2\theta\right)^{1/2} \quad (7.1)$$

where λ_f is the centre wavelength when the filter is tilted, λ_0 is the centre wavelength when it is on axis, known as the design wavelength, n_0 is the refractive index of the environment (≈ 1 in air), n_f is the effective refractive index of the filter and θ is the angle of incidence.

When the angle of incidence increases from zero, the centre wavelength decreases below the design wavelength. In this project, this effect was found to be useful for tuning filter transmission to different wavelengths.

Commercially available laser-line filters are generally designed to work with a specific laser and so transmission spectra tend to correspond to existing laser wavelengths. At the time of writing there was not an available filter in the 340nm range desired for this system. The closest were a 325nm filter [9], corresponding to a HeCd laser line, and a 355nm filter [8], corresponding to a Nd:YAG laser line.

A custom built laser-line filter was obtained, designed specifically for this project. It had a central wavelength of 339nm, matching the longest wavelength of the 339nm wavelength band set. One of the commercially available 325nm filters was also obtained to allow for comparison. The 339nm filter had a FWHM of 3.5nm and a peak transmission of 51%. The 325nm filter had a quoted FWHM of 1.5nm and peak transmission of 78%.

In order to test the behaviour of the laser-line filters with angle, a set of goniometer mounts was used. These were rotating mounts with angular degrees marked to allow filter angle to be varied and measured. The mounts rotated the filters in the vertical axis, holding them stationary in the horizontal axes. They were capable of reliably positioning filters to within ±1°. A photograph of one of the filters in its goniometer mount is shown in Figure 7.8.

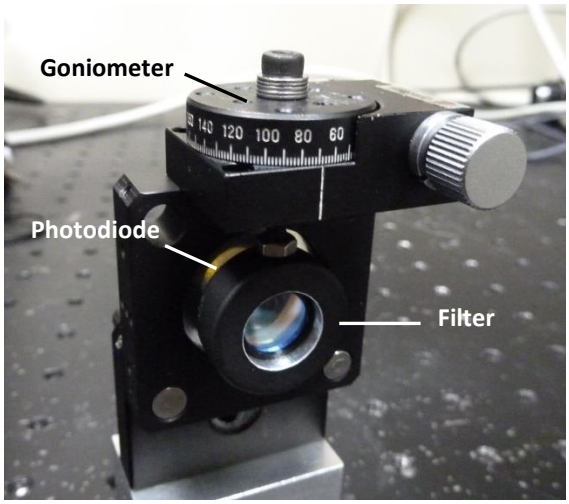

Figure 7.8: Photograph of a laser-line filter in a goniometer mount. One of the photodiodes can just be seen behind the filter.

The transmission spectra of the 339nm filter and the 325nm (Edmund Optics NT47-612, 325nm laser line bandpass filter) [9] filter were tested at a range of angles and the results are shown in Figure 7.9 and Figure 7.10. The UV lamp was used as a light source and the spectrum was measured by the AvaSpec spectrometer. Transmissions were calculated relative to the spectrum of the UV lamp, measured with the same setup for each data set.

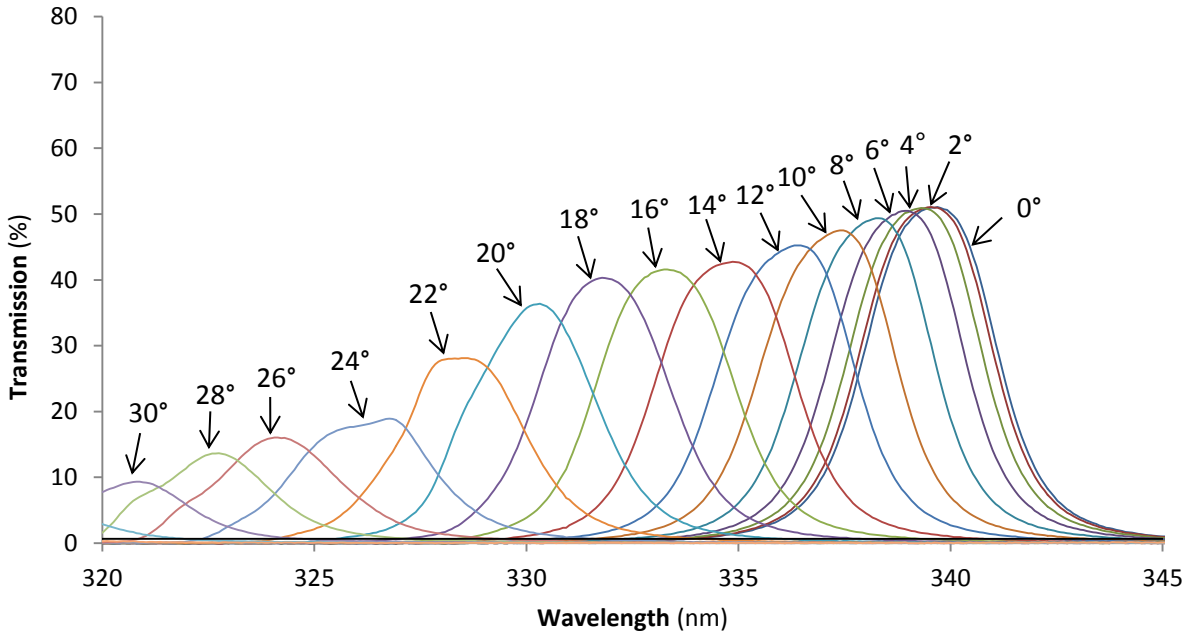

Figure 7.9: Effect of rotating the 339nm filter, showing peak transmission wavelength shifting with angle of incidence. Measurements were taken using the UV lamp and the AvaSpec spectrometer.

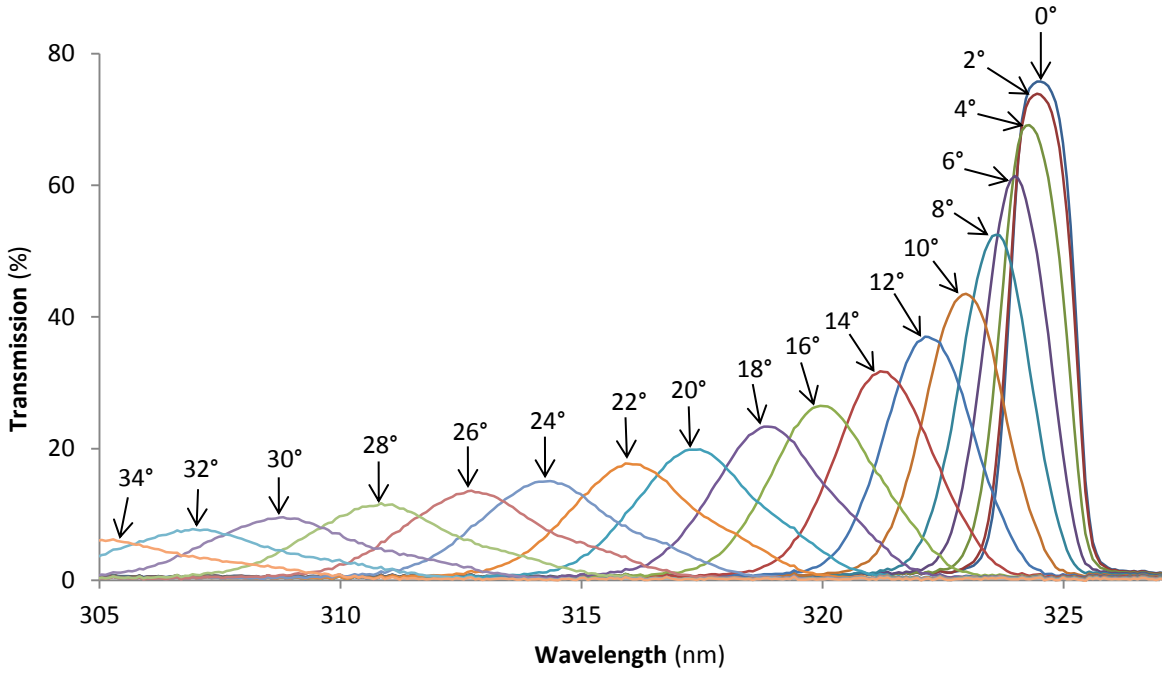

Figure 7.10: Effect of rotating the 325nm filter, showing peak transmission wavelength shifting with angle of incidence. Measurements were taken using the UV lamp and the AvaSpec spectrometer.

In both cases the transmission centre wavelength decreased as expected. However they also show a slight spreading of transmission bandwidth and a significant decrease in peak transmission with increased angle. The peak transmission of the 339nm filter was lower at 0° but the peak transmission of the 325nm filter dropped off more rapidly with angle. At angles above 20°, the transmission peaks of the 339nm filter decrease significantly and start to lose their shape.

Figure 7.11 is a plot of the central wavelength of the two filters with angle, together with theoretical plots from Equation (7.1). Values of effective refractive index were not given by the manufactures and so were empirically fitted at 1.51 for the 339nm filter and 1.64 for the 325nm filter. Both filters show very good correspondence to theoretical results, although the 339nm filter deviated slightly at higher angles due to difficulties identifying the peak in Figure 7.9.

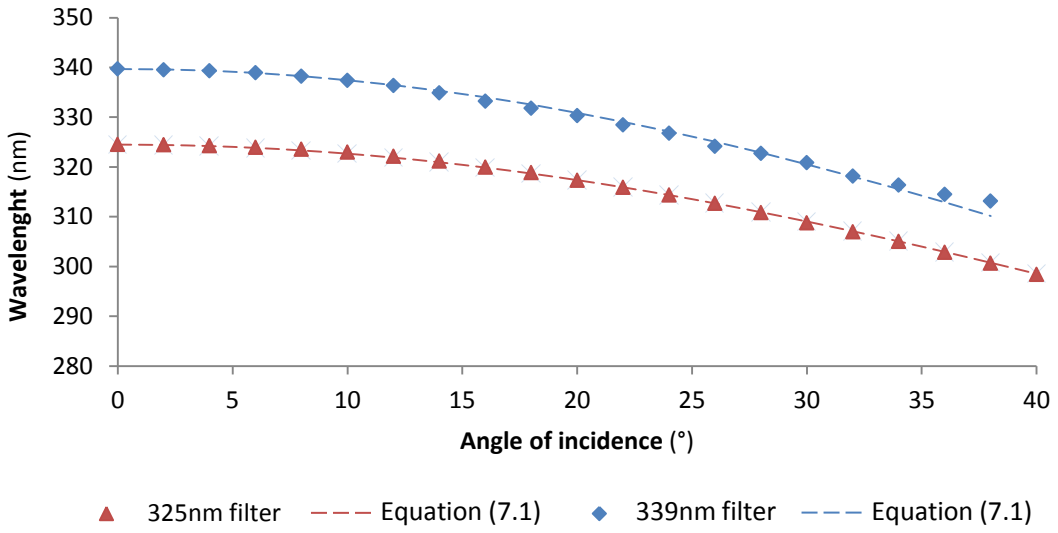

Figure 7.11: Peak wavelengths of the two filters depending on filter angle of incidence. Fit lines are theoretical plots from Equation (7.1) using empirically fitted values of n_f (1.51 for the 339nm filter and 1.64 for the 325nm filter).

Figure 7.12 shows the change in peak transmissions of the two filters. It can clearly be seen how the 339nm has a lower starting transmission, but decreases relatively little for angles less than 20°. Transmission decreases more rapidly for angles greater than 20°. The transmission of the 325nm filter starts higher than the 339nm filter but rapidly drops off with increasing angle, giving a lower transmission by 10°.

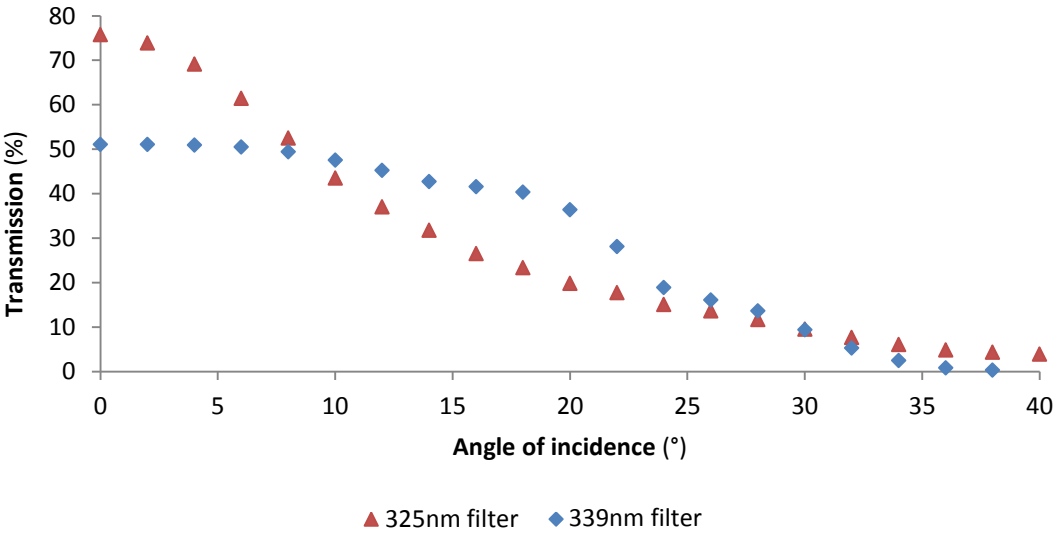

Figure 7.12: Peak transmission of two filters depending on filter angle of incidence. The transmission of the 339nm filter started lower, but initially decreased less quickly with increasing angle.

These results show that tilting laser-line filters can be used to tune their transmissions to shorter wavelengths. However both filters showed a slight spreading of transmission peaks, and a significant decrease in filter transmission. This limits the practical range over which the wavelength can be tuned, with 50% of initial transmission being lost by 24° for the 339nm filter and 12° for the 325nm filter. This corresponds to available wavelength ranges of 326 – 339nm and 322 – 325nm.

While the wavelength shifting of the two filters was similar, the transmission behaviour differed in several ways. The 339nm filter had a lower initial transmission, but it decreased less rapidly with angle. At angles above 20°, transmission of the 339nm filter dropped off more rapidly and peaks started to lose their shape. The 325nm filter started with a higher transmission of 76% which dropped off rapidly but smoothly as angle increased. Consiquently, the 339nm filter had a higher transmission between angles of 10 and 30°.

These differences were attributed to the difference between mass produced and custom made filters. The mass produced filter was likely to have been better optimised for on-axis transmission, with higher initial transmission. The custom filter has lower transmission at angles close to the optical axis. The rapid drop-off in transmission may have been due to the mass produced filter being designed for on-axis performance rather than off-axis performance.

Finally the temperature behaviour of the 339nm filter was tested using the 340nm LED and the AvaSpec spectrometer. The setup was placed in an environmental chamber and the temperature varied from 10°C to 30°C. The emission spectrum of the LED was recorded separately for each temperature to eliminate the effects of temperature change on it. The spectrometer was placed outside the oven, connected by the optical fibre. The resulting shift in the transmission spectrum is shown in Figure 7.13.

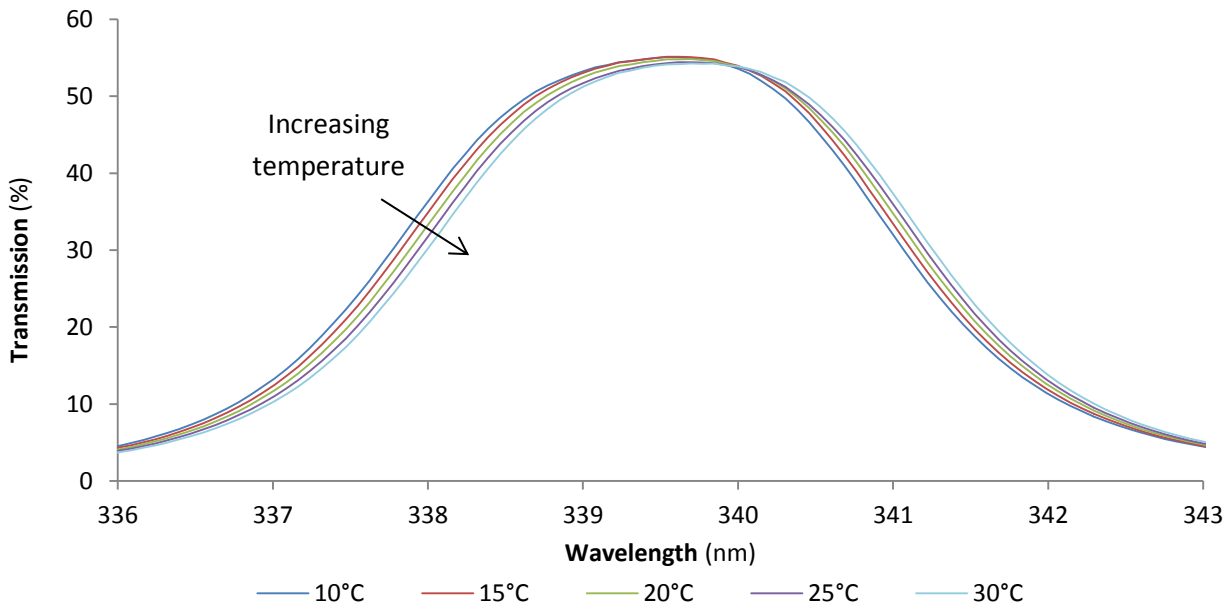

Figure 7.13: Effect of temperature on the transmission spectrum of the 339nm filter. The 340nm LED was used as a light source and spectra were measured using the AvaSpec spectrometer.

Figure 7.13 shows an increase in central wavelength with increasing temperature. This was attributed to thermal expansion of the interference layers. Between 10 and 30°C the peak transmission shifting from 339.60 to 339.72nm, giving a total variation of 0.12nm. This was small in comparison to the FWHM of the filter making the measurement channels of the system, and small compared to the main vibronic peaks of the formaldehyde UV spectrum.

7.2.4. Electronic configuration

In addition to the optical setup, a number of electronic components were used with the two filter system. Components were used for driving the LED, measuring and recording signal from the photodiodes and for removing noise and optimising limit of detection performance. A schematic diagram of the electronic setup of the two filter system is shown in Figure 7.14. A simplified diagram of the optical setup is included in this diagram for reference, the full version of which can be found in Figure 7.3.

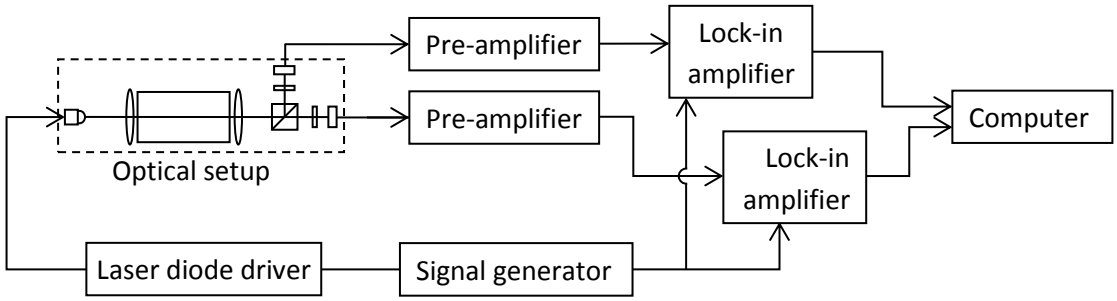

Figure 7.14: Diagram of the electronic setup used for the two filter system The LED was driven by the laser driver with the signal generator providing the modulation frequency and the reference for the lock-in amplifiers. The gain amplifiers converted the photodiode currents to voltages to be filtered by the lock-in amplifiers. The computer processed and recorded the data.

The LED drive current was provided by the laser diode driver (Thorlabs LDC200CV Benchtop LD Current Controller, ±20 mA) [10]. This provided a square wave modulated drive signal with a controlled current. The modulation frequency was provided by the signal generator (Hewlett-Packard 33120a) [11] and was set at 6.5kHz. The signal generator peak to peak voltage was generally set at 8.00mV p-p and the laser diode driver current was 9.41mA.

The signal from the photodiodes was amplified by variable gain amplifiers (FEMTO Messtechnik DLPCA-200). They are quoted as having transimpedance gain ranging from 10^3 to 10^{11} V/A with a gain accuracy of ±1%. They took photodiode current as an input and converted it to output voltage at the set gain ratio. The output voltages from the gain amplifiers were used as inputs for the lock-in amplifiers.

Lock-in amplifiers (Stanford Research Systems SR850 DSP Lock-In Amplifier) [12] operate by extracting only signals with a frequency that matches the specific reference frequency. This allowed any noise that did not match this frequency to be removed from the measurement. The reference frequency was also provided by the signal generator to ensure that it matched that of the LED drive current. The lock-in amplifiers used a time constant of 10ms, bandwidth of 7.8Hz and generally used a gain setting of 200mV although this was sometimes varied due to strength of signal.

Measurements of intensity for this system were given as voltages, being the output of the gain amplifiers as measured by the lock-in amplifiers. Spectroscopy measurements use the ratio of initial and final intensities, so it was not generally necessary to convert figures back to intensities. In this project this was generally referred to as the signal from the intensity, rather than as the intensity directly.

7.3. Wavelength channels

The two filter system was first built using the 339nm wavelength band set as described in Chapter 4. This set had two wavelength bands, a detection band centred at 339nm and a reference band centred at 336nm. It used the $2^1_0\,4^1_0$ formaldehyde absorption peak, one of the strongest formaldehyde absorption peaks in the low interference region described in Chapter 4. The two filter system could only use two channels, so a third (detection) channel was not used. The low interference region of the formaldehyde spectrum is repeated in Figure 7.15.

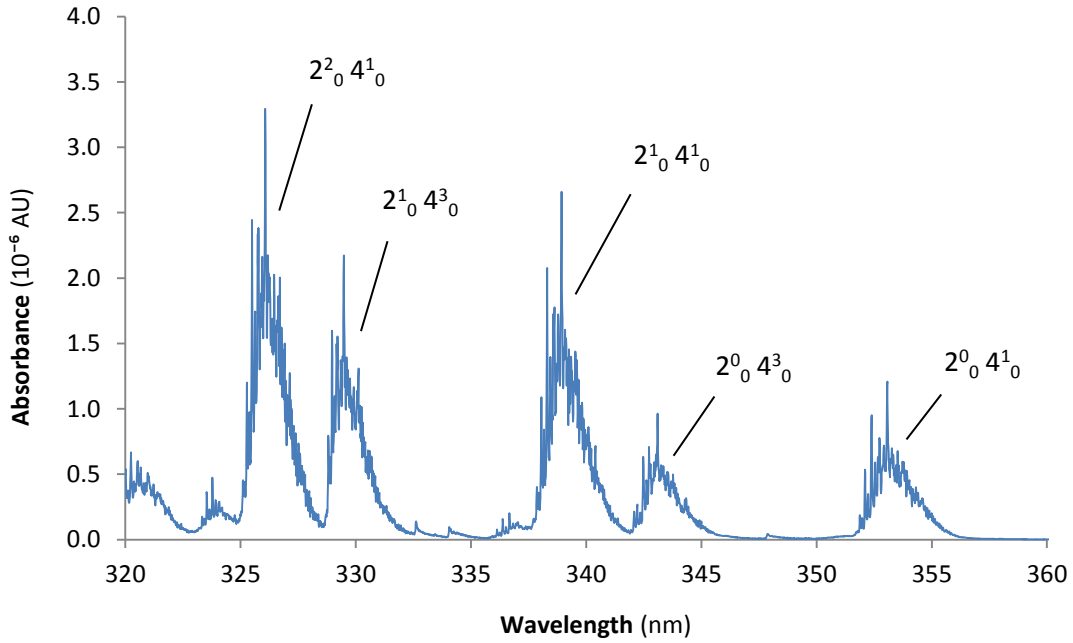

Figure 7.15: Absorbance of formaldehyde in the identified region, assuming a 10ppb concentration and a 100mm path length, calculated from data from Meller et al. [13]. The major vibration state peaks are marked [14]. This region has very little interference from gases common to the indoor environment.

The two filter system was set up using the 340nm LED and a pair of 339nm custom laser-line filters angled at 0° for the detection channel and 14° for the reference channel. The LED intensity and the filter transmission were both lower for the detection channel so the transmission arm of the beam splitter was used for this channel. Figure 7.16 shows the transmission spectra of the two channels as measured by the AvaSpec spectrometer, placed in the positions of the photodiodes (See Figure 7.3).

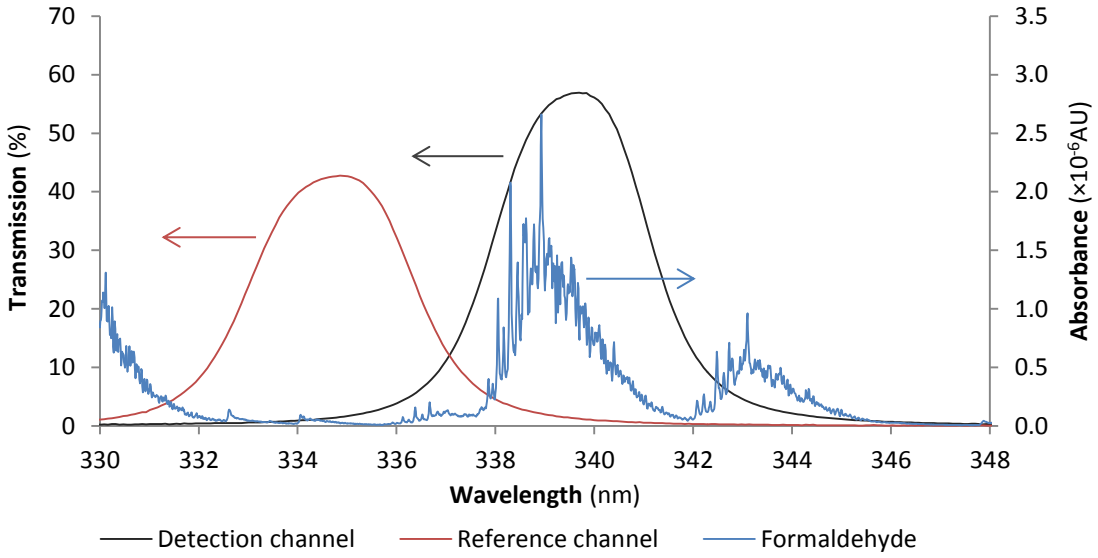

Figure 7.16: Intensity spectra of the detection and reference channels of the two filter system. Data was taken by the AvaSpec spectrometer. The absorbance spectrum of 10ppb of formaldehyde with a 100mm path length, calculated from data from Meller *et al.* [13].

A simulation was run to find the absorbance of these channels using this data and formaldehyde absorption cross-section data from Meller et al. [13]. Using a 19.5cm path length and a simulated formaldehyde concentration of 1ppm, the detection channel and the reference channel were found to have absorbances of 1.04×10^{-5}AU/ppm and 3.48×10^{-6}AU/ppm respectively. The detection channel gives a larger absorbance than the reference channel.

To find the absorbance resulting from a quantity of gas, the difference between the detection and the reference channel was used. As the reference channel did have some absorbance as well, this had the effect of decreasing the measured system absorbance by a factor of $(1.04\times10^{-5}/(1.04\times10^{-5} - 3.48\times10^{-6}) = 1.5$. Hence the system had a total absorbance of 6.9×10^{-6} AU/ppm.

7.4. System optimisation

As explained in Chapter 3, the limit of detection of a spectroscopy based system can be described in terms of the noise equivalent absorbance (NEA), the level of absorbance that is equal to the total noise is set by the signal-to-noise ratio of the detection measurements. The minimum detectable intensity change from gas absorption is equal to the intensity noise level. The concentration required to give this absorption is given by Equation (7.2).

$$\frac{\Delta I(\lambda)}{I_0(\lambda)} = \sigma(\lambda) l N \tag{7.2}$$

The normalised absorbance is given by Equation (7.3) [15]:

$$A = 1 - \frac{I_D}{I_R}\frac{I_{0R}}{I_{0D}} \tag{7.3}$$

A simplified version of the two filter system was used to test and optimise its limit of detection. A diagram is shown in Figure 7.17. The LED, Peltier module, photodiodes and optics were used in the same manner as for the two filter system but the filters and gas cell were removed to simplify optimisation. The electronic setup was the same as described in Section 7.3.5.

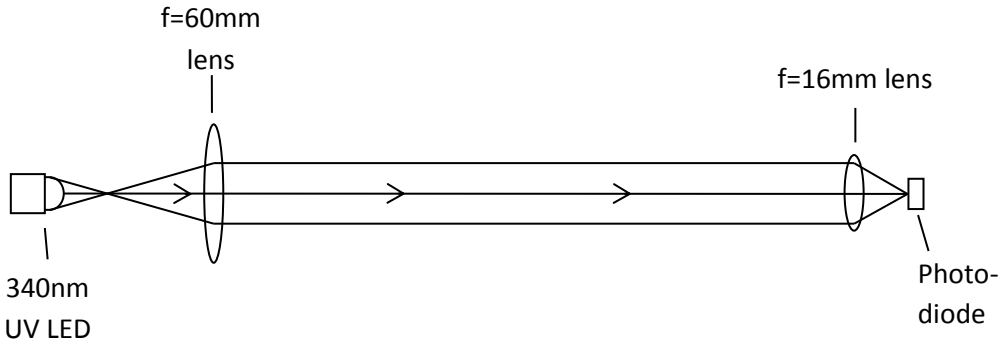

Figure 7.17: Diagram of the setup used for optimising the two filter system. The LED, Peltier module, photodiodes and optics worked in the same way as for the two filter system, but the filters and the gas cell were removed to eliminate any noise from these components.

7.4.1. Drive current and modulation frequency

This refers to the current used to drive the LED. It was provided as a square waveform produced by a signal generator, used to modulate the LED and provide a reference for the lock-in amplifiers. This caused the LED to switch on and off at this frequency, avoiding the need for a chopper or other mechanical modulation. To optimise the two filter system it was important to understand variations in the drive current, and to select a modulation frequency that was relatively clear of electronic interference.

Initially the drive current was provided directly by the signal generator with the voltage controlled and the current allowed to vary. However it was later found that controlling the current provided a more stable LED output [16] so a laser driver was added to the system (see Figure 7.14). The laser driver used the modulation frequency provided by the signal generator but controlled the drive current and allowed the voltage to vary. Figure 7.18 shows measurements of the LED output using voltage control and current control, showing how current control provides a much more stable signal.

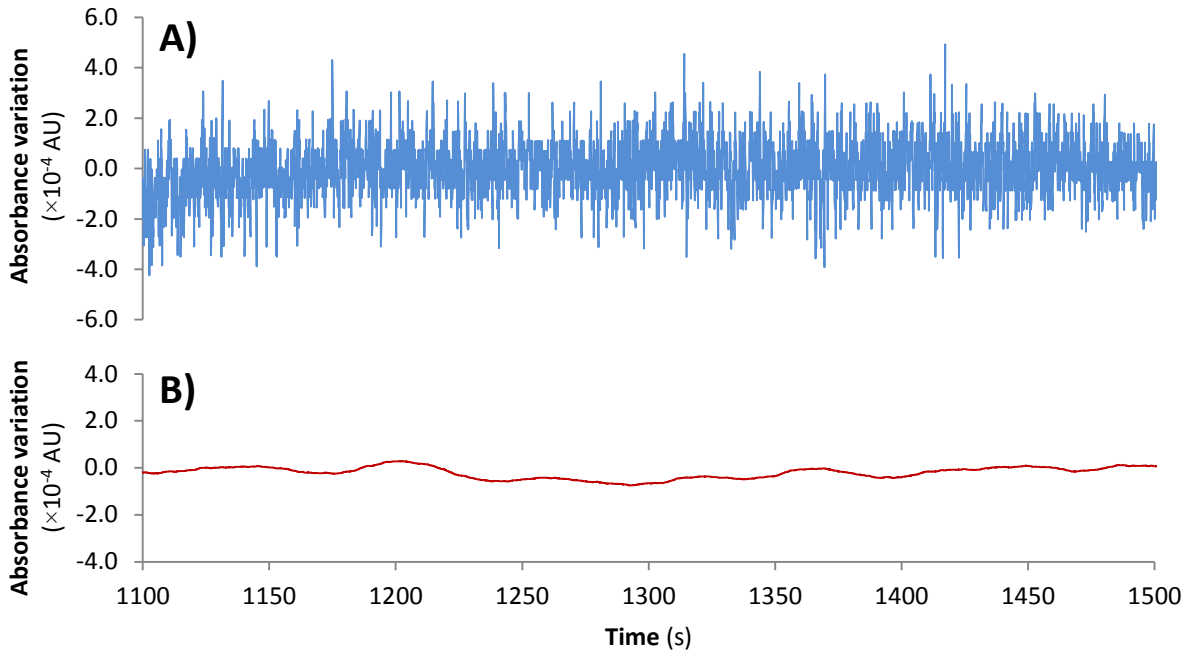

Figure 7.18: System absorbance noise using **A)** voltage-controlled drive current and **B)** current-controlled drive current. It can clearly be seen that the current control gives a more stable output.

It can clearly be seen that current control provides a more stable output. The diode driver was therefore incorporated into the system.

An electronic spectral analyser (Stanford Research SR780 Dynamic Signal Analyzer) [17] was used to select the modulation frequency. This system recorded the magnitude of input signal against the frequency at which it occurred. It was used to measure the electronic noise of the system, covering both electronic interference and fundamental detector noise. The results of which can be seen in Figure 7.19. For this data, the LED was modulated at 25kHz, outside the region of interest (not shown).

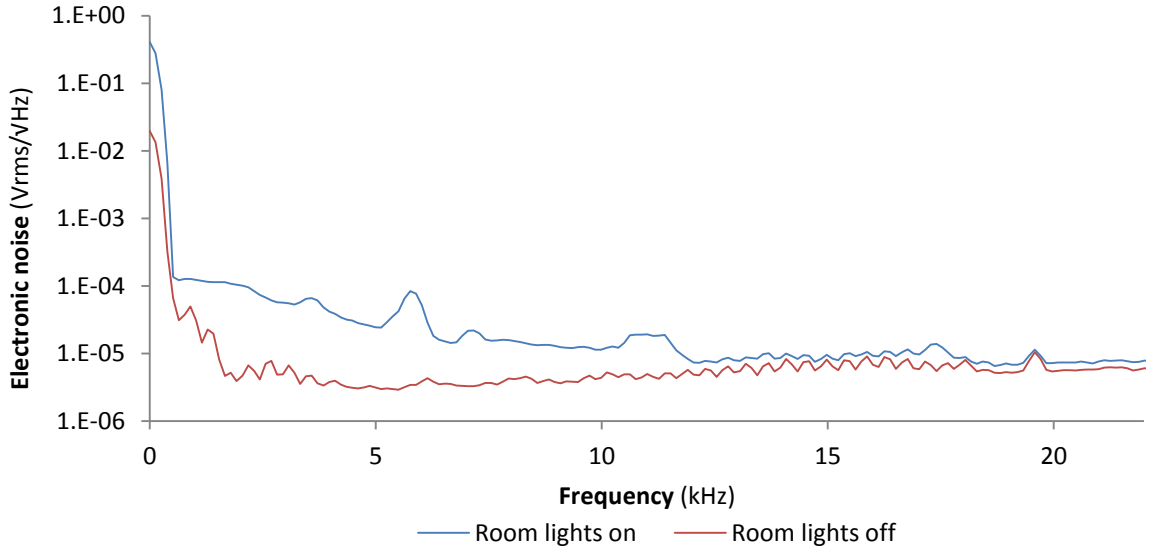

Figure 7.19: Electronic noise spectrum of one of the photodiodes as it measured the output of the LED, as recorded by an electronic spectral analyser, with and without room lights. The LED was modulated at 25kHz for this test. A drive frequency of 6.5kHz was finally selected, giving a noise level of 3.5×10^{-6}Vrms/√Hz.

Figure 7.19 shows that the lowest electronic interference was between around 4 and 9kHz when the room lights were off. A modulation frequency of 6.5kHz was selected as the modulation frequency for the LED as it was within this region and also avoided the main peaks when the lights were on. It gave an electronic signal of 3.5×10^{-6}Vrms/√Hz. Lights were kept off during runs, but lights in near-by rooms could not always be controlled.

It is noticeable that the room lights increased the noise level, predominantly below 12kHz. It was therefore important keep the room lights switched off during testing. Other features were thought to be caused by electrical pickup from the laboratory. For example the oscillating pattern shown between 10 and 14kHz (room lights off) was associated with the monitor of the computer used to record data from the lock-in amplifiers. A signal of 3.5×10^{-6}Vrms/√Hz was found at 6.5kHz with the room lights on.

7.4.2. Temperature dependant uncertainty

Several studies have shown a variation in LED output with temperature [18] [19] [20], finding a decrease in intensity with increasing temperature as well as a shift in peak wavelength. An environmental oven was used to test the temperature dependence of the LED. The temperature of the oven was varied, and the LED was allowed to reach thermal equilibrium in each case. Measurements were taken using the AvaSpec spectrometer, placed outside the oven and connected via the optical fibre. The results are shown in Figure 7.20.

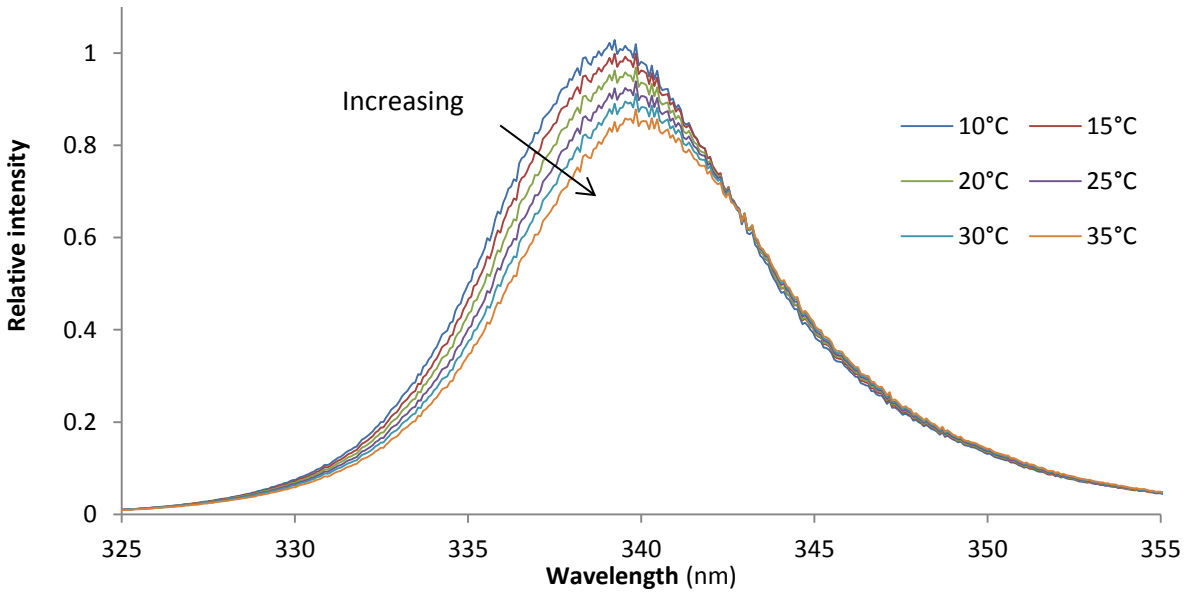

Figure 7.20: Graph of the LED intensity variation with temperature at various wavelengths. Central wavelength increases with temperature and peak intensity decreases.

These results show that an increase in temperature correlates with a decrease in intensity and a shift in transmission spectrum towards longer wavelengths as expected. Over the 25°C test

range, the peak intensity decreased by 16% and the transmission spectrum centre wavelength shifted by 0.84nm. Both were significant issues in the context of this project.

The change in intensity was an issue because intensity changes from absorption were critical to finding concentrations. It was important that intensity change arising from temperature variation were not confused with changes resulting from absorption. The role of the reference channel was to distinguish between absorption variation and variations from other sources.

While the spectral peak shift was small in comparison to the FWHM of the detection and reference channels, the spectral effect was significant. As different channels used different parts of the LED spectrum, wavelength shifts could affect channels differently. For example, the intensity at a 355nm measurement channel would decrease with increasing temperature, while changing little for a 345nm measurement channel. Consequently temperature control of the LED was an important consideration for this project.

When selecting the drive temperature for the Peltier module, it was desirable to find a temperature that could be held as stable as possible. It was also desirable for this temperature to be reached rapidly to minimise LED warm up time before the system could be used. A series of tests were run in which the output of the 340nm LED was recorded over time at a range of different temperature control settings. The results are shown in Figure 7.21.

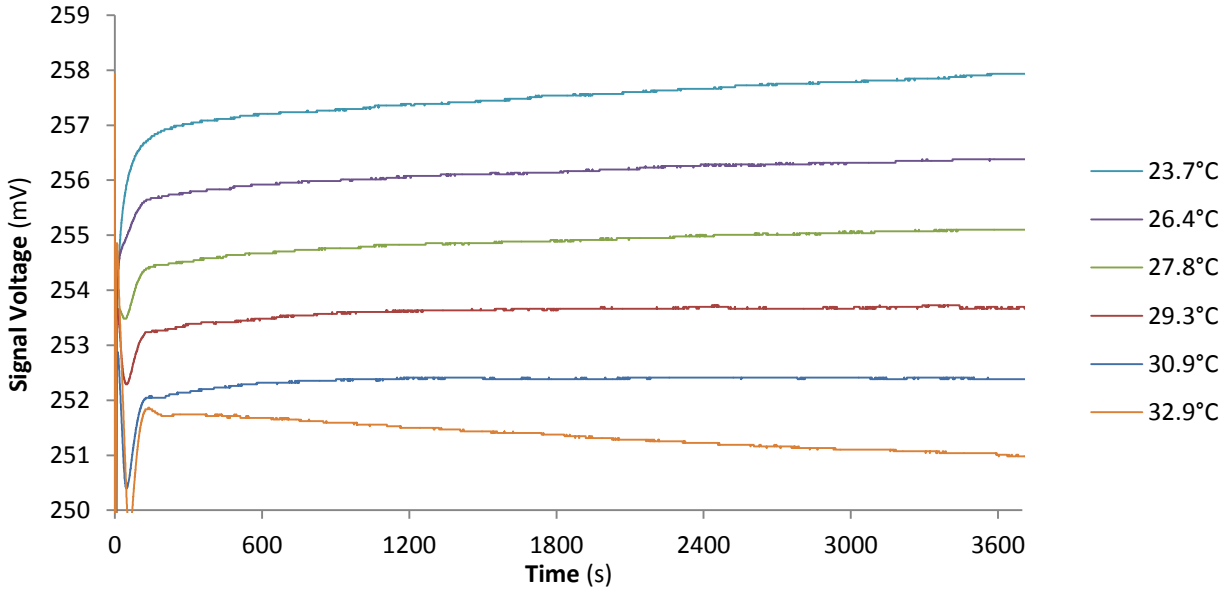

Figure 7.21: Variation of signal from the reference channel over time at various Peltier module temperature settings.

These results show the signal from the LED increases with decreasing temperature as expected. However they also show a significant drift over time, attributed to limitations in thermal contact between the thermistor and the LED element. The most stable LED output was found when the temperature was set to 29.3°C to 30.9°C, taking about 900s (15 minutes) to stabilise. However this value was not fixed and was found to depend on ambient conditions and so vary with time or location. This required the most stable temperature setting to be re-found for every test, making temperature control much more difficult and unreliable.

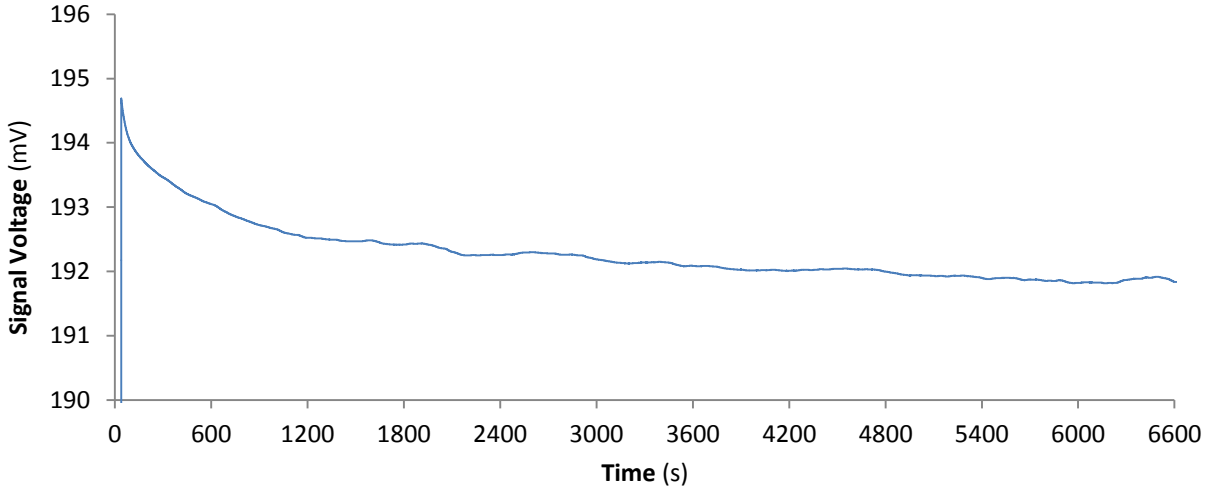

Figure 7.22: Variation of signal from the reference over time as the LED tends to thermal equilibrium with no temperature control.

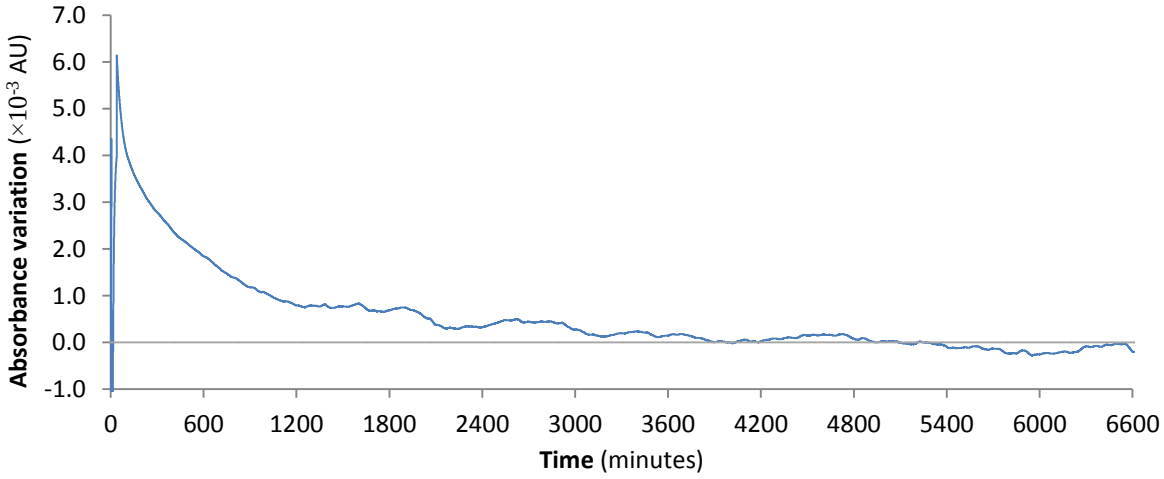

Figure 7.23: Absorbance variation over time as the LED tends to thermal equilibrium with no temperature control.

Figure 7.22 shows the signal from the reference channel with no temperature control (i.e. the Peltier was not used). Figure 7.23 shows the absorbance variation measured by both channels. It took around 3600s (1 hour) to reach thermal equilibrium, significantly longer than when using the Peltier module. However allowing the system to reach thermal equilibrium did remove the requirement to find setting requirements for every test run. It was decided that while improved temperature control would be desirable in a final system, running the system without temperature control would likely provide better noise performance for test measurements.

7.4.3. Noise from lock-in amplifier

One of the main limitations of the lock-in amplifiers used in this project was quantisation. Quantisation is the error on a digital measurement when the precision of the reading cannot be greater than discrete measurement levels. Variations smaller than the measurement levels will not be detected unless they overlap the boundary between two levels. The magnitude of the measurement levels for the lock-in amplifiers was dependent on the gain settings as shown in Table 7.1.

Table 7.1: Details of the gain settings of the lock-in amplifiers.

Gain setting	Precision level	Signal-to-noise ratio	Minimum NEA
1V	0.061mV	1.64×10^{4} : 1	6.10×10^{-5}AU
500mV	0.03mV	1.67×10^{4} : 1	6.00×10^{-5}AU
200mV	0.007mV	2.86×10^{4} : 1	3.50×10^{-5}AU
100mV	0.0038mV	2.63×10^{4} : 1	3.80×10^{-5}AU
50mV	0.0019mV	2.63×10^{4} : 1	3.80×10^{-5}AU
20mV	0.0019mV	1.05×10^{4} : 1	9.50×10^{-5}AU

One of the highest signal-to-noise ratios came from the 200mV gain setting, equal to 2.86×10^{4} : 1. This is equivalent to an NEA of 3.50×10^{-5}AU. While it was important to avoid saturation, best performance could be achieved when the signal was close to the maximum signal of the relevant gain setting.

A technique was devised for improving the performance of the lock-in amplifiers beyond the quantisation limit. By decreasing the measurement period of the lock-in amplifier, random noise phenomena such as shot noise and source fluctuation noise increased in magnitude. Details on the behaviour of this kind of noise phenomena can be found in Chapter 5. By subsequently averaging over many measurements, the random variations could then be used to achieve a better precision than the quantisation limit. An example is shown in Figure 7.24.

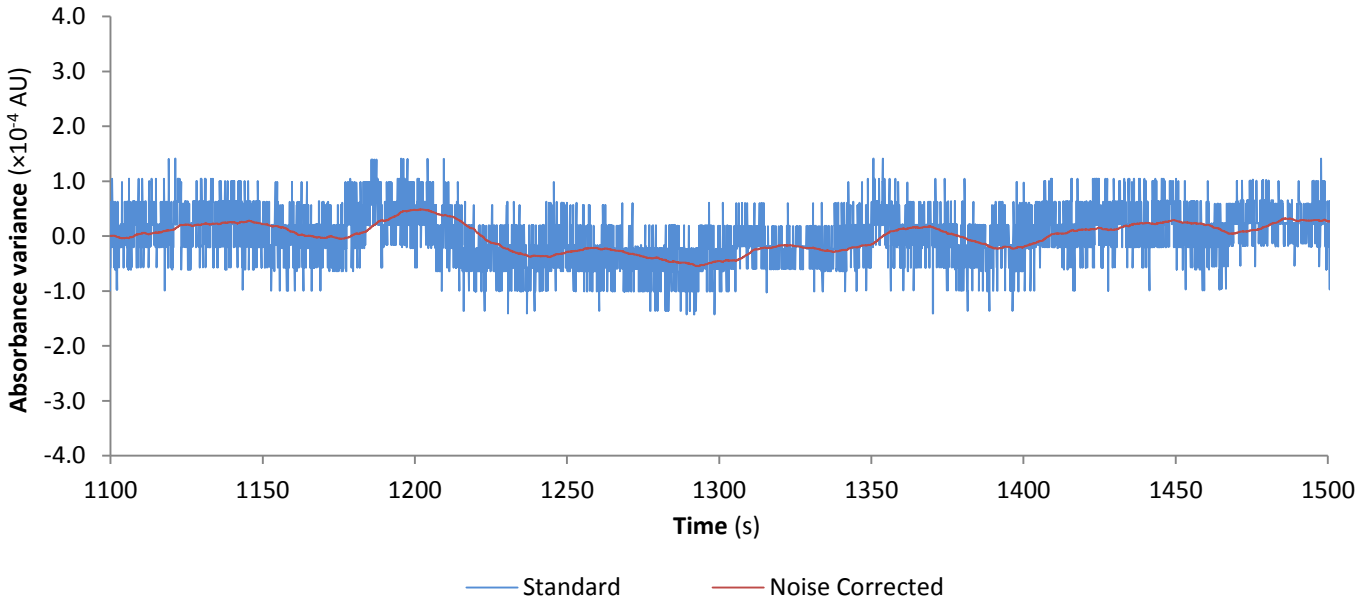

Figure 7.24: Absorbance variation of the system with quantisation limiting processing (Red) and without it (Blue). It can clearly be seen how the method set variations lower than the system precision to be detected.

Quantisation errors can clearly be seen on the unprocessed data set where values were only measured with a precision of 7.0×10^{-5}V intervals. The processed data shows a much improved precision, measuring variations down to 3.5×10^{-7}V. However it is noticeable that the processed data shows a slight delay, caused by the time to take averages over many measurements.

The number of averages to be used was found by measuring the signal from the LED for two hours and then taking an Allan variance of the data [21]. This is an analysis technique in which the variation between measurements is plotted against a varying integration time. The intergration time that gives the lowest variation can be used to minimise measured noise. The technique takes account of both short term fluctuations and long term drifts.

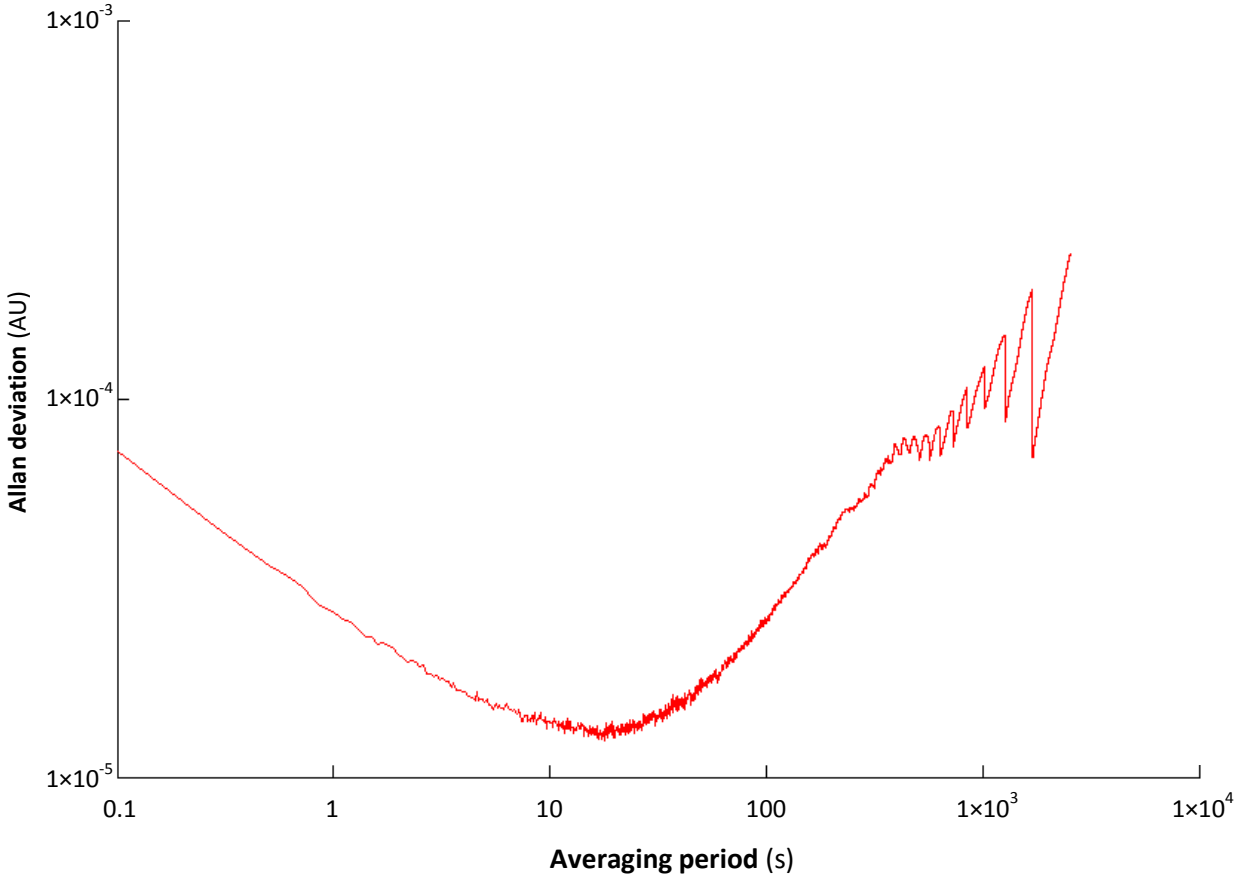

Figure 7.25: Allan variance of the signal from the LED over time. Variation is high at short periods due to short term white noise and high at long periods due to drift effects. The optimum measurement period is found at the minimum variation between about 10 and 60s.

Figure 7.25 shows the Allan variance of the signal from the LED over time. This is a 'classic' Allan variance plot, with high variation at short time periods resulting from white noise such as effects like source fluctuation noise, and also high at long time periods from effects such as temperature related drift. The best compromise between the two can be found at the lowest position on the graph, between about 10 and 60s in this case. The averaging period was set at 20s, within these bounds.

The final noise phenomenon originating from the lock-in amplifiers was a random variation between the outputs from two lock-in amplifiers recording data from the same source. To investigate this, the output of the LED was recorded with a single photodiode and the resulting current was converted to voltage by a single gain amplifier. The voltage signal was then simultaneously recorded by two lock-in amplifiers using the same drive frequency source and the same standard settings.

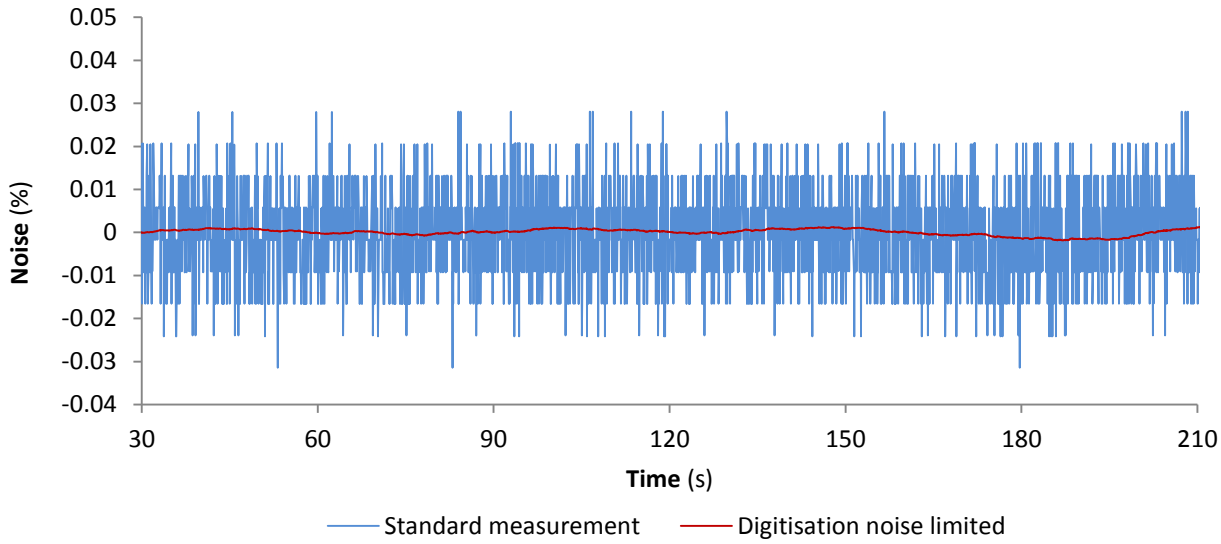

Figure 7.26: Proportional difference between identical signals measured by two lock-in amplifiers as a percentage of total signal.

The proportional difference between the signals recorded by the two lock-in amplifiers is given in Figure 7.26 as a proportion of total signal. Data both with and without quantisation limitation is included. This difference was attributed to noise from the internal electronics of the lock-in amplifier. While well below the precision limit of the lock-in amplifiers, this variation was still significant in the context of this project. Over 20s the quantisation limited data gave an NEA of 3.0×10^{-6}AU.

7.4.4. Noise summary

The main noise phenomena found with the two filter system are summarised in Table 7.2, together with the methods used to control or limit them. NEA values for the optimised performances are given for each, generally calculated over a 20s measurement period. A 10ms time constant was used on the lock-in amplifiers, giving a bandwidth of 7.8Hz. Levels for lock-in amplifier quantisation are given in (V) rather than (V/√Hz) as it does not vary with bandwidth.

Table 7.2: Summary of the noise phenomena affecting the two filter system

Phenomenon	Initial level	Control	Final level	NEA
Electronic noise	Up to 8.4×10^{-5}V/√Hz	Modulation frequency set to 6.5kHz	3.5×10^{-6}V/√Hz	2.4×10^{-5}AU
Thermal drift	Up to 1.5×10^{-6}V/√Hz	Allow system to reach thermal equilibrium	~5.2×10^{-8}V/√Hzs	~3.7×10^{-7}AU/s
Lock-in amplifier quantisation	7×10^{-5}V	Quantisation reduction process	3.5×10^{-7}V	1.8×10^{-6}AU
Lock-in amplifier random noise	4.3×10^{-7}V/√Hz	N/A	4.3×10^{-7}V/√Hz	3.0×10^{-6}AU
Source fluctuation noise	5.3×10^{-5}V√Hz at 0.1s	Averaging over 20s	5.4×10^{-6}V/√Hz at 20s	3.8×10^{-5}AU

The most significant noise phenomena identified for this system were thermal drift, predominantly of the LED, and source fluctuation noise. For a single measurement, source fluctuation noise and electronic noise dominated, giving a limit of detection of 4.5×10^{-5}AU. Thermal drift reaches similar levels after about 3 minutes so baseline measurements needed to be taken soon after or before absorbance measurements.

7.5. System testing with formaldehyde

The two filter system was tested using formaldehyde generated from a permeation tube as described in Chapter 6. The permeation tube yielded formaldehyde gas when heated to 100ºC, which could be mixed with clean air to vary the concentration. In order to minimise disturbance of the setup, the air flow was switched between high and low rates to provide a variation in formaldehyde concentration to detect. The gas taps were set to open to allow a constant gas flow though the gas cell.

Initially the system was tested with a high variation of formaldehyde concentration. Air flow was switched between 500 and 50cm^3/min. Using the formaldehyde flow rates found by the preliminary system in Chapter 6, this provided a comparison between 44 and 4.4ppm, giving a total difference of 40±7ppm. The air flow was switched over multiple times during the run, in the manner of a modulated signal. The results are shown in Figure 7.27.

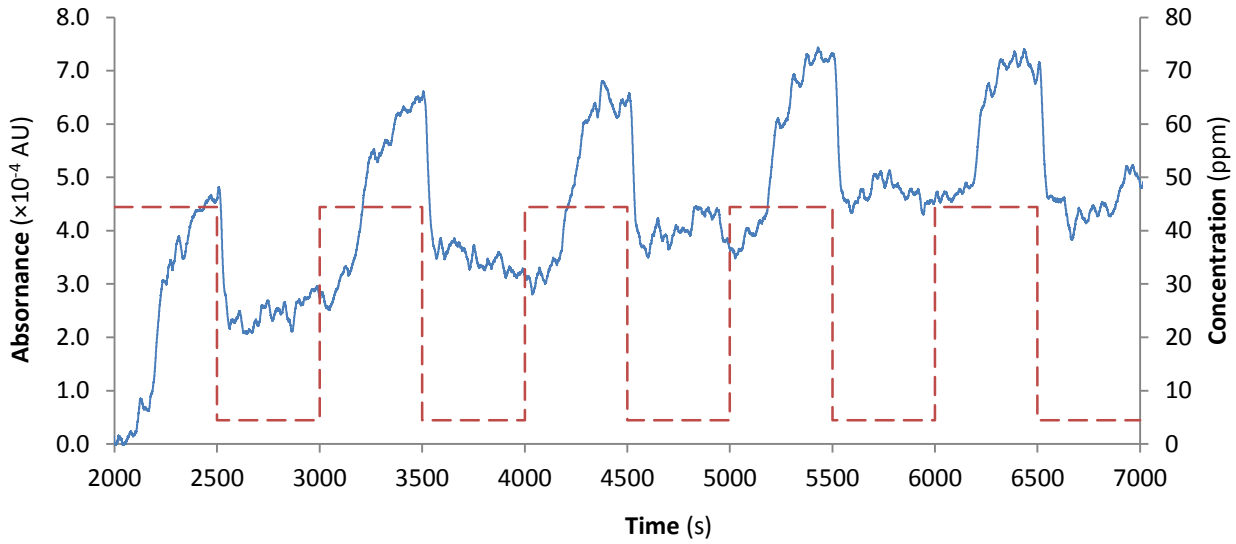

Figure 7.27: Graph of the absorbance detected by the two filter system (Blue) caused by a periodic shift in formaldehyde concentration between 4.4ppm and 44ppm (Red). Absorbance change can clearly be seen above the base-line.

In Figure 7.27 the effect of formaldehyde can clearly be seen as an increase in absorbance correlating with the increases in formaldehyde concentration. This verifies that 40ppm was well above the detection limit of the system. It also shows that the system did not respond as rapidly to the introduction of higher concentration formaldehyde. Absorbance increased slowly after increasing the formaldehyde concentration of the gas flow, decreasing more rapidly when the concentration was decreased.

The main disadvantage of this method is that the change in flow rates may have affected results. Also the concentration could only be decreased to 4.4ppm, not removed completely, limiting the concentration range of the test and preventing the true baseline from being measured. Additional tests were carried out using two vapour generators connected as shown in Figure 7.28. This allowed the supply to the gas cell to be switched between lines with and without formaldehyde without varying the flow rate, although care had to be taken to switch the two switches over at the same time.

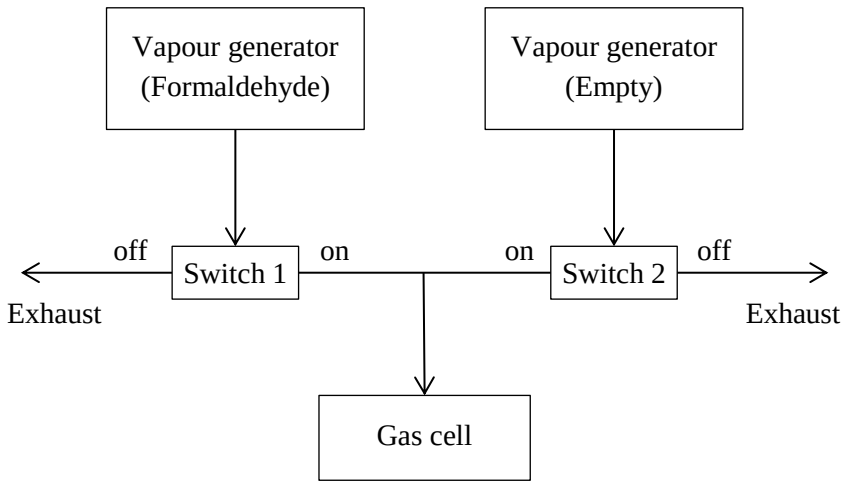

Figure 7.28: Diagram of the formaldehyde delivery system. The two vapour generators supply the same rate of flow and the same temperature. One includes a set concentration of formaldehyde, the other, clean air. The supply to the gas cell can be switched between the two without varying flow rate.

The system was tested in this manner with a range of formaldehyde concentrations. The results are shown in Figure 7.29. 500s were left between baseline and detection measurements to allow the gas cell to fill, increasing the limit of detection to 2.04×10^{-4}AU. The position of the limit of detection is marked on the graph. Figure 7.29 shows a clear increase in detected absorbance with increasing concentration above the limit of detection and little or no correlation below it, as expected.

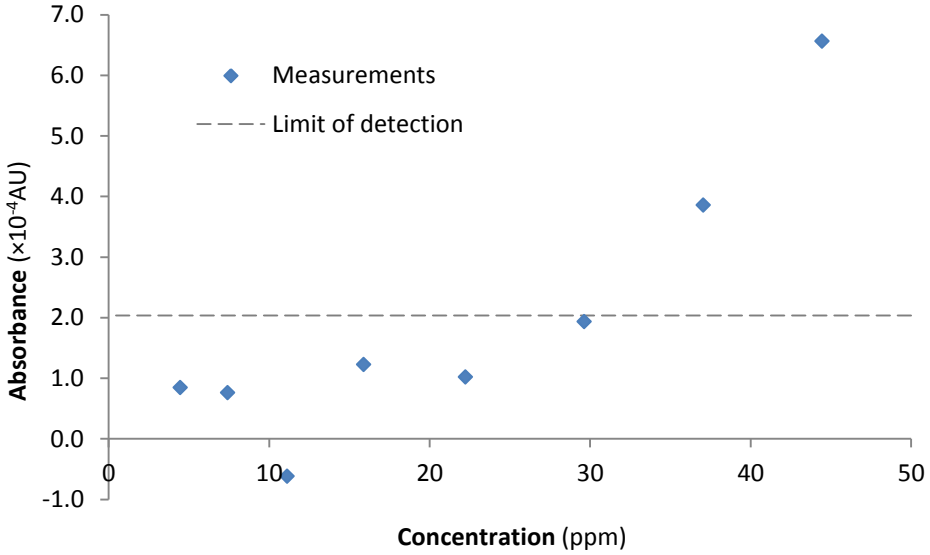

Figure 7.29: Graph of the response of the two filter system to formaldehyde concentration. The position of the calculated limit of detection is shown. The limit of detection was limited increased from 4.5×10^{-5}AU by thermal drift and the time taken to flush samples through the gas cell.

7.6. Chapter summary

The two filter system was used as a proof of concept device, based on laser-line filters. The main advantages of the system were that it was simple in design and came close to the optimum noise performance of the detectors for short term measurements. The main disadvantage was that it had only two channels and therefor had limited selectivity.

The formaldehyde spectrum has a number of strong absorption peaks at wavelengths close to regions of very low absorption. This had potential for use as detection and reference channels for low resolution spectroscopic measurements using minimal components and this system was used to test this. It was also used to test the technique of angling laser-line filters to tune transmission wavelengths.

Light from an LED was collimated through a gas cell and then divided into two channels by a beam splitter. The laser-line filters were used to select the wavelength range of each channel, tilted to tune their transmission wavelengths to match formaldehyde spectral features. The intensity from each channel was measured with a photodiode and the ratio between the detection and reference channels was used to calculate the formaldehyde concentration.

The Laser-line filters were extremely narrow (FWHM around 3nm) band pass filters designed to transmit only the wavelength range of a particular laser. Their peak transmission wavelength could be varied by varying their angle to the optical axis and this behaviour was exploited to tune transmission wavelengths to match features in the formaldehyde spectrum. This allowed absorption measurements to be taken with simple photodiodes and a full spectrometer was not required.

Laser-line filters are generally only mass-produced at wavelengths matching the output of specific lasers so a custom made filter was obtained to match the 339nm formaldehyde absorption peak. It was found to have a lower on-axis transmission than a mass-produced 325nm filter, and that the transmissions of both dropped off rapidly with increasing angle. This limited the practical range over which the transmission spectrum could be tuned. However it was sufficient for use in this project, and there may be potential for improving performance further with additional optimisation of the filter’s fabrication.

The noise performance of this system was characterised and optimised. Noise phenomena that were identified included interference from frequencies matching the modulation frequency, thermal drift, quantisation, lock-in amplifier noise and source fluctuation noise. After optimisation the most significant were source fluctuation noise and thermal drift, giving a best-case limit of detection of 4.5×10^{-5}AU. A simulation of the system channels found this to correspond to 6.6ppm.

A future system could be improved with a thermal control unit placed closer to the LED element. This would preferably be inside the case and installed at the time of manufacture. If all non-fundamental effects, such thermal drift and source fluctuation, could be removed or accounted for, the system would be limited by fundamental detector noise. Assuming all electronic noise not removed by modulation or keeping the room lights off was caused by detector noise, this would give a limit of detection of 2.4×10^{-5}AU.

The two filter system was tested with formaldehyde at a range of concentrations. It was not possible to test the calculated limit of detection 4.5×10^{-5}AU, as it took several minutes for low concentration formaldehyde to fill the gas cell. This allowed thermal drift effects to dominate, giving a higher limit of detection of 2.04×10^{-4}AU. This was due to the size of the gas cell and the formaldehyde delivery method, not the system itself, but it did prevent the short term measurement performance being verified.

This demonstrated that using low resolution wavelength measurements to distinguish between formaldehyde detection and reference channels could be applied to spectroscopic measurements. It also allowed the performance of the UV LED and the photodiodes to be ascertained. However the limit of detection did not reach the target level for the project and having only two channels made accounting for spectral interference particularly difficult. An improvement on this system with multiple channels is discussed in Chapter 8.

7.7 References

[1] Zemax EE 2006 version, Optical Raytrace Software Package, Zemax, Redmond, USA, 2006.

[2] Centronic OSD5.8-7QSD5.8-7Q, *Technical Data Sheet,* Centronic Ltd., Croydon, UK, 2012.

[3] Global Component Sourcing Thermoelectric Module ET-007-06-11, *Technical Data Sheet,* Global Component Sourcing, Hong Kong.

[4] EPCOS NTC thermistors for temperature measurement, Glass-encapsulated sensors, standard type, *Technical Data Sheet,* EPCOS, Munich, Germany, 2013.

[5] EPCOS NTC Thermistors, Standard R/T characteristics, *Technical Data Sheet,* EPCOS, Munich, Germany, 2013.

[6] EPCOS, Standardized R/T Characteristics, *Technical Data Sheet,* EPCOS, Munich, Germany, 2002.

[7] Thorlabs Blueline Series Thermoelectric Temperature Controller, *Operation Manual,* Thorlabs, Newton, USA, 2003.

[8] Edmund Optics NT64-240, *Technical Data Sheet,* Edmund Optics Inc., Barrington, USA.

[9] Edmund Optics NT47-612, *Technical Data Sheet,* Edmund Optics Inc., Barrington, USA.

[10] Thorlabs Laser Dioce Controller LDC200C Series, *Operation Manual,* Thorlabs, Newton, 2013.

[11] Agilent 33120A Function/Arbitrary Waveform Generato, *Technical Data Sheet,* Hewlett-Packard, Palo Alto, USA, 2004.

[12] Stanford Research Systems Digital Lock-In Amplifiers SR850 — DSP lock-in amplifier with graphical display, *Technical Data Sheet,* Stanford Research Systems, Sunnyvale, USA, 2012.

[13] R. Meller and G. K. Moortgat, "Temperature dependence of the absorption cross sections of formaldehyde between 223 and 323 K in the wavelength range 225-375 nm," *Journal of Geophysical Research-Atmospheres,* vol. 105, pp. 7089-7101, 2000.

[14] D. J. Clouthier and D. A. Ramsay, "The spectroscopy of formaldehyde and thioformaldehyde," *Annual Review of Physical Chemistry,* vol. 34, pp. 31-58, 1983.

[15] J. Hodgkinson, R. Smith, W. O. Hob, J. R. Saffell and R. P. Tatama, *Sensors and Actuators B: Chemical,* vol. 186, pp. 580-588, 2013.

[16] M. Johnson, Photodetection and Measurement: Making Effective Optical Measurements

for an Acceptable Cost, New York, USA: McGraw Hill, 2003.

[17] FFT Spectrum Analyzers, SR780 - 100 kHz 2-channel dynamic signal analyzer, *Technical Data Sheet*, Stanford Research Systems, Inc., Sunnyvale, USA, 2013.

[18] Y. Xi, J. Q. Xi, T. Gessmann, J. M. Shah, J. K. Kim, E. F. Schubert, A. J. Fischer, M. H. Crawford, K. H. A. Bogart and A. A. Allerman, "Junction and carrier temperature measurements in deep-ultraviolet light-emitting diodes using three different methods," *Applied Physics Letters*, vol. 86, pp. 031907-031907-3 , 2005.

[19] K. J. Reynolds, J. P. Dekock, L. Tarassenko and J. T. B. Moyle, "Temperature-dependence of LED and its theoretical effect on pulse oximetry," *British Journal of Anaesthesia*, vol. 67, no. 5, pp. 638-643, 1991.

[20] J. C. Wang, C. H. Fang, Y. F. Wu, W. J. Chen, D. C. Kuo and P. L. Fan, "The effect of junction temperature on the optoelectrical properties of InGaN/GaN multiple quantum well light-emitting diode," *Journal of Luminescence*, vol. 132, pp. 429-433, 2012.

[21] P. Werle, R. Mücke and F. Slemr, "The limits of signal averaging in atmospheric trace-gas monitoring by tunable diode-laser absorption-spectroscopy (TDLAS)," *Applied Physics B*, vol. 57, no. 2, pp. 131-139, 1993.

Chapter 8: Single filter, multi-channel system

The single filter, multi-channel system was developed from the two filter system. The transmission wavelength of laser-line filters varies with angle. This was taken advantage of to use a single filter to provide multiple measurement channels. Like the two filter system, this system used a single LED source but used a photodiode array to measure channel intensity. This provides the potential for improving selectivity.

8.1. Principles of operation

The single filter, multi-channel system used the effect of varying filter angle on transmission wavelength. The transmission central wavelength of an interference filter varies with the angle of incidence as given by Equation (8.1) (see Chapter 7).

$$\lambda_f = \lambda_0 \left(1 - \left(n_0/n_f\right)^2 \sin^2 \theta\right)^{1/2} \tag{8.1}$$

Focused light was used to form a cone of multiple angles, as shown in Figure 8.1. The transmission wavelength of light passing through a laser-line filter changes dependent on the angle, so different wavelengths pass through at different parts of the cone. The photodiode array bisected the light cone. Each element of the array was illuminated by a different wavelength band, in the manner of a dispersive spectrometer.

A diagram of this effect is given in Figure 8.1, shown from above and at a slight angle for clarity. It shows unfiltered light converging on the filter from the left and filtered

light diverging to the plane of the photodiode to the right. Different wavelength bands from the LED spectrum are represented by different colours. Where the line of the photodiode array bisects the cone of light is shown to the right.

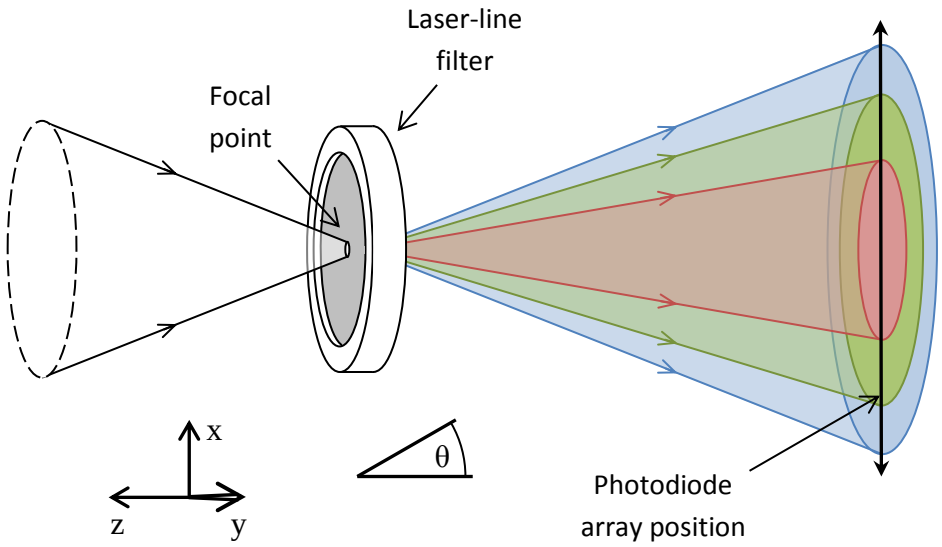

Figure 8.1: Top view diagram of the angular spread of light passing through the filter and reaching the photodiode array. Red represents long wavelengths close to the filter design wavelength, green represents shorter wavelengths and blue represents the shortest wavelengths of this arrangement. The filtered wavelength varies across the photodiode array.

The wavelength band reaching each photodiode element was dependent on the range of angles it subtended. This was dependent on the position of the element, its size and shape, and its distance from the focal point. Equation (8.2) shows the angle of light passing through the filter that reaches a specific point on the photodiode array:

$$\tan\theta = \frac{\sqrt{x^2+y^2}}{z} \tag{8.2}$$

where z is the distance from the focal point to the photodiode array, x is the horizontal distance across the photodiode array and y is the vertical distance across the photodiode array. This influences the peak wavelength reaching the point in accordance with Equation (8.1).

It can be seen from Figure 8.1, and Equation (8.1) that when the filter is aligned with the optical axis, the range of transmitted wavelengths is symmetrical about the optical

axis. This limits the spectral range of the system as the same wavelength bands are repeated on the other side of the photodiode. By imposing an additional tilt ψ, more of the photodiode array and the intensity spread of the LED could be made use of.

The angle of light passing through the tilted filter that reaches a specific point on the photodiode array is given by Equation (8.3).

$$\tan\theta = \frac{\sqrt{(x - z\tan\psi)^2 + y^2}}{z} \tag{8.3}$$

where ψ is the angle of tilt of the filter relative to the optical axis, 24° for this system.

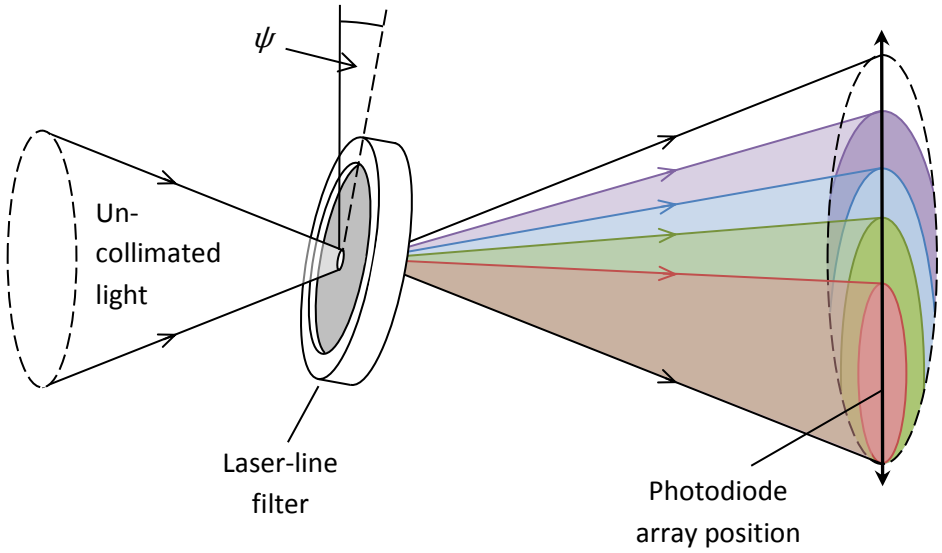

Figure 8.2: Top view diagram of the angular spread of light passing through the filter, tilted at an angle ψ, and reaching the photodiode array. Bands reaching the photodiode array position are of decreasing wavelength in the order red, green, blue, purple and white. By tilting the filter, a greater range of wavelengths reach the photodiode array.

Figure 8.2 shows a diagram of the effect of tilting the filter in this manner. Un-collimated light passes through the filter as before, giving a range of transmission bands at the photodiode. However the angle of the filter results in a shift of the transmitted wavelength bands across the photodiode. Duplicated bands are removed from one end and new bands are introduced at the other.

Unlike dispersive spectrometers, the wavelength band reaching each point was not defined entirely by its position but also by the by the FWHM of the transmission spectrum of the filter. This was about 3nm and results in a minimum spectral resolution for this system, and a slight overlapping of each channel.

The vertical dimensions of the photodiode array elements will have added some spectral spreading. Array elements had a vertical height of 1.45mm, giving a maximum *y* value of 0.725mm. Given a distance from the focal point to the photodiode array of 14.2mm, this adds a maximum angular spread of 1.6°. This corresponds to a spectral spread ranging from 0.7 to 2.0nm. In a future system, this could be limited by using a narrower photodiode array or by masking part of the face. This method was verified using the AvaSpec spectrometer, described in Section 8.6.

8.2. Wavelength channels

For this system, measurement and reference channels must all be within the range of the light source and also of the filter. Two measurement channels and one reference channel were desired for reliable operation with resilience to cross sensitivity. Finally stronger absorption features improve limit of detection, although features closer to the visible range may partially offset this as many components operate more efficiently.

The first wavelength band set to be considered was the 353nm band set described in Chapter 4. This set had two detection bands centred at 353nm and 343nm, and one reference region centred at 348nm. The detection bands in this set did not have as strong absorption as those of the 339nm band set. However, they did all fall within the range of a single LED with a centre wavelength of 350nm.

Figure 8.3 shows the positions of the wavelength channels for this set, along with the formaldehyde absorbance spectrum. The two detection channels predominantly cover formaldehyde absorption peaks, whilst the reference channel covers an area with little or no absorption. However these peaks absorb less than the peaks of the 339nm wavelength band set and that the 355nm filter has low transmission in these positions.

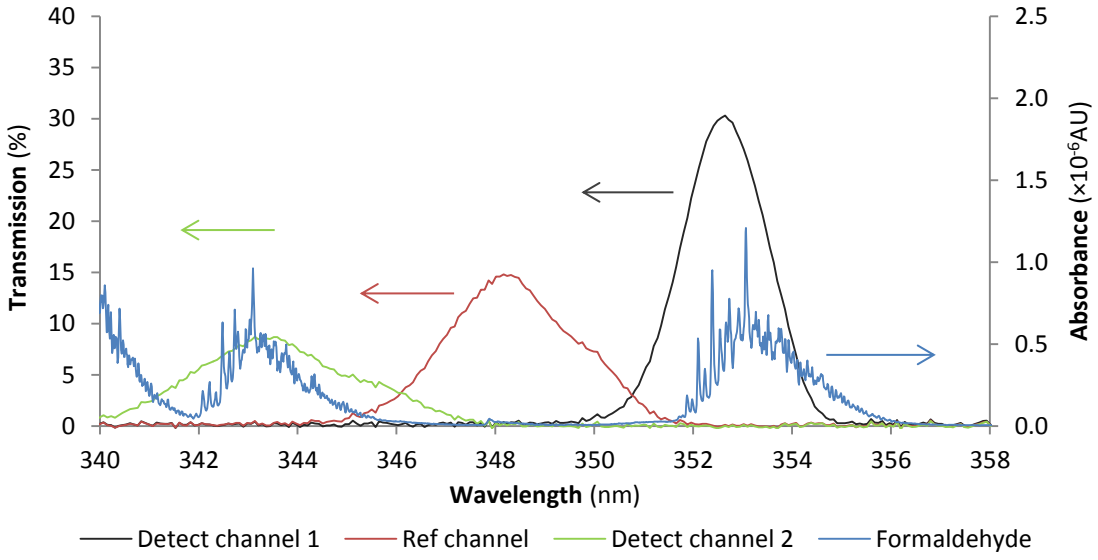

Figure 8.3: Channel transmission spectra of the 353nm wavelength band set using the 355nm filter at 12º (black), 20º (red) and 26º (green). The absorbance spectrum of 10ppb of formaldehyde with a 100mm path length, calculated from data from Meller *et al.* [1].

The 339nm band set was also considered. As discussed in Chapter 7, only one detection channel and one reference channel could be delivered within the transmission of the 340nm LED. However the set does include a strong formaldehyde absorption peak and the 339nm filter has relatively high transmission for these positions. This is shown in Figure 8.4.

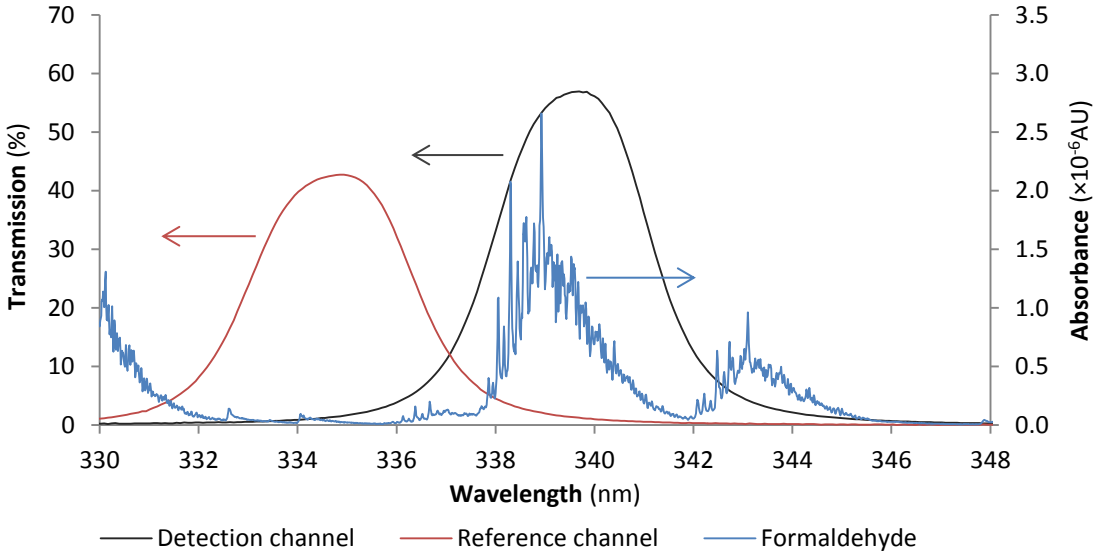

Figure 8.4: Intensity spectra of the detection and reference channels of the two filter system. Data was taken by the AvaSpec spectrometer. The absorbance spectrum of 10ppb of formaldehyde with a 100mm path length, calculated from data from Meller *et al.* [1].

8.3. Setup

A photograph of the single filter, multi-channel system is shown in Figure 8.5. This system used a single laser-line filter to produce multiple measurement channels. Initially the system used the 353nm wavelength band set described in Chapter 4 as a single commercially available LED could be used for three channels.

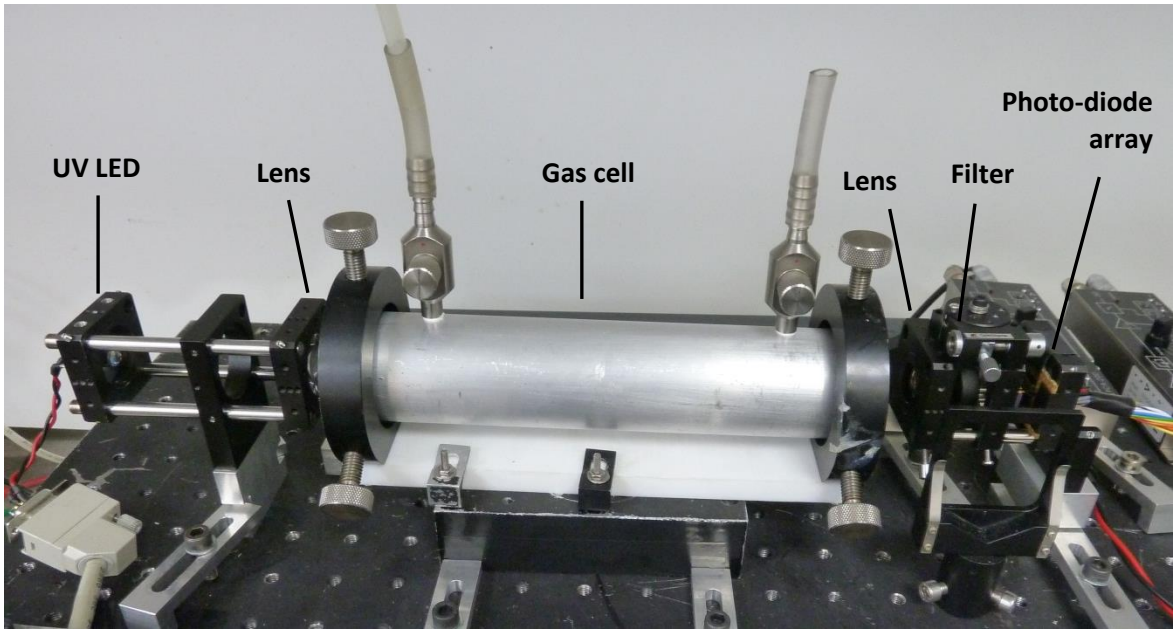

Figure 8.5: Photograph of the single filter, multi-channel system. The setup for the 353nm wavelength-band set was used in this photograph.

A diagram of the single filter, multi-channel system is shown in Figure 8.6. As with the two filter system, the 60mm focal length lens collimated light from the UV LED through the gas cell. The 16mm focal length lens then focused the light to un-collimate it and gave it a range of angles before it passed through the filter.

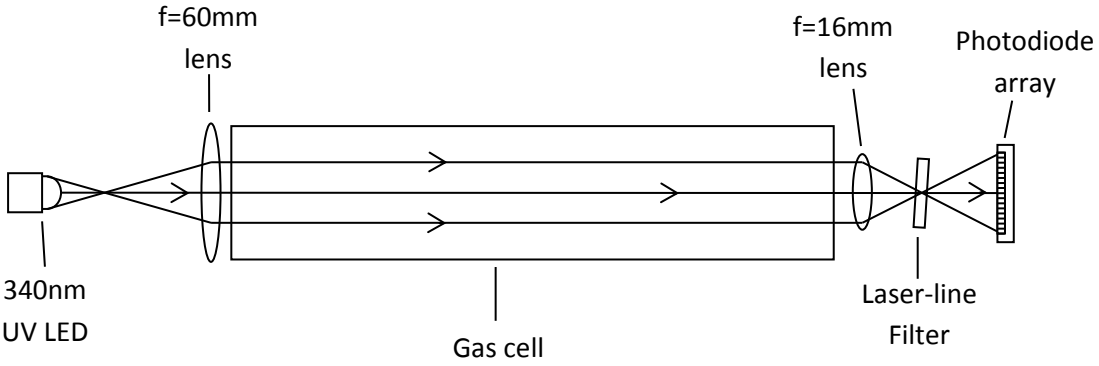

Figure 8.6: Diagram of the optical system of the single filter, multi-channel system. Light from the UV LED is collimated through the gas cell by the 60mm lens. The 16nm lens focuses it and gives it a range of angles. The filter transmission varies with incident angle, so light of different wavelength bands reach the elements of the photodiode array.

The single filter, multi-channel system initially used three channels, one for reference and two for detection. Their central wavelengths were 343.5nm (detection), 348nm (reference) and 354nm (detection). The photodiode array was positioned 14.2mm from the focal point of the 16mm lens to match the desired wavelength channels to the dimensions of the array. This setup was precisely positioned to align photodiode array elements with the desired wavelength bands. More details on the alignment process are given in Section 8.5.

8.4. Apparatus

The single filter, multi-channel system made use of a photodiode array, a 350nm UV LED and a 355nm laser-line filter. It also used the 340nm UV LED described in Chapter 5, the fused silica lenses and the 195mm gas cell described in Chapter 6 and the custom made 339nm laser-line optical filter and the electronic configuration described in Chapter 7. The characterisation of the new apparatus is described in detail in this section.

8.4.1. Photodiode array

The photodiode array used in this system (Hamamatsu S4111-16Q) [2] had 16 array elements arranged linearly. Figure 8.7 is a photograph of the photodiode array and Figure 8.8 is a diagram. Elements were 1.45 by 0.9mm and were separated by 0.1mm of non-active material. Elements were made of silicon and the front window was made of quartz to allow detection in the UV. This gave it a spectral range of 340 to 1100nm.

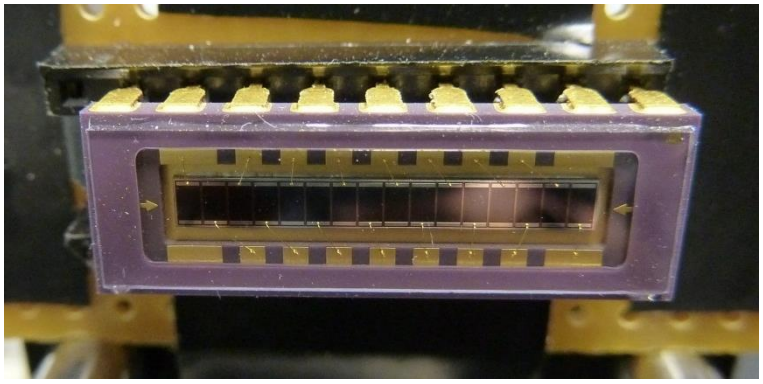

Figure 8.7: Photograph of the photodiode array. Individual elements can be seen in the centre and connection pins can be seen on the top.

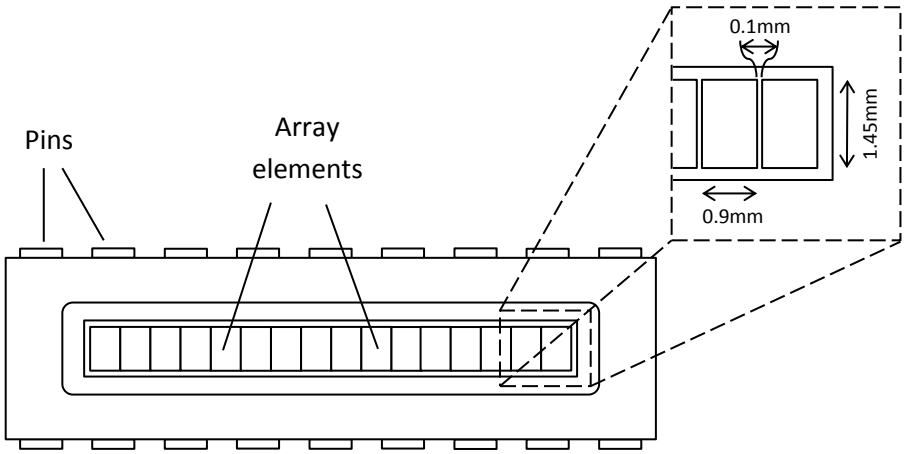

Figure 8.8 : Diagram of the photodiode array. The insert shows a close-up of the array elements with dimensions included.

Like the single photodiodes used in the two filter detection system, the response of the photodiode array was dependent on wavelength. Figure 8.9 is a graph of the response

to wavelength of the array, taken from the manufacturer's data sheet. This shows approximate response of between 0.17 and 0.15A/W for the wavelengths used here. It should be noted that the response is better in this region than for shorter wavelength channels, which was a small advantage for the 354nm wavelength band set.

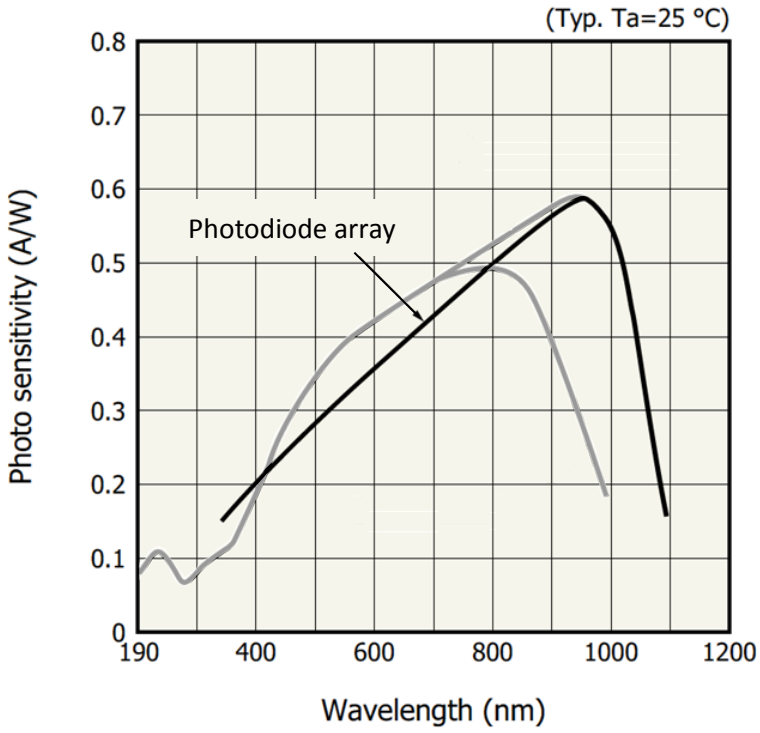

Figure 8.9: Graph of the photodiode array response against wavelength, taken from the manufacture's data sheet and partially re-labelled [2]. Other lines are for other arrays made by the same manufacturer that were not used in this project.

It is noticeable that no sensitivity data is given for wavelengths below about 330 to 340nm in Figure 8.9. This approximately corresponds to the position of the 339nm wavelength band set. While selectivity trends below these wavelengths were not rigorously investigated, the array was responsive to wavelengths as low as 337nm as demonstrated in Section 8.7.

8.4.2 UV LED

For operating with the 354nm wavelength band set, this system used a UV LED (SETi UVTOP350TO39BL) [3] with a quoted central wavelength of 350nm and a

FWHM of 15nm. It was similar to the 340nm LED used with the 339nm wavelength band set (see Chapter 5). Figure 8.10 is a photograph of the 350nm LED. Figure 8.11 shows a graph of the normalised intensity spectrum of the 350nm LED as measured by the AvaSpec spectrometer.

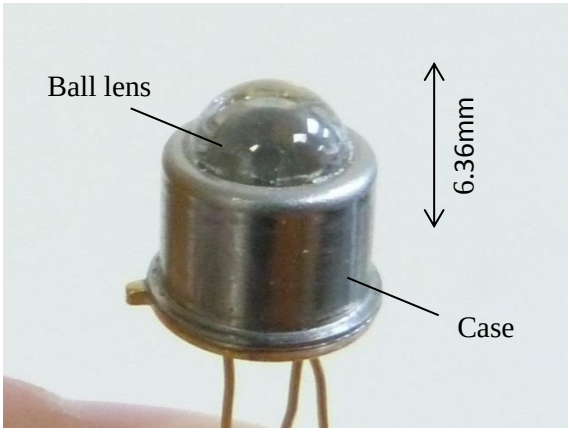

Figure 8.10: Photograph of the LED showing the casing and the ball lens.

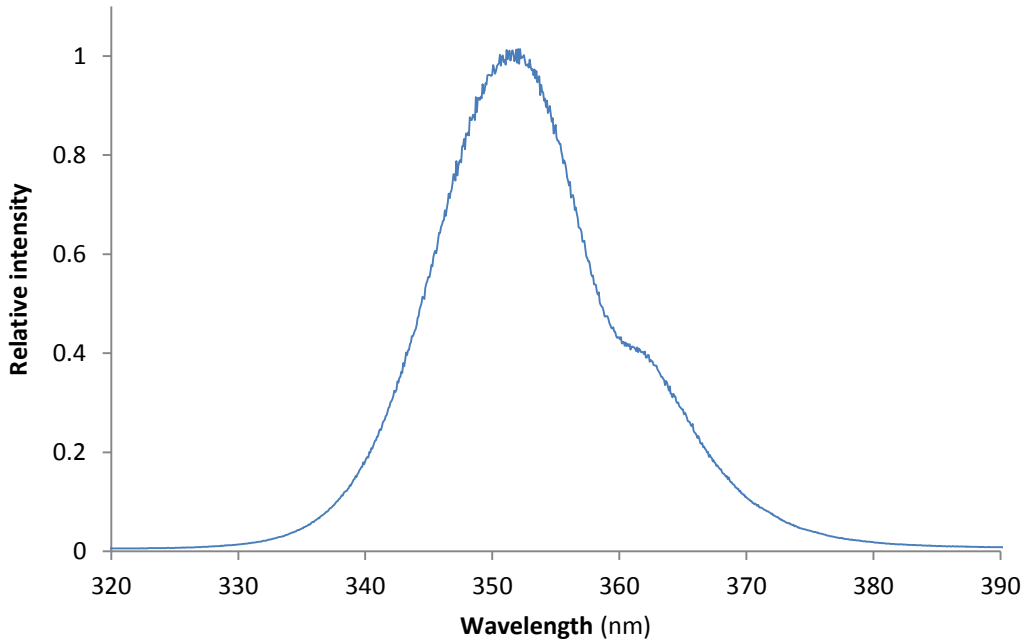

Figure 8.11: Graph of the normalised intensity output of the 355nm LED measured by the AvaSpec spectrometer. It shows a peak wavelength of 351.8nm and a FWHM of 14.0nm.

8.4.3. Laser-line filters

The principles of laser-line filters were described in Chapter 7. They are very narrow band-pass filters (typically around 3nm FWHM), generally designed to permit the output of a specific laser. The single filter, multi-channel system initially used a commercially available 355nm laser-line filter. It had a FWHM of 1.05nm and a quoted peak transmission of 84%, designed to correspond to the Nd:YAG laser line.

$$\lambda_f = \lambda_0 \left(1 - \left(n_0/n_f\right)^2 \sin^2\theta\right)^{1/2} \tag{8.4}$$

The transmission centre wavelength of a laser-line filter varies in accordance with Equation (8.4). This allows the transmission spectrum to be tuned to lower wavelengths by tilting the filter.

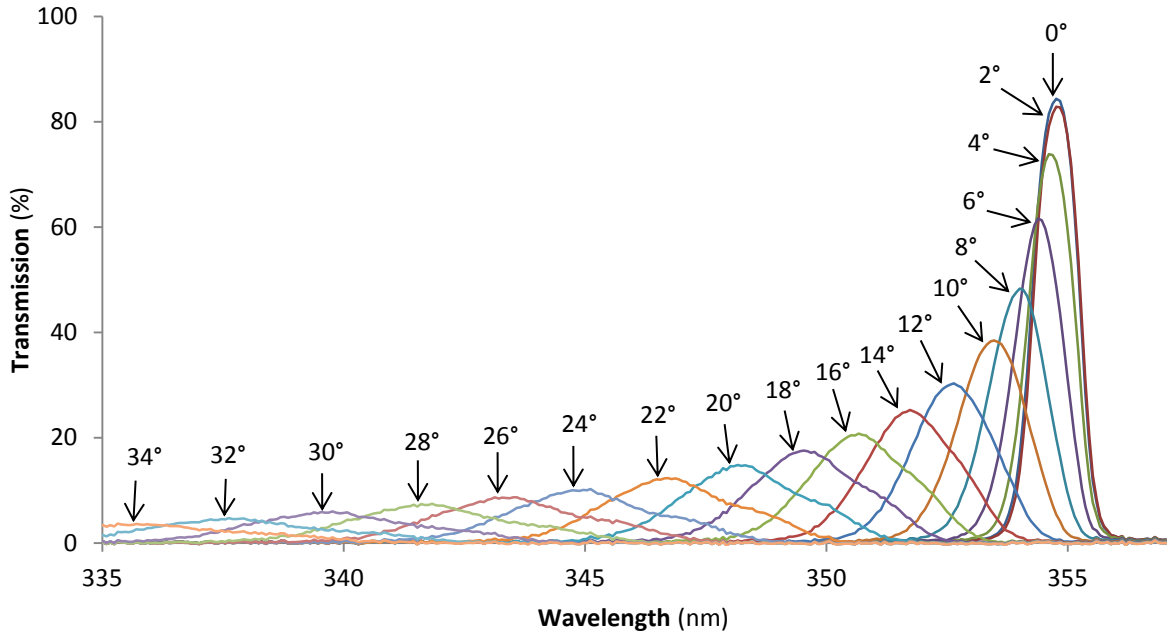

Figure 8.12: Effect of rotating the 355nm filter, showing peak transmission wavelength shifting with angle of incidence. Measurements were taken using the UV lamp and the AvaSpec spectrometer.

The filter was tested using the setup used in Chapter 7. The filter was placed on a goniometer mount to allow its angle to be varied. With the UV lamp as a light source, the AvaSpec spectrometer was used to analyse the transmission spectrum of the filter

at a range of angles. The results can be seen in Figure 8.12. The transmission centre wavelength of both filters decreasing with increased angle as expected, but the transmission decreases more rapidly than for the 339nm filter described in Chapter 7.

Figure 8.13 is a plot of the peak wavelength of the two filters with angle, together with theoretical plots from Equation (8.4). Values of effective refractive index were not given by the manufacture's and so were empirically fitted at 1.74 for the 355nm filter and 1.51 for the 339nm filter. The 355nm filter shows very good correspondence to the theoretical results. The correspondence was slightly better than results for the 339nm filter which deviate slightly at higher angles.

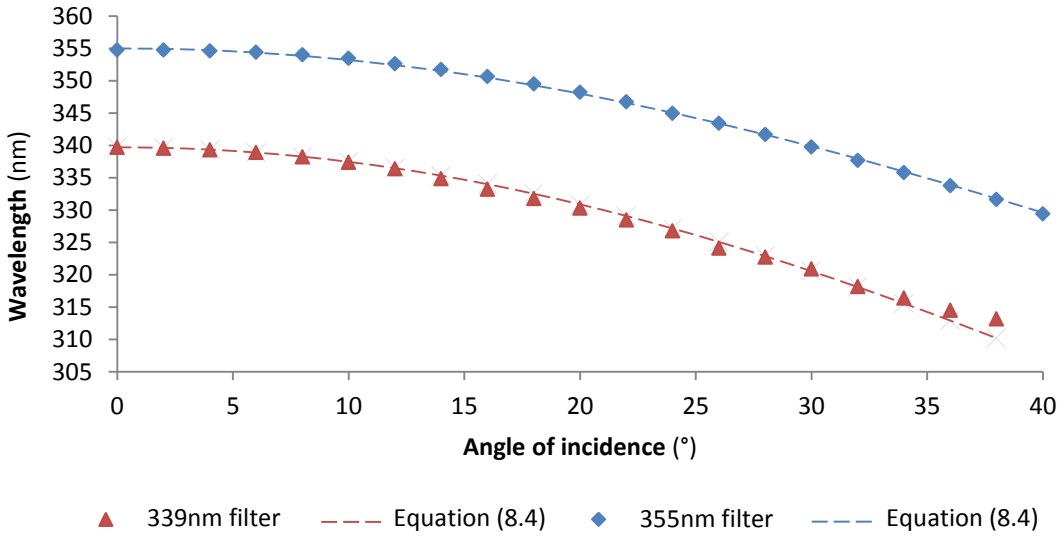

Figure 8.13: Peak wavelengths of the two filters depending on filter angle of incidence. Fit lines are theoretical plots from Equation (8.4). Values of effective refractive index were empirically fitted at 1.74 for the 355nm filter and 1.51 for the 339nm filter.

The peak transmissions of the two filters were plotted with angle, and the results are shown in Figure 8.14. The 355nm filter had a higher starting transmission but it decreased faster than that of the 339nm filter. The behaviour of the 355nm filter was similar to that of the 325nm filter tested in Chapter 7. This was not surprising, given that the 339nm filter was custom built while the 355nm filter and the 325nm filter were both mass-produced by the same manufacturer.

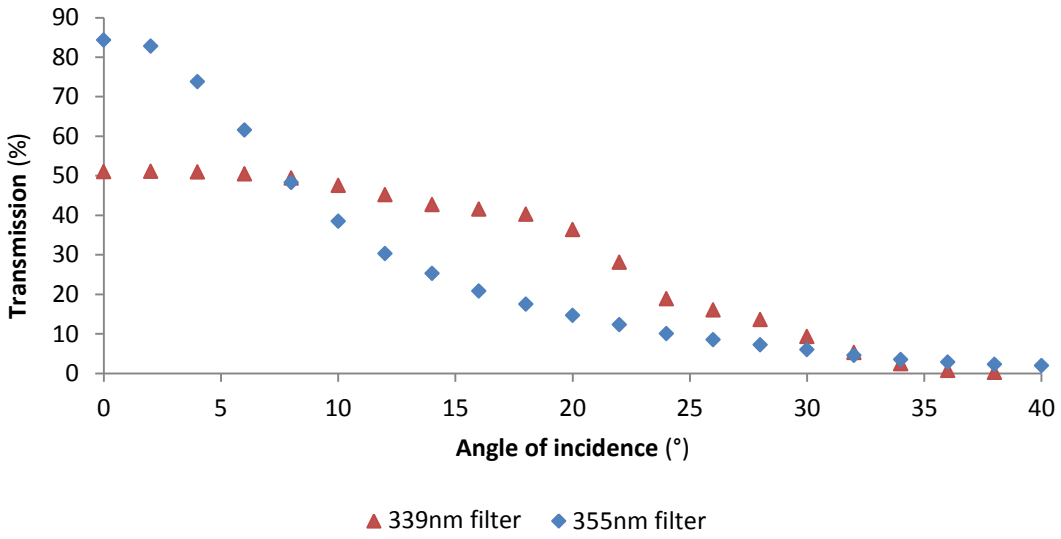

Figure 8.14: Peak transmission of two filters depending on filter angle of incidence. Both filters display a significant drop-off in transmission towards higher angles.

These results show that as for the 339nm filter, the transmission centre wavelength of the 355nm filter could be tuned by varying its angle. They also show that its transmission spectrum decreased more rapidly but more smoothly than for the 339nm filter, and that peaks maintained their shape better. This behaviour was similar to that of the 325nm filter discussed in Chapter 7, supporting the hypothesis that it comes from optimisation for mass-production.

8.4.4. Electronic configuration

The single filter, multi-channel system used the same electronic setup as the two filter system. A schematic diagram of the electronic setup is shown in Figure 8.15. A simplified diagram of the optical setup is included in this diagram for reference, the full version of which can be found in Figure 8.6.

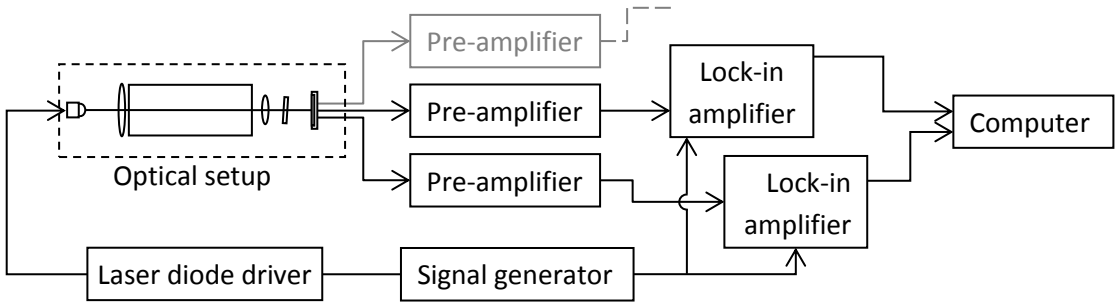

Figure 8.15: Diagram of the electronic setup used for the single filter, multi-channel system. The LED was driven by the laser driver with the signal generator providing the modulation frequency and the reference for the lock-in amplifiers. The gain amplifiers converted the photodiode currents to voltages to be filtered by the lock-in amplifiers. The computer processed and recorded the data. More channels can be added as required.

A square wave modulation frequency of 6.5kHz was provided by the signal generator. This was used as the LED drive frequency of the laser driver. The laser driver controlled the current to the LED at 9.41mA. Current control is known to give a more steady LED output than voltage control (for example directly from the signal generator) [4].

Photodiode array elements gave an output current proportional to the light they received. This current was converted to voltage by the pre-amplifiers and read by the lock-in amplifiers using the signal generator frequency as a reference. The integration time of the lock-in amplifiers was set at 10ms, and averages were taken over a 20s period, to reduce digitisation noise.

8.5. Channel selection

The 353nm wavelength band set had a pair of detection bands, centred at 353nm over the $2^0_0\,4^1_0$ peak and at 343nm over the $2^0_0\,4^3_0$ peak. It also had a single reference band centred at 348nm over a region of low absorption. Its principal advantage was that its three channels fell within the range of the commercially available 350nm LED. This allowed the second detection channel to be used. However it used peaks with low

absorption and angles at which the filter had low transmission, significantly decreasing the formaldehyde sensitivity.

Figure 8.16 shows absorbance measured between the 353nm detection channel and the 348nm reference channel. It can be seen that absorbance from the 353nm wavelength band set was not visible above the noise level. It was decided that lower absorption cross-sections of the peaks it used made it less appropriate of use in a detection system. This meant that there was no three channel wavelength band set in the formaldehyde spectrum that could be used with existing equipment.

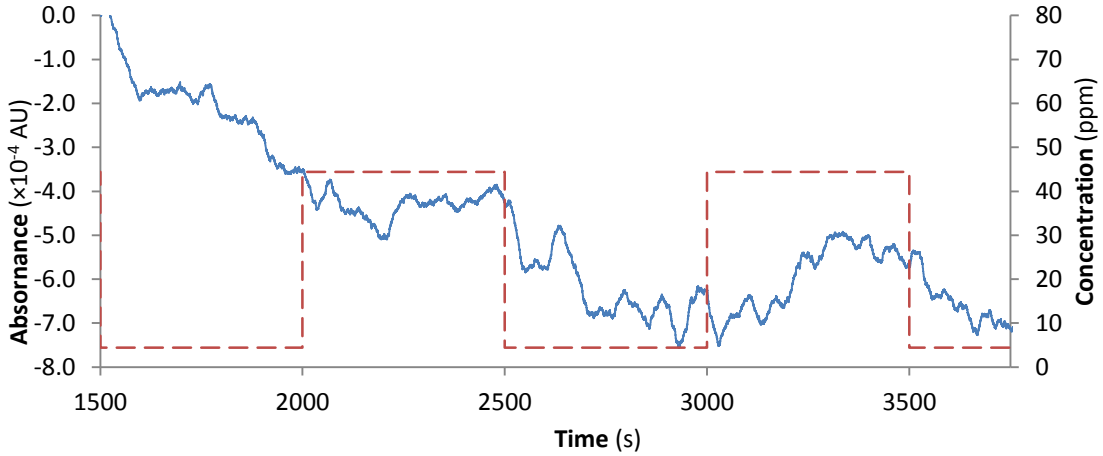

Figure 8.16: Graph of the absorbance detected by the single filter, multi-channel system (Blue) caused by a periodic shift in formaldehyde concentration between 4.4ppm and 44ppm (Red). The 353nm detection channel and the 348nm reference channel were used. No significant absorbance change can be seen above the noise level.

Despite the lack of access to a third detection channel and resulting issues with selectivity, it was decided to test the single filter, multi-channel system using the 339nm wavelength band set. This allowed the system to be tested in principle and to verify its effectiveness if additional equipment becomes available in the future. This set had a detection bands centred at 339 and 329nm, over the $2^1_0\,4^1_0$ peak and the $2^1_0\,4^3_0$ and $2^2_0\,4^1_0$ peaks respectively. It also had a reference band centred at 335nm.

8.6. System tuning

The exact wavelength ranges reaching the photodiode array elements was dependent on the position and angle of the filter and photodiode array and needed to be determined with a high degree of accuracy. Even small shifts in the setup could result in array elements receiving light from a different wavelength range, having a significant effect on results.

Finding the wavelength band reaching a given photodiode array element was not straightforward for a number of reasons. The photodiodes were not wavelength selective and responded only to intensity. Using the spectrometer presented difficulties as precisely placing the fibre launch end in the same position as the elements was not easy. Finally, the limited angle of acceptance of the optical fibre meant that it was difficult to analyse light at extreme angles.

The solution was to use a second 355nm filter placed in a collimated region of the beam to limit transmitted wavelengths. This light would then pass through or be blocked by the main filter. Only wavelengths that passed through both filters could reach the photodiode array, and only elements receiving those wavelengths could register any signal. By rotating the test filter, the transmission wavelength could be changed in accordance with Equation (8.4), scanning light across the array elements.

Figure 8.17 is a set of diagrams of this method. Figure 8.17 (A) shows the single filter, multi-channel system set up as normal. In Figure 8.17 (B) the test filter has been added and tuned to have a transmission wavelength of λ_1. Only light of approximately this wavelength reaches the array and only the element that receives it registers any signal. In diagram C) the test filter is tuned to a different wavelength, λ_2, so a different element registers signal. By rotating the test filter, the spectrum reaching a specific array element can be found.

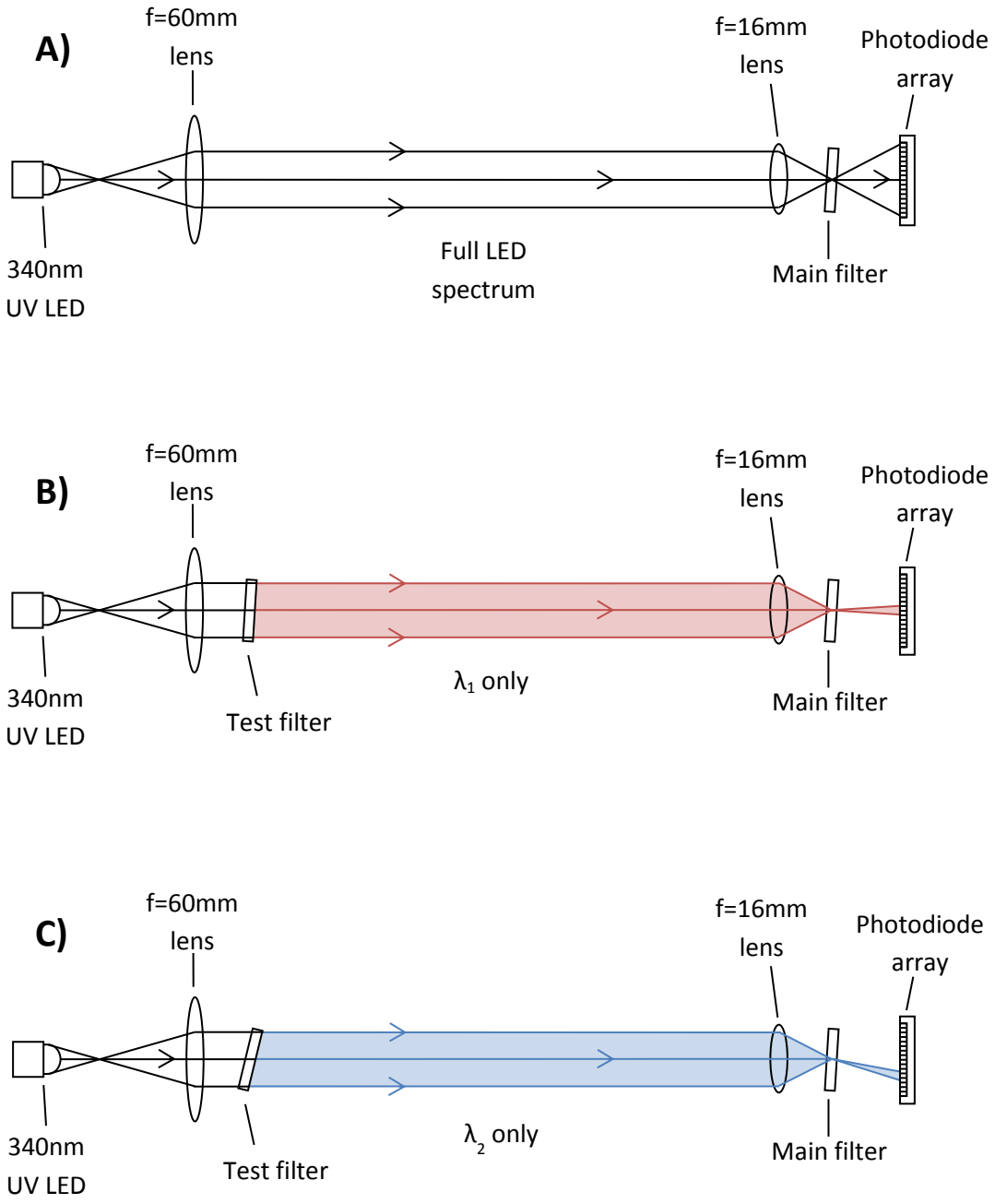

Figure 8.17: Diagrams of the test filter method for wavelength analysis. A) Single filter, multi-channel system set up as normal. B) A test filter has been added, tuned to central transmission wavelength of λ_1. C) Test filter tuned to λ_2, light reaching a different element.

This method was itself tested and verified with the use of the AvaSpec spectrometer. The system was set up as shown in Figure 8.17, but with the fibre for the AvaSpec spectrometer in the centre of the photodiode position. The main filter was tuned to 18°, and the angle of the test filter was varied between 0 and 24°. The resulting

intensity spectra reaching the spectrometer are shown in Figure 8.18 with the intensity spectrum of the main filter on its own given for reference in Figure 8.19. The 340nm LED was used as the light source throughout.

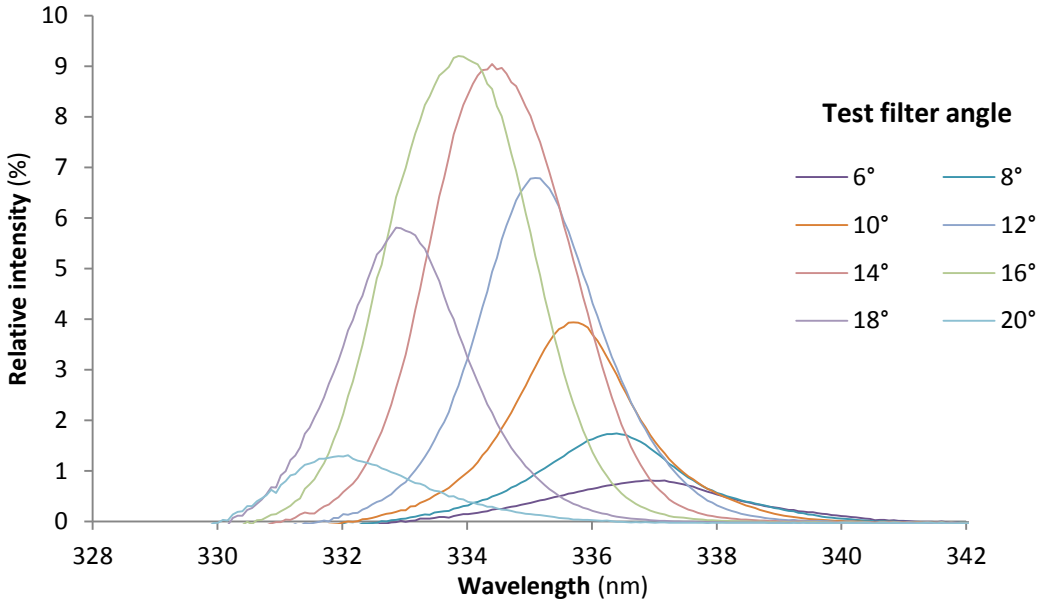

Figure 8.18: Transmission spectrum from the two filter method with the main filter set to 18 degrees and the test filter varying from 6 to 24°. Data was measured by the AvaSpec spectrometer with the fibre launch end placed in the position of the photodiode. This confirms the effectiveness of the test filter for testing transmission of the main filter to a given position.

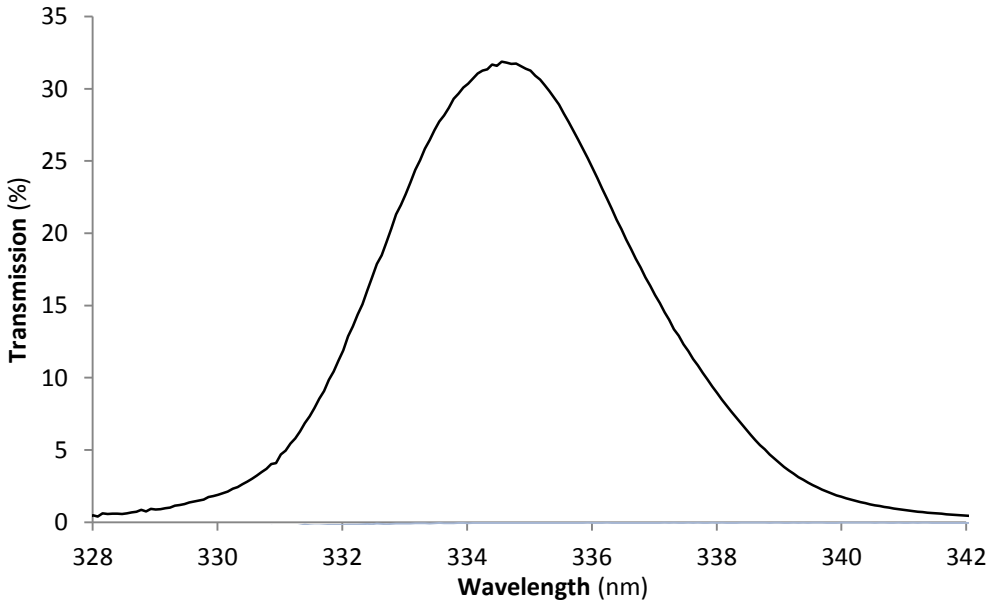

Figure 8.19: Transmission spectrum of the main filter at 18°, provided for reference.

It can be seen from Figure 8.18 that the intensity of light passing through the two filters is strongest approximately when the transmission spectrum of the test filter matches that of the main filter. Shorter wavelengths give a stronger relative intensity, believed to be caused by their lower single-filter transmission. However this data verifies that the inclusion of a test filter can be used to test the wavelength range reaching a given element. It also demonstrates that the spectral resolution of the method was limited by the spectral distribution of the test filter.

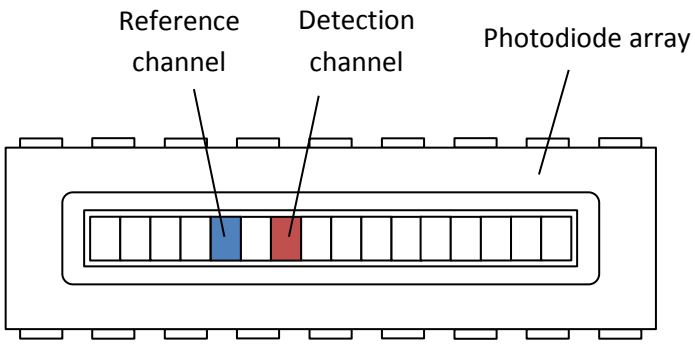

Figure 8.20: Diagram of the photodiode array, with the element used as a measurement channel marked in red and the element used as a reference channel marked in blue.

The single filter, multi-channel system was set up using the two main channels of the 339nm wavelength band set. The positioning was tested using the two filter method described above. Figure 8.20 shows a diagram of the photodiode array, with the elements used for the detection and the reference channel marked. Figure 8.21 is a graph of relative intensity reaching the array elements used for the two channels, plotted against the angle of the test filter. Figure 8.22 is a graph of the relative intensities plotted against wavelength, calculated with Equation (8.4).

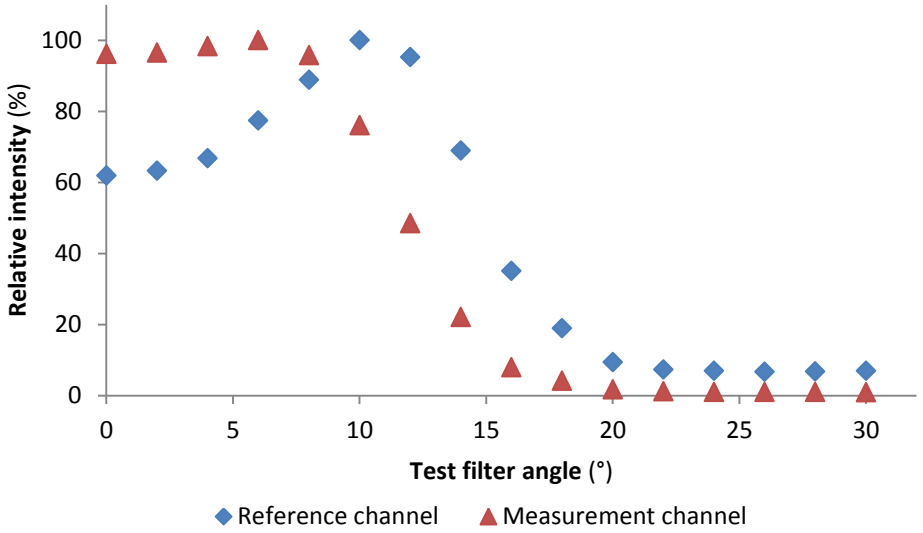

Figure 8.21: Relative intensities of the two channels, as measured by the two filter method, plotted against the angle of the test filter.

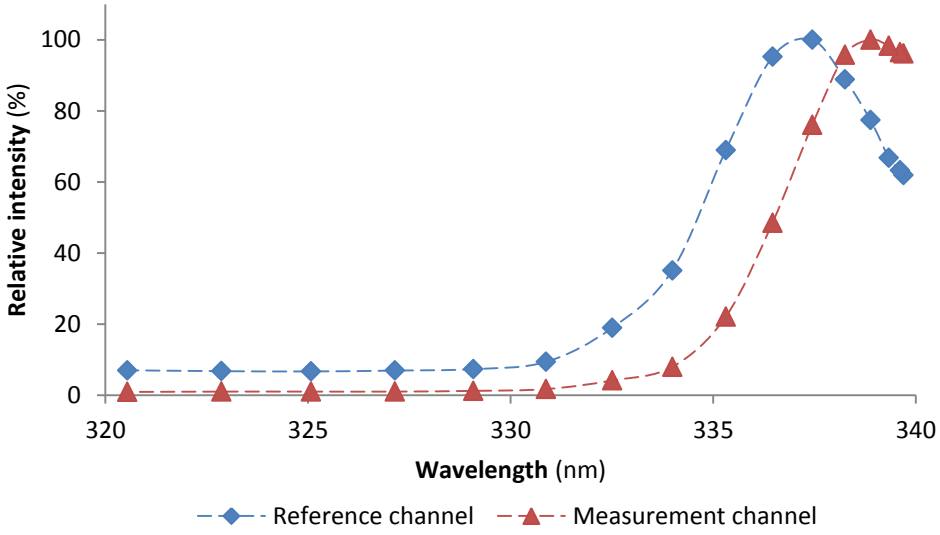

Figure 8.22: Relative intensities of the two channels, as measured by the two filter method, plotted against wavelengths calculated with Equation (8.4).

Figure 8.21 and Figure 8.22 show that a single filter can be used to transmit light at more than one peak wavelength if it has a range of angles. Figure 8.22 shows that the detection channel had a peak wavelength of 339nm and the reference channel had a peak wavelength of 337nm. 339nm is exactly on the main detection band of the set. 337nm is slightly higher than the 336nm reference channel, but still predominantly over the desired low absorption region. Cross-talk appears artificially high in Figure 8.22 because of the resolution of the test filter.

8.7. Noise

Much of the optimisation work carried out on the two filter system was applicable to the single filter, multi-channel system. This system used the same type of LED and similar photodiodes. The same pre-amplifiers and lock-in amplifiers were used. The gas cell and lenses were the same and the laser-line filter was similar, although there were differences in arrangement.

With a pre-amplifier gain of 10^8, the single filter, multi-channel system gave a signal voltage of around 139mV for the detection channel and 117mV for the reference channel. This was slightly lower than the 200mV typical of the two filter system. Some noise phenomena were proportional to signal strength, such as thermal drift and source fluctuation and shot noise. Others were independent of signal strength such as matched frequency interference, digitisation noise and other noise from the lock in amplifier

The main noise phenomena found with the single filter, multi-channel system are summarised in Table 8.1. NEA values are quoted for each, using the signal voltage of the detection cannel. As for the two filter system, electronic interference and source fluctuation noise were the most significant phenomena for single measurements, with thermal drift becoming significant over longer time periods.

Table 8.1: Noise phenomena affecting the single filter, multi-channel system

Phenomenon	Control	Final level	NEA
Electronic noise	Modulation frequency set to 6.5kHz	3.5×10^{-6}V/√Hz	3.5×10^{-5}AU
Thermal drift	Allow system to reach thermal equilibrium	~3.6×10^{-8}V/√Hzs	~3.7×10^{-7}AU/s
Lock-in amplifier quantisation	Quantisation reduction process	3.5×10^{-7}V	2.6×10^{-6}AU
Lock-in amplifier random noise	N/A	4.3×10^{-7}V/√Hz	4.4×10^{-6}AU
Source fluctuation noise	Averaging over 20s	3.8×10^{-6}V/√Hz	3.8×10^{-5}AU

As before the most significant phenomena for this system were thermal drift, source fluctuation noise and electronic noise. For a single measurement, source fluctuation noise and electronic noise dominated, giving a limit of detection of 5.2×10^{-5}AU.

8.8. System testing with formaldehyde

The single filter, multi-channel system was tested with formaldehyde supplied as described in Chapter 7. Formaldehyde was generated from a permeation tube using a vapour generator that provided a fixed concentration determined by temperature and air flow. A second vapour generator contained no permeation tube but used the same settings. By switching between flow from the two generators, formaldehyde concentration could be switched on and off without disturbing the setup.

The system was tested with a range of formaldehyde concentrations and the results are shown in Figure 8.23 . For high concentrations they show a loose correlation between absorbance and concentration and little or no correlation at low concentrations. The trend is less clear than for the two filter system as absorbances were significantly closer to the limit of detection. This was predominantly due to overlap between the reference and detection channels.

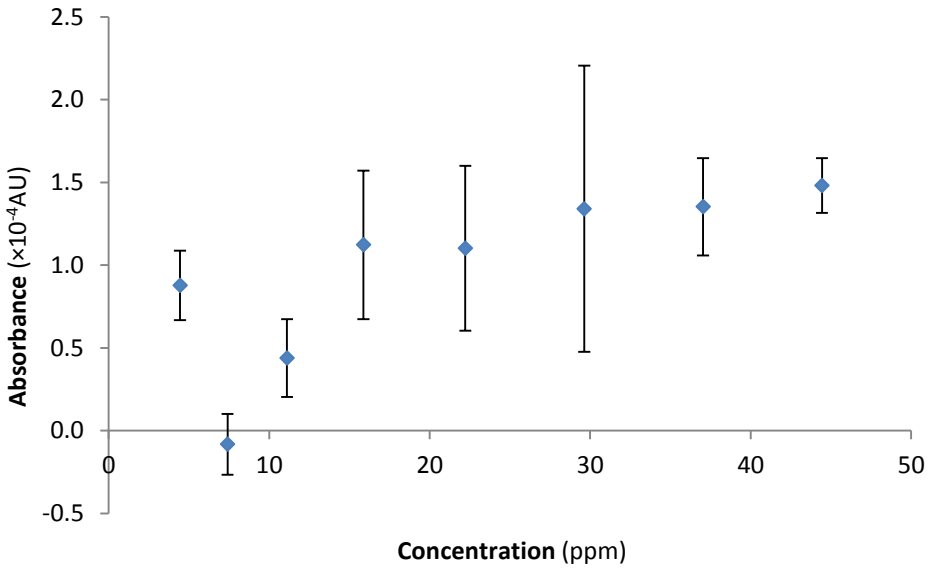

Figure 8.23: Graph of the response of the single filter, multi-channel system to formaldehyde concentration.

As before a period of 500s (8:20 minutes) was given between baseline and detection measurements to allow the gas cell to fill. This would usually give a limit of detection of 1.85×10^{-4}AU, greater than the absorbance of the measurements. However the thermal effects happened to remain relatively constant while taking this set of data. However the other noise phenomena were was still close to the levels of the measurements (see Table 8.1). This made it difficult to draw a clear correlation or to accurately estimate the limit of detection.

8.9. Chapter summary

The single filter, multi-channel system took advantage of the angle dependence of the laser-line filter transmission wavelength to create multiple wavelength channels through a single filter. Focused light with an angular divergence was passed through the filter. Light with different angles of incidence had different transmission spectra, providing different channels. A photodiode array was used for these channels, allowing better resilience to cross sensitivity.

Light from an LED light source was collimated through a gas cell containing the sample. It was then focused and passed through a laser-line filter. Focusing created a cone of light which passed through the filter at a range of different angles. As the transmission centre wavelength of the filter was dependent on angle, this produces a spread of light at a range of different wavelengths.

A photodiode array was used to detect this light spread, with each element receiving a different wavelength band, in the manner of a dispersive spectrometer. By carefully tuning the position of the array and the angle of the filter, these bands could be tuned to correspond to formaldehyde absorption features.

The single filter, multi-channel system was initially designed to use the 353nm wavelength band set described in figure Chapter 4. It included two detection channels and one reference channel, allowing it to be resistant to cross-interference. There was

a commercially available UV LED with a 350nm central wavelength that covered the spectrum of all three channels. Unfortunately the peaks in this region had low absorption cross-sections. This increased the limit of detection to beyond the level that could be safely and reliably produced by the permeation tube.

The 339nm wavelength band set was also used. This set covered peaks with much higher absorption cross-sections and had also been successfully demonstrated with the two filter system. However, while the set did include three separate channels, at the time of writing there was no commercially available LED that covered all three. It was therefore not possible to test the system with three channels.

The system was set up using the reference channel and the first detection channel of the 339nm wavelength band set in order to verify the method of using a single filter for multiple channels. The system was tested with formaldehyde, showing clear detection for high concentrations. However it was less sensitive than the two filter system, predominantly due to decreased signal and cross-talk between channels. For a single measurement the limit of detection was 5.2×10^{-5}AU. A simulation of formaldehyde absorption over these channels found this to correspond to 8.2ppm of formaldehyde.

The two filter system was tested with formaldehyde at a range of concentrations. As with the two filter system, it was not possible to test the calculated limit of detection as the time taken to fill the gas cell allowed thermal drift effects to dominate. This was due to the size of the gas cell and the formaldehyde delivery method, not the system itself, but it did prevent the short term measurement performance being verified.

In the future it may be possible to further optimise the transmission spectrum of the filters, as well as improve their alignment. It may also be possible to test the method using a source with a broader transmission spectrum. The UV lamp described in Chapter 5 could be used in principle, but it would require additional filtering as its transmission spectrum was broader than the region blocked by the laser-line filters.

The single filter, multi-channel system was developed as a simple device using a minimum of complex components for both sensitive and selective formaldehyde

detection. It had the potential of providing three or more wavelength channels using a single filter and a photodiode. It was not possible to test multiple channels in practice because an LED with the appropriate spectrum was not available. However it was demonstrated that a single filter could be used to deliver multiple wavelength channels and that formaldehyde could be detected. If alternative light sources become available in the future, this system could be practically viable.

8.10. References

[1] R. Meller and G. K. Moortgat, "Temperature dependence of the absorption cross sections of formaldehyde between 223 and 323 K in the wavelength range 225-375 nm," *Journal of Geophysical Research-Atmospheres*, vol. 105, pp. 7089-7101, 2000.

[2] Hamamatsu Si photodiode array, S4111/S4114 series, *Technical Data Sheet*, Hamamatsu, Hamamatsu, Japan, 2011.

[3] SETi UVTOP350, *Technical Data Sheet*, Sensor Electronic Technology Inc., Columbia, USA.

[4] M. Johnson, Photodetection and Measurement: maximising performance in optical systems, New Your, USA: McGraw Hill Education, 2003.

Chapter 9: Summary and conclusions

At the time of this research, the methods of formaldehyde detection that were reliable and simple to operate were extremely limited. Semiconductor formaldehyde detectors show cross-sensitivity with acetone and methanol, as well as requiring 600ºC operation for optimum performance. Gas chromatography can be very accurate and reliable but can take several hours to complete a measurement and often requires expensive and bulky equipment.

Optical methods of detecting formaldehyde include TDLS, PAS, CRDS, DOAS and fluorescence detection. Optical methods can be very sensitive, reliable and selective, but can also be complex and require trained operators to interpret results. One electrochemical formaldehyde detector has been produced, found to have a response time at low concentrations of 1 minute and a limit of detection of about at least 0.2ppm.

The aim of this project was test the feasibility of using UV spectroscopy for formaldehyde detection for use in industrial buildings. Using spectroscopy it was considered possible to design a simplified system using low resolution measurement channels specifically targeted at formaldehyde. The UV region was chosen both because the formaldehyde absorption region in the IR has interference from CO_2, and because its UV spectrum had some interesting features to be used.

The following targets for the system's operation were set at the beginning of the project:

* Limit of detection of 0.1ppm or lower.
* Good selectivity from gases commonly found in the indoor environment.

* Response time of 60s or less.
* Simple to manufacture, containing a minimum of complex components.
* Robust and able to operate over a 10 - 30°C range.
* Simple to operate, requiring no extensive training.

9.1. Preliminary work

A literature study of the gases and pollutants common to the indoor environment was carried out and their UV spectra were compared to that of formaldehyde. 85 substances and substance groups were considered, 32 of which were found to have significant absorption in the UV region. Of these, 11 had absorption spectra that significantly overlapped with formaldehyde. By analysing these spectra, a region of the formaldehyde spectrum was found between 320-360nm where the only significant interference came from nitrogen dioxide and nitrous acid. Given the number of potentially interfering gases, this was a surprising result.

This region contained three groups of strong formaldehyde absorption peaks and three regions of very little absorption. The contrast between these two type of regions, and their proximity over only at 40nm range is an unusual property of formaldehyde. A method was devised for spectroscopic detection using a small number of low-resolution detection and reference channels centred over these features.

A preliminary detection system was constructed in order to understand the underlying principles of spectroscopy and to serve as a research tool throughout the project. It was based around a deuterium UV lamp and a UV spectrometer and provided broad-band, high-resolution spectroscopy measurements. This system demonstrated detection of formaldehyde and a range of other gases and was used for characterising optical components throughout the project. However it was too complex and difficult to operate to serve as a final system.

As part of the work on the preliminary system, a detailed investigation into the performance of the UV spectrometer was carried out. The spectral range and spectral resolution were tested and a comparison was made to a different UV spectrometer and to a commonly used visible range spectrometer. Noise phenomena identified and characterised included source

fluctuation and shot noise, dark current and fixed pattern noise (FPN), read noise and photo response non-uniformity (PRNU).

For a high intensity spectroscopy system, PRNU was the dominant performance limiter. When used with a known light source and a known detector, PRNU could be ignored, and source fluctuation and shot noise became the dominant performance limiter. A detailed list of performance optimising procedures was found, including optimum integration time and averaging settings, temperature performance and dark current correction. This investigation was considered a novel contribution to the field of instrumentation. The system could be used as a formaldehyde detector in its own right (NEA of 2.5×10^{-4}AU, LOD of 8.5ppm), but was too complex for the aims of this project.

9.2. Two filter system

Two prototype systems were constructed over the course of this project, the first being the two filter system, a diagram of which is shown in Figure 9.1. This used a beam splitter to provide one detection channel and one measurement channel, using the formaldehyde spectral features mentioned above. It was designed to test the low-resolution formaldehyde detection meth

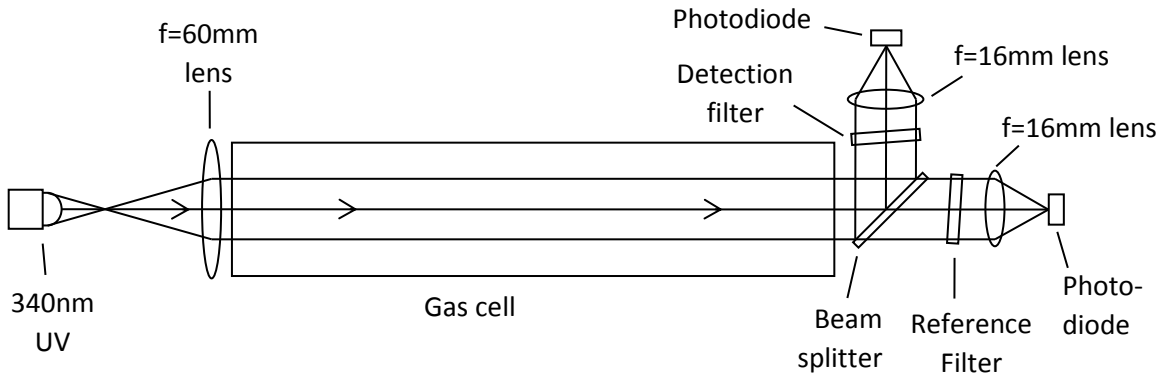

Figure 9.1: Diagram of the optical system. Light from 340nm LED was collimated through the gas cell by the 60mm lens. The beam splitter divided the light into a detection channel (reflection) and a reference channel (transmission). The desired spectral range was then selected by the filters before the 16mm lenses focused light onto the photodiodes for detection.

The light source for both channels was provided by a single 340nm UV LED. It had a FWHM of about 9.2nm, with which it was able to cover a wavelength range of a formaldehyde detection region and a reference region. This was possible with a single LED source because of the unusual property of formaldehyde of having high absorption and low absorption regions so close together. The use of a single LED allowed the reference channel to control for any fluctuations in intensity and simplified the construction.

The other critical components of this system were the laser-line filters. These were narrow-band filters designed to permit light from a single, specific laser waveband. At about 3nm FWHM, these are ideal for the low-resolution formaldehyde detection method. Two custom made laser-line filters were used, having a peak transmission wavelength of 339nm.

Laser-line filters are interference filters and as such their centre transmission wavelength decreased with increasing angle of incidence of the light. This effect was used to tune the centre transmission wavelength to match formaldehyde spectral features. Two filters were used. The first was placed at 0° to give a detection channel at 339nm, corresponding to the $2^1_0\ 4^1_0$ formaldehyde absorption peak. The second was placed at 14° to give a detection channel at 335nm, corresponding to a region of low formaldehyde absorption.

The main noise phenomena affecting the two filter system were temperature drift in the LED, shot noise and electronic noise. Temperature was initially controlled by a Peltier module but it was found to be more stable when allowed to reach thermal equilibrium over a two hour period. Source fluctuation noise was controlled by averaging measurements over a 20s time period. This gave a noise equivalent absorbance (NEA) of 4.5×10^{-5}AU, corresponding to a limit of detection of 6.6ppm.

The system was tested using a controlled concentration of formaldehyde. It clearly showed a linear relationship of absorption signal to concentration at high concentrations, and little or no correlation below the expected limit of detection. The limit of detection for this test was dominated by time dependent thermal drift, as it took several minutes to change the sample in the gas cell. However, this demonstrated the system behaving as expected.

The two filter system had a response time of 20s, in line with the target value. The filters could operate reliably between 10 - 30°C. The system contained few, simple components and

could be made easy to operate. While operation of the prototype was complex, the measured absorbance had a linear relationship with formaldehyde concentration which could be displayed to an operator for a final device.

The system had a formaldehyde limit of detection of 6.6ppm, above the target level. It had issues from thermal drift as temperature changes affected the LED output. The single filter, multi-channel system was designed to be more selective. However practical constraints (availability of LED emission) meant that only two channels could be implemented. (Having only two channels prevented it from removing cross-sensitivity such as from nitrogen dioxide and nitrous acid.)

9.3. Single filter, multi-channel system

The single-filter, multi-channel system was designed as a development of the two filter system. A diagram is shown in Figure 9.2. The system used the same LED and much the same setup as the two filter system but exploited the angular dependence of the filter's transmission wavelength to obtain multiple measurement channels from a single filter. This method was considered to be a novel development.

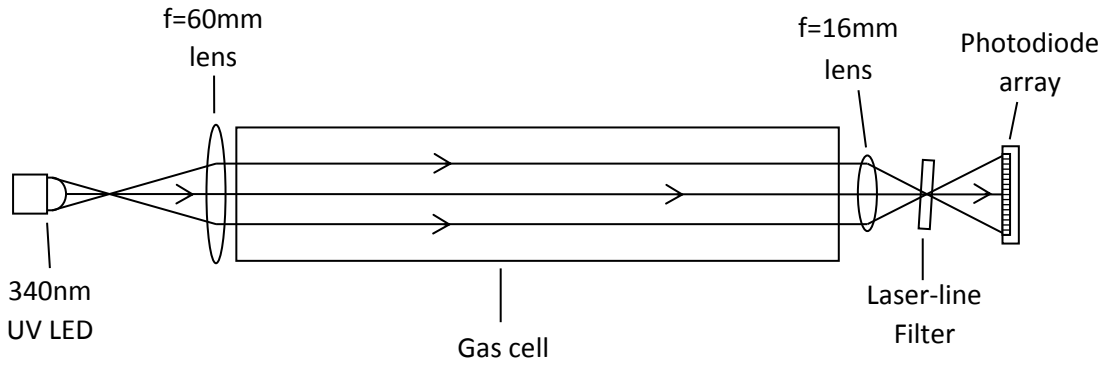

Figure 9.2: Diagram of the optical system of the single filter, multi-channel system. Light from the UV LED is collimated through the gas cell by the 60mm lens. The 16nm lens focuses it and gives it a range of angles. The filter transmission varies with incident angle, so light of different wavelength bands reach the elements of the photodiode array.

When collimated light passes through a laser-line, the entire field is filtered in the same manner. However, focused light has a range of angles depending on its angle to the optical axis, giving a range of peak transmission wavelengths. By placing a photodiode array some distance from the focal point, each element will receive a different wavelength band in the manner of a dispersive spectrometer.

The initial design of the single-filter, multi-channel system used three channels to control for interference from nitrogen dioxide or nitrous acid. These channels were at 339nm, 329nm and 329nm, and used a 350nm LED and a 355nm filter. However the formaldehyde absorption peaks in this region were much weaker than others considered (peak absorption cross-section of $4.7\times10^{-20}cm^2$ as opposed to $1.1\times10^{-19}cm^2$) [1]

As a consequence, the single-filter, multi-channel system was modified to use the 340nm LED, the 340nm filter and the 339nm and 336nm wavelength channels. The formaldehyde spectrum had potential for a third detection channel centred at 329nm, but this was out of the range of the LED. An LED with an output spectrum centred around 335nm could have covered all three channels but one was not commercially available during this research. With only two channels, the system could not correct for cross-sensitivity but its basic functionality could be demonstrated.

The noise phenomena affecting the single filter, multi-channel system were similar to those affecting the two filter system. Single measurements were dominated by source fluctuation noise and electronic noise. Long term measurements were dominated by thermal drift. The system had a NEA of 5.2×10^{-5}AU. This was found to correspond to 8.2ppm of formaldehyde.

The system was tested with a controlled concentration of formaldehyde. It was less sensitive than the two filter system (NEA of 4.5×10^{-5}AU), attributed to overlap between detection and reference channels. The alignment of the filter to give desired wavelength channels was problematic and difficult to check. However it is suspected that the allingment of this system could be improved upon.

The single filter, multi-channel system had similar temperature and response time performance to the two filter system. It used fewer components and had a more compact design, but was more difficult to align. Testing the alignment was also more challenging. It

had a slightly higher limit of detection of 8.2ppm, which was still above the target level. The system could be used to give better selectivity in principle, although additional equipment would have to become available before this could be properly carried out.

This system had a number of advantages over a spectroscopy system using a conventional CCD spectrometer. It used fewer components and would be simpler to construct and operate. The use of lock-in amplifiers and a modulated light source allowed for improved noise reduction. The LED could be modulated electronically removing the need for a chopper. Finally, as high spectral resolution was not required, larger collection areas could be used for the photodiodes, increasing signal.

Table 9.1 summarises of the main points of the three systems. NEA figures for the two filter system and the single filter, multi-channel system are based on calculations from observed noise levels. Formaldehyde LOD figures are based on NEA figures and simulated formaldehyde absorbance from literature data. While formaldehyde detection was observed for both systems, LOD values could not be verified the low flow rate of formaldehyde supply meant that long term drift effects dominating over other noise phenomena.

Table 9.1: Summary of the three systems built during this project

	Preliminary system	Two filter system	Single filter, multi-channel system
Detects formaldehyde?	Yes	Yes	Yes
NEA	2.5×10^{-4}AU	4.5×10^{-5}AU	5.2×10^{-5}AU
Formaldehyde LOD	8.5ppm*	6.6ppm	8.2ppm
Dominant noise	Source fluctuation noise	Source fluctuation noise, thermal drift	Source fluctuation noise, thermal drift
Advantages	Gives full absorption spectrum	Simple to build, best LOD	Few components, potential for many channels
Disadvantages	Complex to build and operate	Only two channels, limited selectivity	Difficult to align, availability of components

* The preliminary system had a formaldehyde LOD only slightly higher than the other systems, despite a much higher NEA. This was because narrow band measurements could covered only the maxima of absorption peaks but required complex, high resolution components.

9.4. Future work

During this project prototype devices were made that met the targets of simplicity of manufacture and operation, and of measurement time period. The target limit of detection was not met, nor was the target of selectivity. The target temperature dependence was met for the filters but not for the LED. Here we describe the future work that could be completed in this area to develop and improve upon these prototypes.

One of the main limiting factors for both systems was temperature stability. While the filters were relatively stable between 10 - 30°C, a peak shift in the LED output with temperature change made temperature a significant issue. Initially a Peltier unit was used to control temperature of the LED, placed on the outside of the casing. However the output of the LED drifted over time, attributed to limitations in temperature control due to the distance between control components and the LED element. Temperature control components placed inside the casing and closer to the element may improve temperature stability.

The second option for temperature control was to use a post-processing algorithm. The shift of LED wavelength spectrum was consistent and predictable. Provided the temperature was known, it may be possible that these variations could be accommodated for mathematically. This would require accurate and precise measurement of the temperature of the LED and knowledge of its temperature behaviour. This method could also be used to account for any temperature effects on the filters.

If all non-fundamental effects such as thermal drift and source fluctuations can be removed or accounted for the system would be limited by fundamental detector noise. Assuming all electronic noise not removed by modulation or keeping the room lights off was caused by detector noise, this would give a limit of detection of 2.4×10^{-5}AU. This was found to be equivalent to 3.5ppm.

Relatively little work was carried out on improving the path length in this project, with a simple, single-pass 195cm gas cell being used. A longer gas cell could be used but as a length of 6.8m would be needed (factor of 35) to achieve the 0.1ppm target, this would make the device impractically bulky.

Options exist for multi-pas cells such as integrating spheres or Herriot cells [2]. McManus *et al.* [3] demonstrated a 36m path length over 182 passes using a 0.3l astigmatic Herriot cell (although they require a high degree of collimation). At the time of writing relatively little work had been done on multi-pass cells for the UV so some more work would need to be done. A potential issue would be obtaining a cell with adequate reflection in the UV region of the spectrum.

Fully analysing the performance of detection systems was limited by the rate of production of formaldehyde. Low concentrations required a low flow rate, taking a long time to change the sample in the gas cell. While this would not be a problem for the short term, open path measurements that the systems were designed for, it prevented their predicted limit of detection being verified. Testing the systems with a more rapid delivery of formaldehyde would be desirable.

One option for doing so would be to use a lower volume gas cell. A thinner gas cell could do this without decreasing the path length, as could a multi-pass cell. Another option would be to generate gas containing a low concentration of formaldehyde but to store it in a syringe or similar reservoir for rapid delivery during the test.

The single filter, multi-channel system would allow three channels to be used if an LED became available with a central wavelength of 335nm and a FWHM of at least 10nm. This would allow the spectrum of the LED to cover all three wavelength bands of the 339nm wavelength band set. Out-of-spec LEDs may also be suitable. The performance of the filter may be improved with further optimisation for mass production, or design for off-axis performance.

9.5. Summary and final remarks

The aim of this project was to investigating whether a formaldehyde detection system could be built using UV spectroscopy. Desired targets included being simple, selective and sensitive to 0.1ppm of formaldehyde. Good temperature stability and a response time of 60s or less was desirable. This system was intended for use in the indoor industrial environment, and specifically needed to demonstrate low cross-sensitivity to gases commonly found there.

A literature study was carried out into indoor gases and their UV spectra. A region of the formaldehyde spectrum was found with very little interference. This region also included a number of strong formaldehyde absorption peaks interspersed with regions of very low absorption. This proved to be very useful for building low resolution spectroscopy devices, specifically tuned to formaldehyde absorption features.

Two prototype detection systems were built and both were shown to be able to respond to formaldehyde. The two filter system was optimised to give the best limit of detection within the limits of the equipment used. It found a limit of detection of 4.2ppm, higher than the target value of 0.1ppm. It was limited by source fluctuation noise, and by thermal drift. It may be possible to reduce the thermal drift by incorporating a thermal controller into the LED casing. A longer path length could also be used to increase absorbance and therefore increase sensitivity.

The two filter system had only two channels and so was susceptible to interference, specifically from nitrogen dioxide. The single filter, multi-channel system was designed to reduce this. It also used fewer components than the earlier system. The exploitation of filter transmission wavelength dependence on angle to give multiple wavelength channels was potentially novel.

Unfortunately it was not possible to test the system with three channels. One wavelength band set had insufficiently strong formaldehyde absorption peaks to be detected, and the other lacked an appropriate LED light source. However the system was tested using two channels, detecting formaldehyde and demonstrating that the single filter, multi-channel method worked in principle.

Both systems demonstrated formaldehyde detection and both were significantly more simple in construction than many gas detection systems. Other than thermal drift of the LED, the system was relatively stable to temperature change. The change in the laser-line filter's transmission wavelength from temperatures from 10 – 30°C was small in comparison to formaldehyde absorption features. Both systems averaged over 20s periods, below the target of 60s.

To summarise, this project demonstrated that it was possible to build a simple formaldehyde detection system using UV spectroscopy. Most of the aims of the project were met but issues remain with formaldehyde sensitivity, thermal control and selectivity with nitrogen dioxide. Suggestions for future work to address these issues have been given. While more work would be required to make these methods practically viable, this work supports their potential as formaldehyde detection systems.

9.6. References

[1] R. Meller and G. K. Moortgat, "Temperature dependence of the absorption cross sections of formaldehyde between 223 and 323 K in the wavelength range 225-375 nm," *Journal of Geophysical Research-Atmospheres,* vol. 105, pp. 7089-7101, 2000.

[2] J. Hodgkinson and R. P. Tatam, "Optical gas sensing: a review," *Measurement Science & Technollogy,* vol. 24, no. 1, pp. 1-59, 2013.

[3] J. B. McManus, P. L. Kebabian and M. S. Zahniser, "Astigmatic mirror multipass absorption cells for long-path-length spectroscopy," *Applied Optics,* vol. 34, no. 18, pp. 3336-3348, 1995.

Appendix 1: Derivations of useful equations

This project focused on absorption measurements of low concentrations of gas, where the change in intensity from absorption was small in comparison to initial source intensity. This allowed a low absorption limiting case of the Beer-Lambert law to be used.

A1.1. Derivation of low concentration absorbance equation

Absorbance of light passing through a sample of gas is governed by the Beer-Lambert law, Equation (A1.1):

$$\frac{I(\lambda)}{I_0(\lambda)} = e^{-\sigma(\lambda) l N} \tag{A1.1}$$

Where I is the intensity of light at a wavelength λ, I_0 is the initial intensity at that wavelength, σ is the absorption cross-section, l is the path length of the light and N is the number density of molecules of the absorbing gas. Using the Taylor expansion for small $\sigma l N$, Equation (A1.1) can be approximated to:

$$\frac{I(\lambda)}{I_0(\lambda)} = 1 - \sigma(\lambda) l N \tag{A1.2}$$

The difference in $I(\lambda)$ when an absorbing gas is introduced can therefore be given by:

$$\frac{I_1(\lambda) - I_2(\lambda)}{I_0(\lambda)} = 1 - (1 - \sigma(\lambda) l N) = \sigma(\lambda) l N \tag{A1.3}$$

where I_1 is the intensity with no absorbing gas present (which is also equal to I_0), and I_2 is the intensity when N gas is present. The maximum detectable variation between I_1 and I_2 is equal to the standard deviation of the measurement of $I(\lambda)$ (to be termed $\Delta I(\lambda)$).

The minimum detectable number density at a given wavelength can therefore be found by equation (A1.4):

$$\frac{\Delta I(\lambda)}{I_0(\lambda)} = \sigma(\lambda) l N \tag{A1.4}$$

Appendix 2: List of indoor pollutants

This appendix includes the list of common gases expected to be present in the indoor environment. Most of the list was obtained from C. J. Weshler [1] but nitrous acid was also found to be present by several studies and so was added to the list [2] [3]. References are given for the UV absorption spectrum data. Substances for which no UV absorption spectrum was found are given no references.

A2.1. Indoor pollutants listed by type or family

Inorganic gases

Carbon monoxide [4]
Nitrogen Dioxide [5]
Nitric Oxide [6]
Ozone
Sulfur dioxide [7]
Radon

Very volatile organic compounds (VVOC)

Formaldehyde [8]
Acetaldehyde [9]
Acrolein [10]
1,3-Butadiene [11]
Isoprene [12]

Volatile organic compounds (VOC), aldehydes

Hexanal
Nonanal
Decanal [13]

VOC, aliphatics

n-Alkanes (e.g., n-octane) [14]
Branched alkanes
Undecane

VOC, aromatics

Benzene [15] [16]
Toluene [17]
Xylene isomers [15] [16]
Ethylbenzene [18]
Trimethylbenzene isomers [15] [16]
Styrene [18]

VOC, terpenoids

Limonene
α-Pinene [19]
Linalool
α-Terpineol

VOC, chlorinated

Dichloromethane

Chloroform [20]

Carbon tetrachloride

1,1,1-Trichloromethane [20]

Trichloroethylene

Tetrachloroethylene (Perc)

Dichlorobenzene [21]

Dichlorophenols

VOC, fluorinated

Freon 11 [22]

Freon 12 [23]

Freon 113 [24]

VOC, other

Dimethyl phthalate

Diethyl phthalate

Cyclopentasiloxane (D5)

Semivolatile organic compounds (SVOC),

Triclosan

Bis(tributyltin)oxide(TBTO)

Butylated hydroxytoluene (BHT)

Pentachlorophenol (PCP)

Trichlorophenols

SVOC, combustion byproducts

ETS

Dioxins

Furans

PAHs

SVOC, degradation products

Bisphenol-A

SVOC, flame-retardants

BDE-47

BDE-99

BDE-209

Tris(chloropropyl)phosphate

SVOC, heat transfer fluids

PCBs

Polydimethyl siloxanes

SVOC, personal care products

Musk compounds

SVOC, pesticides and herbicides

Aldrin

Chlordane

Chlorpyrifos

DDT [25]

DDE

Dieldrin

Malathione

Mirex

Permethrin

SVOC, plasticizers

Dibutyl phthalate [12]

Butylbenzyl phthalate

Di-2-ethylhexyl phthalate

Triphenylphosphate (TPP) [26]

SVOC, stain and water repellents

Perfluorinated surfactants

SVOC, nonionic surfactants and coalescing agents

4-Nonylphenol

Texanol_ isomers

SVOC, waxes and polishes

Fatty acids

Sesquiterpenes

Metals and mineral fibres

Asbestos

Cadmium

Lead

Mercury

Others

Allergens (from dust mites, cats, dogs, etc.)

Mold/fungi

Airborne particles

A2.2. References

[1] C. J. Weschler, "Changes in indoor pollutants since the 1950s," *Atmospheric Enviroment,* vol. 43, pp. 153-169, 2009.

[2] K. A. Ramazan, D. Syomin and B. J. Finlayson-Pitts, "The photochemical production of HONO during the heterogeneous hydrolysis of NO," *Physical Chemistry Chemical Physics,* vol. 6, pp. 3836-3843, 2004.

[3] S. S. Park, J. H. Hong, J. H. Lee, Y. J. Kim, S. Y. Cho and S. J. Kim, "Investigation of nitrous acid concentration in an indoor environment using an in-situ monitoring system," *Atmospheric Environment,* vol. 42, p. 6586–6596, 2008.

[4] W. J. Chaplin, Y. Elsworth, G. R. Isaak, B. A. Miller, R. New and B. Pinter, "Noise characteristics of full-disc helioseismic observations made by resonant scattering spectrometers," *Monthly Notices of the Royal Astronomical Society,* vol. 359, no. 2, pp. 607-614, 2005.

[5] K. Bogumil, J. Orphal, T. Homann, S. Voigt, P. Spietz, O. C. Fleischmann, A. Vogel, M. Hartmann, H. Kromminga, H. Bovensmann, J. Frerick and J. P. Burrows, "Measurements of molecular absorption spectra with the SCIAMACHY pre-flight model: instrument characterization and reference data for atmospheric remote-sensing in the 230–2380 nm region," *Journal of Photochemistry and Photobiology A: Chemistry,* vol. 157, pp. 167-184, 2003.

[6] B. A. Thompson, P. Harteck and R. R. Reeves Jr., "Ultraviolet absorption coefficients of CO2, CO, H2O, N2O, NH3, NO, SO2, and CH4 between 1850 and 4000 Å," *Journal of*

Geophysical Research, vol. 68, pp. 6431-6436, 1963.

[7] A. C. Vandaele, C. Hermans and S. Fally, "Fourier transform measurements of SO2 absorption cross-sections: II. Temperature dependence in the 29000–44000/cm (227–345nm) region," *Journal of Quantitative Spectroscopy & Radiative Transfer,* vol. 110, pp. 2115-2126, 2009.

[8] R. Meller and G. K. Moortgat, "Temperature dependence of the absorption cross sections of formaldehyde between 223 and 323 K in the wavelength range 225-375 nm," *Journal of Geophysical Research-Atmospheres,* vol. 105, pp. 7089-7101, 2000.

[9] W. Schneider, G. K. Moortgat, G. S. Tyndall and J. P. Burrows, "Absorption cross-sections of NO2 in the UV and visible region (200-700nm) at 298 K," *Journal of Photochemistry and Photobiology. A: Chemistry,* vol. 40, pp. 195-217, 1987.

[10] I. Magneron, R. Thevenet, A. Mellouki and G. Le Bras, "A Study of the Photolysis and OH-initiated Oxidation of Acrolein and trans-Crotonaldehyde," *Journal of Physical Chemistry A,* vol. 106, pp. 2526-2537, 2002.

[11] A. Fahr and A. K. Nayak, "Temperature dependent ultraviolet absorption cross sections of 1,3-butadiene and butadiyne," *Chemical Physics,* vol. 189, pp. 725-731, 1994.

[12] V. S. Fihtengolts, Atlas of UV Absorption Spectra of Substances Used in Synhetic Rubber Manufacture, 1969.

[13] H. R. Cooper and H. W. Melville, "The Kinetics of the Autoxidation of n-Decanal. Part I. The Mechanism of Reaction," *Journal of the Chemical Society,* pp. 1984-1993, 1951.

[14] J. W. Au, G. Cooper, G. R. Burton, T. N. Olney and C. E. Brion, "The valence shell photoabsorption of the linear alkanes, CnH2n+2 (n = l-8): absolute oscillator strengths (7-220 eV)," *Chemical Physics,* vol. 173, pp. 209-239, 1993.

[15] A. Bolovinos, J. Philis, E. Pantos, P. Tsekeris and G. Andritsopoulos, "The Methylebenzenes vis-a-vis Benzene," *Journal of Molecular Spectroscopy,* vol. 94, pp. 55-68, 1982.

[16] A. Bolovinos, J. Philis, P. E., P. Tsekeris and G. Andritsopoulos, "The methylebenzenes vis-a-vis benzene - comparison of their spectra in the Rydberg series region.," *Journal of Chemical Physics,* vol. 75, pp. 4343-4349, 1981.

[17] W. Koban, J. D. Koch, R. K. Hanson and C. Schulz, "Absorption and fluorescence of toluene vapor at elevated temperatures," *Physical Chemistry Chemical Physics,* vol. 6, pp. 2940-2945, 2004.

[18] T. Etzkorn, B. Klotz, S. Sorensen, I. V. Patroescu, I. Barnes, K. H. Becker and U. Platt,

"Gas-phase absorption cross sections of 24 monocyclic aromatic hydrocarbons in the UV and IR spectral ranges," *Atmospheric Environment,* vol. 33, pp. 525-540, 1999.

[19] D. Kubala, E. A. Drage, A. M. E. Al-Faydhi, J. Kocísek, P. Papp, V. Matejcík, P. Mach, J. Urban, P. Limão-Vieira, S. V. Hoffmann, S. Matejcík and N. J. Mason, "Electron impact ionisation and UV absorption study of alpha - and beta - pinene," *International Journal of Mass Spectrometry,* vol. 280, pp. 169-173, 2009.

[20] P. C. Simon, D. Gillotay, N. Vanlaethemmeuree and J. Wisemberg, "Temperature-dependence of ultraviolet-absorption cross-section of chlorofluoroethanes," *Annales Geophysicae-Atmospheres Hydrospheres and Space Sciences,* vol. 6, pp. 239-247, 1988.

[21] H. Z. C. Scharping, Substituent effects in the VUV absorption-spectra of monochlorobenzene and ortho-dichlorobenzene, meta-dichlorobenzene and para-dichlorobenzene, Journal of Molecular Spectroscopy: Vol 112, Issue 1, 8-17.

[22] J. W. Au, G. R. Burton and C. E. Brion, "Quantitative spectroscopic studies of the valence-shell electronic excitation of Freons (CFC13, CF2C12, CF3C1, and CF 4) in the VUV and soft X-ray regions," *Chemical Physics,* vol. 221, pp. 151-168, 1997.

[23] C. Hubrich, C. Zetzsch and F. Stuhl, "Absorption-spectra of halogenated methanes in wavelength refion from 275 to 160 nm at temperatures of 298 and 208 K," *Berichte der Bunden-Gesellschaft-Physical Chemistry Chemical Physics,* vol. 81, pp. 437-442, 1977.

[24] J. Doucet, P. Sauvageau and C. Sandorfy, "Photoelectron and far Ultravoplet absorption-spectra of chlorofluoro derivatives of ethane," *Journal of Chemical Physics,* vol. 62, pp. 355-359, 1975.

[25] A. Bartecki, J. Szoke, G. Varasanyi and M. Vizesy, Absorption spectra in the ultraviolet and visible region, vol. 6, New York: Academic Press Inc., 1965.

[26] L. Lang (Editor), Absorption Spectra in the Ultraviolet and Visible Region, Akadémia Kiadó, 1967.

Appendix 3, Gas absorbance and concentration calculations

Several different conventions exist for describing optical absorption, gas concentrations and even the Beer-Lambert law. While information from different sources could use any of these conventions, it was important to be consistent within this project. This section describes how other conventions were converted into those used in this project.

A3.1. Gas absorbance calculations

In figure 5 the absorbances of a range of gases were given over the region of interest, assuming a 10cm path length. Absorbances for most of these gases were calculated from absorption cross-sections taken by other studies. Data was given in terms of absorption cross-section for formaldehyde [1], nitrogen dioxide [2], ozone [3], sulphur dioxide [4], acetaldehyde [5], hexanal [6], toluene [7] and ethylbenzene [8]. The method of converting absorption cross-section data to absorbance is described here.

First concentration in ppm or ppb had to be converted into molecular number density. To calculate molecular number density of air the ideal gas law is used:

$$PV = N_{air} K_B T \tag{A3.1}$$

where P is the pressure, V is the volume being considered, N_{air} is the total number of molecules therein. Rearranging this formula gives the molecular number density as:

$$\frac{N_{air}}{V} = \frac{P}{k_B T} \tag{A3.2}$$

The value of k_B is 1.38×10^{-23}J/K^{-1} and under standard conditions the values of P and T are 101kPa and 293°K (20°C) respectively. This gives a value of molecular number density of 2.503×10^{19}molecules cm^{-3}.

Concentrations given in ppm were then converted to molecular number density for that gas by dividing by 1×10^{6} and multiplying by 2.503×10^{19} or just multiplied by 2.503×10^{13}. Concentrations given in ppb are multiplied by 2.503×10^{10}. These figures were then substituted into Equation (A3.3), along with absorption cross-section figure and the path length of 10cm.

$$\frac{I(\lambda)}{I_0(\lambda)} = e^{-\sigma(\lambda)lN} \tag{A3.3}$$

The data for some gases, decanal [9] DDT [10] dibutyl phthalate [11] Triphenylphosphate [12], used and alternative form of the Beer-Lambert law given by Equation (A3.4) [13]:

$$\frac{I(\lambda)}{I_0(\lambda)} = 10^{-\varepsilon(\lambda)lC} \tag{A3.4}$$

where ε is the molar absorptivity and C is the molar concentration of the gas in question. Molar absorptivity figures were not used to calculate absorbance directly but first converted into absorption cross-section figures. First molar concentration is converted to molecular number density divided by N_A, the Avogadro constant (6.02×10^{23} mol^{-1}). This gives:

$$\sigma(\lambda) = \ln\left(10^{\varepsilon(\lambda)/N_A}\right) \tag{A3.5}$$

Hence absorption cross-section figures can be calculated and substituted into Equation (A3.3).

A3.2. Concentration conversions

Gas concentrations given in this document are generally quoted in ppm (parts per million by volume) or ppb (parts per billion, being 10^{-3} ppm). This is only one way of quantifying concentration. The section describes how other conventions were converted to ppm.

The molecular number density of a gas describes the number of molecules present in a given volume of air, generally quoted in units of cm^{-3}. In Section A.4 the molecular number density of air under standard conditions was calculated to be 2.503×10^{19} molecules cm^{-3}. Under standard conditions the molecular number density of a gas in air can therefore be converted into ppm by dividing by 2.503×10^{13}.

Some sources quote concentration in μg m^{-3}, describing the mass of the gas present in a given volume. The conversion to ppm depends on the mass of the gas in question, which is 30.026g mol^{-1} [14] for formaldehyde. 1μg m^{-3} of formaldehyde is therefore equivalent to

$$\frac{1\times10^{-12}\times6.0221\times10^{23}}{30.026\times2.53\times10^{13}} = 8.013\times10^{-4}\text{ppm}$$

where 1×10^{-12} is the unit conversion from μg m^{-3} to g cm^{-3} and 6.0221×10^{23} is the Avogadro constant.

Particularly high concentrations are sometimes quoted as a percentage. This refers to the percentage of molecules in a given volume are the type in question and is therefore the proportion of the gas by volume. 1% is equivalent to 1×10^{4}ppm.

A3.3. References

[1] R. Meller and G. K. Moortgat, "Temperature dependence of the absorption cross sections of formaldehyde between 223 and 323 K in the wavelength range 225-375 nm," *Journal of Geophysical Research-Atmospheres,* vol. 105, pp. 7089-7101, 2000.

[2] K. Bogumil, J. Orphal, T. Homann, S. Voigt, P. Spietz, O. C. Fleischmann, A. Vogel, M. Hartmann, H. Kromminga, H. Bovensmann, J. Frerick and J. P. Burrows, "Measurements of molecular absorption spectra with the SCIAMACHY pre-flight model: instrument characterization and reference data for atmospheric remote-sensing in the 230–2380 nm region," *Journal of Photochemistry and Photobiology A: Chemistry,* vol. 157, pp. 167-184, 2003.

[3] D. Daumont, J. Brion, J. Charbonnier and J. Malicet, "Ozone UV spectroscopy I: Absorption cross-section at room-temperature," *Journal of Atmospheric Chemistry,* vol. 15, pp. 145-155, 1992.

[4] A. C. Vandaele, C. Hermans and S. Fally, "Fourier transform measurements of SO2 absorption cross-sections: II. Temperature dependence in the 29000–44000/cm (227–345nm) region," *Journal of Quantitative Spectroscopy & Radiative Transfer,* vol. 110, pp. 2115-2126, 2009.

[5] W. Schneider, G. K. Moortgat, G. S. Tyndall and J. P. Burrows, "Absorption cross-sections of NO2 in the UV and visible region (200-700nm) at 298 K," *Journal of Photochemistry and Photobiology. A: Chemistry,* vol. 40, pp. 195-217, 1987.

[6] H. Plagens, R. Bröske, M. Spittler, L. Ruppert, I. Barnes and H. K. Becker, "Atmospheric loss processes of hexanal. Photolysis and reaction with OH and Cl radicals," *Proceedingsof the Second Workshop of the EUROTRAC-2 Subproject Chemical Mechanism Development,* pp. GPP10-1-GPP10-4, 1998.

[7] W. Koban, J. D. Koch, R. K. Hanson and C. Schulz, "Absorption and fluorescence of toluene vapor at elevated temperatures," *Physical Chemistry Chemical Physics,* vol. 6, pp. 2940-2945, 2004.

[8] T. Etzkorn, B. Klotz, S. Sorensen, I. V. Patroescu, I. Barnes, K. H. Becker and U. Platt, "Gas-phase absorption cross sections of 24 monocyclic aromatic hydrocarbons in the UV and IR spectral ranges," *Atmospheric Environment,* vol. 33, pp. 525-540, 1999.

[9] H. R. Cooper and H. W. Melville, "The Kinetics of the Autoxidation of n-Decanal. Part I. The Mechanism of Reaction," *Journal of the Chemical Society,* pp. 1984-1993, 1951.

[10] A. Bartecki, J. Szoke, G. Varasanyi and M. Vizesy, Absorption spectra in the ultraviolet and visible region, vol. 6, New York: Academic Press Inc., 1965.

[11] V. S. Fihtengolts, Atlas of UV Absorption Spectra of Substances Used in Synhetic Rubber Manufacture, 1969.

[12] L. Lang(Editor), Absorption Spectra in the Ultraviolet and Visible Region, Akadémia Kiadó, 1967.

[13] D. L. Pavia, G. M. Lampman and G. S. Kriz, Introduction to Spectroscopy, third edition, Stamford: Thomson Learning, 2001.

[14] D. R. Lide, Handbook of Chemistry and Physics, 82nd Edition, Boca Raton: CRC Press, 2001-2002.

Appendix 4, Safe handling of formaldehyde

A4.1. Safety procedures during formaldehyde generation

As described in Chapter 1, formaldehyde is an extremely hazardous chemical and so safety was of paramount importance when generating the gas. In the United Kingdom the EH40 work place exposure limit for formaldehyde is 2ppm. Care was taken to avoid exposure when generating concentrations of formaldehyde above this level, or when concentration was uncertain but could pass this level. Table A4.1 is a list of hazards identified when working with formaldehyde and paraformaldehyde.

Table A4.1: List of hazards identified when working with formaldehyde and paraformaldehyde.

Hazard	Details
Inhaled	Acute toxicity, may cause respiratory irritation, limited evidence of causing cancer.
Contact with skin	Causes skin irritation, may cause allergic skin reaction, may cause skin sensitisation.
Contact with eyes	Causes serious eye damage, eye burns.
Swallowed	Acute toxicity, limited evidence of causing cancer.
Exposure to fire	Highly flammable in solid or gas form. Should be kept away from fire, sparks or excessive heat.
Environmental hazard	Toxic to aquatic invertebrates and other aquatic life. Should be disposed of safely and not introduced into waterways.

Consequently safety procedures had to be followed. Personal protective equipment was used including lab coat, goggles and nitrile gloves. This was to limit the risk of contact with skin or eyes of any formaldehyde derivative. Additionally, hands and face were thoroughly washed after leaving the lab, specifically before eating. None of this equipment was protection against gaseous formaldehyde.

All generation or use of formaldehyde was carried out in a fume cupboard (Labspace F7 x 2000). It had a surface flow velocity of $0.5ms^{-1}$ and a flow rate of $1{,}620m^3hr^{-1}$ or $0.45m^3s^{-1}$. The limiting factor on the concentration used in the fume cupboard alone was exhaust outflow as it could not be guaranteed that no one was present near the chimney during use.

The cupboard flow was at maximum when the hood was raised to the highest safe level, when a higher volume flow was needed to maintain the surface flow velocity. To keep exhaust outflow to a safe level it was necessary to limit the release of formaldehyde gas in the cupboard to below $0.9cm^3s^{-1}$. Figures assume perfect mixing in the ducting.

When the rate of formaldehyde generation was above this level, or there was a risk of it rising above this level, a glove box was used (Scienceware Bel-Art 500402011 medium clear view glove box). The box was placed inside the fume cupboard to guard against leaks and for the removal of exhaust gas. Gas fittings were attached to allow controlled release of the internal atmosphere. The glove box was selected to have as much internal space as possible within the limits of the fume cupboard. An airlock was also necessary to allow items to be passed in and out without opening the box, as was construction material compatible with formaldehyde.

Before use with formaldehyde, the glove box was tested for leaks. This was done by pumping 2.5% by volume of methane in air into the box, and then running a combustible gas detector (Kane-May CD 100) around all joins to search for methane on the outside. The detector measured relative methane concentration and so did not give a quantitative measurement of leaks but was sufficient to locate them. A few were found on joints where bolts had come loose. These joints were re-sealed with silica sealant and the bolts were retightened. Once the sealant had dried the test was performed again, finding no further leaks.

When formaldehyde concentration inside the glove box was higher than 2ppm, the contents were pumped out at a fixed rate rather than releasing it in an uncontrolled manner into the fume cupboard. This was done with the use of a mass flow controller attached to the box via gas fittings. Similar fittings were attached to the air lock to allow it to be pumped down independently of the main chamber. A lookup table was produced for the safe rate of gas flow depending on internal formaldehyde concentration. The table is included in the Appendix.

The final piece of safely equipment was an electrochemical formaldehyde detector (PPM Technologies Formaldemeter). It did not have a quoted limit of detection but was found to give readings down to 50ppb. It had a response time of 60s. It was used to check room concentration levels whenever formaldehyde was used, as well as in the glove box when appropriate.

Whilst other precautions were intended to prevent exposure to formaldehyde at unsafe concentrations, the detector was kept as a backup to make sure that this remained the case. It was therefore run frequently whenever formaldehyde gas was present or expected to be present. The detector could also be passed into the glove box through the airlock in order to determine the safe rate of gas flow for pumping down the glove box.

A.4.2 Look-up table for formaldehyde flow rates

Calculated assuming an LEV flow of $0.45m^3/s$ (0.5m/s x 0.505m x 1.80m) with fume cupboard hood at maximum level (red stop position). Flow rate aims to ensure the concentrations are diluted to a safe level in the fume cupboard exhaust. Airlock volume: $0.033m^3$ (0.38m x 0.31m x 0.28m). Main chamber volume: $0.30m^3$ (1.07m x 0.508m x 0.61m – $0.033m^3$ / 2). The results are given in Table A4.2

Table A4.2: Look-up table for formaldehyde purge flow rates from glove box

Concentration	Maximum air flow rate (up to 1300 cc/min)	Approximate purge time (airlock)	Approximate purge time (main chamber)
≤ 2ppm	N/A*	N/A*	N/A*
≤ 41,000ppm	1300 cc/min	26 min	3:51 hrs
≤ 54,000ppm	1000 cc/min	33 min	5:00 hrs
≤ 108,000ppm	500 cc/min	1:06 hrs	10:00 hrs
≤ 540,000ppm	100 cc/min	5:30 hrs	50:00 hrs
≤ 1,000,000ppm	54 cc/min	10:12 hrs	92:36 hrs

*Considered safe to emit directly into fume cupboard